GEOMAR REPORT

GEOMAR

Helmholtz-Zentrum für Ozeanforschung Kiel

RV METEOR Fahrtbericht / Cruise Report M127

Extended Version

Metal fluxes and Resource Potential at the Slow-spreading TAG Midocean Ridge Segment (26°N, MAR) – Blue Mining@Sea

Bridgetown (Barbados) – Ponta Delgada (Portugal)
25.05.-28.06.2016

Berichte aus dem GEOMAR
Helmholtz-Zentrum für Ozeanforschung Kiel

Nr. 32 (N. Ser.)

November 2016

GEOMAR

Helmholtz-Zentrum für Ozeanforschung Kiel

RV METEOR Fahrtbericht / Cruise Report M127

Extended Version

Metal fluxes and Resource Potential at the Slow-spreading TAG Midocean Ridge Segment (26°N, MAR) – Blue Mining@Sea

Bridgetown (Barbados) – Ponta Delgada (Portugal)
25.05.-28.06.2016

Berichte aus dem GEOMAR
Helmholtz-Zentrum für Ozeanforschung Kiel

Nr. 32 (N. Ser.)

November 2016

GEOMAR
Helmholtz-Zentrum für Ozeanforschung Kiel

Das GEOMAR Helmholtz-Zentrum für Ozeanforschung Kiel ist Mitglied der Helmholtz-Gemeinschaft Deutscher Forschungszentren e.V.

The GEOMAR Helmholtz Centre for Ocean Research Kiel is a member of the Helmholtz Association of German Research Centres

Herausgeber / Editor:
Petersen, S. and Shipboard Scientific Party

GEOMAR Report
ISSN Nr.. 2193-8113, DOI 10.3289/GEOMAR_REP_NS_32_2016

Helmholtz-Zentrum für Ozeanforschung Kiel / Helmholtz Centre for Ocean Research Kiel
GEOMAR
Dienstgebäude Westufer / West Shore Building
Düsternbrooker Weg 20
D-24105 Kiel
Germany

Helmholtz-Zentrum für Ozeanforschung Kiel / Helmholtz Centre for Ocean Research Kiel
GEOMAR
Dienstgebäude Ostufer / East Shore Building
Wischhofstr. 1-3
D-24148 Kiel
Germany

Tel.: +49 431 600-0
Fax: +49 431 600-2805
www.geomar.de

Content

1 Summary

Cruise M127 is an integral part of the EU-FP7 project "Blue Mining: Breakthrough Solutions for the Sustainable Deep Sea Mining Value Chain" and is addressing research questions regarding the nature and resource potential of marine minerals, especially seafloor massive sulfides (SMS) along mid-ocean ridges. The cruise left from Bridgetown (Barbados) in the evening of May 25th and reached the working area at 26°N on the Mid-Atlantic Ridge on May 30th (Fig.1.1). One of the main tasks during the cruise was mapping of the TAG segment (26°N) in various resolutions. This included ship-based multibeam mapping over the entire length of the ridge segment as well as high-resolution mapping using an autonomous underwater vehicle (AUV) flying close to the seafloor (40-100 m altitude).

The ship-based multibeam mapped along 710 nautical miles of profile lines covering approximately 7,000 km^2 in the working area. Another 1,800 nautical miles of lines were mapped on the transit from Barbados to the working area and from there back to the Azores. The AUV was used on 19 missions, usually with survey times close to the seafloor of between 10 and 12 hours. Most dives provided maps with a resolution of 2 m and collected a number of other parameters with its sensors at the same time. Two dives were devoted to mapping points of interest in 50 cm resolution.

Seismic work, as the 2nd important part of the cruise, included refraction and reflection seismics with airgun shots and multichannel seismic streamer records being compiled along 49 profiles on 8 survey runs (230 nautical miles in total length). Additionally, 22 ocean bottom seismometers (OBS) and 9 ocean bottom hydrophones (OBH) deployments were undertaken. The seismic work was hampered by problems with the compressor, for which the oil could not be cold enough at the beginning. This was later solved with the help of the ships crew. Deep-towed streamer work could also not be performed because of continued problems with the streamer that could not be resolved on board. A series of 6 ocean bottom electro-magnetic stations (OBEM) were deployed as preparation for the up-coming RRS James Cook cruise, which is also part of the Blue Mining project.

A modular towed instrument platform (HYBIS) was used to deploy 10 of the (OBS) to the seafloor with high precision. Since this platform has built-in cameras and can be equipped with a sampling module we used this instrument later in the cruise to further visually inspect the seafloor and select locations for sampling.

The final instrument being used was a short (3m) gravity corer for sediment sampling. In the course of the cruise 35 stations were attempted of which 22 stations successfully retrieved sediment for some of which ship-board analyses showed very high concentrations of copper. Rock fragments were recovered in 9 stations indicating the volcanic nature of those sampling stations. At the end of the cruise all Ocean Bottom Seismometers (OBS) were recovered. Only the six OBEM were intentionally left behind.

Station work in the working area ended on 20:30 LT on June 23rd when the 5 day transit to Ponta Delgada was started. During the transits from and to the working area 3 ARGO floats were deployed and the ship-based multibeam and the 75-kHz ADCP collected data in international waters. The cruise ended 09:00 LT of June 28th with docking in Ponta Delgada.

Overall on 1/3 of the cruise was used for the transit and 2/3 for stations work and transits within the working area (Fig. 1.2). Most of station time was devoted to geophysical work including seismic profiling and the deployment and recovery of the instruments.

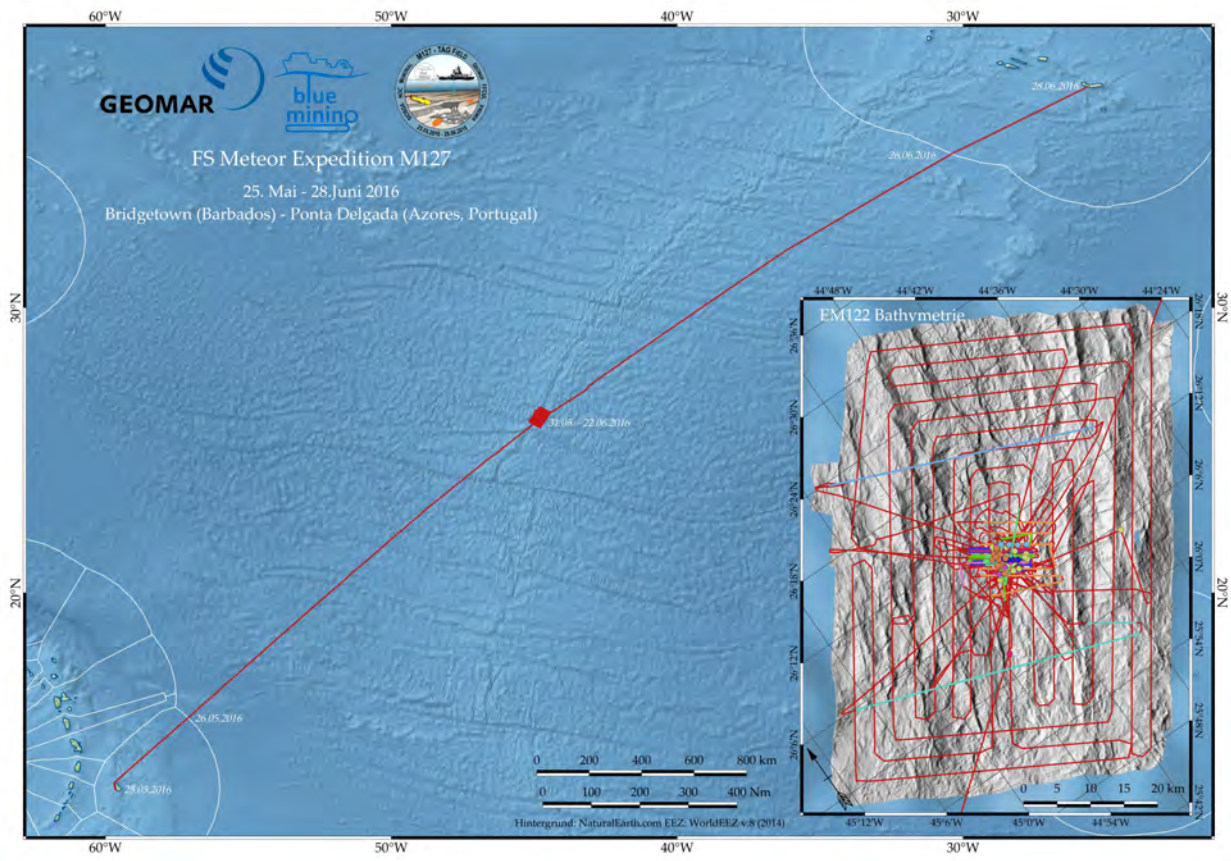

Fig. 1.1: Map of the cruise track from Bridgetown (Barbados) to Ponta Delgada (Azores, Portugal). Insert shows cruise track in the working area with ship-based bathymetry (red lines) and seismic profiles (other colors). Other station work is limited to the very center of this map.

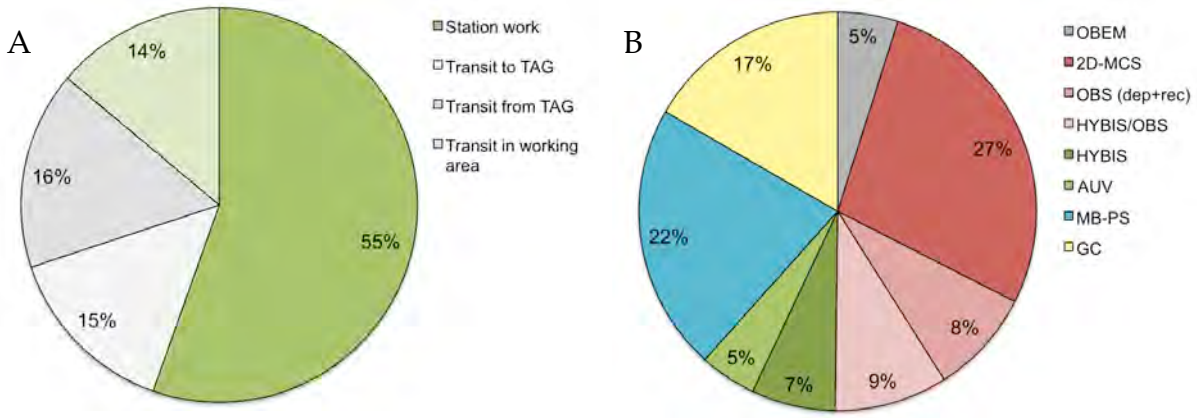

Fig. 1.2: Cruise time-use statistics. A) About 2/3 of the ship time was spend in the working area with the remaining 1/3 spend on the long transits to and from the working area. B) Seismic profiling (27%) and ship-based multibeam mapping account for most of the station time being used. This is followed by the deployment/recovery of OBS and OBH (17%; combining deployments in free-fall mode and by HYBIS), gravity coring, and geological dives using HYBIS. Deployments of the OBEM via cable as well as the deployment and recovery of the AUV used minimal ship-time. The AUV used 20.5 h of ship-time while mapping the seafloor for 161 h.

2 Participants

Name	Discipline	Institution
Dr. Sven Petersen	Chiefscientist	GEOMAR
Dr. Jörg Bialas	Co-chief scientist, Seismics	GEOMAR
Dr. Anke Dannowski	Ocean Bottom Seismometers	GEOMAR
Dr. Alba Gil	Ocean Bottom Seismometers	NOC
Dr. Nico Augustin	Bathymetry	GEOMAR
Dr. Isobel Yeo	AUV bathymetry	GEOMAR
Dr. Florent Szitkar	AUV self-potential & magnetics	GEOMAR
Prof. John Jamieson	Mineral resources	Memorial
Prof. Fernando Barriga	Mineral resources	FFCUL
Dr. Kai Zhang	Mineral resources	SIOSOA
Dr. Honglin Li	Mineral resources	SIOSOA
Dr. Anna Lichtschlag	Sediment porewater chemistry	NOC
Iain Stobbs	Geology/GIS	NOC
Sofia Martins	Sediment geochemistry	FFCUL
Adeline Dutrieux	Sediment porewater chemistry	NOC
Marcel Rothenbeck	AUV	GEOMAR
Lars Triebe	AUV	GEOMAR
Emanuel Wenzlaff	AUV	GEOMAR
Henning Schröder	DeepTow MCSeismics	GEOMAR
Tammy Jacobsen-Bialas	DeepTow MCSeismics	GEOMAR
Torge Matthiessen	Technician	GEOMAR
Gero Wetzel	Electronic engineer	GEOMAR
Meike Klischies	Structural geology	GEOMAR
Sebastian Graber	Structural geology	GEOMAR
Florian Besson	Geology	IFREMER
Holger Jens	Meteorology	DWD
Andreas Raeke	Meteorology	DWD
Laura Raeke	Meteorology	MPI

GEOMAR	Helmholtz-Centre for Ocean Research, Kiel (Germany)
NOC	National Oceanography Centre, Southampton (UK)
SIOSOA	State Oceanic Administr. – 2nd Institute of Oceanography, Hangzhou (China)
IFREMER	Institut français de recherche pour l'exploitation de la mer, Plouzané (France)
FFCUL	Fundação da Faculdade de Ciências da Universidade de Lisboa (Portugal)
MPI	Max-Planck-Institut für Meteorologie, Hamburg (Germany)
Memorial	Memorial University of Newfoundland, St. Johns (Canada)
DWD	Deutscher Wetterdienst, Seeschiffahrtsberatung, Hamburg (Germany)

Fig. 2.1: Participants of cruise M127.

3 Research program

(S. Petersen)

Cruise M127 is an integral part of the EU-FP7 project "Blue Mining: Breakthrough Solutions for the Sustainable Deep Sea Mining Value Chain" that is, among others, addressing research questions regarding the nature and resource potential of marine minerals, especially seafloor massive sulfides (SMS) along mid-ocean ridges. These deposits are often seen as a possible future contribution to a secure metal supply for global human needs. Resource estimates, however, are lacking several of the fundamental answers that need to be addressed. There are currently several orders of magnitude between resources estimates based on observations at the seafloor and those based on calculated metal fluxes. In order to provide realistic resource estimates, we need to understand how much of the metal that is released by high-temperature fluid convection over a given length of a ridge axis and over a specific geological time frame is actually deposited as massive sulfides. Additionally, exploration is currently only targeting active deposits. It is assumed that 10 times more inactive massive sulfides are occurring within the neovolcanic zone, but until recently the technology to identify those deposits was lacking thereby underestimating the global resource potential. Within the framework of the Blue Mining project some of these technical limitations are addressed and this provides us with the tools to address, for the first time, the full metal potential and fluxes of a slow-spreading mid-ocean ridge.

Slow-spreading mid-ocean ridges, such as the Mid-Atlantic Ridge are known to host accumulations of large submarine massive sulfide (SMS) deposits. The TAG Hydrothermal field at 26°N on the Mid-Atlantic Ridge, for instance, is characterized by a large active black smoker complex and by several similar-sized inactive (eSMS) sites, despite the fact that only small areas of this ridge segment were ever investigated in detail. This area was therefore chosen as the working area for the seagoing activities within "Blue Mining". In the time between submitting the Blue Mining proposal to the EU in 2013 and the Meteor M127 cruise in 2016, the French Research Institute for Exploitation of the Sea (IFREMER), has obtained an exploration license for seafloor massive sulfides from the International Seabed Authority in 2014.

During our cruise, detailed high-resolution AUV-based mapping on a segment scale combined with 2D seismic observations and the investigation of surface sediments will help to answer the following scientific questions:

1) What is the accumulation rate of sulfide formation at a slow-spreading ridge and how does it change over time?
2) Is there more sulfide present in inactive deposits compared to active deposits?
3) What are the regional and local spatial controls of these large hydrothermal fields?
4) What is the 3-dimensional structure of inactive sulfide deposits?
5) How far out (back in time) can we trace hydrothermal activity using geophysical and geochemical instrumentation (AUV-based surveys plus sediment geochemistry)?

The rationale behind these questions is the following:

Q1) What is the accumulation rate of sulfide formation at a slow-spreading ridge and how does it change over time?

We do not know how much of the metal that is released by high-temperature fluid convection over a given length of a ridge axis and over a specific geological time frame is actually deposited as massive sulfides. There are simply no systematic surveys for massive sulfide abundance on a ridge segment scale and back in time (away from the ridge axis). Even the amount of sulfide along the neovolcanic zone is likely highly underestimated. In a recent survey within known vent sites at the Endeavour Segment, AUV-based high-resolution bathymetry was used to identify extinct sulfide chimneys and mounds. There, in only eight 18-hour dives the number of chimneys and mounds present was quadrupled (*Jamieson et al., 2014*). This is especially noteworthy since this vent site has seen well over one hundred submersible and ROV dives over the past 30 years and is considered to be the best studied submarine hydrothermal field on Earth. The total sulfide tonnage estimated from the high-resolution data at this vent field is now 1.2 Mt, a four-fold increase compared to the previous estimate of 0.3 Mt largely based on active structures. Thus, the global inventory of submarine hydrothermal deposits may be similarly biased towards active systems, and the 3 x 10^9 t Cu+Zn global estimate by *Hannington et al (2011)* should be considered a minimum, even for the neovolcanic zones.

Q2) Is there more sulfide present in inactive deposits compared to active deposits?
and
Q3) What are the regional and local spatial controls of these hydrothermal fields?

If there is indeed more sulfide present in inactive deposits, how do we explore for such inactive occurrences in a fast and cost-efficient way? The hypothesis is, that large eSMS deposits can be found in a strip of a few tens of kilometers away from mid-ocean ridges at only a few meters below a sediment or lava carapace. The potential to find sulfide deposits that far from the ridge axis opens up a vast area of the seafloor for future exploration. However, without a distal signature, *e.g.* a geochemical or geophysical anomaly that is detectable over hundreds of meters or even kilometers away from deposit, and with only poorly constrained geophysical properties, inactive deposits are difficult to locate or evaluate. Without a better understanding of their size, structure, and distribution, the resource potential of eSMS remains uncertain. Knowledge about the regional and local spatial controls of sulfide deposition are currently still lacking. This is largely a reflection of the lack of high-resolution investigations away from the spreading centers. However, large inactive deposits have been discovered in the past few years, especially at slow-spreading ridges. These include the Krasnov, Semyenov, and Petersburg sites (*Cherkashov et al., 2010; Shilov et al., 2012*) that are estimated to contain up to 14 million tonnes of sulfides in the case of Semyenov and Krasnov (*Cherkashov et al., 2010*). As stated above, these systems cannot be found with traditional exploration technologies that are looking for geochemical or geophysical tracers in the water column. Russian scientists used time-consuming towed geophysical and electrochemical sensor-package operations for their discoveries up to 12 km away from the ridge axis (Petersburg deposit; *Shilov et al., 2012*). Their systematic surveys use a so-called self-potential sensor package that is towed close to the seafloor. In order to be able to cover larger areas of the seafloor, the Russian research vessel spends about 6 months at sea every

year on exploration. Techniques to identify such deposits time and cost efficiently on a regional scale are still lacking. We currently also lack the ability to identify buried deposits (beneath a few meters of sediments or lava) thereby further underestimating the resource potential of explored areas. This limitation results in a narrow exploration corridor as we can only venture off-axis, when we can detect deposits under cover. Sediments may provide such a far-field halo around inactive deposits at a scale comparable to that of plume mapping. Although sediment geochemistry has been a standard tool in marine geology for over a century, there have been few modern advances to adapt this technique to the search for marine minerals. This contrasts with the search for ore deposits on land, where exploration geochemistry has achieved a high degree of sophistication, including the application of ultra-sensitive tracers such as mobile metal ions and pore-fluid gases. Depth profiles of metals in the sediments can potentially be used to estimate the age of a source (and how far away it might be, based on spreading rates), but few sensitive mineralogical, geochemical or isotopic vectors have been tested that could be traced back to metal sources more than 1-2 km distant or at depth below the sampled core. Gravity coring and ship-based analytics (e.g. portable XRF, PIMA, portable XRD) in combination with structural interpretation of AUV-based high-resolution self-potential, magnetics, and bathymetry data may open up a new frontier in exploration technology and were tested during this cruise. Geophysical and geochemical vectors to ore may then help answering scientific questions on metal accumulation rates over time and metal fluxes.

Q4) What is the 3-dimensional structure of sulfide deposits?

SMS deposits are three-dimensional bodies and therefore any resource estimate must build on depth information. Tonnage calculations reported for most known seafloor deposits, however, are only based on interpretation of visual surface information of the outcrop thickness and lateral extension as well as on distribution of Fe-staining at the surface. In many cases, these estimates are considered to overestimate their size and tonnage (*Hannington et al., 2011*). For example, the tonnage estimates for Krasnov and Semyenov are entirely based on visual surface observation in combination with chemical composition of surface samples. Finding these deposits is not enough. Resource estimates need reliable subsurface information. Drilling is currently the only technology that provides depth information of SMS deposits and has only been performed for few deposits. Since drilling is very expensive, there is a pressing need to develop or modify existing technologies to gain subsurface information. Geophysical tools such as seismic and marine electromagnetics (EM) could provide this information. Due to the rough morphology reflection seismic data collected at the sea surface will be heavily disturbed by side echoes and diffraction events, which can partly be suppressed with modern seismic processing techniques (e.g. *Peirce et al., 2007*). Refracted seismic events from Ocean Bottom Seismometers (OBS) can be used to further improve reflection seismic images (e.g. *Planert et al., 2010*). These techniques have so far mainly been applied to crustal scale investigations and were, in the framework of this cruise, tested for investigating shallow eSMS deposits.

Q5) How far out (back in time) can we trace hydrothermal activity using geophysical and geochemical instrumentation (AUV-based surveys plus sediment geochemistry)?

As stated above, exploration for inactive sulfide occurrences is mainly limited to the immediate surrounding of active vents sites. One of the aims of cruise M127 is to test, if AUV-based mapping technologies or sediment sampling at the surface are able to detect mineralization under cover. In the case of the TAG segment, the detection of indications for mineralization under the sediment cover along the eastern rift valley wall, where slumps are expected to occur that cover the younger volcanic rocks was tested. Time depending, we wanted to extend the map as far east, and away from the ridge axis, as possible. Ground truthing of these targets, however, was beyond the scope of this project, as this would rely on drilling operations.

Specific technology topics of interest within "Blue Mining" that were adressed during cruise M127 were:

1) Test of AUV-based self-potential sensor package for use in exploration of inactive sulfide occurrences (eSMS).
2) Produce regional, high-resolution topographic maps to aid a geochemical study of surface sediments (cover rocks) to identify concealed sulfide mineralization.
3) Produce high-resolution topographic maps of eSMS to aid the drilling program for RRS JAMES COOK cruise JC138, scheduled for July/August 2016.
4) Provide high-resolution geophysical sections across type examples of eSMS.

4 Narrative of the cruise

(S. Petersen)

Preparations for the seismic work and the setup of the AUV during the port call in Bridgetown resulted in the presence of several members of the scientific crew well before the official boarding. Leaving the ROV Quest on board for M128 provided additional constraints on the logistics since five containers with material came from Kiel, and were met by two containers with seismic gear that came from RV SONNE via New Zealand. Preparations were interrupted on May 23rd by an official banquet on the vessel organized by the German consulate/embassy and the ship's crew. Guests from the island were introduced to the ship and the scientific instruments were presented. The science party was complete on the evening of Wednesday May 25th when RV METEOR left port at 21:00 LT after a search for stowaways. The luggage of 3 scientists and 8 crewmembers never made it to Bridgetown. The transit time was used to set up the labs of the various working groups, to prepare the AUV, HyBis and the mobile winch (Werner-Winde), and for scientific talks describing the goals of the various working groups. Since leaving the Exclusive Economic Zone of Barbados on 20:00 LT on May 26th (May 27th 00:00 UTC) the 75 kHz ADCP and the Kongsberg EM122 multibeam echosounding system collect transit data that will be made publically available directly after the cruise.

In the afternoon of May 29th, the transit was interrupted in order to deploy an ARGO float for the MOCCA project. Two more floats follow at the end of the cruise as we approach Ponta Delgada. The stop was used to obtain a sound velocity profile (#557XBT), for a short test deployment of HyBis (#558HYBIS) and the AUV (#559AUV), both showing the need for additional maintenance, and a test of all releasers to be used for OBS/OBH/OBEM deployments

(#560REL). The ARGO float was deployed as the final station of this stop before continuing the transit (#561ARGOS). After repairing HyBis, a second short break of the transit at noon on May 30th allowed a further test of this instrument (#562HYBIS) as well as of the releasers that didn't perform the day before (#563REL). A few hours later, station work in the working area (TAG segment at 26°N on the Mid-Atlantic Ridge) started just before midnight on May 30th with acquiring a new sound velocity profile (#564XBT).

The early morning hours of May 31st saw a multibeam survey that mapped the central part of the segment (#565MB) before testing and adjusting the AUV buoyancy and trim (08:00 – 11:20 LT; #566AUV). The afternoon was used to deploy the first of six Ocean Bottom Electro-Magnetic stations (#567OBEM) that will be recording variations in the electromagnetic field in passive mode for the duration of this cruise. They stayed on the seafloor, however, and were used for passive and active controlled-source EM works before and during the following RRS JAMES COOK cruise in July/August 2016. In order to provide more accurate positions of these stations they are deployed on the cable and aided with subpositioning using POSIDONIA. At 18:30 LT the AUV was deployed for its first real mission (#568AUV; ABYSS dive 224). The night was used to enhance the coverage of the existing bathymetric map of the area (#569MB).

June 01st was used to deploy four more OBEM stations (stations #570OBEM, #571OBEM, and #573OBEM to #575OBEM) with two short breaks related to the recovery of the AUV in the late morning and its redeployment in the afternoon (#572AUV; ABYSS dive 225). One OBEM station did not release and had to be deployed a second time. The OBEM stations are located on a WNW-ESE profile line spanning a distance of 3 km across two known inactive sulfide mounds in the Alvin Zone, the Shinkai Mound and the Southern Mound.

A first gravity corer was placed in the northern part of the working area (#576GC) on June 2nd to obtain background sediment, followed by a short multibeam survey (#577MB). Two OBS instruments were placed near the active TAG mound (#578OBS and #579OBS). A seismic profile line was started using the surface streamer (#580MCS), but had to be cancelled after six hours due to a failure of the air compressor. The two OBS instruments were released and recovered (#581OBS). In the evening the AUV was launched (#582; ABYSS dive 226).

During night-time of June 03rd two gravity corers were deployed in the faulted terrain in the west (#583GC, #584GC), both returning empty. These stations were followed by a short multibeam survey to detect water column signals associated with active venting (#585MB). Three OBS instruments were deployed on the flanks and the top of Shinkai Mound using the cable to aid deployment with POSIDONIA subpositioning (#586HYBIS, #587HYBIS, #588HYBIS). Between these stations the AUV was recovered at 11:25 LT.

The early morning hours of June 4th were devoted to gravity coring on a profile line towards the active TAG mound. Station #589GC was placed close to a previous location and returned empty again, while station #590GC returned volcanic glass. Later, a series of 6 OBS instruments was deployed in free-fall mode (#591OBS to #595OBS and #598OBS). Two further OBS instruments were deployed at the flanks of Shinkai Mound via the cable to finalize the network

over this extinct sulfide deposit (#596HYBIS, #597HYBIS). From 19:40 LT to 22:00 LT the AUV ABYSS was occupying the vessel as it was send on a calibration mission for the magnetometer at shallow water depth (#599AUV; ABYSS dive 227) and was supposed to be reprogrammed for the next mission at the sea surface via WIFI connection (ABYSS dive 228). The connection was lost, however, and the AUV had to be recovered, was reprogrammed in the LARS and then redeployed for ABYSS dive 229 all under the same station number. During the night two gravity corer stations were performed in small basins near the western side of the working area (#600GC, #601GC).

These two stations were followed on Sunday June 05th by a series of 6 OBS and OBH deployments (in free-fall mode) covering the periphery of the seismic network (stations #602OBS to #607OBH). Later that day, a set of three OBS instruments was deployed on the top and the flanks of Southern Mound, a second large inactive sulfide occurrence in the Alvin Zone (#608HYBIS, #609HYBIS, #611HYBIS). In between the HYBIS stations the AUV ABYSS was recovered at 11:42 LT and then later deployed again at 18:00 LT for its next mission (#610AUV; ABYSS dive 230). Just before midnight the last 3 free-falling OBS stations were deployed (#612OBS, #613OBS, #614OBS).

The early morning hours of Monday June 06th started with 3 gravity coring stations (#615GC, #616GC and #617GC) in the eastern part of the working area that collected short (< 2m) sections of hydrothermally influenced sediments. Around 09:10 LT the AUV Abyss was recovered after finishing its 5th mission of the cruise (#610AUV; ABYSS dive 230). During the day, HYBIS was used to deploy the two remaining OBS on the Southern Mound (stations #618HYBIS and 619HYBIS). The day was finished with yet another AUV launch (#620AUV; ABYSS dive 231).

A long multibeam profile was conducted during the night covering parts of the western rift flank and the northern continuation of the ridge segment (#621MB). In the morning of June 07th the AUV was recovered at 08:09 LT (#620AUV) while rain showers and winds up to 7 Bft from a small weather front passed the vessel. These conditions improved slightly for the following deployment of the deep-tow streamer and airguns that started at 09:50 LT (#622MCS). Seismic profiling continued during the day, however, problems with the electronics and an overturning air gun required pulling in both, the airgun and the deep-tow streamer, and replacing them with the surface streamer and a second airgun.

Seismic profiling using the surface streamer continued through most of June 8th and was only briefly interrupted for the deployment of the AUV in the late evening (21:05 LT; #623AUV; ABYSS dive 232). Seismic profiling continued during the night (#624MCS) and finished on Thursday June 9th at 10:59 LT. The Meteor moved then to the recovery position for the AUV, which was taken aboard on 12:30 LT (#623AUV; ABYSS dive 232). Since the problems with the deep-towed streamer were not resolved, the surface streamer was redeployed for additional profile lines over the inactive sulfide mounds and the proposed detachment fault hosting the deposits (#625MCS). The streamer was recovered just before midnight (LT).

A series of three gravity corers was deployed on June 10th recovering 120 cm of variably hydrothermally influenced sediment from the Shimmering Mound area in the northern part of the Alvin Zone (#626GC) and 300 cm of Fe-oxyhydroxides and sulfides from a distinct basin structure (called "Central Area"; #627GC). The third station was placed in the vicinity of Shinkai Mound and returned empty (#628GC). Beginning at 07:55 (LT) a series of five OBH instruments (#629OBH to #633OBH) were released and recovered. One instrument did not release. A short multibeam profile (#634MB) was followed by the launch of the AUV at 20:43 LT (#635AUV; ABYSS dive 233). The mission was aborted shortly after its start due to a mission timeout when the AUV dropped its weight and resurfaced. The mission was restarted as ABYSS dive 234 at 21:35 LT.

The night to June 11th saw the deployment of three gravity corer stations, all of which had low recoveries (#636GC to #638GC). The morning was used to redeploy four OBH instruments. The instruments were positioned along a 4 km long profile over a proposed detachment fault in the northeastern part of the working area (#639OBH to #642OBH). The AUV was recovered at 13:02 LT. A 22-hours long multibeam station extended the existing bathymetry to the next segments in the north and south (#643MB).

Two gravity corer stations were deployed in the afternoon of June 12th. The first corer (#644GC) was deployed in the "Central Area" and recovered 269 cm of strongly layered hydrothermal sediment. Station #645GC recovered 131 cm of pelagic sediment from a basin west of the MIR Zone with a small interval of hydrothermally influenced material at shallow depth. Seismic profiling (#646MCS) started at 20:57 LT and continued until the early afternoon of June 13th. The remainder of that day was used for two gravity corer stations (#647GC in the Central Area and #649GC east of the MIR Zone) interrupted by the deployment of the AUV (#648AUV; ABYSS dive 235) at 20:11 LT.

The night hours of June 14th were used to extend the bathymetric map (#650MB). During the day HYBIS was used twice to investigate the nature of targets identified in the AUV-based bathymetric data either by their relief or by their geophysical response to the AUV sensor package (magnetics, SP, temperature, Eh). Station #651HYBIS confirmed the hydrothermal nature of mound 27, while station #652HYBIS showed that mound 29 is also a structure formed by hydrothermal processes. The AUV was recovered between the two HYBIS stations. At 19:49 LT seismic work continued with a surface streamer survey during station #653MCS that lasted until the next afternoon. The evening of June 15th was used to recover 11 OBS stations (#654OBS to #664OBS). The AUV was deployed for its next mission on 22:12 LT surveying the southern part of the working area (#665AUV; ABYSS dive 236).

The early morning hours of June 16th saw the deployment of 2 gravity corers (#666GC and #667GC) followed by the recovery of another set of OBS instruments (#668OBS to #676OBS). One station did not return and will hopefully be recovered after the time release on June 21st. Following these recoveries, the AUV was picked up at 11:55 LT after successfully completing its 10th mission (#665AUV; ABYSS dive 236). A mound in the northern part of the working area, near Shimmering Mound, was then proven to be hydrothermal in nature by visual inspection and

sampling during station #677HYBIS in the afternoon. In the evening, 2 OBH instruments were recovered (#678OBH and #679OBH), followed by a short ship-based multibeam profile at slow speed over the inactive sulfide mounds to get high-resolution backscatter data (#680MB).

Three gravity corer stations marked the beginning of June 17th targeting the Shimmering Mound area (#681GC, 300 cm of mixed pelagic and light-brown hydrothermal sediment; #682GC, 281 cm of intercalated pelagic as well as green, red and orange hydrothermal layers) and a basin west of the active TAG mound (#683GC, 15 cm of carbonate ooze). The first of two HyBis stations began at 08:42 LT and investigated a mound in the central, faulted area (#684HYBIS). This mound (mound 01) consists of pillow basalt. A second dive confirmed the hydrothermal nature of yet another target, this time mound #09, called "Rona Mound" in remembrance of the late Peter Rona, who worked in the TAG hydrothermal field for many years (#685HYBIS). AT 19:26 LT the AUV was launched for its next mission to extend the bathymetric map further to the east (#686AUV; ABYSS dive 237). The night and morning hours were used for mapping the segment end in the south (#687MB).

June 18th started with the recovery of the AUV at 11:09 LT, followed by the launch of HyBis to investigate the area characterized by a strong magnetic low in the AUV-data for the presence of past hydrothermal activity. Several mounds were investigated that proved to be volcanic in origin until mound 11 was reached, where hydrothermal Fe-Mn-oxyhydroxides were observed and sampled at its summit (#688HYBIS). In the evening the AUV was launched for a mission targeting the northeastern part of the working area including the upper parts of a detachment fault (#689AUV; ABYSS dive 238). Gravity coring started at 18:46 LT and continued throughout the night with 4 stations sampling the foot of the slope north of Shimmering Mound (#690GC, 80 cm of carbonate ooze), a basin in the eastern part of the working area (#691GC, 66 cm of carbonate ooze), the MIR Zone (#692GC, 79 cm of carbonate ooze interlayered with hydrothermal sediment), and the summit of mound 11 (#693GC, 71 cm of Fe-Mn-oxyhydroxide gravel).

On June 19th, the AUV was recovered and this station was followed by the final geological HYBIS station targeting a mound showing a prominent magnetic low north of Shimmering Mound (mound 19), however, visual inspection and sampling showed the presence of angular and slightly altered greenstone-like rocks in this area (#694HYBIS). The last remaining of the originally 6 OBEM stations was deployed in the afternoon (15:34 LT; #695OBEM) in order to passively measure the electromagnetic field until the RRS JAMES COOK returns mid-July. Following this, the AUV was deployed for a 400 kHz mission to map the Mir Zone with 50 cm resolution (#696AUV; ABYSS dive 239). Starting at 21:40 LT, seismic profiling was performed over the eastern valley wall and continued until 22:56 LT of June 20th (stations #697MCS and #698MCS). The profiles needed to be interrupted shortly in order to recover the AUV around noon.

Shortly after midnight on June 21st, the AUV was launched for its next mission (#699AUV; ABYSS dive 240) mapping the southeastern corner of the working area. A series of 4 gravity corer stations started at 03:00 LT and targeted the sediment covering the toe of the detachment fault (#700GC, empty), a small basin in the east (#701GC recovering only few pieces of volcanic

pebbles), the northwestern flank of Southern Mound (#702GC, 092 cm of hydrothermally influenced sediment), and a small basin south of mound 27 (#703GC, 300 cm of layered carbonate ooze overlying hydrothermal sediment). Gravity coring finished at 12:49 LT and was followed by the recovery of the 2 OBH instruments that could not be released previously. The set time release worked and both instruments were recovered by 19:39 LT (#704OBH and #705OBH). At 20:02 LT the AUV was launched for its 15th and final mission mapping the southwestern corner of the working area next to the ridge axis (#706AUV; ABYSS dive 241).

During the night and morning hours of June 22nd a multibeam station mapped the northern end of the segment as well as the eastern flank (#707MB). The 2 AUV LBL transponders were on deck by 12:19 LT (#708AUV-T and #709AUV-T). The afternoon was used to take a background sediment sample far away from the ridge axis. The first station (#710GC) returned empty, however, after repeating this station the corer recovered 300 cm of shell-rich sediment (#711GC). The time before leaving the working area was used to finish the last profil line to the north (#712MB), before starting the Transit to Ponta Delgada, which began at 20:30 LT on June 23rd. The transit was interrupted on June 25th and June 26th for the deployment of the two remaining ARGO floats (#713ARGOS and #714ARGOS). Data collection for the Kongsberg EM122 and the 75kHz ADCP stopped just before entering the Portuguese EEZ at 20:00 LT on June 26th.

Cruise M127 ended in the morning of June 28th with meeting the pilot at 08:00 LT and entering the port of Ponta Delgada. Scientific equipment was sent back to Kiel or was set aside for the RRS JAMES COOK arriving a week later.

5 Preliminary results

5.1 Ship-based multibeam bathymetric mapping (EM122)

(N. Augustin, M. Klischies, S. Graber, H. Li)

5.1.1 Acquisition and processing

During cruise M127 extensive multibeam mapping was conducted with the onboard EM122 echosounder system provided by Kongsberg Maritime. The EM122 collects bathymetric data in water depths up to 11,000 m with an angular coverage sector of up to 150 degrees (controlled by the operator), a nominal sound frequency of 12 kHz and up to 864 soundings per ping. The system consists of the EM122 transceiver unit, the hydrographic workstation, a motion/heading sensor, a GPS receiver and a sound velocity sensor. Data were acquired using the SIS acquisition software, which output regularly spaced .all files containing the bathymetric and backscatter information. Sound velocity profiles were measured using Lockhead Martin XBT (eXpandable Bathy Thermograph) probes. XBT probes were launched at 6 kn ship's speed and reached a maximum water depth of 2,000 m. Sound velocity profiles (.edf-files) were loaded into SIS's SVP-Editor, manually edited and automatically extended from 2,000 to 12,000 m water depth.

The majority of surveys (710 nm in total) in the working area were conducted with a symmetrical beam spacing of 45° to both sides (90° full swath angle), a survey speed of 6-8 kn and a line spacing of 3 km, giving a typical swath width on the seafloor of around 7 km and yielding bathymetric grids with a final resolution of up to 30 m without major gaps. Backscatter data were logged throughout the cruise and a single small section of water column data was obtained over the TAG field as well as the ATA water column anomaly reported by IFREMER. However, acoustic water column anomalies could not been observed during M127 over the ATA target area. Transit data (1,800 nm) were collected at approximately 9-11 kn and a swath angle of 120°. The transit data towards the survey area were of fairly good quality, but due to poorer weather conditions and rougher seas the transit from the working area to Ponta Delgada achieved bathymetric data of lesser quality.

Post-processing and gridding of data was carried out using the QPS Qimera and Fledermaus software suite: Qimera 3D Editor for 3D editing, Fledermaus for gridding of the data and FMGT for processing and mosaicking the backscatter data. Multibeam data were cleaned manually to remove outliers and then gridded and imported to Global Mapper (Blue Marble), which contained the M127 GIS project. The final bathymetric maps were produced with ArcGIS and QGIS. Figure 5.1.1 shows an overview of the bathymetry of the working area using the texture shading technique (TTS) developed by *Leland Brown (2010)* merged with minor weighted shaded relief and slope maps to remove any bias associated with the position of a light source. Apparently, when the data was imported to Fledermaus/Qimera, a ping appeared to be being 'dropped' between data file changes resulting in small (<30 m) data gaps in the gridded datasets. This data is recorded, however SIS does not complete the line during a file change and, as Fledermaus cannot read partial lines, these small data gaps were interpolated for the final grids. Kongsberg can provide a program to correct this in post processing if required. Backscatter mosaics were exported as greyscale GeoTiff images from FMGT at 25 m resolution (Figure 5.1.3). The raw

data of the transits is publically available for download from the Pangaea data repository (https://doi.pangaea.de/10.1594/PANGAEA.864817).

5.1.2 Coverage and geological description

During cruise M127 50,000 km^2 of the seafloor were imaged during the transits and were gridded at 100m resolution. The main working area at the TAG segment was mapped at higher resolution (cell size 30 m) and consists of about 3,900 km^2 near 26°N on the Mid-Atlantic Ridge. The aim of the bathymetric surveys during M127 was to cover the entire length of the TAG segment including the non-transform offsets to the north and south (Fig. 5.1.1 and 5.1.2).

The segment of the MAR between 25°46N and 26°33N that hosts the TAG hydrothermal field is characterized by tectonic extension typical for many slow-spreading ridges. However, abundant volcanism can also be observed along this section of the Mid Atlantic Ridge displayed by semi-circular volcanoes on- and off-axis, axial volcanic ridges and hummocky terrain. The sediment thickness in this area is generally low and allowing the underlying rugged topography to be clearly visible. The sediment cover increases with distance to the active spreading centre covering smaller features.

The neovolcanic valley extends in a northeast-southwest direction and is dominated by axis parallel volcanic ridges, hummocky terrain and circular volcanoes. The latter exhibit diameters up to 3 km and heights up to 200 m. Furthermore, the valley shows two deep basins at 26°01N and 26°17N, which exceed depths of 4,500 m. The valley floor rises to depth of 3,700 m at the shallowest part of the valley in the vicinity of the TAG hydrothermal field.

The western ridge flank is characterized by southeast dipping normal faults with prominent fault scarps. In addition, axis parallel, linear ridges occur along the central and northern part while the southern part towards the offset shows a smoother morphology featuring few basins. The eastern flank of the ridge axis is dominated by a massif extending over 30 km along axis. It is formed by three consecutive, axis parallel ridges of which the largest one to the east rises up to a water depth of 1,400 m. Each of these ridges exhibits major northwest facing escarpments. The northern part of the eastern flank is characterized by parallel ridges that are separated by basins. A large basin is also located south of the massif spanning over 17 km along axis. In contrast to the fault pattern on the western ridge side, faulting at the eastern side is more complex. Few major fault systems are separated by tectonized areas, which show several small scale faults with varying dipping directions.

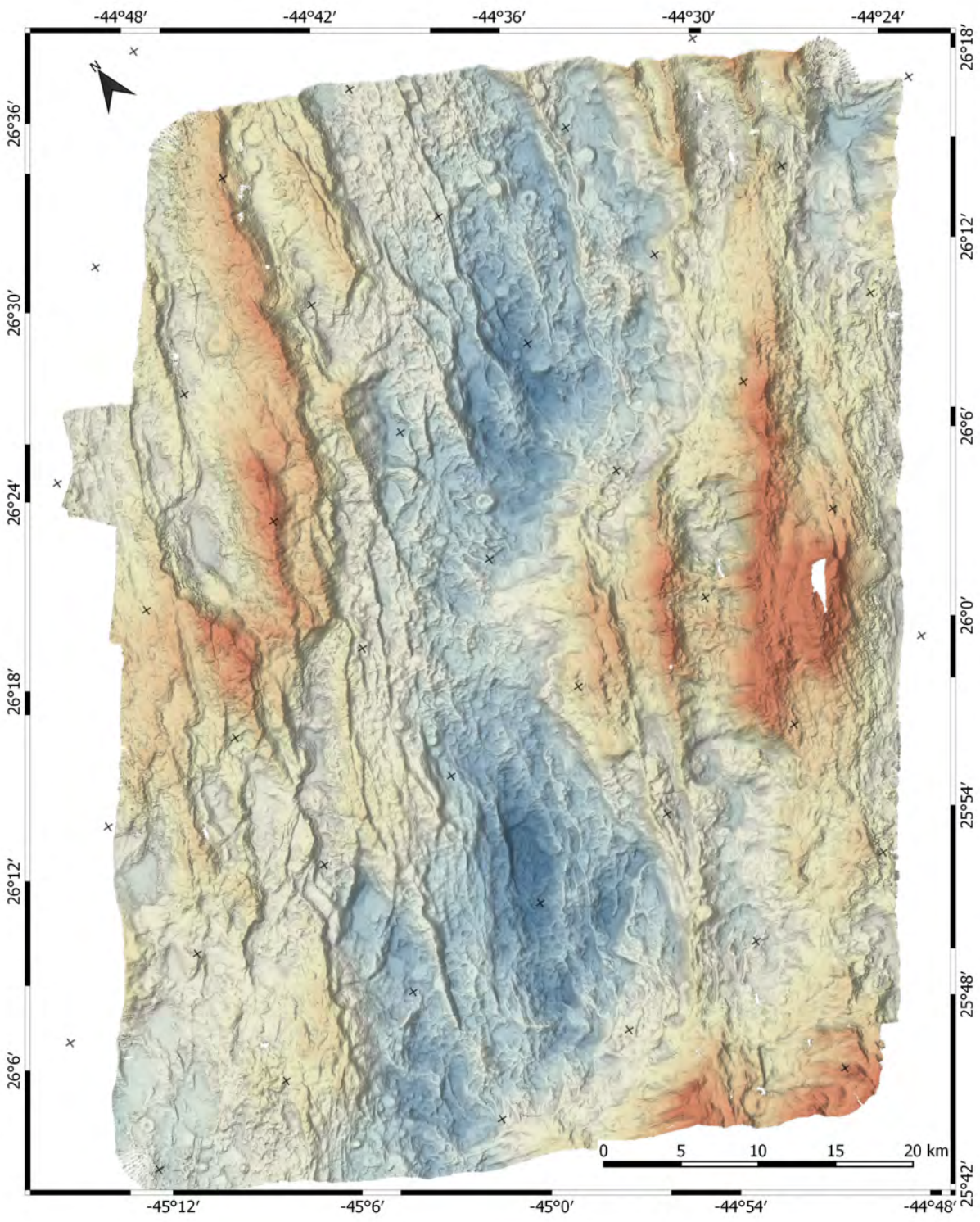

Fig. 5.1.1: *Texture-shaded bathymetry of the TAG segment with data collected during expedition M127. The shown area includes the central axial high where the TAG hydrothermal field is situated, the eastern and western ridge flanks as well as the segment offsets to the north and south.*

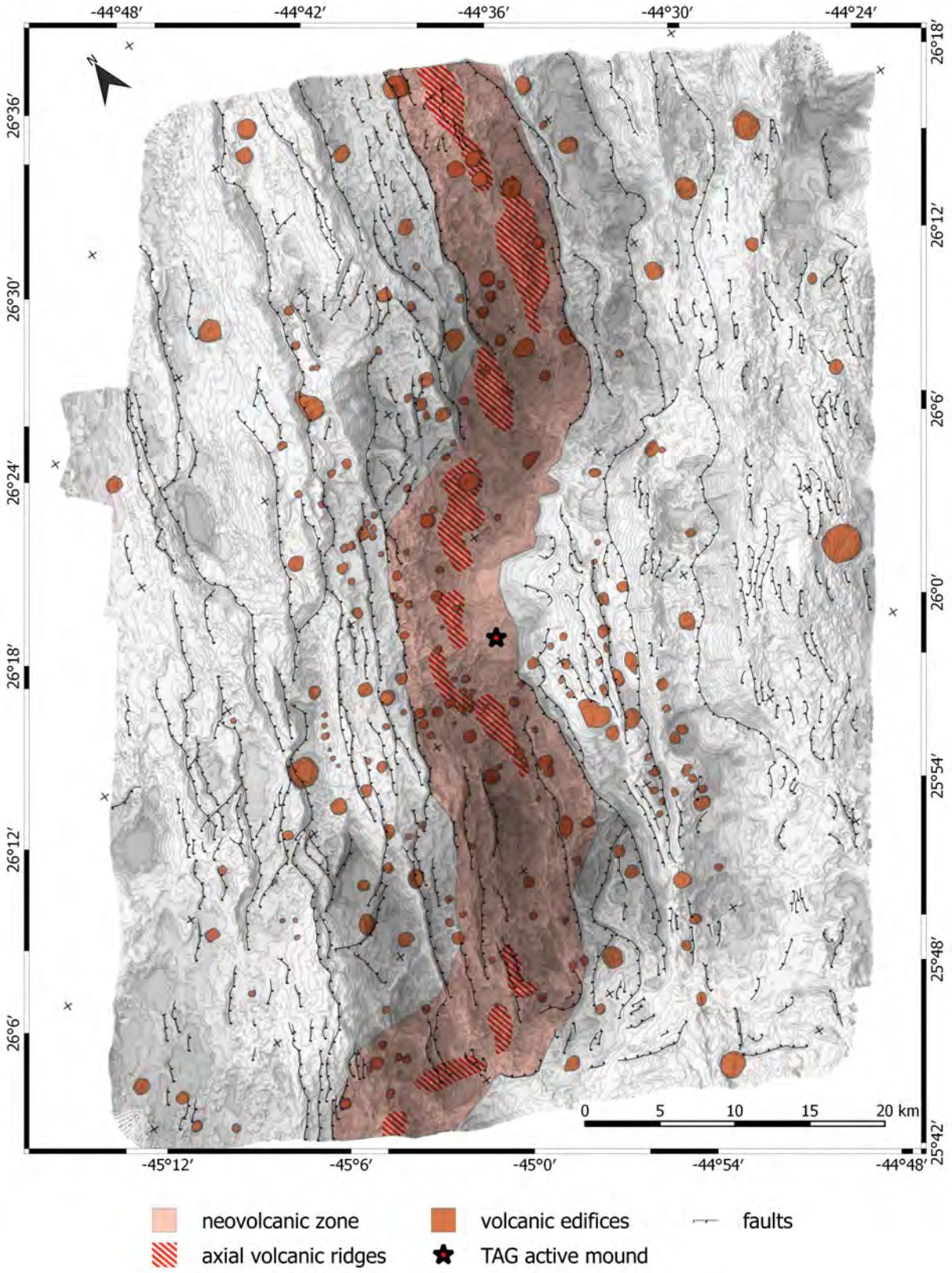

Fig. 5.1.2: *Map of the survey area showing the location of the TAG hydrothermal field, the main tectonic features, volcanoes and the neovolcanic zone on the axial valley floor. Contour lines at 100m interval.*

5.1.3 Data from transits

The recording of transit multibeam is a standard procedure for German research vessels to increase the availability of bathymetric data worldwide. Transit data will be made publically available as raw-data and gridded files (100 m cell size) through the Pangaea data repository. The grid-files are processed as described above.

The transit grids are used for the identification of formerly unknown seafloor features and may aid future cruise planning as they often provide surprising new data. During M127 at least one old core complex (crustal age 35 Ma) and an area that appears to show younger lava flows within an area of apparently 20 Ma old crust have been identified (Figure 5.1.3).

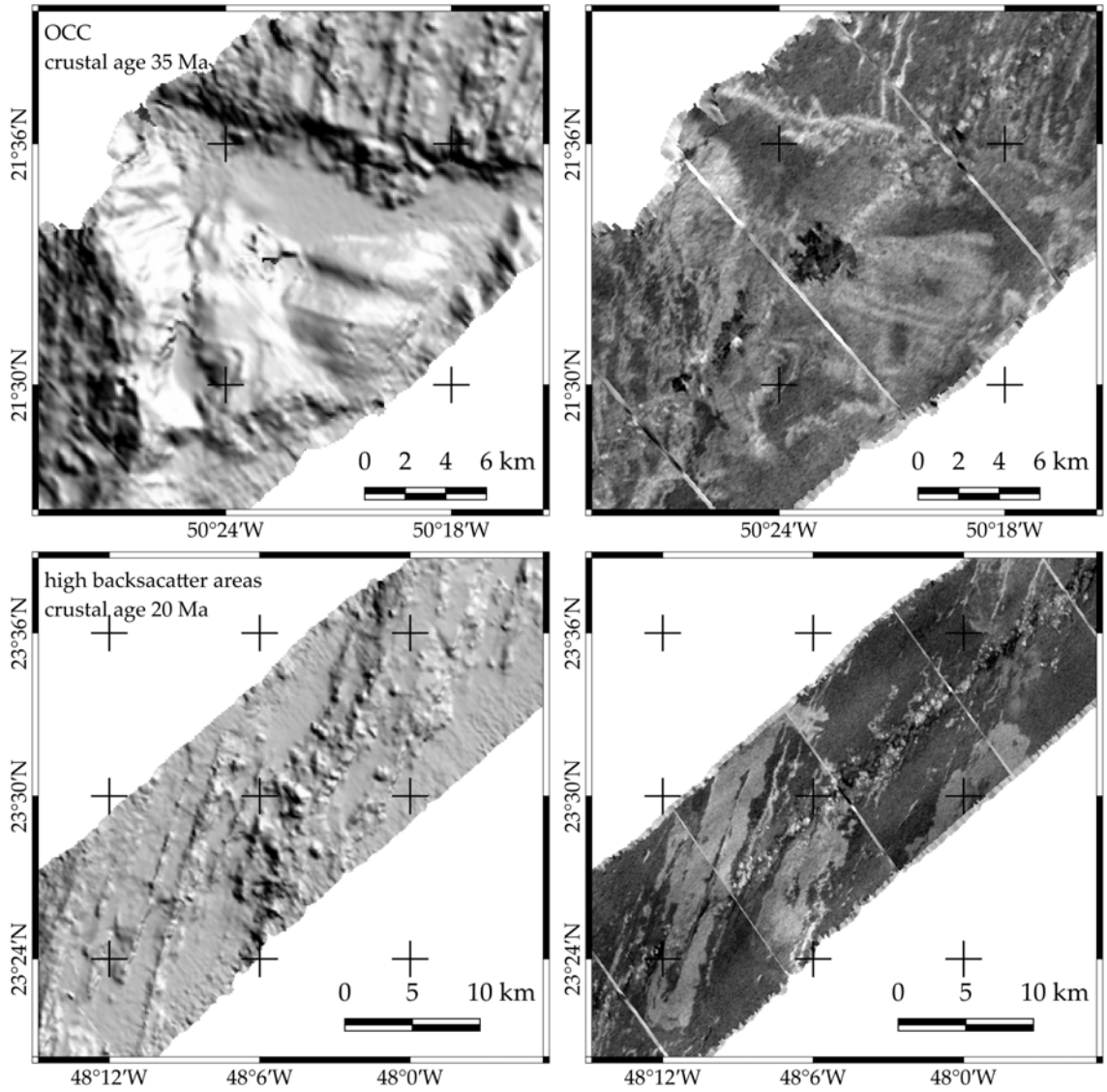

Fig. 5.1.3: *Old oceanic core complex in 35 Ma old crust (c. 500 km west of the MAR axis) at the southern wall of a transform fault. The rift perpendicular corrugated surface is well visible in both, shaded relief (A) and backscatter data (B). North of the transform fault the N-S striking, rift parallel fabric of volcanic ridges continues. Within the rift parallel pattern of volcanic ridges (C) surprisingly large areas of high backscatter intensities (D), maybe related to significantly less sedimented lava flows, found in ca. 20 Ma old crust, 300 km west of the MAR axis. Spatial resolution of multibeam grid is 100 m, the backscatter mosaic yields a resolution of 25 m.*

5.2 AUV ABYSS operations

(M. Rothenbeck, L. Triebe, E. Wenzlaff, I. Yeo, F. Szitkar, J. Jamieson, S. Petersen)

The Autonomous Underwater Vehicle (AUV) Abyss (built by HYDROID Inc.) from GEOMAR can be operated in water depths up to 6,000 m. The system comprises the AUV itself, a control and workshop container, and a mobile Launch and Recovery System (LARS) with a deployment frame that was installed at the stern of the afterdeck of RV METEOR. The self-contained LARS was developed by WHOI to support ship-based operations so that no Zodiac or crane is required for launch and recovery. The LARS is mounted on steel plates, which are screwed to the deck of the ship. The LARS is configured in a way that the AUV can be deployed over the stern or port/starboard side of the German medium and ocean-going research vessels. The AUV Abyss can be launched and recovered at weather conditions with a swell up to 2.5 m and wind speeds of up to 6 Beaufort. For the recovery the nose float pops off when triggered through an acoustic command. The float and the ca. 19 m recovery line drift away from the vehicle so that a grapnel hook can snag the line. The line is then connected to the LARS winch, and the vehicle is pulled up. Finally, the AUV is brought up on deck and secured in the LARS. The AUV missions were planned based on ships bathymetry.

The Long Baseline (LBL) transponders 1B and 2C which are used for missions 224-241 were dropped on 31.05.2016 (10:05/10:21 LT). The ship sailed one circles around the center between both transponder drop positions with a diameter of approx. 1.5 kilometers to measure the slant ranges to the transponders. The calibration took 1.0 hour without transit time. The positions were calculated using the software "Survey" (Hydroid). The transponders were released and recovered on 22.06.2016.

Table 5.2.1: Positions of the LBL transponders

Station	Beacon	Transponder positions	Depth	Offset range	Offset bearing	Mean error
M127/566	1B	26°08.412'N 044°49.106'W	3641 m	120.7 m	320.6°	2.1
M127/566	2C	26°07.897'N 044°49.114'W	3669 m	114.2 m	317.6°	1.6

During cruise M127 19 missions were flown by the AUV Abyss (Table 5.2.2). The missions were flown using exclusively the multibeam configuration. The primary sensor was the Kongsberg RESON Seabat 7125 (multibeam echosounder), which is a combined system for 200 and 400 kHz. The frequency of 200 kHz was used during 13 mapping dives and during 2 dives the working area was mapped using 400 kHz. The combination of a magnetometer (Applied Physics System APS 1540 Digital 3-Axis Miniature Fluxgate Magnetometer; S/N 685) and a Self Potential sensor (Silvion CCS1-Port Electrodes) was used for the first time during this cruise. Both magnetic and self-potential data were logged on a combined datalogger (Magson GmbH). The turbidity sensor (WetLabs ECO FLNTU Fluorometer and Turbidity sensor; S/N FLNTURTD-939), the REDOX potential sensor (by Koichi Nakamura) and the CTD (Seabird SBE49 FastCAT; S/N 4948793-0168) ran simultaneously and served as secondary sensors.

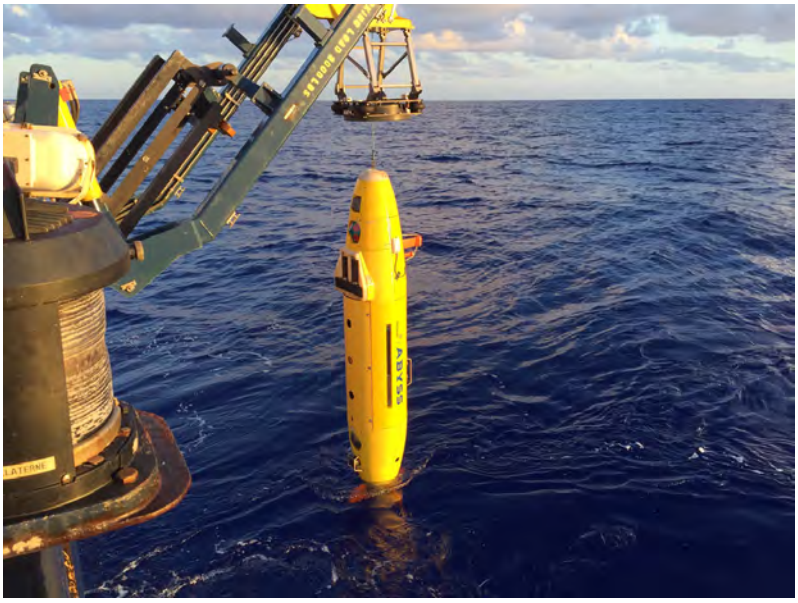	***Fig. 5.2.1a:*** *AUV Abyss (in multibeam configuration) during recovery (Photo: S. Petersen).*
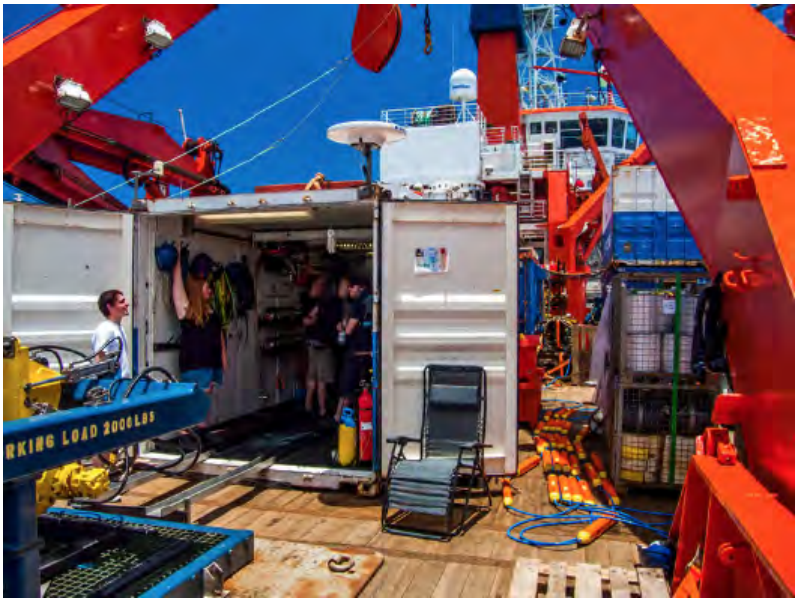	***b****: AUV container, rails and LARS on the deck of RV METEOR (Photo: J. Jamieson).*
	***c****: Preparation for launch (Photo: I. Stobbs)*

5.2.1 Mission summaries

(M. Rothenbeck, L. Triebe, E. Wenzlaff)

The AUV Abyss mapped the eastern flank of the spreading segment area around two previously defined target areas, the Alvin Zone in the north and the TAG active mound in the south. The map was than extended with each additional dive in order to combine the data for those two areas and to extend the coverage to the east, into older crust and to the south (Fig. 5.2.2). The final multibeam-echosounding (MBES) map was aimed at a resolution of 2 meter and was therefore flown with the 200 kHz multibeam configuration. Areas of special interest, such as the known inactive sulfides deposits were mapped at a resolution of 50 cm. This data was also used to aid the selection of drill targets in the Alvin Zone or the Mir Zone for the follow-up "Blue Mining" cruise in July/August 2016 onboard the RRS JAMES COOK. These missions were flown using the 400 kHz configuration and at 3 different altitudes all of them closer to the seafloor than the 200 kHz dives. Table 5.2.2 shows an overview of the missions carried out on this cruise. Detailed technical information on the dives and the data obtained can be found in Appendix 2.

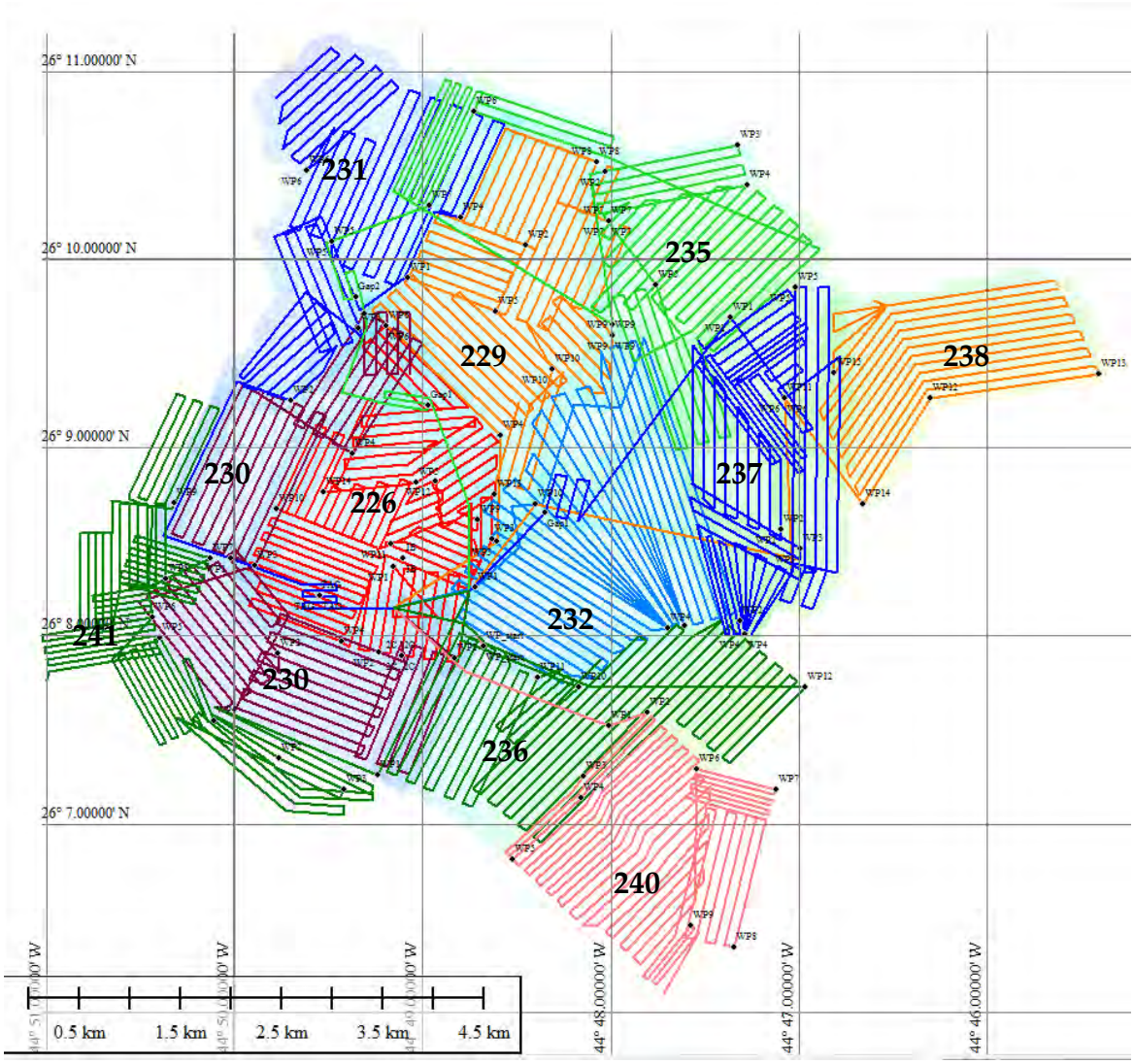

Fig. 5.2.2: *Overview of the locations of the various AUV dives (200 kHz). This figure gives an indication of the overlap necessary between adjacent maps and shows also the complicated dive planning due to the rough terrain in certain areas. Partial infilling of data-gaps in previous dives was also needed. Two additional dives used the 400kHz option to map the Alvin Zone and Mir Zone with 50 cm resolution.*

Table 5.2.2: Mission Statistics for cruise M127.

Station	Area	Dive	Date	Survey time	Mission time	Distance travelled	Sensors (Comments)
M127/559	Stop during transit	223	May 29	0.2 h	0.8 h	2.9km	Mag / SP (Test dive)
M127/568	central box south	224	May 31	12.1 h	14.6 h	80.9km	MB 200 kHz / Mag/SP
M127/572	central box north	225	June 1	10.0 h	12.5 h	69.0km	MB 200 kHz / Mag/SP
M127/582	central box south	226	June 2	11.7 h	15.2 h	84.3km	MB 200 kHz / Mag/SP
M127/599	-	227	June 4	0.3 h	0.7 h	3.5km	Magn. / SP calibration
M127/599	-	228	June 4	-	0.1 h	0.4km	Aborted mission
M127/599	central box north	229	June 4	10.0 h	11.4 h	62.5km	MB 200 kHz / Mag/SP
M127/610	central box southwest	230	June 5	12.2 h	14.7 h	80.2km	MB 200 kHz / Mag/SP
M127/620	central box northwest	231	June 6	9.9 h	11.5 h	67.7km	MB 200 kHz / Mag/SP
M127/623	central box southeast	232	June 8	12.3 h	14.8 h	81.6km	MB 200 kHz / Mag/SP
M127/635	-	233	June 10	-	0.2 h	0.4km	Aborted mission
M127/635	Alvin Zone	234	June 10	12.0 h	13.7 h	75.4km	MB 400 kHz / Mag/SP
M127/648	central box northeast	235	June 13	12.3 h	14.9 h	81.3km	MB 200 kHz / Mag/SP
M127/665	South of dive 232	236	June 16	10.3 h	11.9 h	64.5km	MB 200 kHz / Mag/SP
M127/686	East of dive 232	237	June 17	13.0 h	14.5 h	82.0km	MB 200 kHz / Mag/SP
M127/689	East of dive 237	238	June 18	10.2 h	12.5 h	69.0km	MB 200 kHz / Mag/SP
M127/696	MIR zone	239	June 19	11.7 h	14.3 h	80.4km	MB 400 kHz / Mag/SP
M127/699	South of dive 236	240	June 21	10.4 h	12.3 h	66.5km	MB 200 kHz / Mag/SP
M127/706	SW of dive 230	241	June 21	12.0 h	13.0 h	74.1km	MB 200 kHz / Mag/SP
			Total:	**161 h**	**204 h**	**1127 km**	

(Survey time = time spent mapping on the seafloor; Mission time = time including descent, survey and ascent phase; Distance travelled = total distance during mission; MB = Multibeam Echosounder; Mag = Magnetometer; SP = Self Potential Sensor)

5.2.2 Data processing

(M. Rothenbeck, L. Triebe, E. Wenzlaff, I. Yeo)

MBES 200 kHz workflow

The following workflow describes the processing of the individual missions and the main map, which was extended step by step during the cruise. MB-Systems[1] (Version 5.5.2) and Fledermaus were used to process the MBES raw data. Global Mapper (Version 15) was used to visualize grids and to convert data formats. Where "grids" are referred to these were created using a Gaussian Weighted Mean algorithm with a spline interpolation set to fill data gaps up to 2 times the grid cell size (4m in the 200kHz data and 1m in the 400kHz data).

1. Create a project / data list for the recent dive in MBSystem
2. Modify the processing parameter (lever arms of the MBES transducer array / offsets roll, pitch, heading)
3. Process / apply parameter changes to the data set
4. Create grid of the data set / check quality
5. Modify filter settings (medium spike filter, slope filter, local medium depth filter)
6. Process / apply filter to the data set
7. Create grid of the data set for checking process result
8. Check data quality and vehicle navigation

[1] Caress, D.W., „MB-Systems – A public domain software for processing swath mapping sonar data", Undersea Exploration, 1999

9. Successive application of navigation adjustment at different levels
10. Process / apply navigation adjustment to the data set
11. Create grid of the processed data set
12. Measure position difference between the adjusted grid and the known position of an ODP drilling cone visible in the data
13. Change parameter file (XY drift)
14. Process / apply parameter settings to the data set

This first grid over the TAG active mound represents the central reference for all neighbouring dives since it includes the well-navigated mound itself as well as two ODP funnels with known locations that were left at the seafloor in 1995 and are visible in the new high-resolution data. Tasks 1 to 11 are also done for the following 200 kHz dives. The following steps are done to merge the new (now internally consistent) grid relative to the central first dive grid.

15. Create a new project
16. Check overlap in Global Mapper and, if necessary, apply XY shift to achieve overlap
17. Load the first reference data set
18. Set the files of the first data set/s as fixed in terms of XYZ
19. Load the second data set into the project
20. Successive application of navigation adjustment at different levels (see Fig. 5.2.3)
21. Process / apply navigation adjustment to the data set

This workflow was carried out for every MBES data set. Task 16 was only used if there was a realistic overlap between the reference grid and the to be added data set but the positional drift was so large that MB Navadjust wasn't able to find crossing data files. The final step is a detailed cleaning of the entire data set carried out using Fledermaus followed by gridding in MBSystem (Fig. 5.2.4).

MBES 400 kHz workflow

The data sets logged during the two 400 kHz dives were planned using a slightly different approach. Each dive was separated in three survey patterns, all laterally identical but at vertically different levels. This allowed us to achieve good data within the ideal range from the vehicle across very uneven terrain without too much reduction in data quality due to pitch (which would be expected if running at constant altitude). These individual survey patterns were processed separately following the 200 kHz workflow (Task 1 to 11) before being combined. The subsequent processing tasks were:

1.b Create a new project
2.b Create a grid of the combined data set to assess navigation
3.b Load the data set of the lowest level of survey pattern 1
4.b Navadjust to produce internally consistent grid
5.b Process data to create new navadjusted dataset
6.b Repeat steps 1.b – 5.b for each survey level
7.b Create new Navadjust project and add lowest survey pattern

8.b Set the files of this data set as fixed in terms of XYZ
9.b Load the data sets of the higher level of survey pattern 1
10.b Successive application of navigation adjustment at different levels
11.b Process / apply navigation adjustment to the data set
12.b Create a grid of the navadjusted data set to check fixes
13.b Modify navigation as necessary
14.b Reprocessing and regridding of data
15.b Export of XYZ data
16.b Final cleaning of the combined data set in Fledermaus
17.b Gridding of the cleaned dataset in MBSystem

Further processing of these datasets will probably involve applying vertical gates to the data to limit the sounding included in the dataset to only those that fall within the ideal ranges of the gates.

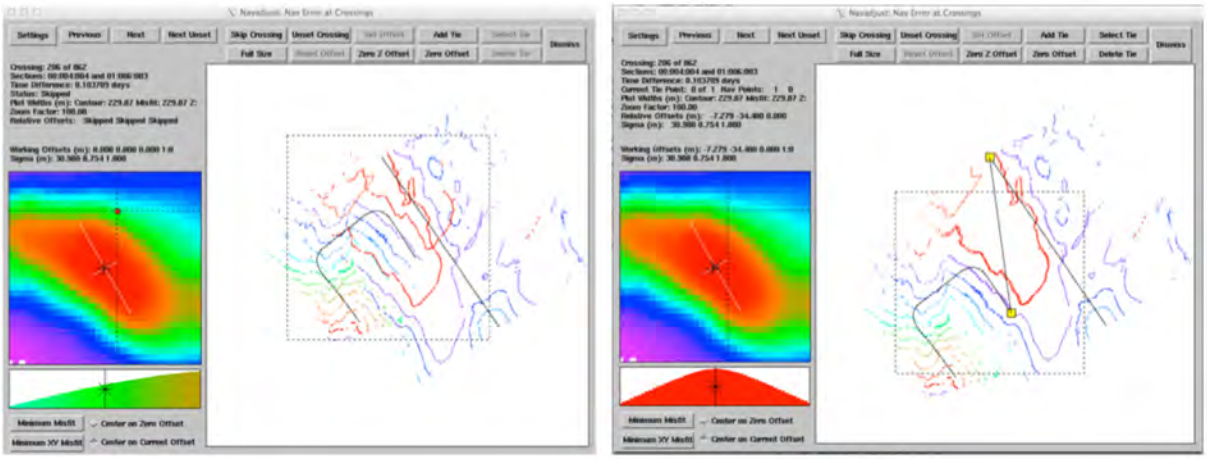

Fig. 5.2.3: *MBnavadjust module of MBSystem showing 2 sections of overlapping data before and after feature matching.*

Data quality

The first two MBES missions (#568AUV; ABYSS dive 224 and #572AUV; ABYSS dive 225) were planned with fixed depths according the the shipbased bathymetric map. The initial grid of those data sets were very noisy with a decreased amount of data especially in the steeper terrain (see Fig 5.2.4). There is no obvious reason for the unexpected noisy data set since the vehicle attitude at a fixed depth should have been more stable than in bottom following mode. Due to the very rough terrain the vehicle altitude was often below the ideal range, however, this should not have caused the level of noise observed.

AUV ABYSS dives 224 and 225 were then re-mapped by dives 226 (#582AUV) and 229 (#599AUV) using a fixed altitude of 80 meters (bottom following). The improvement in the quality of the raw data set can be seen in figure 5.2.4. The noise is still present but the vehicle accepted these wrong soundings much less commonly, resulting in more “good” soundings being recorded. This was despite the pitch changes during the survey being noticeably larger and more frequent than at fixed depth as a result of the bottom-following mode.

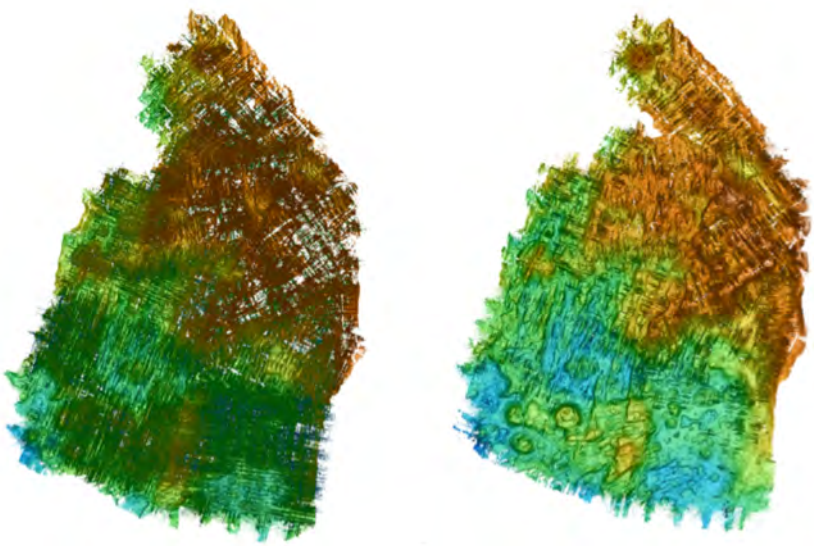

Fig. 5.2.4: *The noisy data set of mission 224 compared to 226 (right; bottom following).*

The exact source or cause of the noise in the data remains unclear. The swath replay from mission 229 showed that the vehicle was getting a reflection of the seafloor but this was commonly being replaced by a louder reflection from below the seafloor. This may be related to the Doppler Velocity Log (DVL; 300 kHz), although that does not explain why this has only been a problem on this expedition. Additionally, the noise did not appear evenly throughout all the missions. In at least 2 surveys a marked reduction in noise was observed corresponding with different seafloor terrains.

Several MBES settings were checked on a single repeated leg at the beginning of dive 226 (#582AUV) to see if an adjustment in one of the RESON settings could reduce this effect, however the only noticable difference was observed when modifying the power settings and the MBES was already running at almost maximum power. Figure 5.2.5 shows the data quality with respect to the different settings. In the end good data quality was managed by increasing the overlap so that areas where good data were lost to noise were covered by other swaths, running all the 200 kHz missions in fixed altitude mode, running the MBES with high-power and running a media depth deviation filter and a spike filter on data import to remove the majority of the noise before processing.

Final Data Sets

The following data set are saved and stored for future use:

1. MBES raw data (224-226, 229-232, 234-241) (Format: .s7k)

2.a Final Grid of the merged 200 kHz MBES dives (226, 229-232, 234-241) (Format: .xyz)

2.b Final MB-System data set of the merged 200 kHz MBES dives (226, 229-232, 234-241) (all parameter changes applied) (several formats)

3.a Final grid of the dive 234 (400 kHz MBES dive) (Format: .xyz)

3.b Final MB-System data set of the 400 kHz MBES dive 234 (several formats)

4.a Final grid of the dive 239 (400 kHz MBES dive) (Format: .xyz)

4.b Final MB-System data set of the 400 kHz MBES dive 239 (several formats)

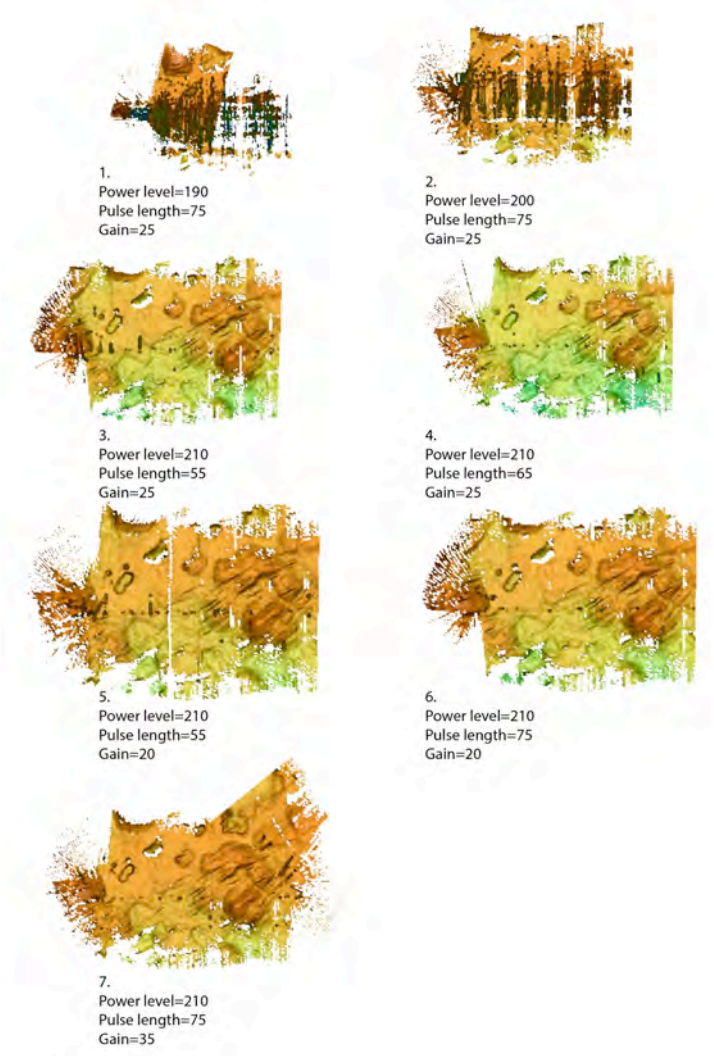

Fig. 5.2.5: *Comparison of data collected on same leg with different Reson settings.*

5.2.3 Preliminary interpretation of bathymetric data

(I. Yeo, S. Petersen, M. Rothenbeck, J. Jamieson, N. Augustin)

The bathymetric data was combined into a single grid and plotted using QGIS (version 2.14). The maps show a large variability of the tectonic and volcanic processes in the area. The combined map covers the rift valley floor from the neovolcanic zone and its volcanic pillow mounds in the west to the eastern flanks of the adjacent rift valley wall (Fig. 5.2.6). The central part of the working area is charaterized by hummocky volcanics that are, to various degrees, affected by extensional faulting developing west-facing and east-facing faults (Fig. 5.2.7). A small lava lake is situated in the east of the TAG active mound and is characterized by partial roof collapse. Large-scale faults, indicated by bathymetric troughs, and variations in the direction of the faulting pattern seem to control the location of the active TAG hydrothermal field as well as that of the inactive sulfide mounds in the north. Slump features and a pronounced detachment fault showing evidence for corrugations are present in the northeastern part of the working area (Fig. 5.2.8). The westernmost part of the working area is characterized by volcanic pillow mounds and ridges and shows no prominent faulting (Fig. 5.2.9). Extensional faulting seems to start 1.5 km east of the

neovolcanic ridge and is restricted to a narrow band. Some hummocky areas, including the area with the lava lake to the east of the TAG active mound are not affected by this N/S trending extensional faulting. Since these areas do not appear to be younger than the faulted terrain, based on sediment cover and fabric, this may indicate that these are "islands" of the original hummocky terrain that escaped extensional faulting.

The geology and evolution of the inactive sulfide occurrences in the so-called Alvin Zone (*Rona et al., 1993*) was investigated during station #635AUV (ABYSS dive 234) using the 400 kHz multibeam configuration. This allows a final grid file resolution of 50 cm (Fig. 5.2.10). Three sulfide mounds in the west (Shinkai, NewMound#2, and NewMound#3) appear to be younger based on their steeper slopes and because they seem to be unaffected by the extensional N/S faulting. Double Mound and Southern Mound are, despite being located only 500 m further to the east, intensly cut by these faults. A small mound, located even further to the east, was proven to be hydrothermal in origin by visual observation and sampling during station #685HYBIS and was later named Rona Mound. Ths mound appears to be bounded by two faults but otherwise has a gentle slope. The MIR Zone in the southeast, a large zone of inactive chimneys, was also mapped with 50 cm resolution during station #696AUV (ABYSS dive 239; Fig. 5.2.11). The bathymetry shows that the MIR Zone is located just east of a west-facing fault that runs for over a kilometer in N/S direction. This fault might be a continuation of the detachment fault further to the north. Small mound structures on the sides of the central MIR Zone are probably also related to hydrothermal activity. The overall size of the constructive part of the MIR Zone is smaller than previously published information suggests (*Rona et al., 1993*). The N/S trending fault does also show up in the magnetic maps (see below) and might therefore represent a feeder zone to that deposit. The 400 kHz high-resolution maps will also allow a preliminary size and volume estimate of the inactive deposits and may be used to attempt a first estimate of their resource potential assuming typical chemical compositions for these mounds. The 50 cm resolution maps will also be used to prepare the drilling operations that are performed by the RRS JAMES COOK in July/August 2016 as part of the Blue Mining project.

Another important discovery based on the mapping is the abundance of collapse structures or pits in several of the inactive sulfide occurrences. It was originally proposed only for the TAG active mound and inferred to be the result of anhydrite dissolution within the deposits (*Humphris et al., 1995; Petersen et al., 2000*) due to its retrograde solubility (*Blount and Dickson, 1969*). However, our detailed AUV bathymetry shows that mound collapse is also present at the MIR Zone, Mont de Reliques, New Mound#3, and at target #20 in the north. Partial collapse of sulfide mounds seems therefore to be more common in basalt-hosted hydrothermal systems than previously thought and may actually be a common phenomenon in the evolution of modern seafloor massive sulfide deposits.

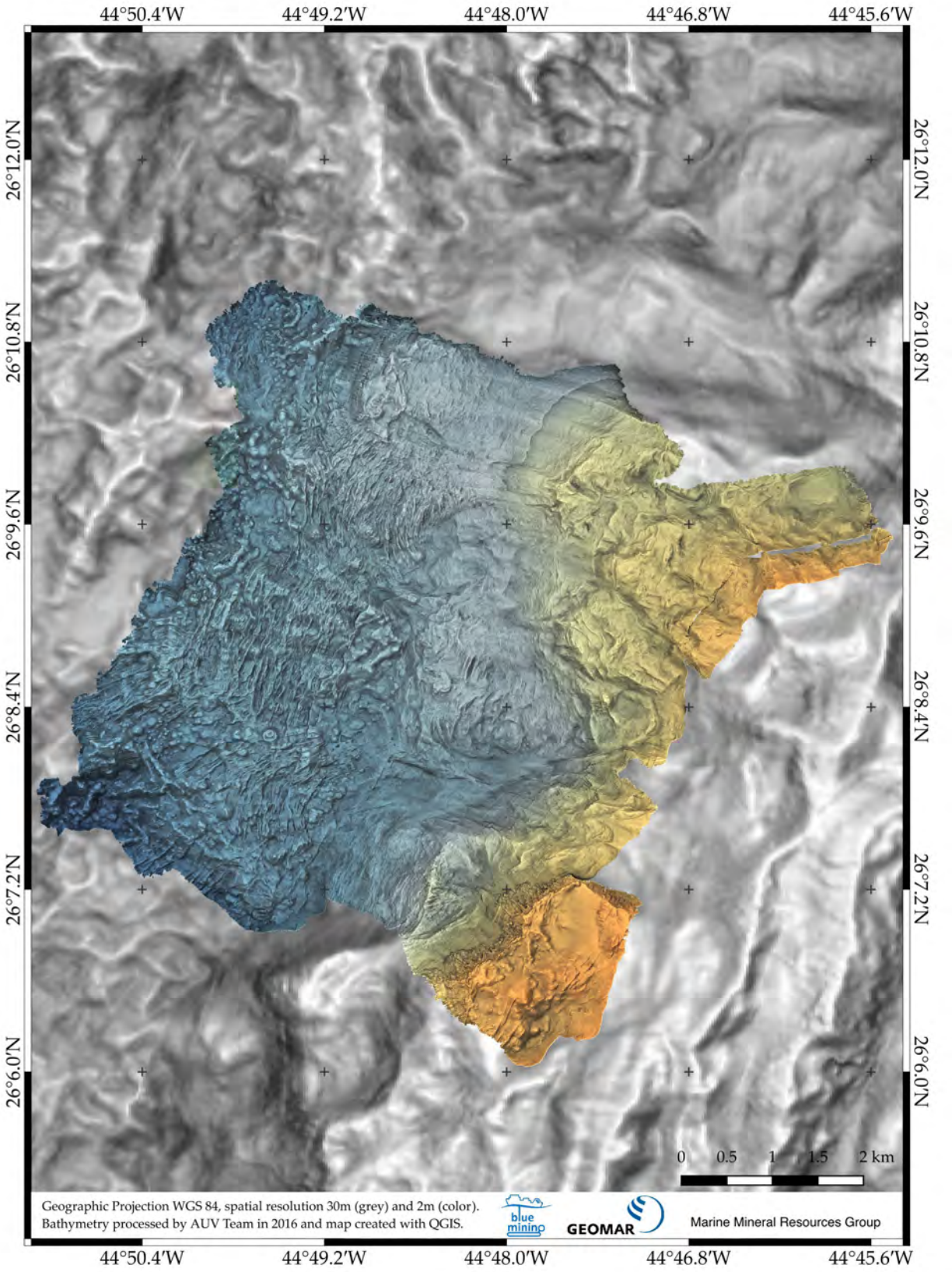

Fig. 5.2.6: *Texture-shaded high-resolution AUV-based bathymetry of the TAG segment reaching from the neovolcanic zone in the west to the eastern flank of the rift valley. The data set covers an area of 47 km^2 in 2m resolution. The underlying texture-shaded ship-based bathymetry (30 m resolution) was obtained during M127. Data is only roughly cleaned; final editing will be performed on-shore.*

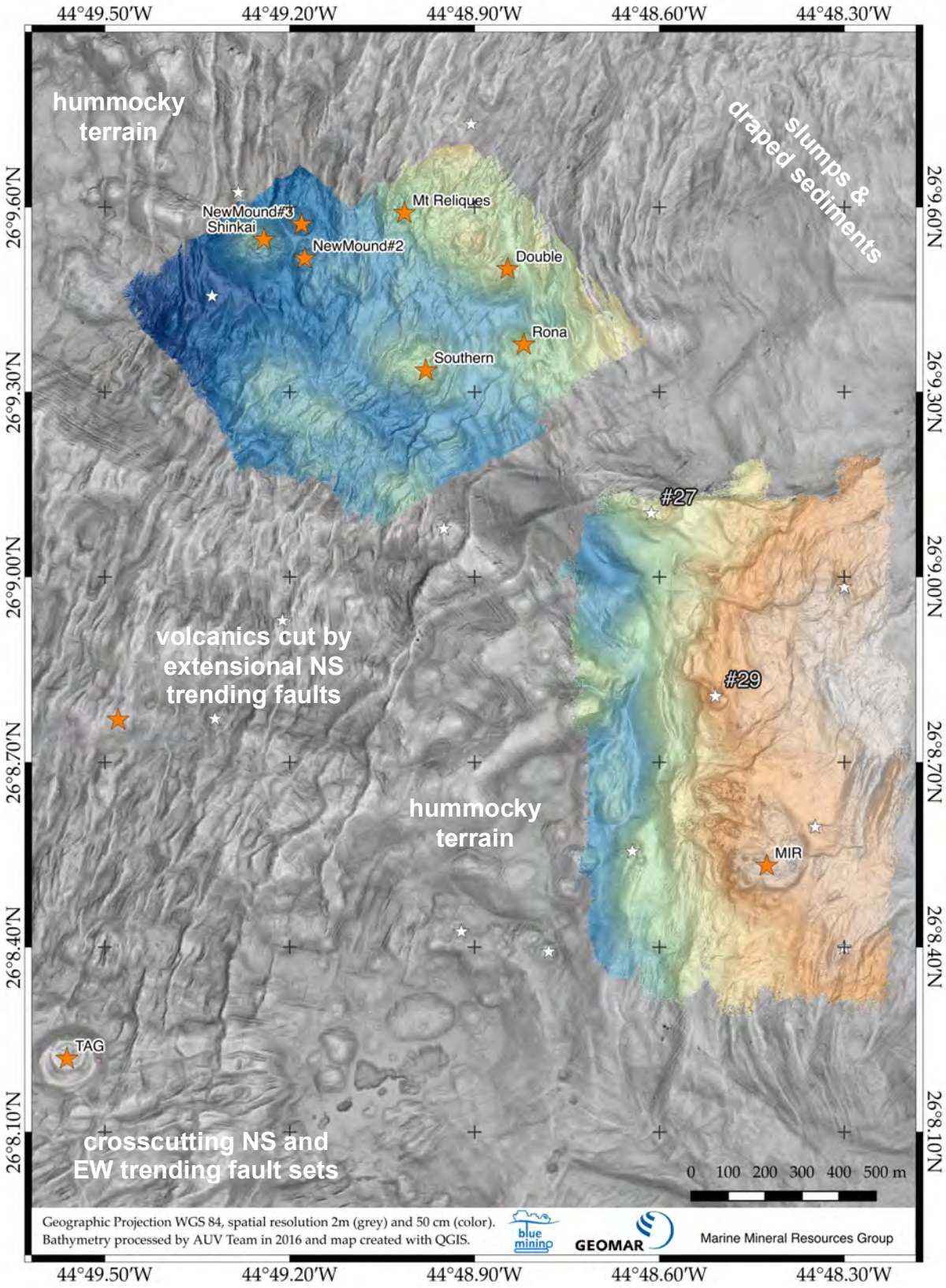

Fig. 5.2.7: *High-resolution AUV-based bathymetry obtained over the central part of the working area, including the TAG active mound and the known inactive massive sulfide deposits (2m resolution; hill-shaded). The color-coded areas have been mapped at 50 cm resolution using the AUV's 400kHz option during two missions (see below). White stars denote possible hydrothermal targets. Targets #27, #29 and Rona Mound have been confirmed to be hydrothermal by HyBis dives. Data is only roughly cleaned; final editing will be performed on-shore.*

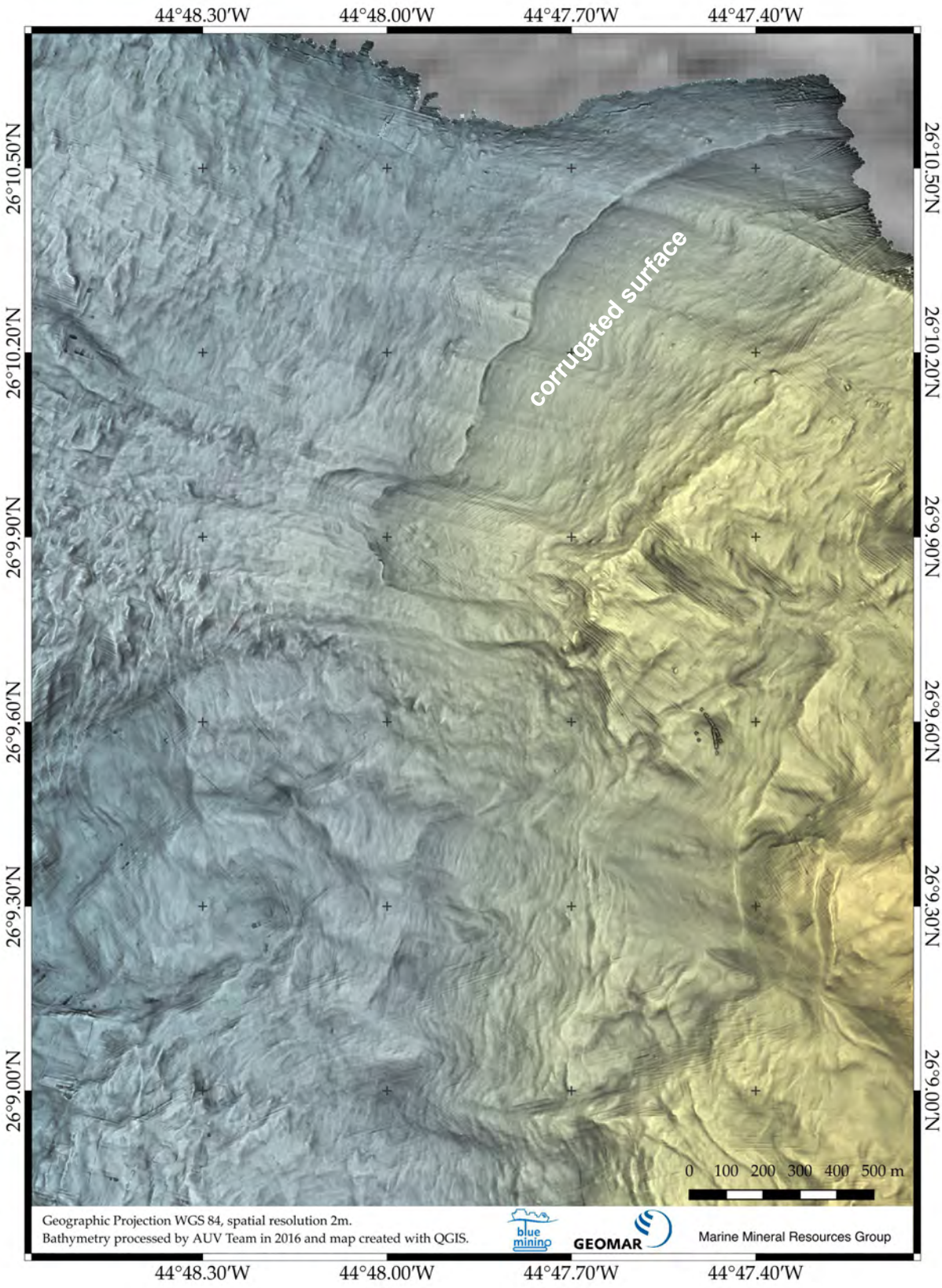

Fig. 5.2.8: *Detail of the high-resolution AUV-based bathymetry showing the foot of a possible detachment fault and associated corrugations in the northeastern part of the working area as well as slump features, common in the eastern part of the working area (2m resolution; texture-shaded). Data is only roughly cleaned; final editing will be performed on-shore.*

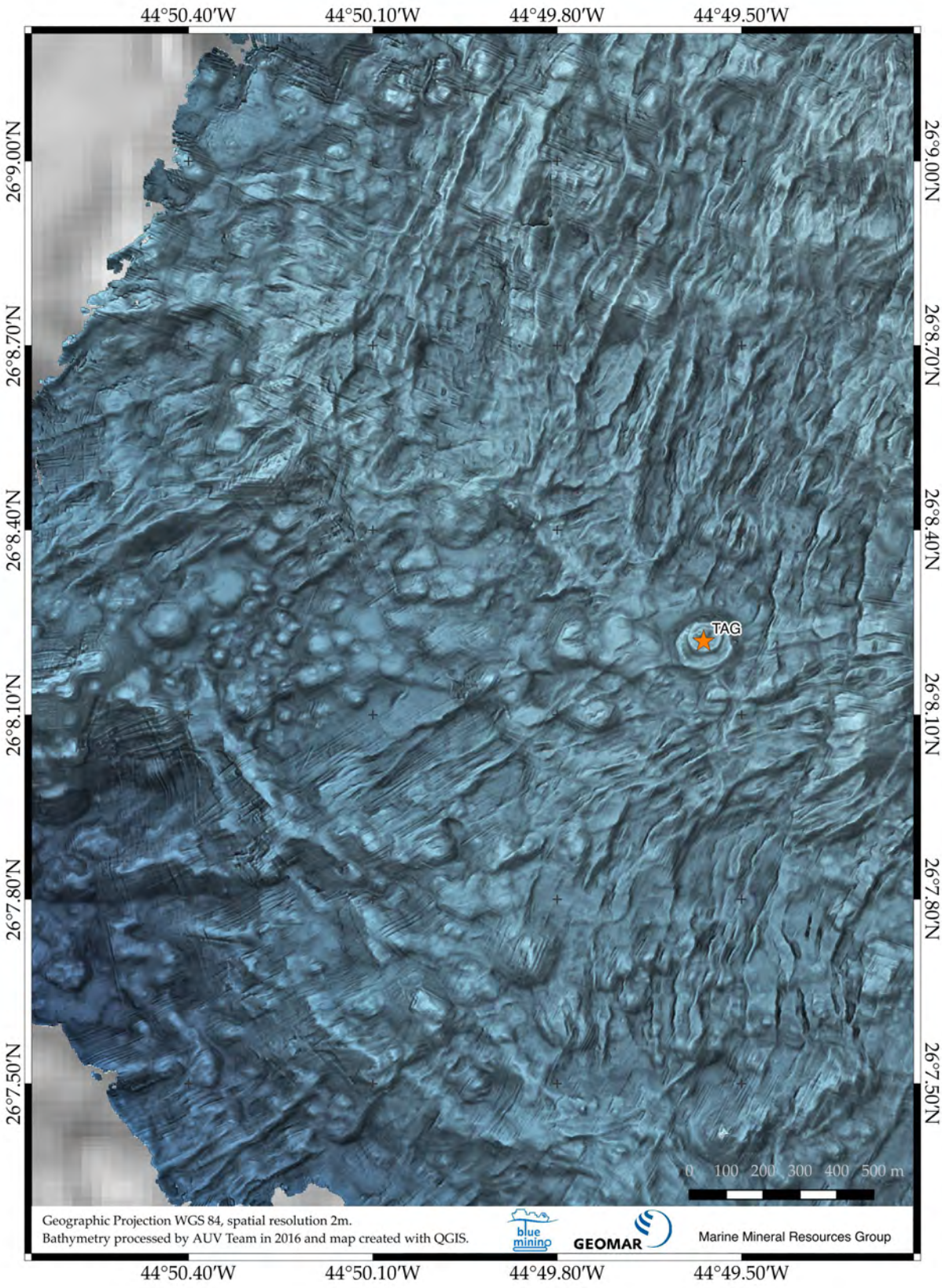

Fig. 5.2.9: *Detail of the high-resolution AUV-based bathymetry showing part of the neovolcanic zone in the SW of the working area and the intense bi-directional faulting close to the TAG active mound (red star). Map with 2m resolution; texture-shaded. Data is only roughly cleaned; final editing will be performed on-shore.*

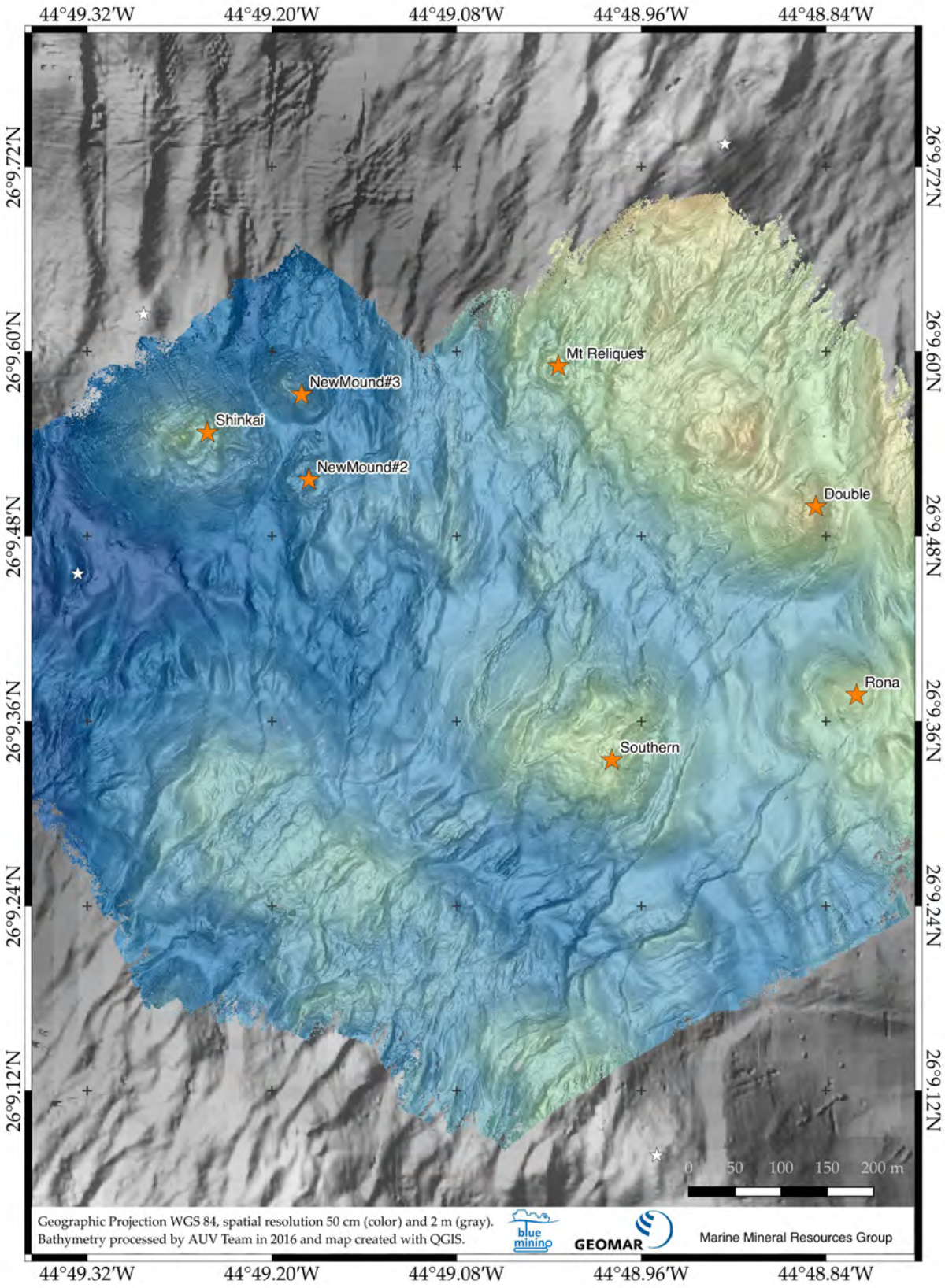

Fig. 5.2.10: *High-resolution AUV-based bathymetry obtained over the central Alvin Zone (400 kHz data gridded at 50 cm resolution). The underlying grey-shaded bathymetry is the 200kHz AUV bathymetry gridded at 2m resolution. The red stars denote inactive sulfide mounds and white stars possible hydrothermal targets that were not ground-truthed during M127. Data is only roughly cleaned; final editing will be performed on-shore.*

Fig. 5.2.11: *High-resolution AUV-based bathymetry obtained over the MIR Zone (400 kHz data; gridded at 50 cm resolution). The underlying grey-shaded bathymetry is the 200kHz bathymetry (2m resolution). Unlabled white stars denote possible hydrothermal targets that were not ground-truthed during M127. Data is only roughly cleaned; final editing will be performed on-shore.*

5.2.4 Magnetic and self-potential data from AUV surveys
(F. Szitkar)

Hydrothermal deposits have the potential to become economically viable mining targets in the near future, but localizing and characterizing such targets is not an easy task. Moreover, inactive deposits are generally more interesting than active ones but they are even more difficult to locate, as they can no longer be detected through their associated geochemical or geophysical anomalies (plume) in the water column. It is therefore of utter significance to use specific geophysical properties of the deposits that remain after the end of hydrothermal activity to optimize the chances of finding them. To do so, we consider a combination of high-resolution magnetic and self-potential (SP) measurements with the AUV ABYSS of GEOMAR (Fig. 5.2.12) along the TAG hydrothermal field that consists not only of an active black smoker systems, but also several inactive deposits in its surroundings.

The Earth's magnetic field undergoes changes in polarity with an average frequency of about once every million years. When rocks from the seafloor cool down below the Curie temperature of their magnetic minerals, these minerals acquire a natural remanent magnetization parallel to the magnetic field's direction at that time. Another magnetization, called induced magnetization, is generated by the ambient field and is proportional and parallel to it.

The remanent magnetization of volcanic rocks such as extrusive basalts from the oceanic crust, is usually strong and dominates the induced magnetization. Consequently, the oceanic crust is characterized by a succession of normal (i.e. same orientation as today's Earth magnetic field) and reverse polarities (i.e. opposite direction), generating symmetrical magnetic anomalies that are observed on both sides of mid-ocean ridges. These anomalies played a key role in the understanding of plate tectonics.

As a result of alteration, the titanomagnetite within the basalt slowly turns into titanomaghemite, which has a weaker magnetization, and finally into non-magnetic minerals. Therefore, circulation of fluids in extrusive basalts reduces their average magnetization and the intensity of associated magnetic anomalies. Consequently, anomalies associated to young volcanic structures (ridge axis, active volcanoes, etc.) are comparatively stronger than those from the surroundings. At a local scale, alteration becomes dominant in hydrothermal areas, generating a lack of magnetization that remains after the end of hydothermal activity. Therefore, high-resolution magnetic data seem to be a highly efficient tool to locate and characterize inactive deposits that cannot be detected through their associated water column anomalies.

To conduct our magnetic measurements the AUV Abyss followed a regularly spaced parallel survey track at a roughly constant altitude above the seafloor (i.e., draping the topography) and collected a combination of high-resolution magnetic, self-potential (see below) and bathymetric data.

Fig. 5.2.12: *One of the self-potential electrodes mounted on the starboard side of the AUV.*

Magnetometer and initial processing

The APL1540 magnetometer that was used during cruise M127 is a three-component fluxgate magnetometer rigidly fixed to the AUV structure. It collects data along X-, Y- and Z-axis at a 10 Hz sample rate. Magnetic and self-potential measurements are logged by the newly designed Magson datalogger as binary files (each file corresponding to 5 minutes of data acquisition).

Using magnetometers on deep-sea instruments like AUVs or ROVs represents the ideal way to considerably improve the measurement precision by moving the magnetometer closer to the sources (the magnetic field intensity decreases with the cube of the distance). This improvement only allows relatively small zones to be surveyed and therefore focuses on potentially interesting targets. It cannot currently be used to survey large areas of the seafloor in high resolution.

Unlike for surface measurements, where the magnetometer is towed at sufficient distance to eliminate the magnetic influence of the ship, the immediate proximity of the underwater vehicle strongly affects the raw data. The magnetic influence of the AUV has therefore to be quantified and removed, in order to resolve the crustal magnetic anomaly. However, as the AUV does not have any moving part, apart from the engine, and does not modify its geometry during the dive (no sampling arm collecting samples, no rotating cameras etc…), this influence remains steady, guaranteeing a high stability of the data acquisition and therefore really good data quality.

Regardless of the vehicle (AUV, ROV etc.) their magnetic influence at the beginning of the dives has to be determined using, in this case, a calibration pattern made of a series of "figure-8's" to estimate the effect of heading with varying roll, followed by a succession of ascents and descents to estimate the influence of pitch at zero roll (*Isezaki, 1986; Honsho et al., 2009*). This pattern has to be made when the AUV is far enough from both the ship and the seafloor, so that no external source influences the data acquisition. However, as this pattern is time and energy consuming (i.e., shortening the duration of the dive itself by roughly 30 minutes), and considering the high stability of the AUV, only one calibration pattern has been completed during this cruise (station #599AUV, Abyss dive 227) and it was enough to get magnetic anomaly maps without any remaining influence of the vehicle.

Preliminary results for magnetic data acquisition

Once the influence of the vehicle is removed from the data, the raw magnetic anomalies can be calculated by subtracting the Earth's local geomagnetic field approximated by the International Geomagnetic Reference Field (IGRF) (*IAGA Working Group V-MOD, 2010*; Fig. 5.2.13), but these anomalies are phase-shifted, i.e., not centered above their causative sources, as a result of the Earth geomagnetic field inclination and declination. To remove the phase-shift and therefore to place the anomalies above their sources, a mathematical transformation called Reduction to the Pole (RTP) must be applied. The anomalies presented in Fig. 5.2.10b have been reduced to the pole, in order to get a first idea of potentially interesting zones (see "Interpretations" below) however, this transformation has been done using the direct RTP operators and is not 100% mathematically rigorous yet although it already provides really reliable results. Indeed, these operators are applied in the Fourier domain and require the data to be collected on a level datum plane, which is not the case for an AUV draping the topography. Further processing will be done, using the high-resolution bathymetric data, to obtain a rigorous RTP anomaly but the requested computer power for the magnetic inversion is only available onshore at GEOMAR.

For the magnetic data acquisition, the AUV dives for the high-resolution bathymetry (200 kHz) dives were extremely interesting as they allowed data collection on a specific target but at different altitudes above the target (Fig. 5.2.14).

Magnetic anomalies reveal subsurface information depending on the altitude of the survey. Whereas near-seafloor magnetic data reveal short wavelength (i.e., small dimensions), shallow subseafloor sources, data collected at higher altitudes corresponds to longer wavelengths and hence deeper sources. A dataset collected at various altitudes above the same target is therefore an ideal way to map what happens at all depths and gives precise information concerning the geometry and size of the source. Such work, however, requires lots of additional processing and has not been carried out onboard.

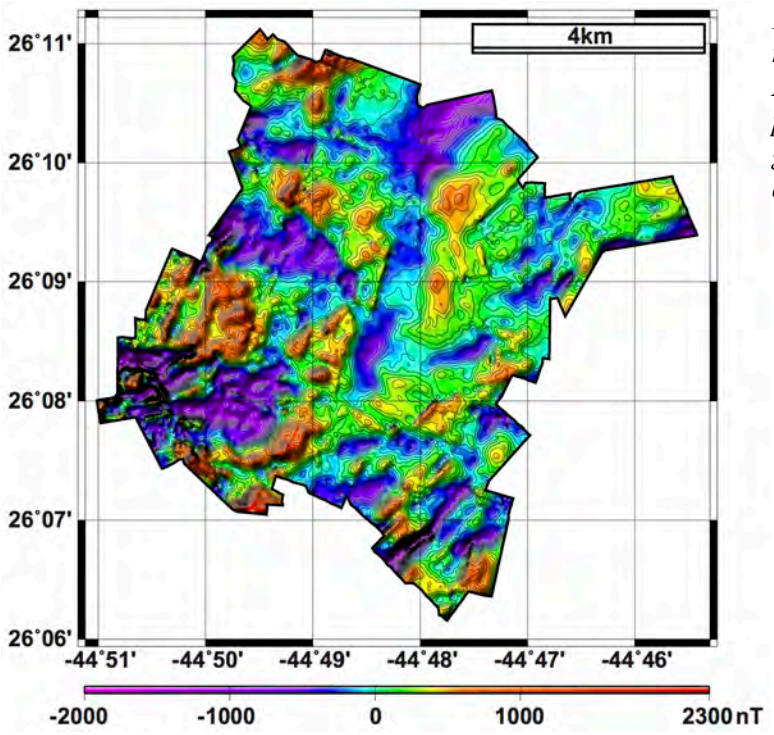

***Fig. 5.2.13a**: Final magnetic anomaly map obtained by combining all the AUV dives. The anomalies are still phase-shifted as a result of the geomagnetic fields local inclination and declination*

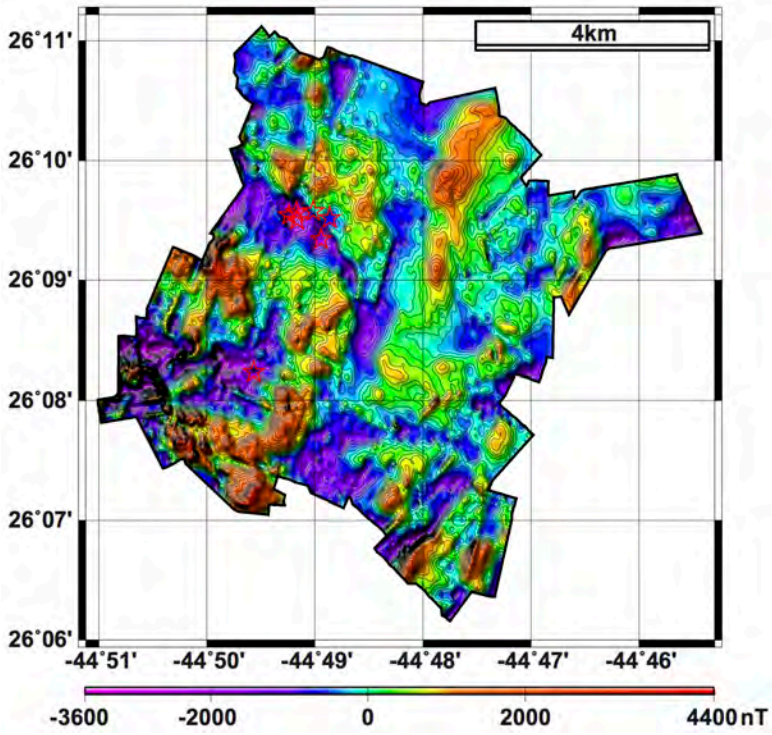

***Fig. 5.2.13b**: Preliminary anomaly map after reduction to the pole (RTP). The anomalies are shifted northwards, which is consistent with our location in the northern hemisphere. They are now centered above their causative sources. The red stars correspond to some of the identified active and inactive basalt-hosted hydrothermal targets (the southern-most star corresponds to the TAG active mound). As expected, these targets are all associated with a negative RTP anomaly, i.e., a lack of magnetization.*

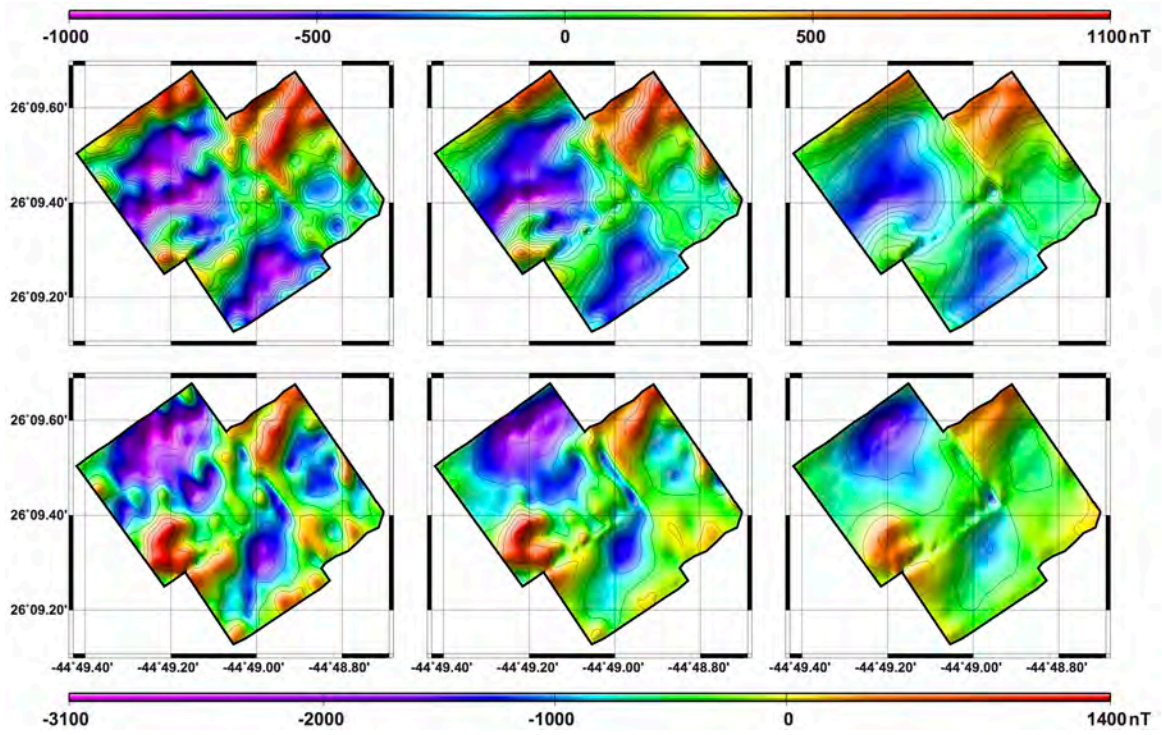

Fig. 5.2.14*: Data from ABYSS dive 234 in the Alvin Zone. Up: Magnetic anomaly from the three different altitudes of data acquisition. Down: Same data, but with RTP anomaly. The color scale remains the same on the three maps, underlining the loss of amplitude and of short wavelength because of the higher altitudes.*

Interpretations

In basalt-hosted environments, both active and inactive hydrothermal systems are associated with a negative RTP anomaly, i.e., a lack of magnetization (*Tivey et al., 1993; Tivey and Johnson, 2002; Tivey and Dyment, 2010; Zhu et al., 2010; Caratori Tontini et al., 2012; Nakamura et al., 2013; Honsho et al., 2013; Szitkar et al., 2014; Szitkar et al., 2015a*). This specific signature is a result of the alteration of titanomagnetite in the basalt into less magnetic minerals such as titanomaghemite by contact with hydrothermal fluid circulation (*Ade-Hall et al., 1971; Johnson and Pariso, 1987; Watkins and Paster, 1971; Tivey and Johnson, 2002; de Ronde et al., 2011*), the accumulation of a thick and non magnetic deposit (*Szitkar et al., 2014*) and (at least for active sites) a small thermal contribution if the temperature of the site exceeds the Curie temperature of titanomagnetite. It is now proven that the thermal contribution is of second order (*Szitkar et al., 2015a*), i.e., the specific magnetic signature remains after the end of hydrothermal activity because mineral alteration and the deposit accumulation are non-reversible processes. It is therefore possible to use this permanent geophysical property as a way to locate and characterize the deposits using high-resolution, near-seafloor magnetic data.

Previous magnetic investigations have proven that the TAG hydrothermal field is associated with a lack of magnetization (*Tivey et al., 1993; Szitkar et al., 2015b*), consistently with all other active and inactive basalt-hosted sites. The submersible *ALVIN*, however, collected these data at a lower altitude above the seafloor. Our new dataset was collected at higher altitudes, i.e., it provides additional information concerning the deep structure of the hydrothermal field and

extends way beyond the site itself in all the directions. These data largely contributed to identify new targets, also confirmed by other kinds of measurements and revealed that these basalt-hosted hydrothermal structures (Double Mound, Mir Zone etc.) are all associated with a lack of magnetization. Moreover, the negative anomaly associated with the Double Mound is strong enough to create a negative "hole" within a large positive anomaly, suggesting that the demagnetized source below this mound extends potentially deeper than that of the others (Fig. 5.2.15). However, it is worth noting that further processing is required and more precise interpretations will only be done later. It will then become possible to precisely study the shape and amplitudes of these anomalies to provide an estimation of the mining potential, and volume of each target.

Self-Potential measurements

Self-potentials (SP) are naturally occurring electric voltages that result from a number of different physical processes. Electrokinetic potentials arise when a fluid flows in porous media as a consequence of a pore-pressure gradient, while regions with temperature gradients may give rise to thermoelectric potentials. Diffusion (or mineral) SP is of greatest significance in geophysical exploration and occurs across boundaries with differing geochemical compositions.

In a mineral exploration point of view, an electrical conducting ore is required to connect electronically two different electrochemical environments. A vertical gradient in reduction-oxidation (redox) potential Eh facilitates a relative excess of oxidizing agents in the upper part of the ore body and a relative excess of reducing agents in the lower part. Reducing agents undergo oxidation at the lower host source boundary, producing electrons and positive ions. Electrons travel up the source where they are used to help reduce the oxidizing agents at the upper host source boundary; the ohmic potential drop of this current is measured as the resulting SP anomaly. The upper half-reaction produces negative ions that flow back through the host rock (and, in our case, seawater).

As the redox chemical reactions between the deposit and the surrounding seawater still exist after the end of hydrothermal activity, SP measurements represent another potential way to locate inactive deposits (Fig. 5.2.15). Collecting high-resolution SP data with an AUV on such a large area had never been undertaken before. In terms of SP exploration, cruise M127 is therefore the first of its kind, to test the efficiency of these highly specific data.

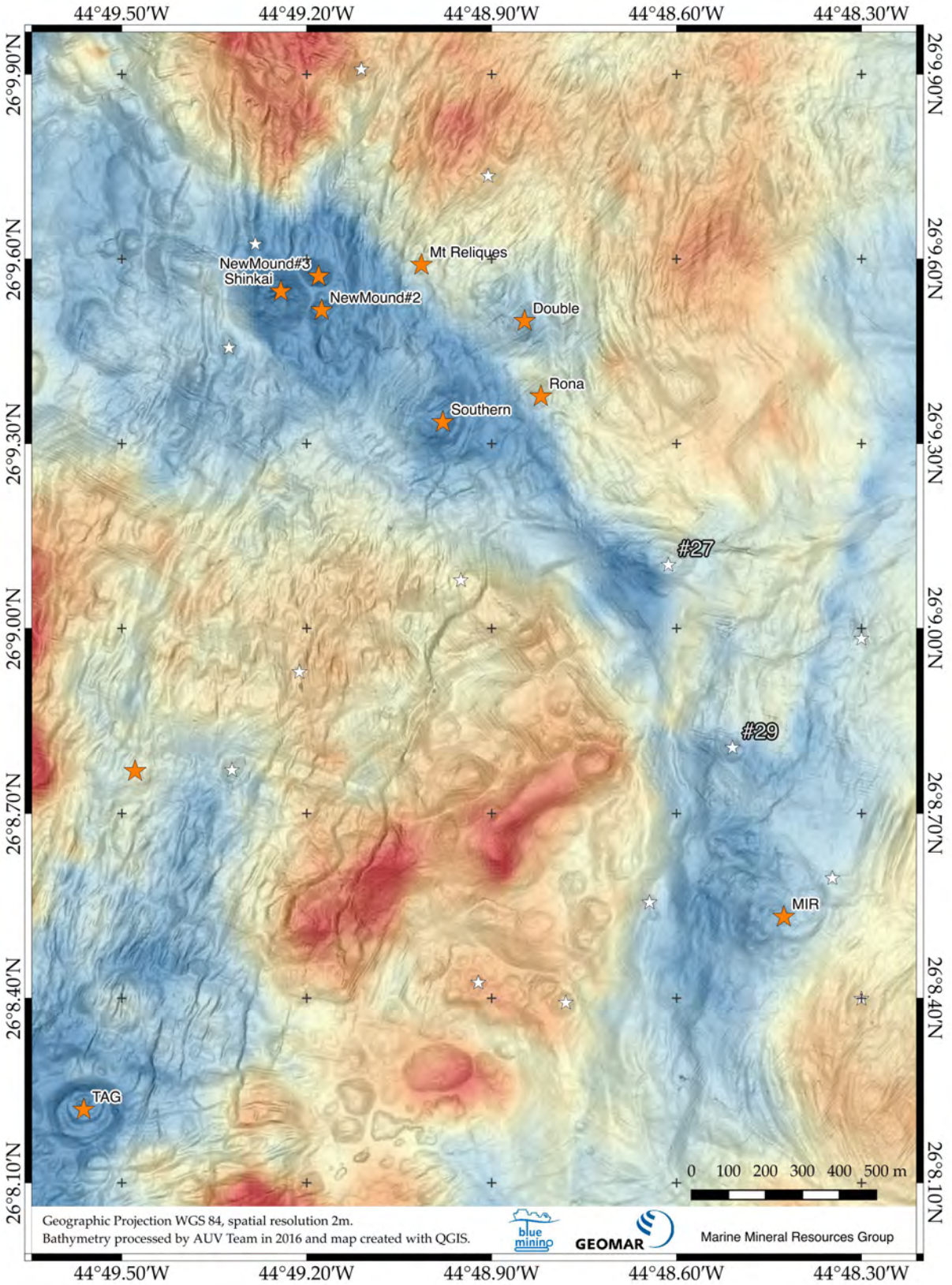

Fig. 5.2.15: *Preliminary magnetic data draped over bathymetry. The image shows the association of magnetic lows (blue) with known and suspected hydrothermal systems. The underlying bathymetry is the 200kHz bathymetry (2m resolution). White stars denote target sites suspected to be hydrothermal in origin based on AUV-mapping. Note that targets #27 and #29 were confirmed to be hydrothermal during HYBIS dives during cruise M127. Rona Mound, another suspected target based on bathymetry (target #09) was confirmed to be hydrothermal in origin during M127 and later drilled during the subsequent RRS JAMES COOK cruise JC138 in August 2016.*

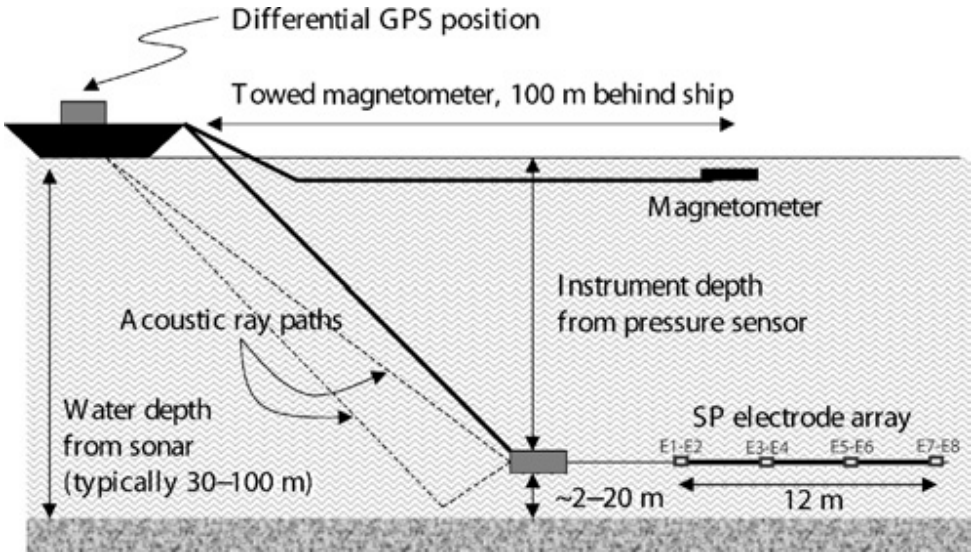

Fig. 5.2.16*: Principle of at sea SP measurements (adapted from Heinson et al., 2005). This figure shows how to collect SP data from a ship with a SP electrode array. The AUV is equipped with two sets of electrodes (respectively across and along axis) to measure the SP anomalies in both directions.*

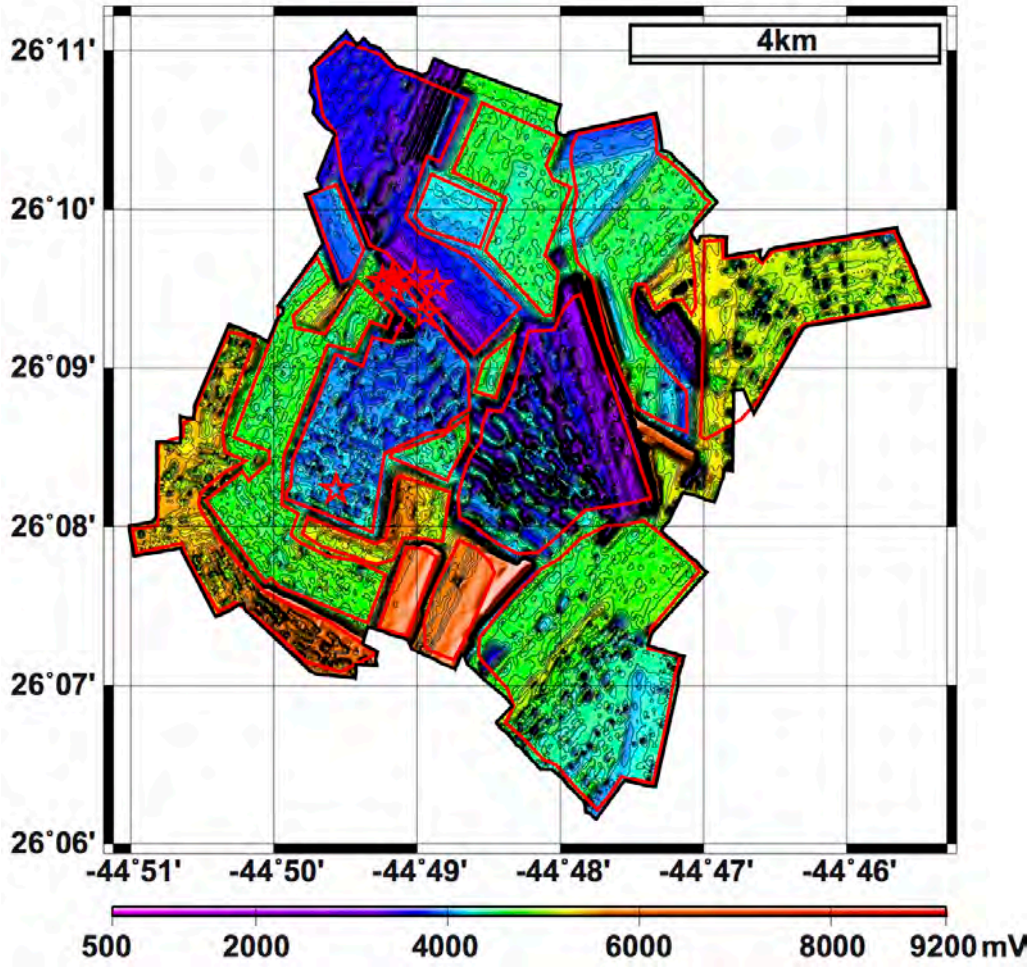

Fig. 5.2.17*: Self-Potential (SP) map of the investigated area. As the results are highly altitude-dependent, the dive was split into smaller patches delineated by the red lines and each one plotted separately with a different color palette.*

The AUV-based SP-data shows strong dependance on altitude. Further post-cruise reprocessing is therefore needed to fully evaluate the data obtained during cruise M127. At first sight, the typical altitude of 70–80 m of the AUV during our exploration surveys, which is determined by the speed of the AUV, the local topography, and the final resolution of the bathymetric grid that is required for this type of exploration (2m resolution) seems to be too high with regards to the weak electrical currents that we are measuring. The two dedicated high-resolution surveys, collecting data at three different target altitudes, however, indicated that altitudes of 30 m are sufficient to detect signals over known inactive deposits (Fig. 5.2.18). The data from these two dives will be used to model best practise for future exploration surveys using combined SP and magnetic data with associated bathymetry.

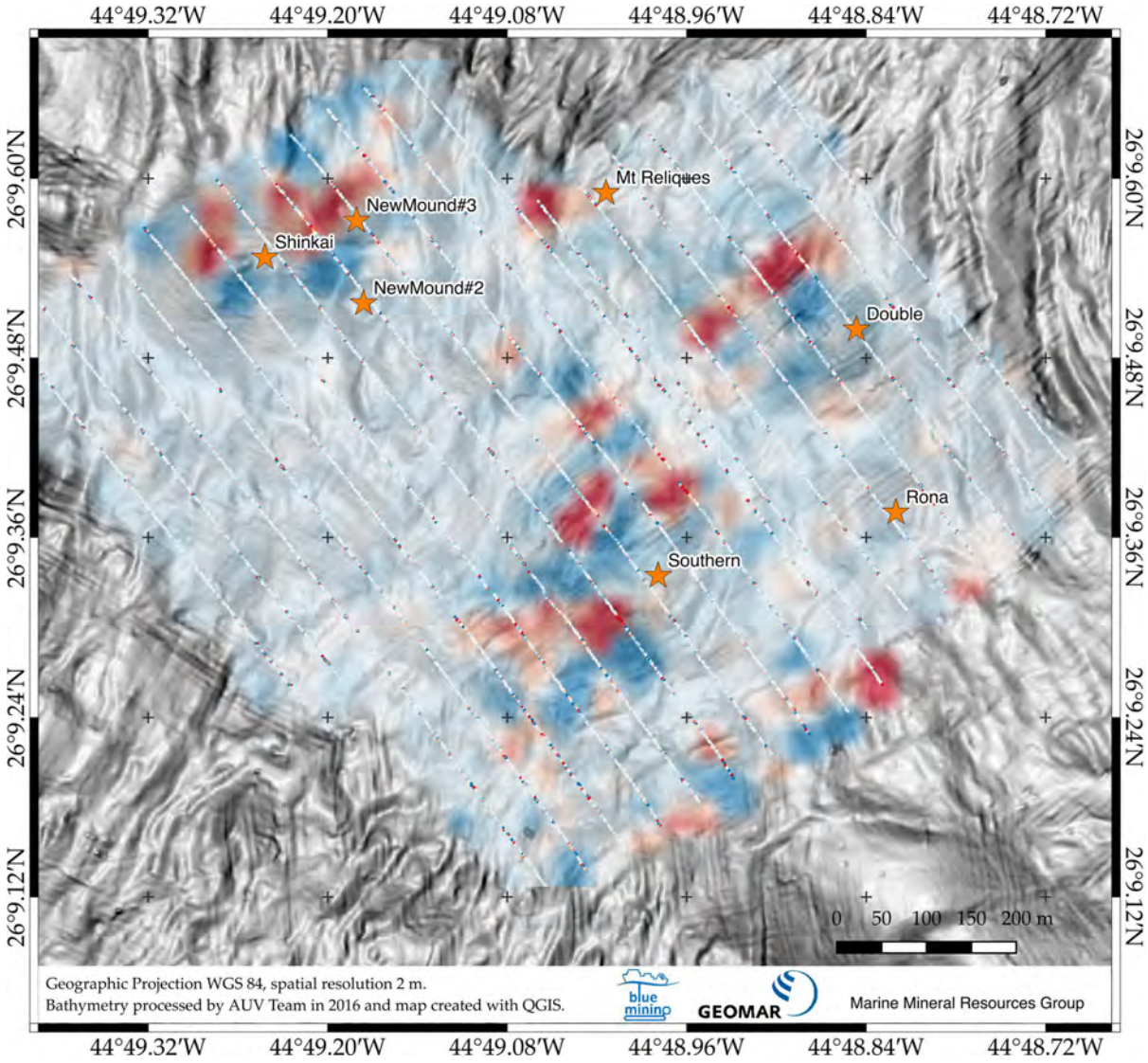

Fig. 5.2.18*: Plot of filtered and interpolated Δ-SP data (preliminary data from AUV mission #234 flying at <40m altitude) over bathymetry indicating the capability of the SP-sensor to detect known deposits (orange stars). Note the absence of strong positive (red) or negative (blue) anomalies in the western part of the survey area. The known deposits have diameters up to 200 m (Southern Mound) and are therefore potentially interesting for industry, depending on grade. The non-filtered and non-interpolated data is also plotted as a thin line to show the corresponding line spacing.*

5.2.5 Resource consideration

(J. Jamieson)

A combination of AUV bathymetry, AUV magnetic data and ship multibeam backscatter data was used to identify possible hydrothermal deposits on the seafloor. Individual targets were identified using each method independently. Targets were identified in the AUV bathymetry as mound features on the seafloor such as targets #27 (Fig. 5.2.19a), #09, or #29. Criteria used to define a target as hydrothermal are based on *Jamieson et al. (2014)*, and include the shape, slope angles and smoothness of the mounds. Based on similar work at the Endeavour hydrothermal fields, rough, irregularly shaped mounds tend to be hydrothermal in origin, compared to volcanic mounds, which are generally smooth and symmetrical. The recent volcanic and tectonic history of the area is not yet well constrained enough to use timing based on cross-cutting relationships in order to differentiate hydrothermal features from volcanic features in the bathymetry. Targets were also identified based on presence of magnetic lows (Fig. 5.2.19b). These targets were selected without taking into consideration whether or not there was a corresponding bathymetric feature (e.g., targets #34 and #40 in Fig. 5.2.19b). The magnetic anomaly map used to pick targets during the cruise had not yet been corrected for seafloor topography, and many magnetic features in the preliminary map corresponded to topographic features or boundaries between different AUV dives. Targets will be re-picked once a final magnetic anomaly map is available.

Finally, it was noticed that, in several cases, a low backscatter anomaly from the ships multibeam was associated with known hydrothermal sites such as the Shinkai Mound (Fig. 5.2.19c). The cause of the low backscatter is still uncertain. The association of these anomalies with mounds on the seafloor may simply be the result of the effects of slope and aspect of these features relative to the ship. They may, however, also be a result of the physical properties of the substrate, such as density or roughness of the surface. If the magnetic lows are primarily a result of the physical properties of the substrate, ship-based backscatter has the potential to be a useful tool for identifying hydrothermal material on the seafloor. However, further examination of these data is necessary before any conclusions can be drawn.

Each target identified using the three methods described above was then separately evaluated for its likelihood of being hydrothermal in origin using each of the three methods, and each target was given three separate ratings as being either 1) likely hydrothermal; 2) possibly hydrothermal; or 3) likely not hydrothermal. This method allowed for the most and least probable hydrothermal targets to be identified, and also allowed for the different prospecting techniques to be directly compared to each other. Targets that scored highest were identified as “likely hydrothermal” using all three methods. Likewise, targets that scored the lowest were identified as “likely not hydrothermal” using all three methods. Both high and low combined scores thus represent the highest confidence that a target is either hydrothermal or volcanic in origin.

Targets that have different ratings from the different methods offer the opportunity to evaluate and compare each method. For example, there are several targets that are thought to be likely hydrothermal based on the bathymetry, but have no corresponding magnetic anomaly (targets #21 and #23 south of Shimmering Mound; Fig. 5.2.19d), and vice versa (e.g., targets #34 and #40 in Fig. 5.2.19b). There are also two occurrences of mounds that may be hydrothermal but are

associated with a positive, as opposed to the expected negative magnetic anomaly (for instance target #10; Fig. 5.2.19e).

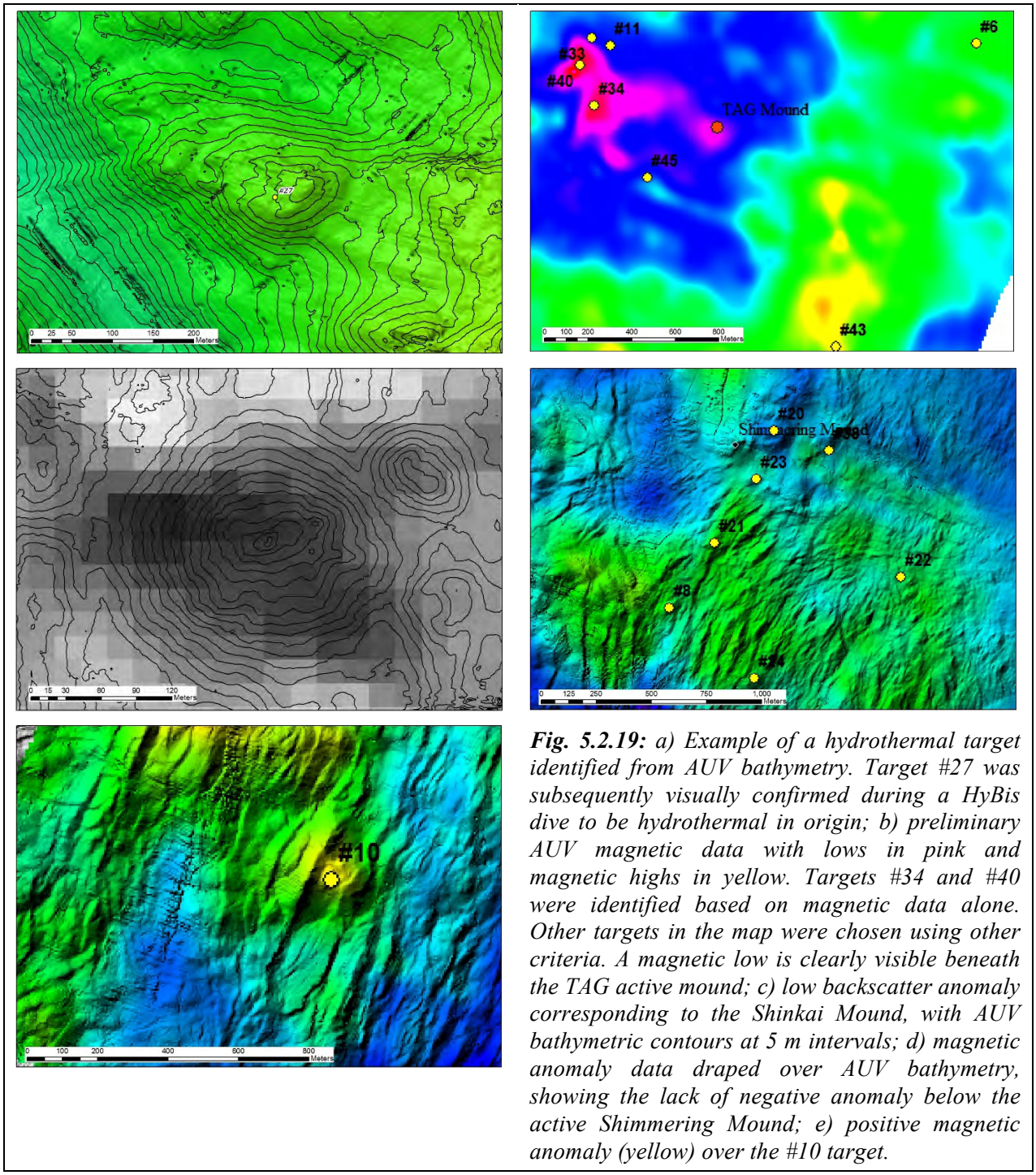

Fig. 5.2.19: *a) Example of a hydrothermal target identified from AUV bathymetry. Target #27 was subsequently visually confirmed during a HyBis dive to be hydrothermal in origin; b) preliminary AUV magnetic data with lows in pink and magnetic highs in yellow. Targets #34 and #40 were identified based on magnetic data alone. Other targets in the map were chosen using other criteria. A magnetic low is clearly visible beneath the TAG active mound; c) low backscatter anomaly corresponding to the Shinkai Mound, with AUV bathymetric contours at 5 m intervals; d) magnetic anomaly data draped over AUV bathymetry, showing the lack of negative anomaly below the active Shimmering Mound; e) positive magnetic anomaly (yellow) over the #10 target.*

It is important to note that many of these discrepancies may turn out not to be real once the data are re-examined using fully processed ship-based bathymetry and magnetic data. However, ground-truthing (with ROV, submersible, video surveys, etc…) will be the critical next step to fully evaluate the exploration methods discussed here. Limited validation of targets on this cruise using HyBis video surveys and sampling resulted in the confirmation that 4 target sites were confirmed to be hydrothermal in origin (targets #09 Rona Mound, #20, #27, #29; Tab. 5.2.3; Fig.

5.2.20) and 6 sites were confirmed to be volcanic rather than hydrothermal in origin (targets #10, #11, #19, #33, #34, #40). The confirmed hydrothermal sites were originally targeted primarily based on their combined bathymetric and magnetic attributes. For the sites confirmed to not be hydrothermal, all were rated as "likely not hydrothermal" or "maybe hydrothermal" based on AUV bathymetry.

However, 3 of the non-hydrothermal sites (targets #33, #34, and #40; all located west of the active TAG mound) were rated as "likely hydrothermal" based on their strong negative magnetic signature, suggesting that magnetic surveys alone may not necessarily be an optimal exploration tool. Evaluation of the fully-processed AUV-based magnetic data is required before any firm conclusions can be made. Regardless, confirmation of the genetic origin of targets that display different, or even opposing indications of a hydrothermal origin (e.g., strong bathymetric indication but no associated negative magnetic anomaly) is necessary to not only validate each method but to evaluate how best to combine the data from different methods in order to maximize the chances of successfully identifying hydrothermal deposits on the seafloor.

A combination of different exploration tools will likely be the most effective way to locate hydrothermal deposits. The weighting, or confidence assigned to each method is yet to be fully evaluated, but short of direct visual surveys or sampling, the results so far suggest that high-resolution bathymetry will likely be the most important and reliable exploration tool for finding deposits, but a combination of several methods will enhance the chances of success. Further to this, shore-based analyses of the AUV-based backscatter and self-potential data may further help delineate targets.

Table 5.2.3: Rock samples recovered by HyBis.

Station	Date/Time	Lat./Long.	Depth	comment)
M127/651	14.06.2016 / 13:46	26°09.091'N / 044°48.580'W	3534 m	variety of Fe-oxyhydroxides some with Mn-crust from top of target #27
M127/652	14.06.2016 / 21:36	26°08.805'N / 044°48.483'W	3439 m	red Fe-oxyhydroxides and thick Mn-crusts from top of target #29
M127/677	16.06.2016 / 18:32	26°10.344'N / 044°48.844'W	3418 m	small pieces of red Fe-oxyhydroxides and sulfides from target #20; video shows outcropping sulfides and possibly chimney relics on the slope of this mound
M127/684	17.06.2016 / 15:32	26°08.711'N / 044°49.190'W	3590 m	beige sediment with few tiny bits of basaltic glass shards from target #01; video showed no evidence for hydrothermalism
M127/685	17.06.2016 / 19:51	26°09.373'N / 044°48.825'W	3539 m	orange Fe-oxyhydroxides with trace atacamite from top of target #09 (Rona Mound)
M127/688	18.06.2016 / 19:20	26°08.465'N / 044°49.929'W	3632 m	few pieces of Fe-oxyhydroxides from top of flat pancake-like mound; video showed no evidence for hydrothermalism at targets #11, #33, and #34
M127/694	19.06.2016 / 15:50	26°10.683'N / 044°48.630'W	3436 m	large block of chloritized (?) greenish microgabbro (dolerite) in weakly Fe-stained sediment from target #19

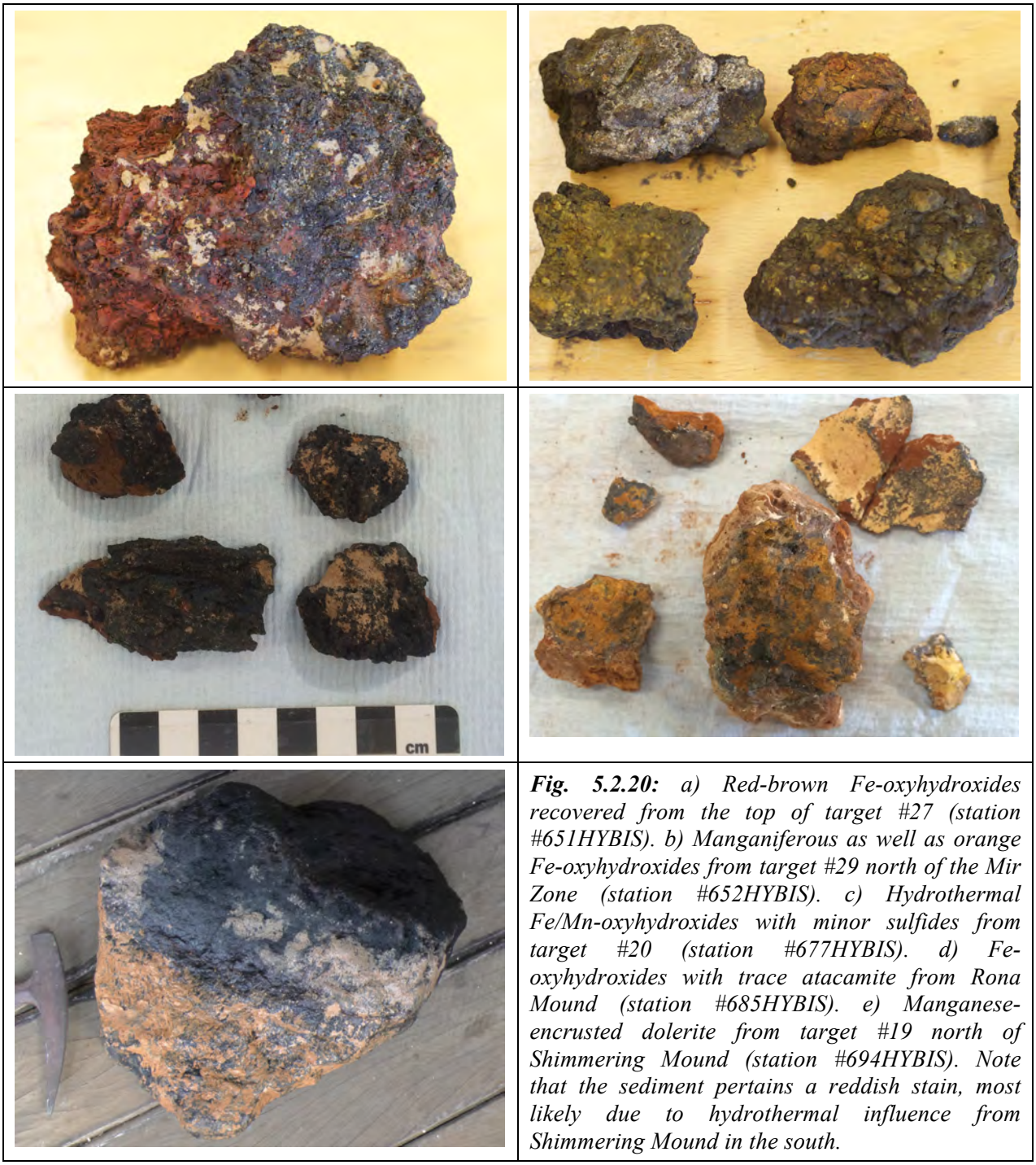

Fig. 5.2.20: *a) Red-brown Fe-oxyhydroxides recovered from the top of target #27 (station #651HYBIS). b) Manganiferous as well as orange Fe-oxyhydroxides from target #29 north of the Mir Zone (station #652HYBIS). c) Hydrothermal Fe/Mn-oxyhydroxides with minor sulfides from target #20 (station #677HYBIS). d) Fe-oxyhydroxides with trace atacamite from Rona Mound (station #685HYBIS). e) Manganese-encrusted dolerite from target #19 north of Shimmering Mound (station #694HYBIS). Note that the sediment pertains a reddish stain, most likely due to hydrothermal influence from Shimmering Mound in the south.*

5.3 Seismic work

(J. Bialas, A. Dannowski, A. Gil, H. Schröder, G. Wetzel, T. Matthiessen, T. Jacobsen-Bialas)

Task 2.2 of WP2 of Blue Mining project sets out to acquire multichannel and ocean-bottom seismic data in order to analyse the structure and lateral extend of one or more eSMS deposits. For this purpose 20 Ocean-Bottom Seismometers (OBS) and five Ocean-Bottom Hydrophones (OBH) together with a 30 channels deep towed and a 192 channels surface towed streamer were provided by GEOMAR. Gun volumes and available compressor capacity of 10 m^3/min need to be adjusted in order to provide a sufficient strong source signal while the frequency content should still be kept as high as possible to allow the highest possible resolution. Simulations of the acquisition geometry, the expected geologic conditions in the working area and the expected shot rate of 10 s to 12 s suggested to either use two GI airguns (105/105 cinch) or a G-gun cluster (380/380 cinch).

In a pre-cruise meeting at GEOMAR, Kiel, the involved parties GEOMAR, NERC and SOTON discussed the research targets within the TAG field. Active TAG mound has been investigated quite intensively and could serve as basis for theoretical pre-cruise modelling. However, it was decided to put major emphasis on the inactive Shinkai and Southern Mound. In addition, the Shimering Mound area should be covered by the seismic acquisition. As a service for the follow on cruise with RRS JAMES COOK and the colleagues of the electromagnetic group six Ocean-Bottom Electro-Magnetic stations (OBEM, Fig. 5.3.1) were deployed for passive monitoring during cruise M127 already.

In total 22 OBS and 9 OBH deployments were undertaken (Fig. 5.3.1). Airgun shots and multichannel seismic streamer records were compiled along 49 profiles. For the profiles P20 and following an onbaord GPS receiver solution for the airgun floatation could be applied and supported the navigation processing.

Airgun shots were provided during eight survey runs, which sum up to a total of 49 profiles. The first test profile P01 was recorded by OBS26 & OBS27 only as it was thought as calibration run to test source strength and amplification for the OBH and OBS sensors. Profiles P02 to P27 were recorded by OBS01 to OBS 21 and OBH17, OBH22 to OBH25 (Fig. 5.3.2). After recovery of OBH22 to OBH25 and redeployment of OBH28 to OBH31 all instruments recorded profiles P28 to P46 (Fig. 5.3.3). After recovery of the ocean-bottom instruments, OBH17 and OBH30 did record the final profiles P47 to P49 (Fig. 5.3.4) as they surfaced from their time release only. While profiles P35 to P46 were shot with two GI airguns all other lines were shot with two G-guns.

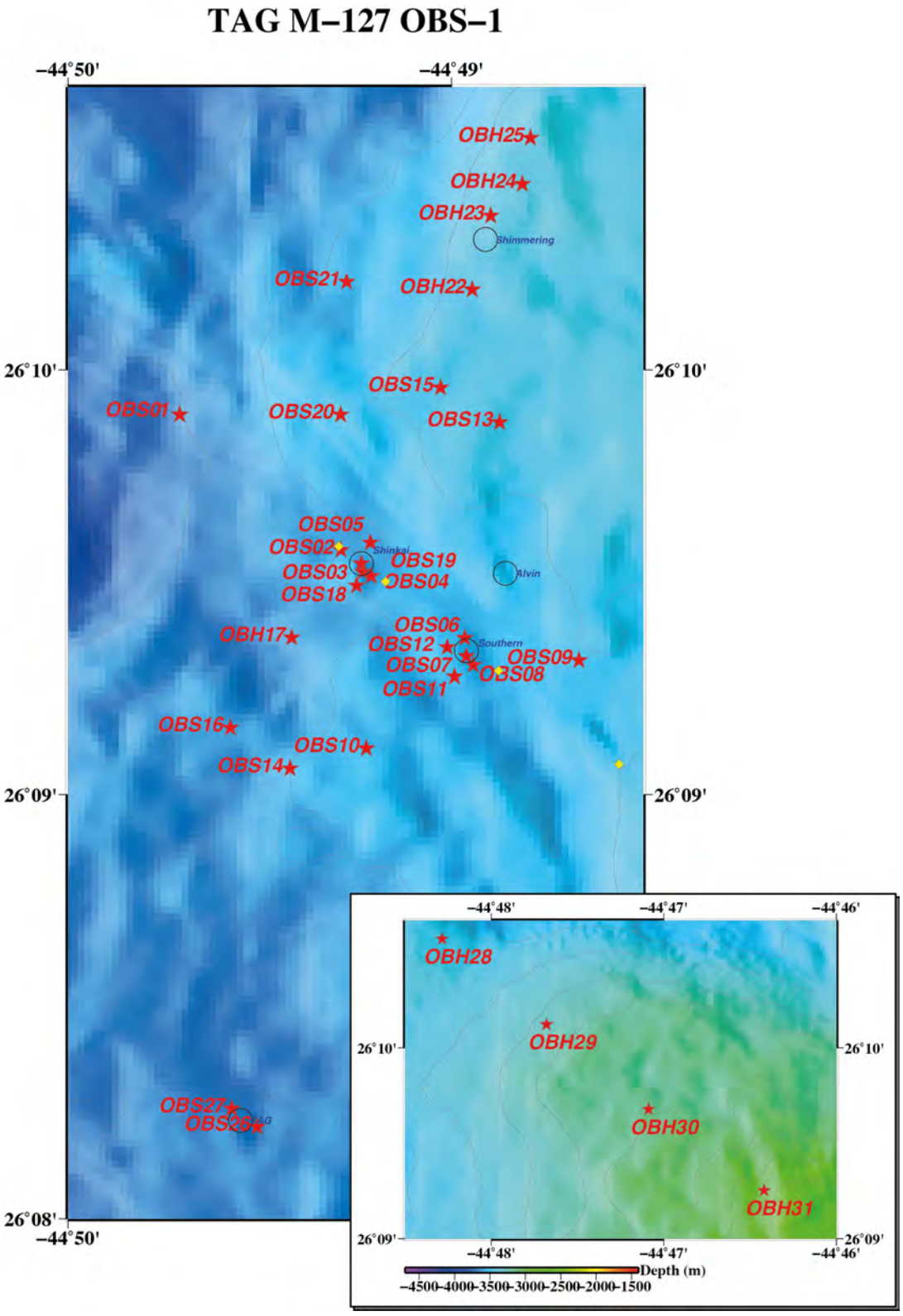

Fig. 5.3.1: *Map of the OBS and OBH positions deployed during the M127 cruise.*
OBS26 and 27 were deployed for a short test profile only. OBH22 to OBH 25 were recovered once all instruments deployed on and around Shinkai, Southern and Shimmering mound did record airgun shots from at least two crossing lines. The four instruments were redeployed on positions OBH28 to OBH31. OBH17 and OBH30 did surface on time release only. Yellow dots mark the deployment positions of OBEM stations in this area.

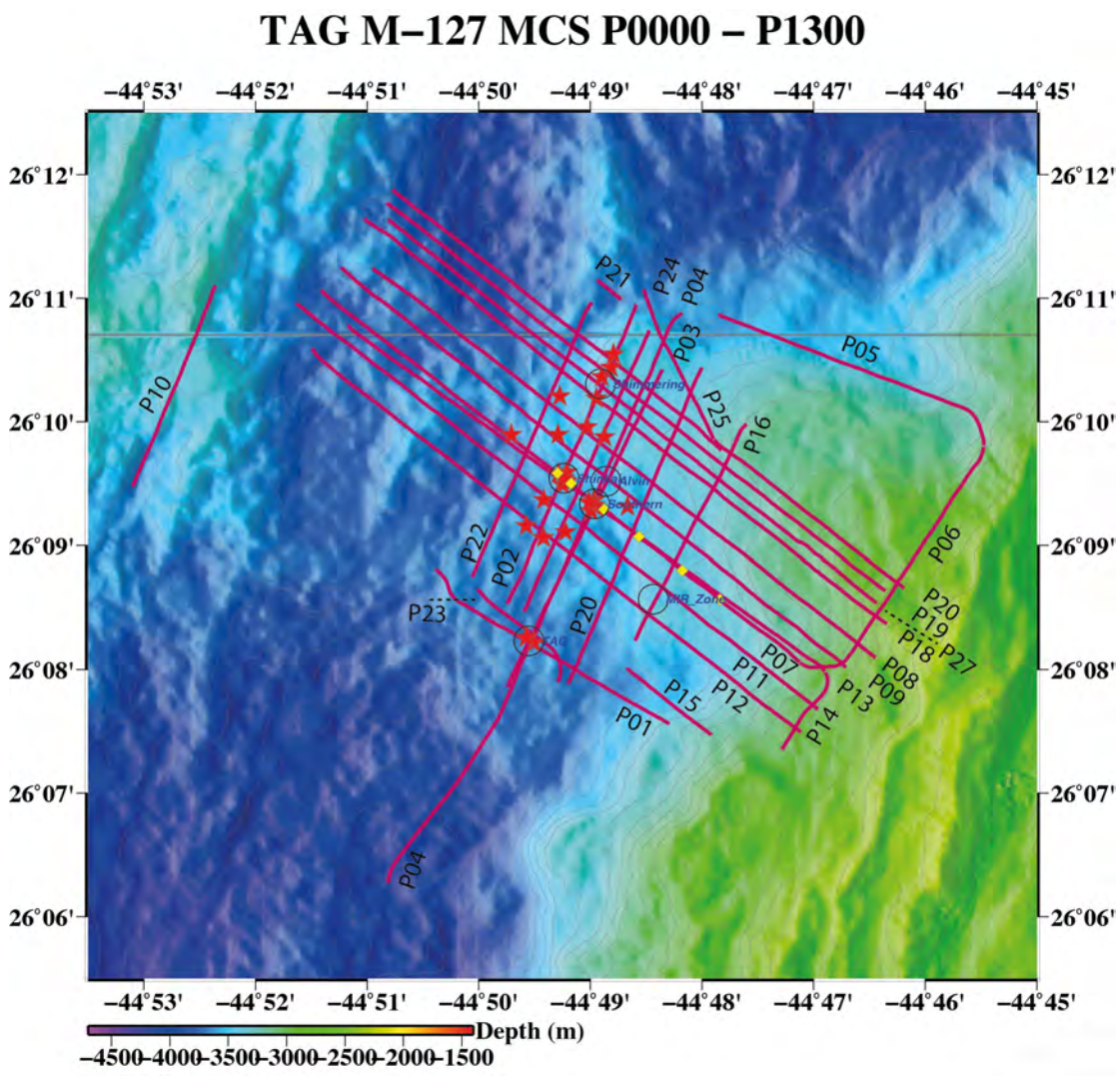

***Fig 5.3.2**: Map of the airgun profiles P01 to P27. The shots were provided from a two times 380 cinch G-gun cluster. While OBS26 & OBS27 did record test profile P01 only all other instruments recorded profiles P02 to P27.*

5.3.1 Airguns

For cruise M127 a carrier for two GI-guns was build, but could not be tested beforehand. During a test profile in the working area it turned out that the GI-gun carrier was not stable enough to withstand the wave state in the area. Therefore the G-gun cluster (380/380 cubic inch) was deployed together with the surface streamer and two OBS. The G-gun cluster was towed at 6 m depth and proved to provide reliable signal strength for the topographic and tectonic complicated terrain of the Mid-Atlantic Ridge. It was used throughout the most seismic profiles at a shot rate of 12 sec. Later the GI-gun carrier could be refitted and allowed to use the two GI airguns (105 cubic inch each) towed at 2.5 m depth along the main OBS observation lines. In order to provide very dense shot offsets the survey speed of R/V METEOR was reduced to 2.5 - 3 kn through water resulting in 2 kn to 3 kn across ground and shot offsets of 16.5 m to 19.8 m. Airgun triggers were generated based on GPS clock timing, providing the time base for all recording devices.

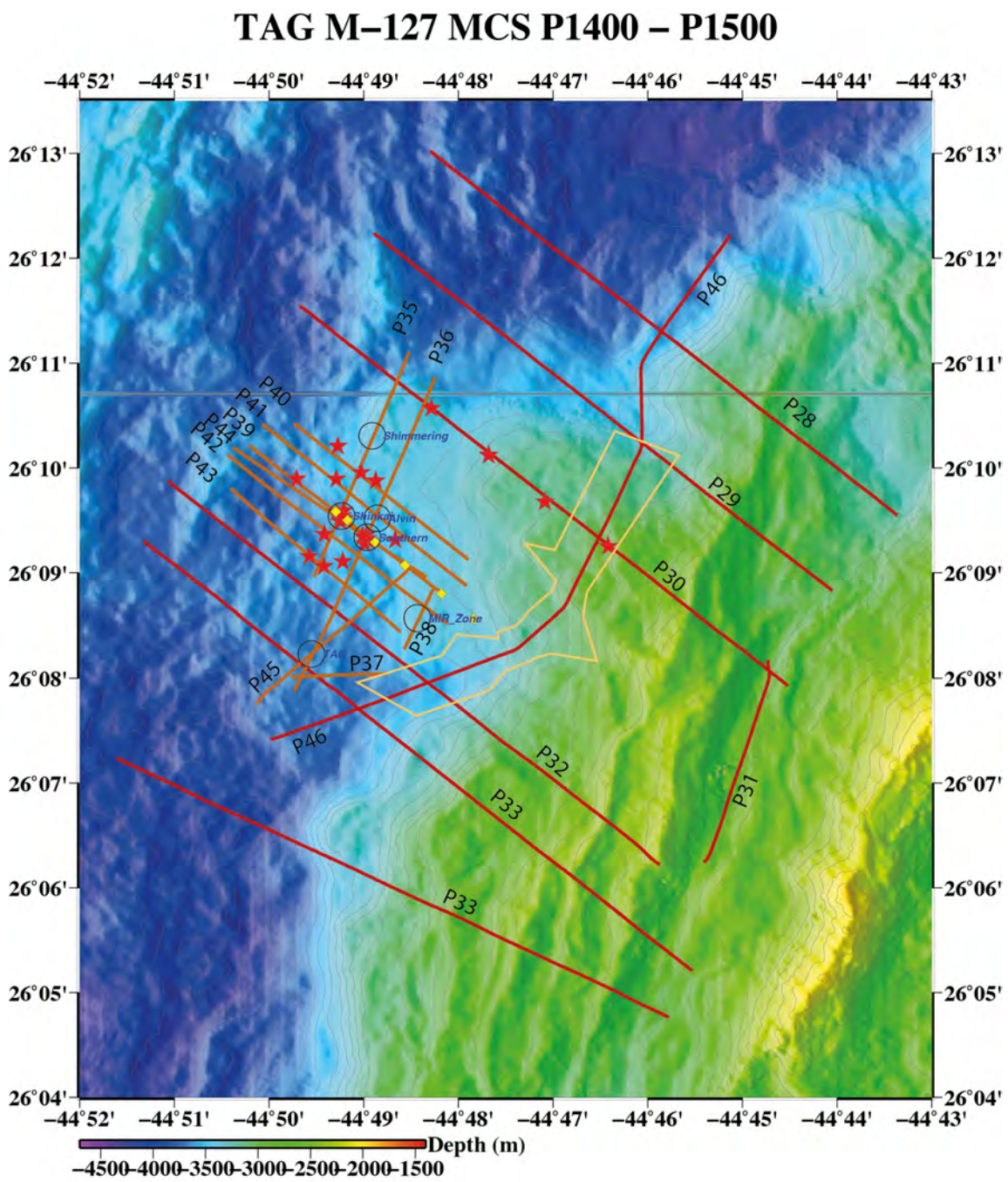

Fig 5.3.3: *Map of airgun profiles P28 to P46. After recovery of OBH22 to OBH25 and redeployment of OBH28 to OBH31 all instruments recorded these lines. Profiles P28 to P34 were shot with the G-gun cluster, while profiles P35 to P46 were shot with the double GI airgun.*

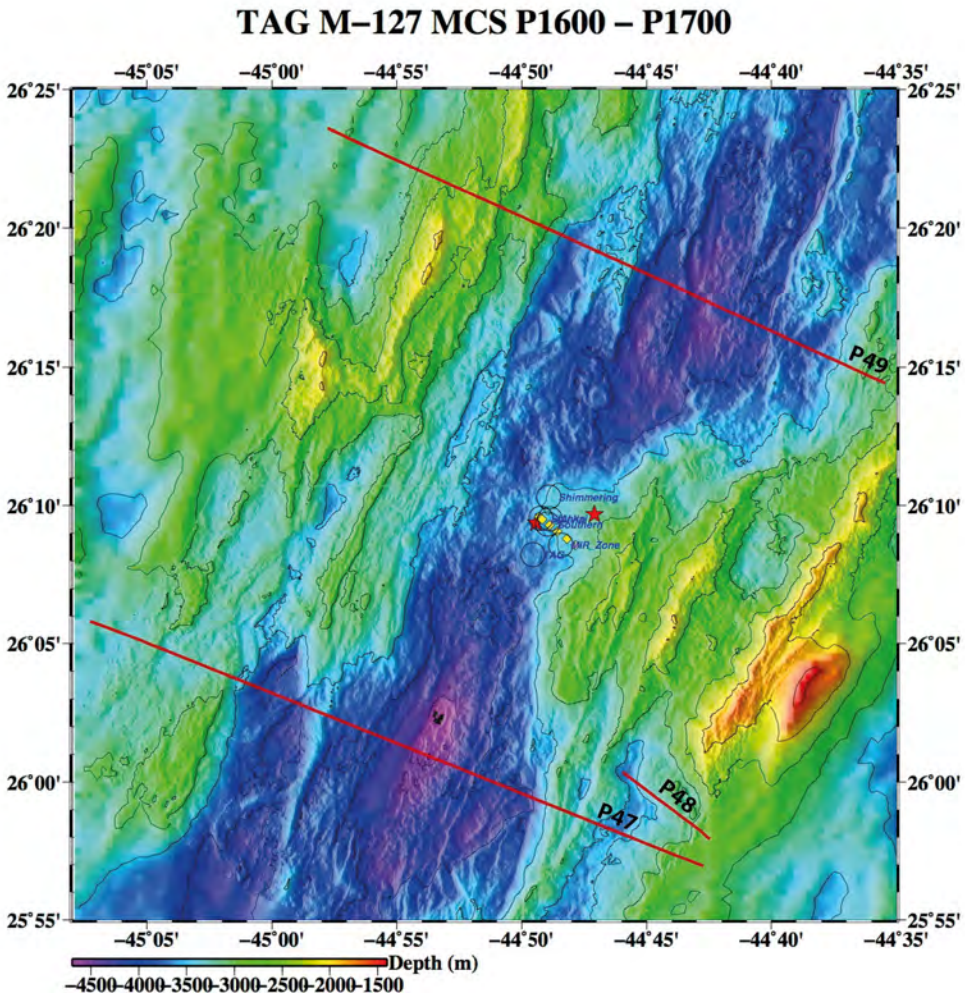

Fig 5.3.4: *Map of airgun Profiles P47 to P49. The G-gun cluster served as source while the remaining OBH17 and OBH30 did record the source signals.*

5.3.2 OBS

Within the Blue Mining proposal, 20 OBS systems (4 components) were quoted for seafloor seismic observations. However, GEOMAR could provide another 5 OBH (single component) for additional observations of the airgun shots. Pre-cruise modelling (deliverable D2.21) suggested an OBS offset of about 75 m only for the central part of the mounds. Further instruments should be deployed along crossing seismic profiles in the offset of 350 m and 750 m. The long record of experience with the GEOMAR OBS let us trust in a reasonable precise bottom positioning with free fall deployment of the 350 m and 750 m offset instruments. With respect to the short offsets and the expected rough topography on the mounds it was decided to deploy those instruments using HYBIS as a video guided propelled deployment frame hanging on a deep-sea cable. For this purpose the sample grab was replaced by a newly build OBS deployment carrier. New LED lights and improved camera systems completed the HYBIS upgrade for this mission. Ten instruments were sucessfuly deployed during three to four hours long diving missions distributed over three days. During these missions, video observation of the designated deployment site was undertaken. Due to the observed roughness of the seafloor the scheduled deployment positions were modified when a reasonable flat seafloor came into sight. One of the additional five OBH

was used to fill a gap in the OBS deployment geometry, while the remaining four instruments were used for investigations of the Shimmering mounds area.

In order to provide the best record capabilities nine of the long time used MBS data logger devices were replaced by the new GEOMAR GEOLOG generation. GEOLOG does provide reduced power consumption by increased bandwidth for the hydrophone component and an atomic clock based autononmous time base. All OBS and OBH devices were operated at 1 ms sample rate.

The deployment of OBS and OBH was done along three 2D profiles. A WNW-ESE trending profile crosses Shinkai and Southern Mound while two additional NNE-SSW oriented parallel profiles provide rectangular observations of the two mounds. The western profile was extended to cover Shimmering mounds as well. First all three profiles and deployment positions were crossed while later additional profiles with various offsets were shot to provide additional fan observation for a 2.5D interpretation.

During relocation of the OBS it turned out that the instruments deployed in free fall mode drifted far further away from their surface deployment position as usually expected (Fig. 5.3.5). As this has never been observed before it was assumed that the new squared shape of the floatation does serve as a plane during descend in the water column. This is not the case for the former tube shaped floatation, which allows more water to penetrate between the individual floatation bodies. As almost all instruments drifted in NW direction, the direction of the major surface current observations, it was assumed that NW water currents are active over a significant water depth.

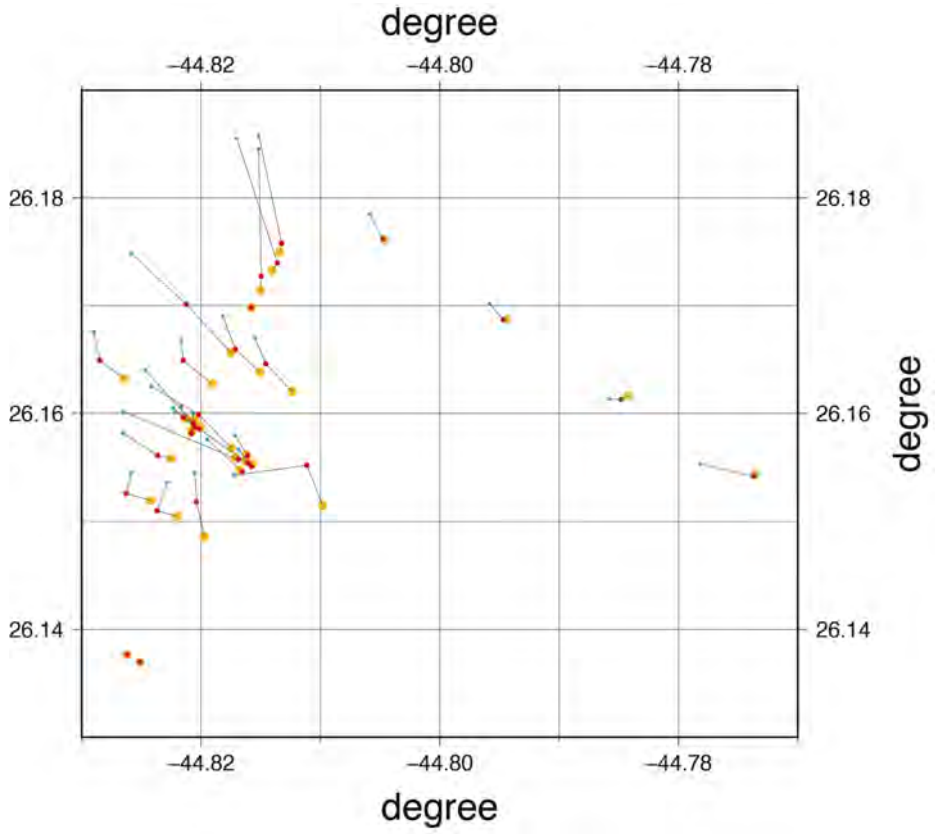

Fig 5.3.5: *Map with drift indicators for the deployed ocean-bottom instruments. Yellow dots indicate the sea surface drop position, while red points indicate the relocated position at the seafloor. Blue dots indicate the surface recovery position.*

Reflection events of the raw OBS data can be correlated with corresponding reflections in the streamer sections. Comparison of the near seafloor events do show a depth resolution of about 50 m for the OBH data as shown in the comparison of an OBS dataset with the corresponding streamer section (Fig. 5.3.6). This is in the range of the expected extension of the sulfide mounds. However, events in the multiple are of much higher frequency and promise for higher resolution after sophisticated processing.

On 13.06.16 an earthquake was recorded during seismic profiling (Fig. 5.3.9). As the OBS/OBH recorded continuously during the entire period of deployment their data sets were quickly checked for passive events especially during the gaps of active source profiling. Without using any detection code an average of 25 earthquakes per day could be identified. This sums up to more than 250 local and regional events during the time when OBS and OBH have been on the seafloor. With the 3D distribution of the instruments above the young developing oceanic core complex an analysis of the deeper structure by passive seismology should be possible.

The observation of young corrugated seafloor expressions and their continuation to depth underneath the hanging wall as interpreted from the multichannel reflection seismic data (Fig. 5.3.11) lead to an inspection of the corresponding arrivals on OBH28 to OBH31. Although the downward dipping top of the corrugated surface could not be identified in a first quick check of the data a second event parallel to the surface could be imaged and modelled with the OBH data of stations OBH28 to OBH31 (Fig. 5.3.7). The velocities of the model are relatively high from the seafloor down to depth. This was expected and confirms thin sedimentation above the volcanic basement. With dip towards the ridge axis velocities become higher. Refracted events observed on the OBH with variable lateral extend need later confirmation but showed to be in the range of 7 km/s and above. Hence, shallow Moho events seem to be recorded along profile P30. The layer boundary modelled here corresponds to the second lower reflection event shown in Fig. 5.3.11.

5.3.3 Surface streamer

2D multichannel seismic profiles were acquired using a 192 channels streamer with 1.5 m group offset (268 m active length) along all seismic tracks. The streamer is comprised from 12.5 m long sections. The 14 sections closest to the vessel are oil filled, while the remaining 10 sections are manufactured as solid-state sections. For the oil filled part three birds were used to secure a towing depth of 3 m. However, due to the variable sea state during the cruise depth variations between 2 m and 4 m were observed. For the solid-state sections no active depth control was available, as bird coils are not foreseen in this type of streamer. Streamer ghost effects observed with the second half of the streamer suggest that these sections might have been deeper than the scheduled 3 m. During deployment, additional floatation was tested with these sections but it seemed to keep the sections on the sea surface and was taken off again. Records were done at 0.5 ms sample rate with a record length of 8 s, which includes the first multiple. Onboard brute processing of the multichannel data include trace Q/C, bandpass filter of 25-55-400-500 Hz, stacking and time migration. Group offset and shot rate allow computing brute sections with trace spacing of 1.5 m.

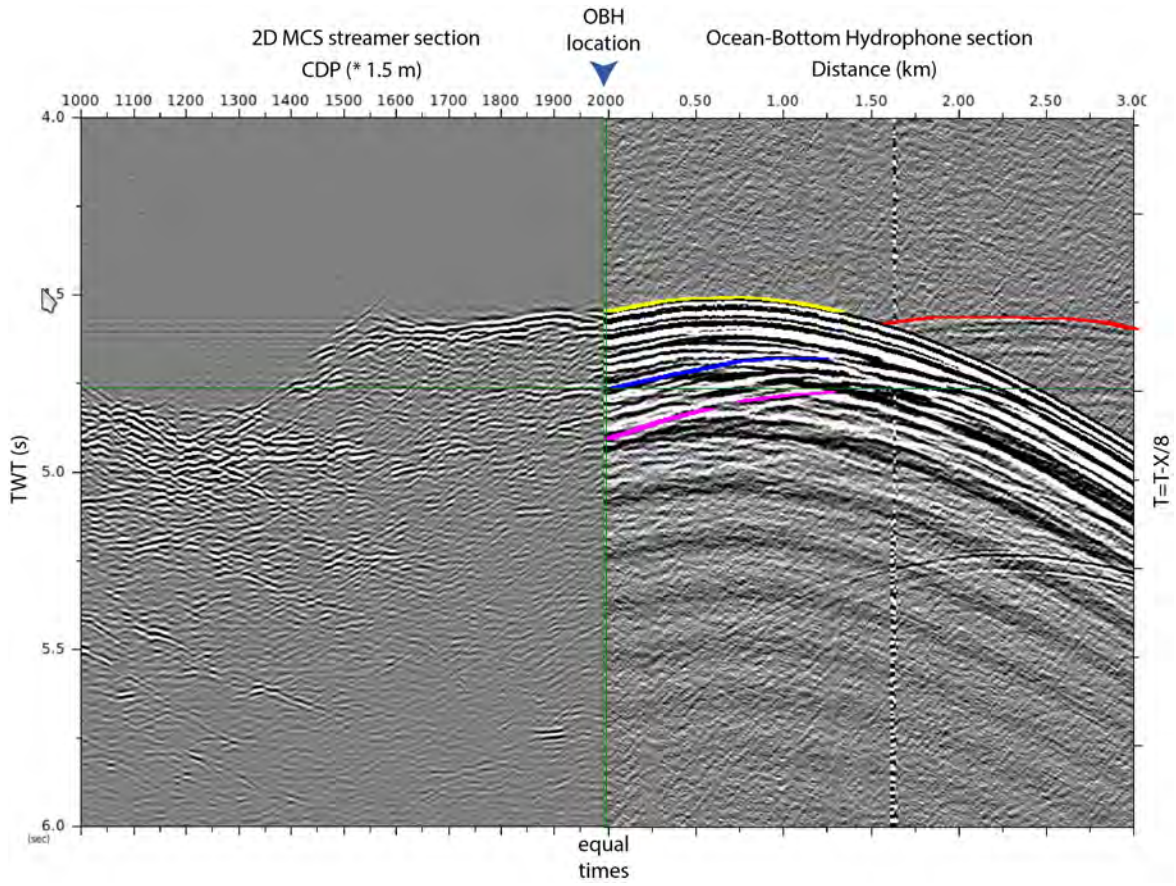

***Fig 5.3.6**: Comparison of multichannel streamer section of profile P30 (left) with a hydrophone section from OBH30 (right). Both sections are connected at the seafloor location of OBH30. Here, traveltimes of both sections are almost vertical and are corresponding. Yellow marked event of the OBH section is the seafloor reflection, Blue and purple lines mark later events that correspond with increased amplitude events at depth in the streamer section. Red picks in the OBH section indicate refracted energy corresponding to the uppermost layers of the profile.*

Figure 5.3.8 shows an example of profiles P36 and P44 crossing at Southern mound (Fig. 5.3.3). Both lines were shot with two GI airguns. As expected in this ridge axis environment the reflection image is dominated by short ranging reflecting events of variable dip direction. The young crust has not yet developed clear layers and has been deformed by fracturing and uplift. However, several events are visible from within Southern Mound and should provide information on internal structure and extension. On top of the seismic data seafloor depth of the onboard multibeam has been displayed. It is clearly visible that there is a significant mismatch. Faint reflections above the picked seafloor and within the expected topographic footprint of the bathymetry indicate that the streamer has not crossed Southern mound at its centre but did record some diffracted energy from the peak. Consequently, navigation of the streamer need to be adjusted and interpretation of the data need to take care for this situation. Nevertheless, the resolution of the MCS data does allow the investigation of the mounds as planned.

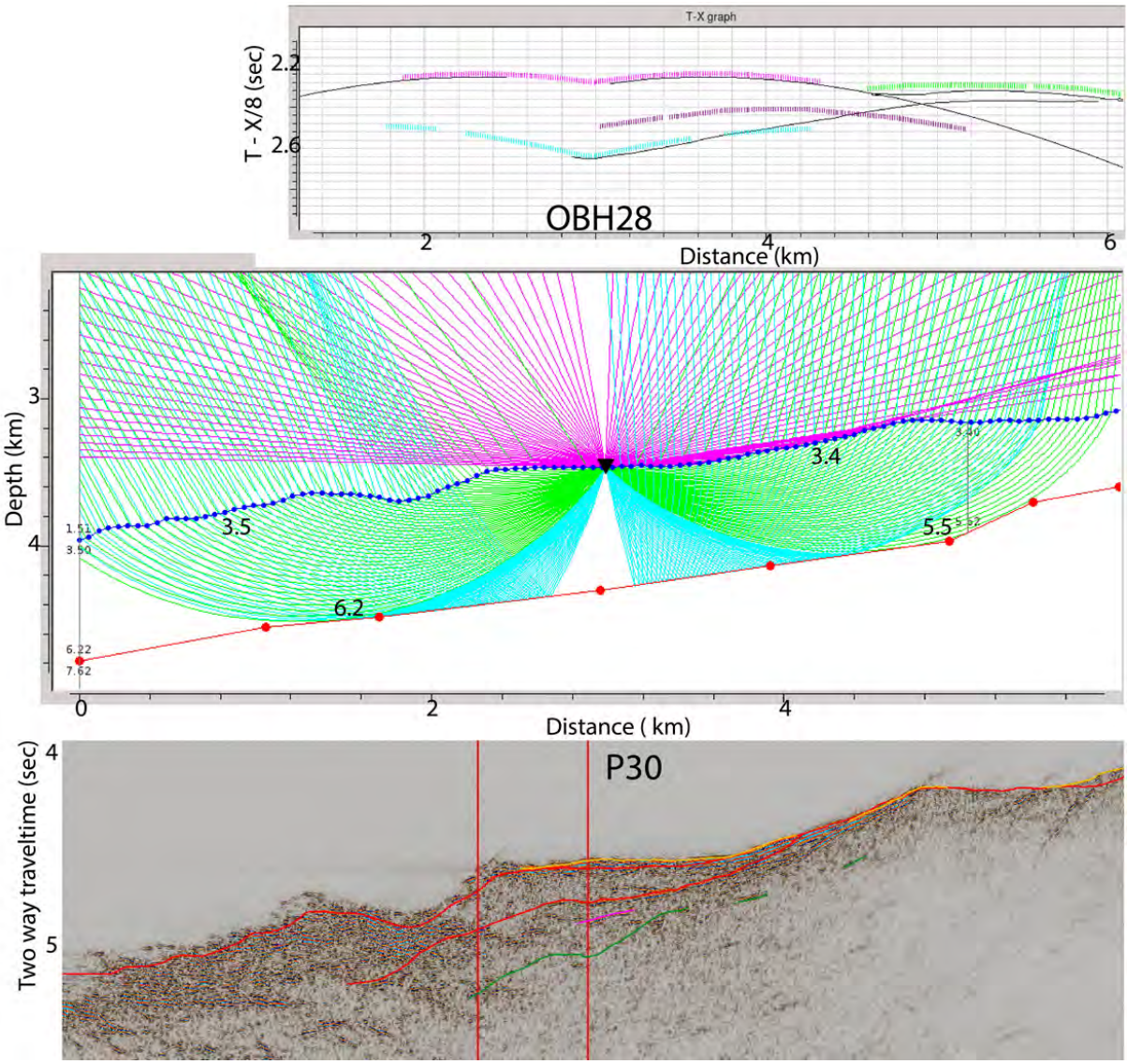

Fig 5.3.7: *OBS model of profile P30. High velocities (depth model in the middle) increasing with westward dip towards the ridge axis confirm thin sedimentation. As an example of the coverage only rays calculated for OBH28 are shown in the top of the figure. The modelled interface corresponds well with the second and deeper (green) reflection events identified on the MCS data of profile P30 (bottom).*

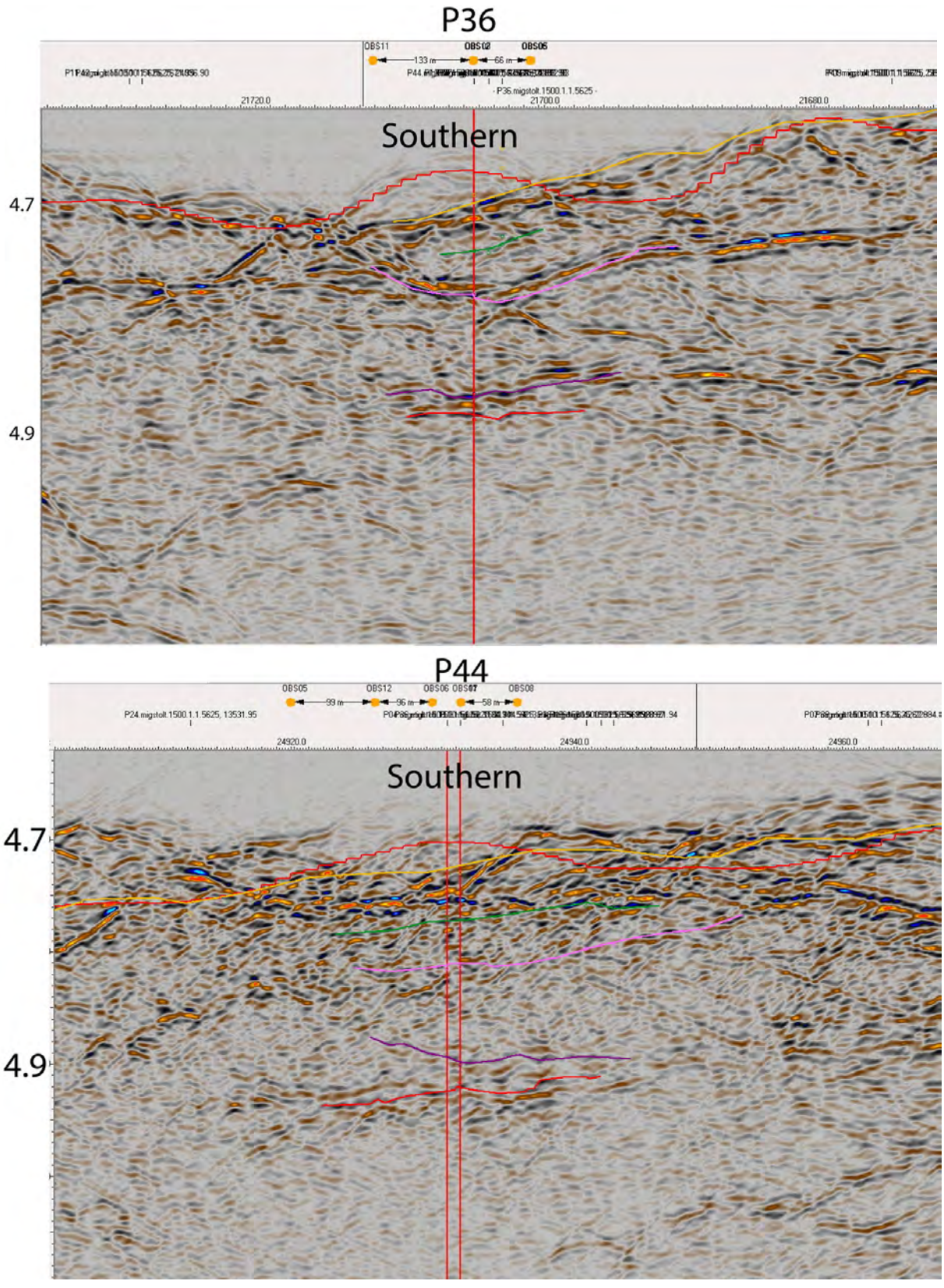

Fig 5.3.8: *Time migrated seismic sections of profile P36 and P44 across Southern mound. The picked seafloor is indicated in yellow, while the red line shows the time converted expected seafloor depth drawn from the multibeam bathymetry. The offset between expected seafloor depth and measured seafloor indicates that the streamer did not cross the mound at centre and navigation need be adjusted.*

During the night watch on Monday 13.06.16 an unusual event was observed. All hydrophone channels were overdriven for a single shot. Inspection of a single channel display showed that accidently an earthquake took place while the streamer was recording (Fig. 5.3.9). P and S arrival were well separated and appeared with much stronger energy than the airgun shots. A quick estimation based on travel time delay between P and S arrival, neclecting slow sediment velocity contribution, resulted in an assumed hypocentre distance of about 7 km. With respect to the tectonic structure of the working area the event is interpreted as normal slip event that might have taken place right underneath the OBS/OBH network.

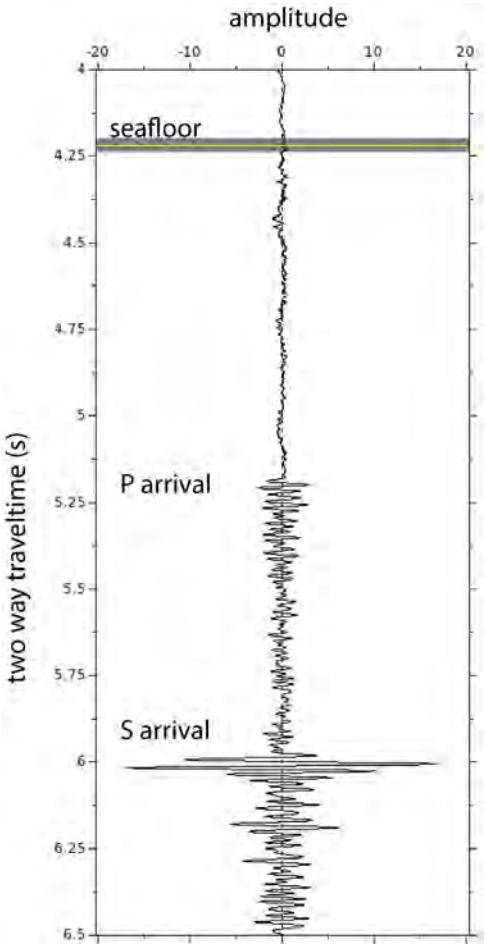

Fig 5.3.9: *Single channel display of an earthquake recorded on 13.06.16 at 03:15 UTC with the multichannel streamer. Due to the strong energy of P and S wave arrival the onset of the seafloor is marked by the green line. A quick traveltime estimation reveals that the hypocentre should be expected at about 7 km offset.*

With the high-resolution AUV multibeam mapping small scale topographic undulations become visible that were less well expressed in the shipboard multibeam maps. Among such features is the discovery of a short section of exposed seafloor with well expressed corrugations, the birth of an oceanic core complex. Although map data were recorded after deployment of the OBS/OBH network and after the multichannel seismic survey it happened that some of the lines did cross this feature (Fig. 5.3.10). Within profile P30 the upcoming young seafloor with its corrugations could be imaged downdip well beyond the hanging wall (Fig. 5.3.11).

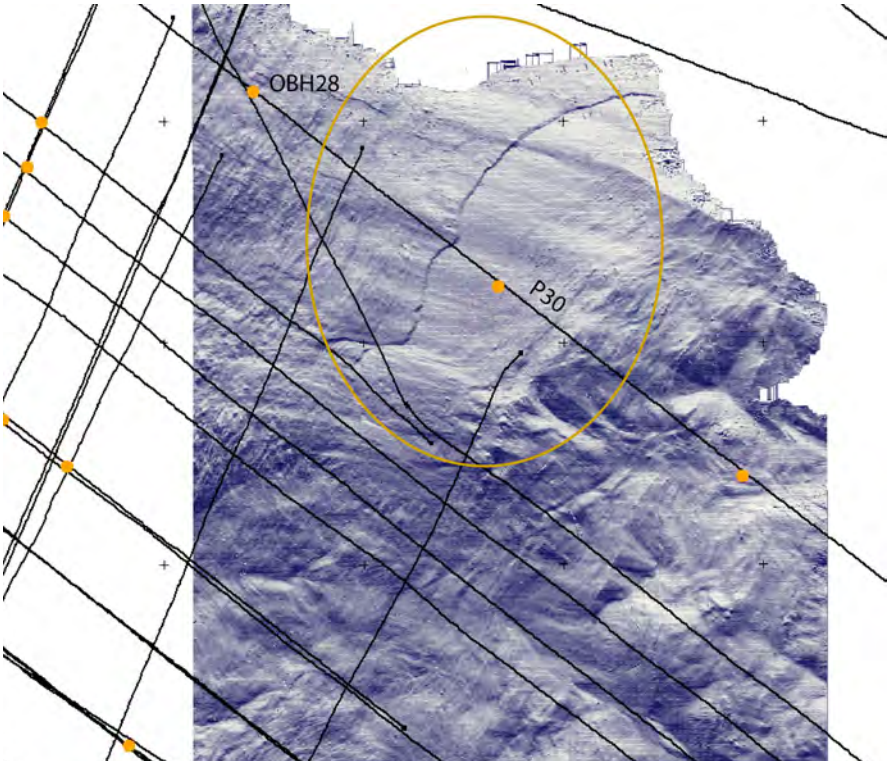

Fig 5.3.10: *With the AUV mapping small scale strucutres like this young corrugated surface become visible. Fortunately the OBH28 to OBH30 did cover this region as well as some of the seismic profiles.*

A second slightly deeper reflection event does not appear as continuous but could be correlated with a well-pronounced event on the OBH recordings (Fig. 5.3.11). The cross cutting profile P35 does show the event of the top of the down dipping corrugated surface and seems to show a similar topography. Further processing and interpretation will better image this event on the other lines as well. Furthermore it should be possible to identifiy the depth to which the corrugations can be followed.

5.3.4 Deep-towed streamer

The deep towed streamer device was successfully applied during test cruise POS-484 in 2015 acquiring data across the eSMS deposits of the Palinuro volcanic complex in the Mediterranean. During a first deployment on cruise M127 data connection was broken when the system was lowered to about 1200 m water depth. After recovery it turned out that the system carrier must have done a full 360° turn during deployment spooling the data cable of the streamer. During this unforeseen operation, the security loop in the streamer cable became too short and the 300 V power connector was pulled while emersed in water. Fortunately the bulkhead plug served as melting fuse and prevented the electronics from damage. After improvement of the tow point on the system carrier and repair of the connector a second dive was undertaken. Again, the connection of the streamer was lost at about 1400 m water depth. This time the Chinese fingers, which should take the towing stress of the streamer cable slipped and the power connector was pulled under water again. A failure in the power distribution of the system could be repaired. While the digitisers of the hydrophone nodes could be addressed, they failed to deliver data records after this second deployment failure. Despite intensive inspection the cause of this failure

could not be identified and repaired with onboard capabilities. Unfortunately the deep towed service could not be completed for this cruise.

As the surface streamer did proof to deliver excellent data quality by that time already it was decided to use the scheduled working time for additional surface streamer profiles, which add further fan observations to the deployed OBS and OBH network.

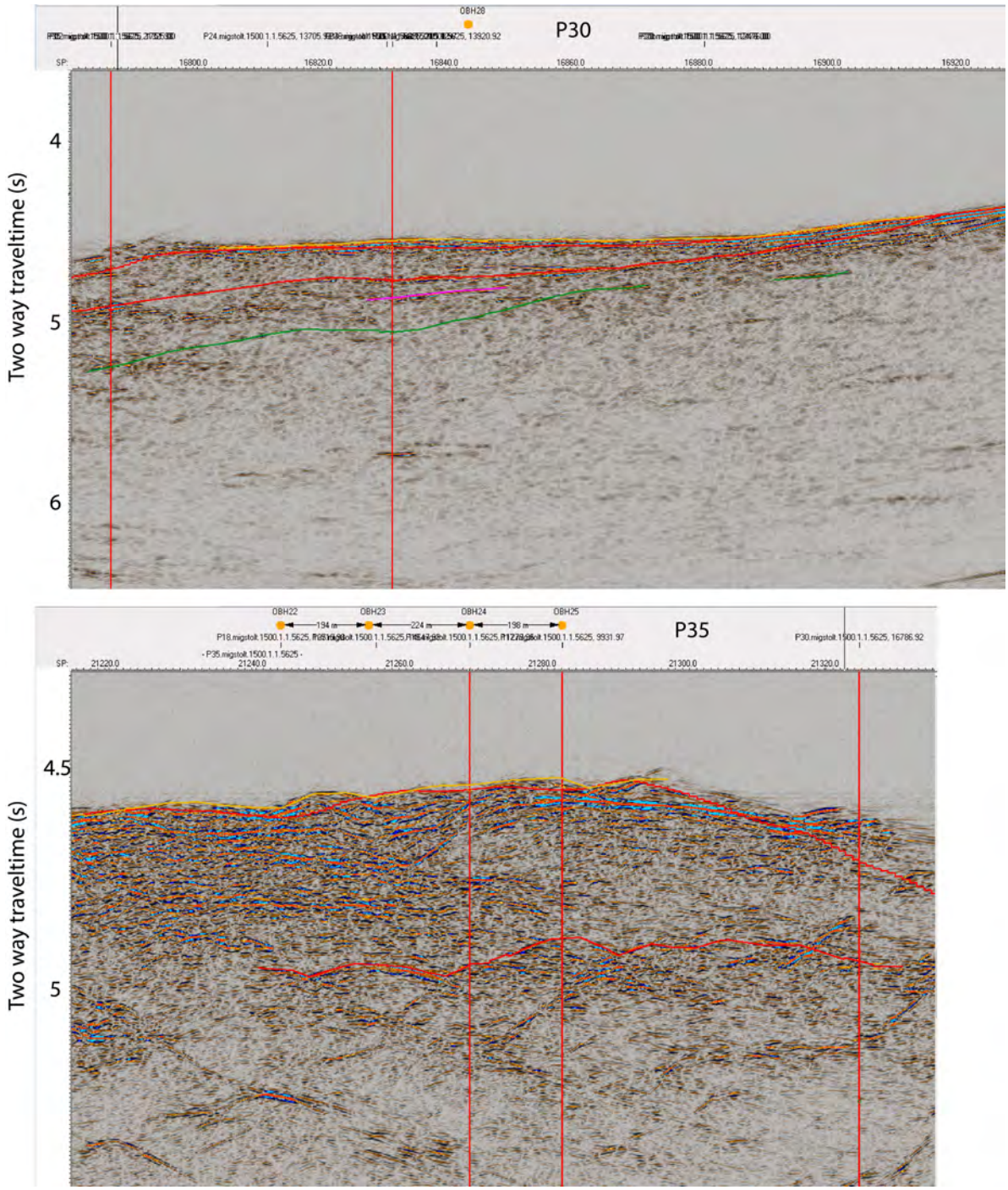

Fig 5.3.11: *The downward dipping corrugated surface could be well imaged in profiles P30 (top) and P35 (bottom). The red line indicates the young seafloor and its continuation underneath the hanging wall. On the cross profile the continued undulations of the corrugations are still visible. A second less continuous reflector parallel to the dipping surface could be well correlated with a prominent reflection in the OBH (Fig. 5.3.9).*

5.3.5 OBEM

Magnetotellurics is a passive electromagnetic geophysical method for imaging the electrical resistivity structure (reciprocal to conductivity) of the subsurface. Electrical resistivity varies strongly due to temperature and presence of fluids, such that this type of measurement is of great interest in the investigation of a mid ocean ridge system. The method is based on the observation that naturally occurring fluctuations of the Earth's magnetic external field induce electric currents whose strength and distribution depend on the subsurface resistivity.

Variations of the horizontal electric and three-component magnetic fields are recorded on the ocean bottom to derive a spectral, complex-valued impedance tensor Z given by Z Hh = Eh where Eh and Hh denote the frequency-dependent horizontal electric (Eh) and magnetic (Hh) field vectors. In a homogenous half-space, the so-called skin depth d is a crude estimate of detection depth with d = sqrt (r T) in kilometers, (where T is the period in seconds and r is the bulk resistivity). At periods shorter than approximately 1 s, seafloor electromagnetic signals are very small. This is due to the high conductivity of the sea water above, which causes attenuation according to skin depth and thus reduces the resolvability of shallower sea-bottom features.

Six OBEM stations were deployed during cruise M127 (Fig. 5.3.1). The systems are designated to be recovered after a recording time of approximate two months when RRS JAMES COOK returns to TAG field for the second Blue Mining cruise. As the systems can remotely be switched from passive to active CSEM recording precise positioning informations at the seafloor are essential. Therefore, the instruments were deployed with the deep-sea cable, using an acoustic release transponder. Due to the water resistivity of the four 5 m long electrode levers the instrument descends with 0.67 m/s only. Hence, the deep-sea cable was lowered with 0.5 m/s winch speed only. POSIDONIA USBL system was used to provide coordinates of the acoustic release transponder at the time of release of the OBEM station at about 50 m above seafloor.

Fig 5.3.12: *Photograph of deployed OBEM01 taken from the video camera of HYBIS during the deployment of OBS02.*

5.4 Gravity Coring

(F. Barriga, F. Besson, A. Dutrieux, S. Graber, A. Lichtschlag, S. Martins, I. Stobbs)

Overall 35 gravity core stations (3 m length, 125 mm diameter, 600 to 900 kg weight on top) were completed during M127. Of these, 33 stations were in the TAG Hydrothermal Field area and two additional stations were taken as reference stations about 15 km east of TAG (26°05.485N - 44°38.770W). Locations of possible coring stations (Table 5.4.1) were selected with the help of the high-resolution AUV bathymetry and backscatter data. Twenty-three of the cores contained abundant sediment, 8 contained only fragments of gravel, basalt and traces of sediments in the core catcher and 4 were completely empty. Among the 23 sediment cores, 10 had visible indications of hydrothermal-influenced sediments; the other cores had the visual appearance of background sediments (carbonate ooze), but 2 cores showed layers of volcanic origin.

Table 5.4.1: Details of gravity coring stations obtained during M127. Positions are POSIDONIA recordings (CC = core ctacher).

Station	Latitude	Longitude	Depth	Recovery	Comment
M127/576GC	26°10.422'N	44°48.318'W	3434m	1.16 m	Carbonate ooze
M127/583GC	26°09.659'N	44°48.818'W	3510m	0.01m	Few pieces of basaltic glass in CC
M127/584GC	26°08.772'N	44°49.140'W	3605m	-	Empty
M127/589GC	26°08.779'N	44°49.134'W	3600m	-	Empty
M127/590GC	26°08.228'N	44°49.383'W	3628m	0.01m	Only few pieces of basaltic glass in CC
M127/600GC	26°09.184'N	44°49.042'W	3559m	0.02m	Only few pieces of basaltic glass in CC
M127/601GC	26°08.422'N	44°49.401'W	3664m	0.02m	Some sediments with basalt fragments in CC
M127/615GC	26°07.863'N	44°48.180'W	3555m	1.08m	Carbonate ooze with 2 shelly layers
M127/616GC	26°09.391'N	44°48.464'W	3500m	1.31m	Carbonate ooze overlying brown to red silty-sandy layers with a few gray volcaniclastic layers
M127/617GC	26°09.253'N	44°48.519'W	3462m	0.64m	Carbonate ooze
M127/626GC	26°10.401'N	44°48.747'W	3407m	1.20m	Carbonate ooze overlying brown to red silty-sandy sediments and basalt fragments
M127/627GC	26°09.139'N	44°48.860'W	3519m	3.14m	Repeating series of brown-red-orange silty-sandy sediment layers with some sulfide beds
M127/628GC	26°09.635'N	44°49.270'W	3558m	-	Empty
M127/636GC	26°09.088'N	44°49.540'W	3604m	1.08m	Carbonate ooze
M127/637GC	26°07.986'N	44°48.726'W	3639m	0.01m	About 0.1cm of basalt fragments, glass and red fragments in CC
M127/638GC	26°08.015'N	44°50.152'W	3753m	0.20m	Carbonate ooze
M127/644GC	26°09.006'N	44°48.695'W	3515m	2.69m	Repeating series of brown-red gravel and silty-sandy sediment layers and red-green patchy layers
M127/645GC	26°08.713'N	44°48.725'W	3562m	1.31m	Carbonate ooze with one brown layer
M127/647GC	26°09.146'N	44°48.858'W	3520m	3.00m	Repeating series of brown-red-orange silty-sandy sediment layers with few sulfide beds
M127/649GC	26°08.534'N	44°48.245'W	3423m	1.78m	Carbonate ooze overlying brown to red silty-sandy sediments with a few gray "ash" layer
M127/666GC	26°08.593'N	44°46.920'W	3000m	0.37m	Carbonate ooze with 1 light brown layer and grey volcaniclastic layers
M127/667GC	26°08.161'N	44°47.095'W	2992m	0.03m	Few basalt fragments and shells in CC
M127/681GC	26°10.444'N	44°49.076'W	3510m	3.00m	Carbonate ooze overlying repeating series of brown-red silty-sandy-gravely sediment layers
M127/682GC	26°10.243'N	44°48.706'W	3445m	2.81m	Carbonate ooze overlying repeating series of brown-red silty-sandy-gravely

Station	Latitude	Longitude	Depth	Recovery	Comment
					sediment and patchy layers
M127/683GC	26°08.341'N	44°49.933'W	3700m	0.15m	Carbonate ooze in CC
M127/690GC	26°10.774'N	44°49.041'W	3644m	0.80m	Carbonate ooze
M127/691GC	26°08.417'N	44°47.184'W	3067m	0.66m	Carbonate ooze
M127/692GC	26°08.559'N	44°48.397'W	3422m	0.79m	Carbonate ooze overlying patchy red-brown-green gravel layers
M127/693GC	26°08.466'N	44°49.917'W	3654m	0.71m	Brown-beige gravel with some sediments
M127/700GC	26°10.053'N	44°48.027'W	3345m	0.08m	Empty, with basalt pieces stuck in the core catcher
M127/701GC	26°09.367'N	44°47.611'W	3248m	0.02m	Some carbonate ooze and basalt fragments in CC only
M127/702GC	26°09.436'N	44°49.063'W	3560m	0.92m	Brown silty-sandy sediment with green patches
M127/703GC	26°09.984'N	44°48.576'W	3460m	3.00m	Carbonate ooze overlying dark brown-red-green gravel
M127/710GC	26°05.485'N	44°38.763'W	2137m	-	Empty
M127/711GC	26°05.485'N	44°38.770'W	2130m	3.00m	Repeating series of beige and thin light-brown carbonate ooze and shelly layers

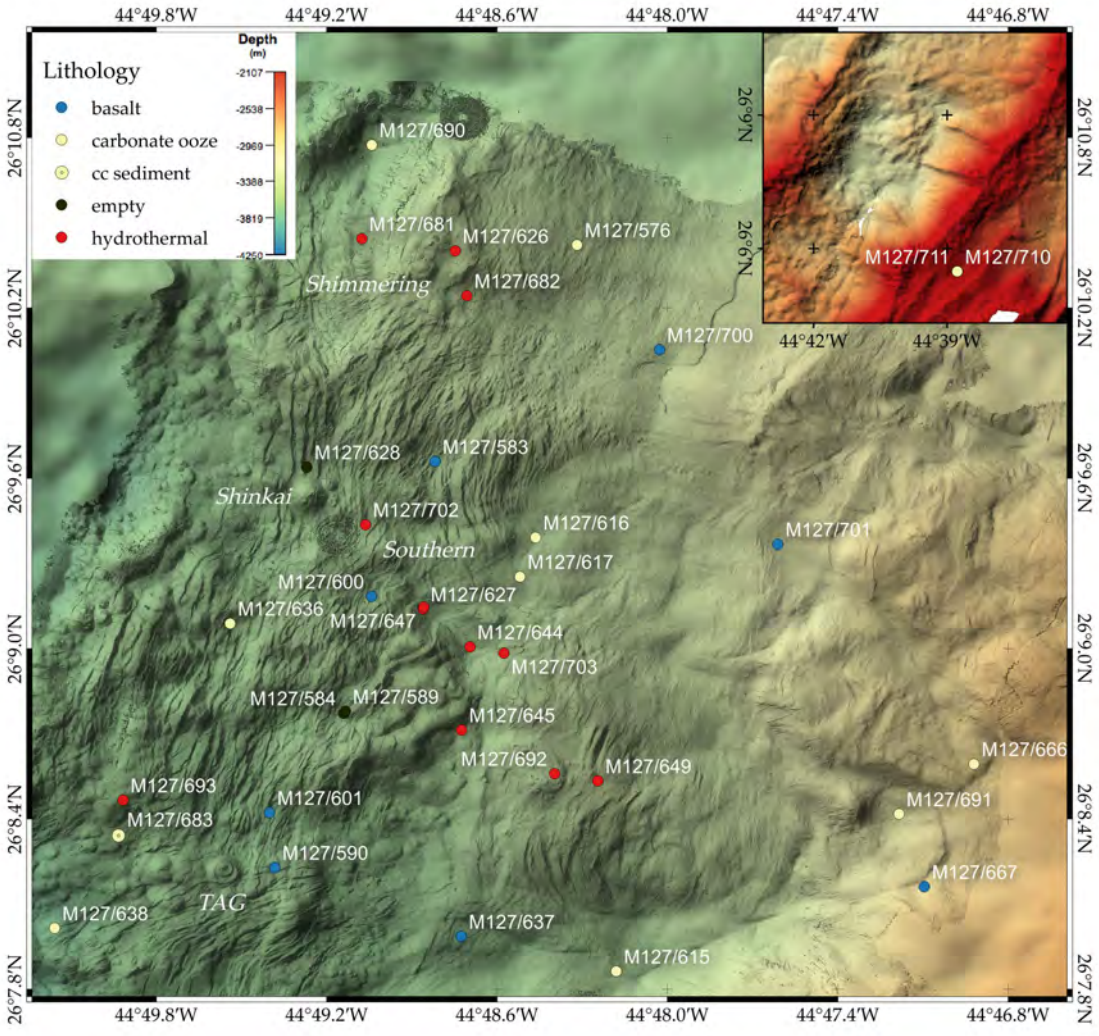

Fig. 5.4.1: *Map showing the locations of gravity corer stations within the TAG Hydrothermal Field; the insert shows the locations of the reference coring stations high on the eastern flank of the segment. The lithology retrieved in the cores is shown by the colour of the circles; blue: cores with fragments of basalt and/or volcanic glass; yellow: carbonate ooze; yellow with dot: carbonate ooze in the core catcher only; black: empty; red: hydrothermally influenced sediments.*

Upon recovery, the first operation was the removal of the core catcher and measurement of several parameters (pH, Eh and temperature) with a multiparametric probe in the sediment, if present. The liners loaded with sediment were cut into 1 m long sections and the ends were sealed with caps, after measurement of properties. The core sections were subsequently transported to a controlled temperature room (7 °C) for pore water extraction (see Fig. 5.4.2). After pore water sampling, the core sections were split longitudinally using a hand-held, power disc-saw, opened in two halves, photographed (as well as permitted by conditions), described and subsampled (see Fig. 5.4.2). After subsampling both halves were stored in plastic sleeves flushed with N_2 and heat-sealed. The working half of the core was frozen at -20°C (final destination FFCUL Lisbon). The archive half remained undisturbed and is going back to GEOMAR.

5.4.1 Pore water sampling

(A. Dutrieux, A. Lichtschlag, I. Stobbs)

For pore water sampling, holes were drilled into the liners at selected intervals (usually 5 cm intervals in the first 50 centimetres, 10 cm intervals up to 1.50 m, and 20 cm intervals up to 3 meters) and water was extracted with Rhizon Soil Moisture samplers (Fig. 5.4.2). These samplers consist of a small microporous polymer tube (approximately 0.2 μm pore size) that is supported by a stabilizing glass fibre wire and connected to a PVC tube (*Seeberg-Elverfeldt et al., 2005*). The pore water was recovered using negative pressure produced by the attached 10 mL syringes (Luer-Lock connection). Small dead volume (< 0.5 mL) allows sampling of very small volumes of pore water. The applied method permitted extraction of the pore water with minimal disturbance of the sediment. To minimize it furthermore, the pore water was collected along the splitting line. The first 0.5 mL of the pore water samples were discarded. Oxidation of pore water and sediments samples by air was minimized by (1) connecting the Rhizon soil moisture samplers to syringes before the core section was opened and (2) covering drilled holes with oxygen impermeable tapes while no Rhizon was inserted. About 10 mL was collected for every interval and has been distributed in following aliquots: (i) 2 mL for cations in acid cleaned 7 mL plastic vials; (ii) 1.5 mL for anions and dissolved sulfide in Eppendorf cups prefilled with 0.5 mL of 2% Zinc acetate (iii) 2.2 mL for dissolved inorganic carbon (DIC) filled without headspace in glass vials; (iv) 2.2 mL for total alkalinity (TA) filled without headspace in glass vials and (v) approximately 2 mL frozen in plastic vials at -20°C for nutrient analyses.

After sampling, the aliquots for cations were acidified with 5 uL of suprapur concentrated nitric acid to prevent metal precipitation. DIC and TA were poisoned with mercury chloride (1%) to prevent microbial turnover. At NOC Southampton cations will be analysed by ICP-OES/ICP-MS; TA measurements will be conducted by titration, anions (chloride, sulfate, bromide) will be measured by ion chromatography and sulfide by photospectrometry (Cline 1970). Nutrients (ammonium, silica, phosphate) will be measured with a nutrient analyser. Overall 411 pore water samples have been collected (see Appendix). When a core had indications of hydrothermal influence (i.e. targeting a hydrothermal area or the core catcher/the end of the sections had the typical red color), narrower intervals (5 cm) have been sampled.

On the first cores, oxygen micro-profiling has been conducted, but hard layers and non-transparent core liners made the measurement impossible without breaking the sensitive probe.

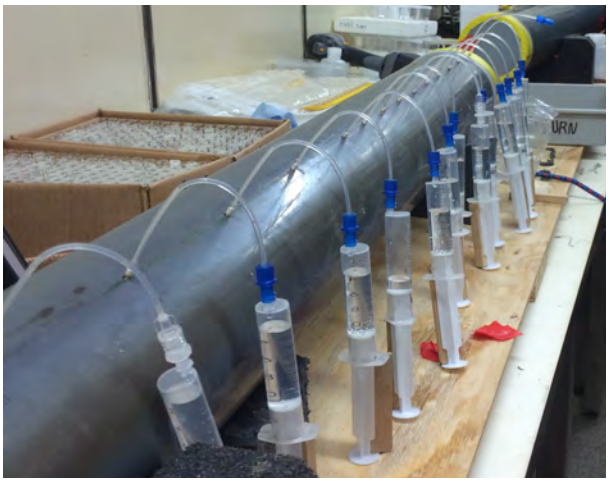

Fig. 5.4.2: *Pore water sampling using Rhizon soil moisture samplers (photo Florian Besson).*

5.4.2 Sediment description and subsampling

Several photographs were taken of each half-core (representative examples in Fig. 5.4.3 and 5.4.4). Additionally, visual core description sheets were produced. These include the lithotype and features (lineations, faults, gradations, impregnations, bioturbation, etc) general description, subsampling positions and various numerical data (colorimetry, multi-parameters, etc). See Appendix 3 for the individual sheets.

Several cm^3 of sediment have been sampled at approximately the same depth as the pore water extraction (shifted by about 1 cm), along the opposite side from the drilled holes. A subsample, taken with a cut-off syringe is stored at 4°C for porosity and density measurement. Gravel layers have not been sampled for porosity. Another subsample of the sediment was frozen in a plastic bags for isotopic measurements such as ^{210}Pb (determining the bioturbation mixing layers), ^{14}C dating and/or U-Th series dating (most likely $^{230}Th_{excess}$ and $^{231}Pa_{excess}$ dating methods) with α-spectrometry or γ-spectrometry at NOCS. In addition 3 cm^3 of sediment have been sampled in hydrothermally-influenced cores for methane analyses by gaschromatography. The volume was transferred to a glass vial filled with 5mL of NaOH, crimp-sealed, and the vials are stored upside-downed to avoid any gas leakage.

5.4.3 In-situ measurements with portable instruments (pH, Eh, temperature, Colorimetry, XRF, XRD, PIMA)

(F. Barriga, S. Martins, F. Besson)

Immediately upon core recovery, the accessible ends of core sections, including core catcher, were tested for pH, Eh and temperature with a single, multi-sensor probe (Lange senSION + portable meter and 50 45 Probe). After pore water extraction and sediment subsampling, new measurements of pH, Eh and temperature were undertaken at precisely the same locations as the

subsampling for FFCUL. The instrument was frequently calibrated, and about 1000 measurements were recorded.

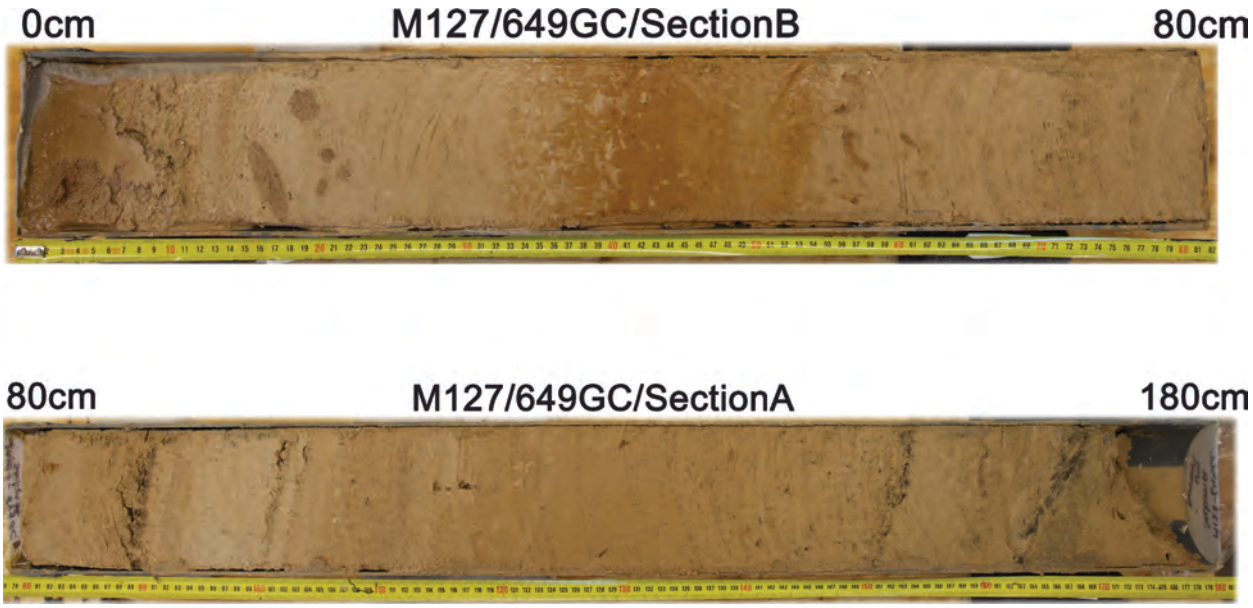

Fig. 5.4.3: *Core M127/649GC/SectionsA+B. Carbonate ooze with relatively minor hydrothermal impregnations and thin volcaniclastic layers in some core intervals.*

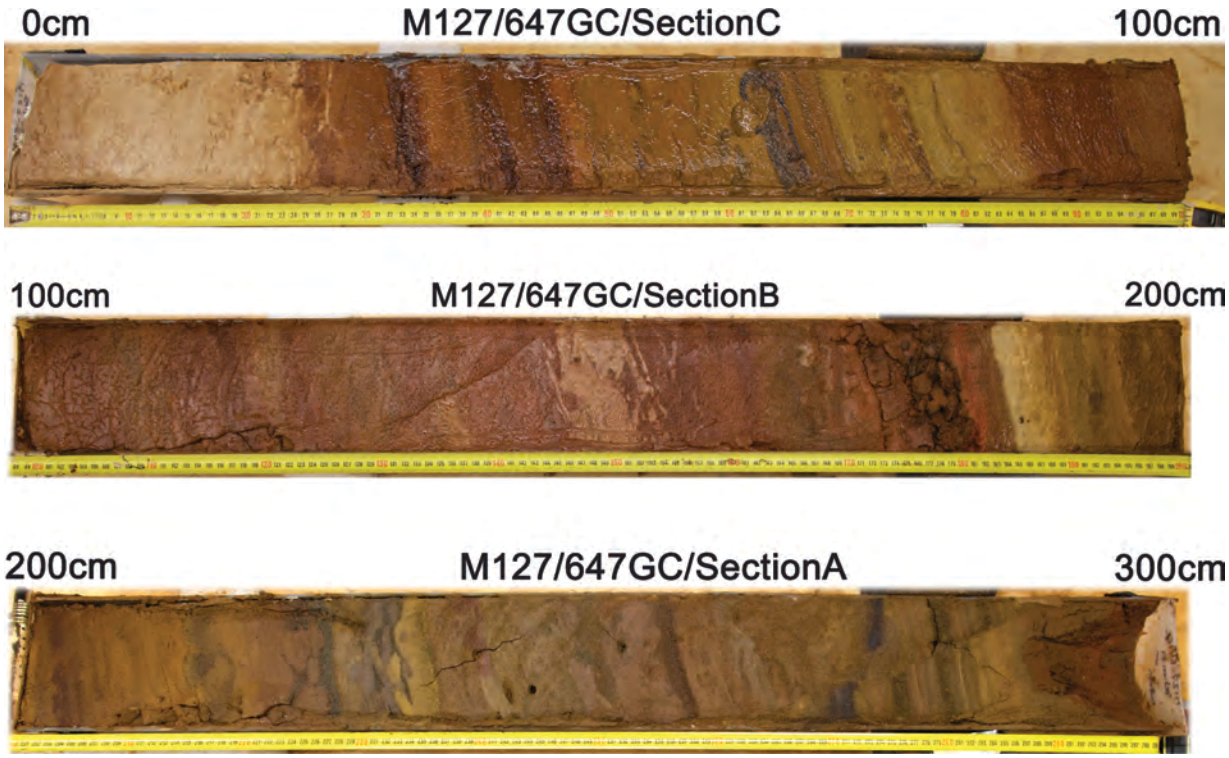

Fig. 5.4.4: *M127_647GC_SectionsA+B+C, largely composed of laminated hydrothermal sediments including sulfides as both, impregnations and separate layers.*

A hand-held colorimeter (Spectrophotometry - CM - Konica Minolta 700d) was used to record a variety of colour and visible reflection parameters including the Munsell sediment parameters. The archive half cores were covered with spectrophotometrically tested film (Glad®; *Balsam et al., 1997*) to enable contact of the colorimeter sensor, and analysed every 5 cm, to a total of over 650 spots analysed.

Table 5.4.2: Selected representative XRF analyses of hydrothermally influenced sediments comparing samples measured using the "soil" routine (in ppm; usually used for elements with concentrations less than 0.5 wt.%) and the "mining" routine (in wt.%; for elements > 0.5 wt.%).

Sample	Units	Zn	Cu	Fe	Mn	S	Ca	Ba
M127/626GC_A_55	ppm	191	816	55136	6441	1966	>100000	< LOD
M127/626GC_A_55	wt.%	0.02	0.09	5.65	0.70	0.32	30.25	< LOD
M127/626GC_A_110	ppm	255	5146	-	>100000	1933	8436	1468
M127/626GC_A_110	wt.%	0.02	0.57	14.65	18.12	0.20	0.77	0.14
M127/626GC_A_104	ppm	682	8160	-	>100000	2242	6125	427
M127/626GC_A_104	wt.%	0.06	0.89	21.01	12.88	0.26	0.57	0.05
M127/627GC_C_57	ppm	2806	33634	-	17011	2233	7561	428
M127/627GC_C_57	wt.%	0.23	3.31	32.35	0.67	0.34	0.70	0.04
M127/627GC_C_118	ppm	5852	44975	-	3113	23828	4502	414
M127/627GC_C_118	wt.%	0.48	4.31	37.11	0.11	3.22	0.49	0.02
M127/627GC_A_241	ppm	5976	82873	-	851	68448	1433	843
M127/627GC_A_241	wt.%	0.46	7.37	36.60	0.03	10.04	0.23	0.04
M127/627GC_A_263	ppm	2110	10131	-	1252	5178	3366	230
M127/627GC_A_263	wt.%	0.18	1.06	40.11	0.05	0.68	0.36	0.02
M127/627GC_A_280	ppm	2783	54697	-	1071	30482	2015	591
M127/627GC_A_280	wt.%	0.23	5.17	39.88	0.04	4.35	0.27	0.03
M127/627GC_A_284	ppm	7114	>100000	-	611	>100000	458	823
M127/627GC_A_284	wt.%	0.51	9.82	34.28	0.02	29.02	0.13	0.02
M127/627GC_A_285	ppm	3242	30663	-	891	53835	1954	664
M127/627GC_A_285	wt.%	0.26	2.96	39.56	0.03	7.91	0.26	0.02
M127/627GC_A_300	ppm	2523	19106	-	1259	9387	2279	284
M127/627GC_A_300	wt.%	0.22	1.92	42.90	0.04	1.26	0.25	0.01
M127/627GC_A_307	ppm	5737	>100000	-	927	89442	1169	814
M127/627GC_A_307	wt.%	0.37	21.47	27.81	0.02	13.95	0.19	0.02

A portable XRF instrument (XRF, Niton Ultra XL3t Thermo Finnigan) was used, with a variety of routines and accessories, including light elements (initially with He purge) and a large number of trace elements with variable detection limits, and precisions generally better than 20% relative to the amount present. The use of a stand, and sample holders with calibrated polyethylene windows permitted not only extended probe time spans but also constant distance between sample and X-ray source and sensor, thus optimizing the analytical conditions. The analyses were conducted in dry, ground samples. Tests indicate that the values obtained are devoid of sampling errors, as part of the samples were remounted and reanalysed without significant differences in the results. In total, 96 samples were analysed, with two routines (trace

and major elements), the more conservative values are reported. Before each batch of measurements, the instrument was calibrated using certified materials (Al6061 and NIST)

Overall 75 samples, dry and ground, were analysed by Portable Infrared Mineral Analyser (PIMA), in a darkened laboratory and with a cover on the samples (to reduce interference with lighting). Determinations were triplicated, and samples were stirred between determinations to minimize sampling errors. PIMA discriminates between carbonate ooze, ooze impregnated with hydrothermal material, sometimes proximity of igneous mafic rocks, and hydrothermal precipitates, but the individual minerals listed by the instrument are not always confirmed by X-ray diffraction (see below).

Some samples (18) were also analysed by XRD (Rigaku Miniflex II), to calibrate the PIMA results, which enabled detection, and elimination, of a few PIMA artefacts. Also, less abundant minerals, including copper chlorides were tentatively detected in some samples.

All the mineralogical and geochemical measurements made offshore will be repeated onshore by FFCUL, to evaluate the precision of the portable instruments working under real conditions and completed with additional major elements and trace elements, various species of volatiles such as C, S, N, P, and still others. Additionally, smear slides, thin and polished sections and electron microprobe work will be completed, to determine the use of the sediments in seafloor exploration and in genetic studies.

5.5 Sun-photometric aerosol measurements

(L. Raeke)

The Meteor cruise M127 from Bridgetown (Barbados) to Ponta Delgada (Azores, Portugal) was used to make sun-photometric aerosol measurements in the central Atlantic in order to extend the database of the Maritime Aerosol Network (*Smirnov et al., 2009*) that is operated at the Goddard Space Flight Center (GSFC) of the NASA. Surface based direct measurements of aerosol optical depths are important to evaluate and improve retrieval assumptions (e.g. aerosol size) for satellite retrievals and to offer reference data for aerosol column properties for model simulations and satellite observations over ocean areas. The Maritime Aerosol Network has gathered sun-photometric aerosol measurements from research cruises in all ocean basins and all seasons since 2004. Aerosol measurements in the Mid-Atlantic Ridge and along the ships track (Bridgetown – Ponta Delgada), are still rare. The M127 cruise increased the number of surface based aerosol measurements in this region substantially.

The Microtops II sun photometer

The Microtops II is a hand-held multi-band sun photometer that measures sun light at five wavelengths, which for our device are at 380, 440, 675, 870 and 936 nm, across the visible into the infrared of the solar spectrum. The optics has a narrow viewing angle of only 2.5° so that the sensors see the light from the sun disk alone, if the device is pointed directly at the sun.

The sun photometer is used to measure the intensity I_k of the sun beam at these five wavelengths. I_k depends on the extraterrestrial intensity $I_{0,k}$ and the attenuation of the beam on its way through the atmosphere to the sun photometer. Attenuation is due to either absorption by gases or scattering due to molecules – so called Rayleigh scattering – of aerosol, clouds, or rain. For our instrument the wavelengths are chosen to work well for the detection of aerosol particles by avoiding solar spectral regions with significant trace-gas absorption, provided no clouds are in the way.

The aerosol attenuation of the solar beam depends mainly on the number and size of aerosol particles along the beam. Small particles are more efficient in attenuating at shorter solar wavelengths than at longer solar wavelengths, while larger particles attenuate more evenly over the solar spectrum. Cloud droplets, which are larger than aerosol particles, exceed the size of the wavelength and therefore scatter at all wavelengths almost evenly (or all colours of the suns spectrum, equally), which also explains why clouds appear white. Comparing the solar attenuations at different wavelengths therefore gives indication of the size of the scattering particles. The extinction of the beam through the atmosphere obviously depends on the amount of air passed by the beam and therefore on the viewing angle of the instrument with respect to the zenith. The lower the sun, the longer the path of the sun beams through the atmosphere, the higher the atmospheric mass along the beam's path and the higher the chance for scattering and absorption. If the sun is directly above the observer, the solar zenith angle is 0° and the beam crosses one atmosphere. For a solar zenith angle of 48° the beam crosses 1.5 times the atmospheric and for 80° the beam passes through 6 atmospherics. UTC time and latitude from the GPS unit altogether, define the solar zenith angle and with it the atmospheric mass factor along the path of the beam. From the detected surface pressure the attenuation from scattering by air-molecules can be detected at each sample wavelength and is automatically removed so that the remaining attenuation normalized to the zenith direction (by air-mass factor division) yields “aerosol optical thickness” (AOT) at each of the five sampled wavelengths k.

The accuracy of these results is practically dominated by two factors: first of all, if the sun photometer is not pointed exactly in the direction of the sun, then the sensors see only a part of the sun disk and hence the extraterrestrial intensity I 0,(k) is smaller than assumed. As the sun photometer has no direct information on the pointing quality it makes internally several measurements – 20 in our device – within about 10 seconds and keeps only that with the highest intensity, which is assumed to have been pointed directly at the sun. On a moving platform, such as RV METEOR, the observer cannot always point correctly at the sun (e.g. rough sea, wind conditions), and hence some measurements receive less sun light and the sun photometer interprets this as a higher aerosol optical thickness instead of a lower extraterrestrial intensity $I_{0,k}$. This sun pointing error is discussed in *Porter et al. (2001)* and *Knobelspiesse et al. (2003*), where also a post-processing algorithm is proposed to filter out the measurements possibly affected by the sun-pointing-error. The second factor limiting the accuracy is thin cirrus, which cannot be easily detected in automatic filters looking for temporal variability and is even hard to detect by the observer. If measurements are taken in the presence of thin cirrus, then the extinction will be slightly increased, which again causes a weak overestimation of the aerosol optical thickness by the sun photometer. Ii is also important to find a good position on the ship for the measurements.

The higher the deck position, the better the chance to avoid sea spray on the detection window (although ignoring near surface aerosol extinction may yield small AOT underestimate. Further I had to pay attention to the ships funnel and its smoke (due to unfavourable wind directions).

The Microtops II sun photometer delivers the following parameters:
• Signal strength at 380, 440, 675, 870 and 936 nm
• Ratio of signal strengths: 380nm/440nm, 440nm/675nm, 675nm/870nm and 870nm/936nm.
• Aerosol optical depth at 380, 440, 675, 870 and 936 nm
• Water vapor column amount

With each measurements the following metadata are saved:
• Date and time
• Longitude and latitude
• Height and pressure
• Solar zenith angle and corresponding atmospheric mass
• Temperature

From these parameters the following aerosol characteristics can be derived:
• The Angstrom exponent, characteristic for the size and nature of the aerosols
• The fine mode fraction and aerosol optical depth
• The coarse mode fraction and aerosol optical depth

Fig. 5.5.1: *Microtops II sunphotometer and GPS unit provided by the Marine Aerosol Network of AERONET at NASA-GSFC. (c) MPI-M.*

Quality assurance

The sun photometer measurements are screened in three steps:

1. **Level 1.0**: On board screening for false measurements, which are triggered unintentionally. Such data are deleted. The remaining data were submitted to Dr. Alexander Smirnov at GSFC/NASA for further screening.

2. **Level 1.5**: At GSFC/NASA, to remove outlier data. If the sun photometer is not pointed accurately towards the sun, or a measurement is affected by clouds drifting into the optical path, then the intensities are reduced substantially, and consequently cannot be

used. Outliers are removed by an algorithm that compares single measurements to a series mean and the series standard deviation. This data reduction is done separately for each frequency.

3. **Level 2.0**: At GSFC/NASA, to remove suspicious data possibly influenced by cirrus and to apply the final correction from the instrument calibration.

Measurements

Measurements were taken during all day light hours when the sun was not obscured by clouds. When possible, series of 10 to 15 measurements were taken in intervals of 10 to 15 minutes. Measurements within a series vary mostly due to the sun pointing error, while measurements across all series resolve the variations along the ship track. No measurements were possible on May 26, June 8 and 9 due to cloudy conditions and on May 25 when the vessel was in the exclusive economic zone (EEZ) of Barbados, where no measurements could be taken. Table 5.5.1 shows the number of measurements and series taken during the M127 cruise. In total 7707 measurements were taken, resulting in 829 level 1.0 series.

Table 5.5.1: Number of measurements for all days of the cruise and resulting number of measurements series after Level 1.0.

Date	Measurements Lev 1.0	Series Lev 1.0	Days Lev 1.0	Comment
25 May 2016	0	0	0	EEZ of Barbados
26 May 2016	0	0	0	Cloudy
27 May 2016	123	14	1	
28 May 2016	193	20	1	
29 May 2016	309	28	1	
30 May 2016	401	39	1	
31 May 2016	243	26	1	
1 June 2016	489	41	1	
2 June 2016	274	32	1	
3 June 2016	82	9	1	
4 June 2016	319	36	1	
5 June 2016	382	46	1	
6 June 2016	316	39	1	
7 June 2016	110	13	1	
8 June 2016	0	0	0	Cloudy
9 June 2016	0	0	0	Cloudy
10 June 2016	239	28	1	
11 June 2016	386	42	1	
12 June 2016	254	28	1	
13 June 2016	165	18	1	
14 June 2016	281	33	1	
15 June 2016	337	38	1	

Date	Measurements Lev 1.0	Series Lev 1.0	Days Lev 1.0	Comment
16 June 2016	433	47	1	
17 June 2016	415	45	1	
18 June 2016	267	29	1	
19 June 2016	279	32	1	
20 June 2016	129	17	1	
21 June 2016	163	18	1	
22 June 2016	317	34	1	
23 June 2016	259	28	1	
24 June 2016	337	33	1	
25 June 2016	92	8	1	
26 June 2016	26	2	1	
27 June 2016	87	6	1	
28 June 2016	0	0	0	EEZ of Portugal
Total	**7707**	**829**	**30**	

Results

The photometric aerosol measurements can be evaluated at the level of single measurement series or of daily means and at five frequencies. Figure 5.5.2 shows the measurements for June 17, when measurements could be taken through the whole day. The measurements show a diurnal variation related to the changing zenith angle, which is most pronounced in the 380 nm channel. A view of the aerosol amount at wavelength 440nm in Fig. 5.5.3 indicates the daily progress as well as the development for the entire cruise M127. Both transits show increased values of aerosol amount. The transit to the TAG hydrothermal field lastet from May 25th until 31st May and the transit to the Azores started on June 23rd.

To calculate the aerosol size, the Angstrom parameter (AnP) will be used, because it is a general indicator for particle size. In this case it is the logarithmic ratio of the thicknesses at 440nm and 870nm in relation to the logarithmic wavelength ratio. Larger (super-micron) aerosol particles display little spectral dependence (AnP ~ 0.5 to 0), whereas smaller (sub-micron) aerosol particles have a stronger spectral dependence (AnP ~ 1 to 2). Dust and sea-salt are mainly contributing as super-micron sizes to the AOD, while pollution or wildfires aerosol mainly contributes to sub-micron AOD. Thus, AnP indirectly offers some insights on aerosol type. For cruise M127 the values of the Angstrom Parameter indicate small as well as larger aerosol particles, which is clearly visible in Fig. 5.5.4.

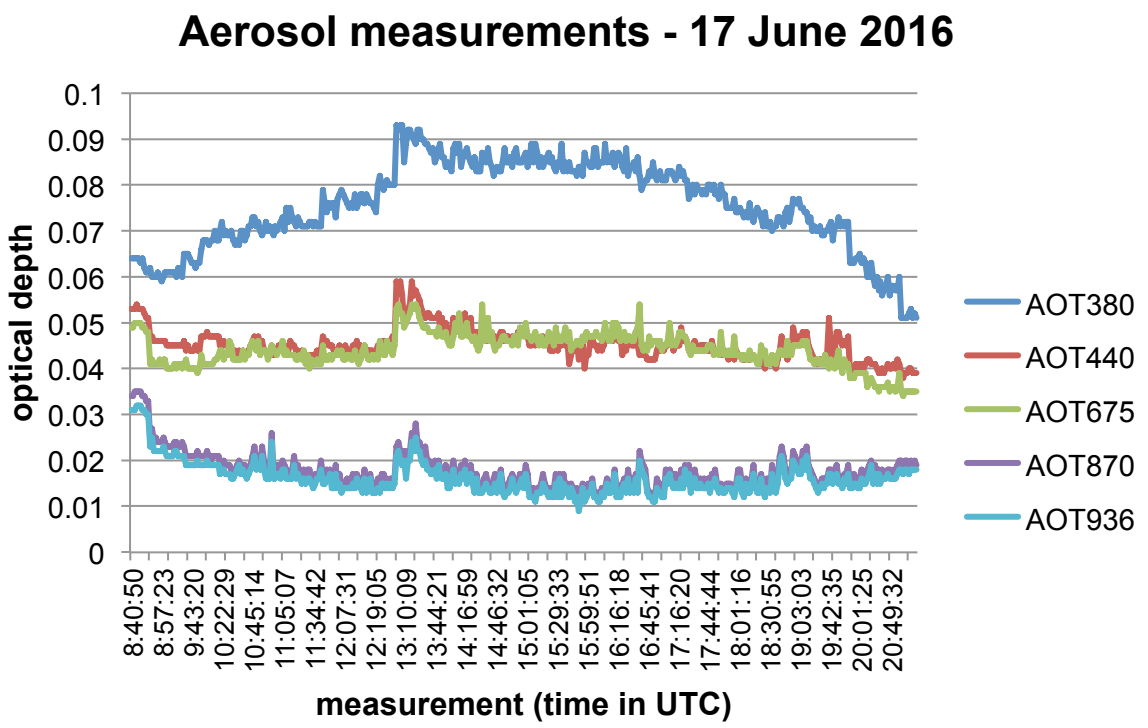

Fig. 5.5.2: *Aerosol optical depth at five wavelengths (380, 440, 675, 870 and 936 nm) as measured aboard RV METEOR on the Mid-Atlantic Ridge on June 17th 2016. The first measurement started at a zenith angle of 83.98° at 26.139°N/44.832°W. At noon (LT) the minimum zenith angle reached 2.75° at 26.145°N/44.820°W. The last measurement was taken at a zenith angle of 83.65° at 26.135°N/44.816°W. The data is result of Level 1.0.*

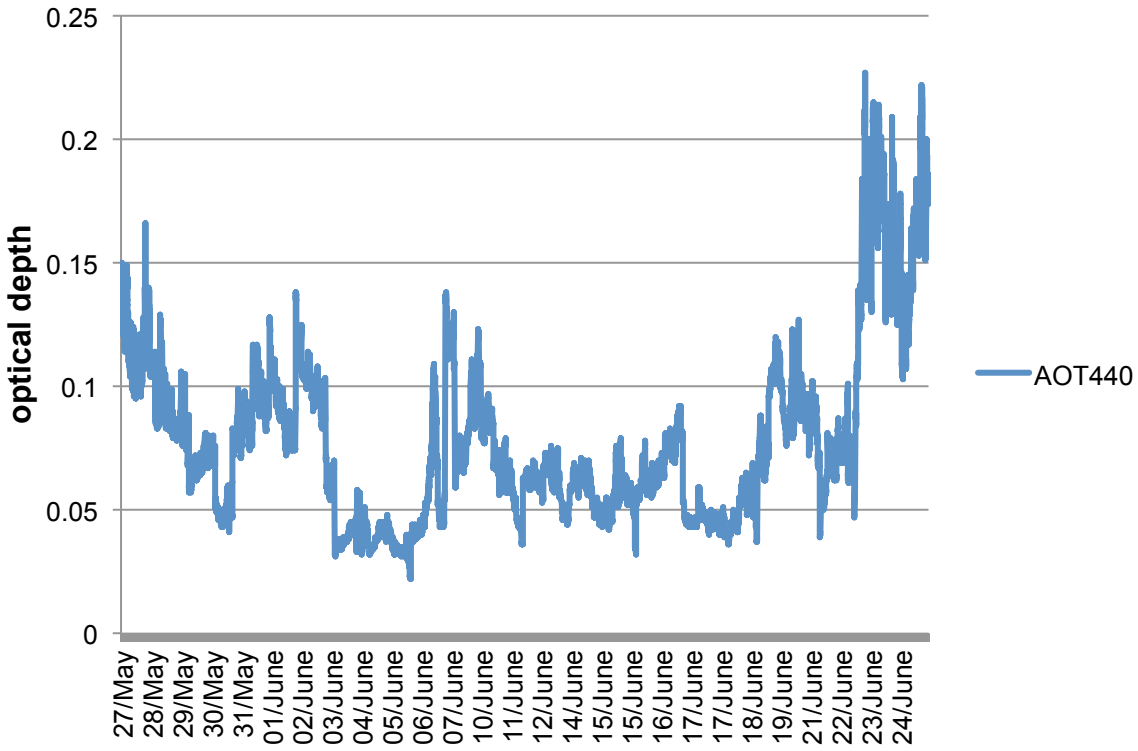

Fig. 5.5.3: *Aerosol amount at wavelength 440nm for the cruise M127 at Level 1.0.*

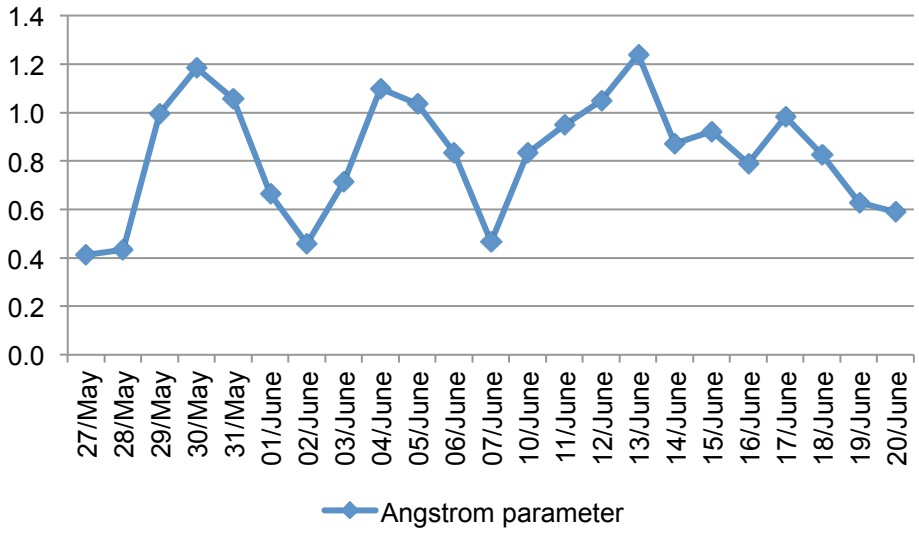

Fig. 5.5.4: *The Angstrom parameter between 440 and 870nm on cruise M127.*

The data is submitted directly to GSFC/NASA and integrated in their database. The daily mean aerosol optical depth at 500 nm wave length along the track of M127, for example, is shown in Fig. 5.5.5. A comparison with all available cruise data (Fig. 5.5.6) indicates the data from cruise M127 is one of a few datasets that sampled aerosol optical depths along a diagonal track from the Caribbean island Barbados to the Acores with the opportunity to collect data from the same area (TAG hydrothermal field at 26°N) over a prolonged time period. Weather conditions allowed measurements on 30 days.

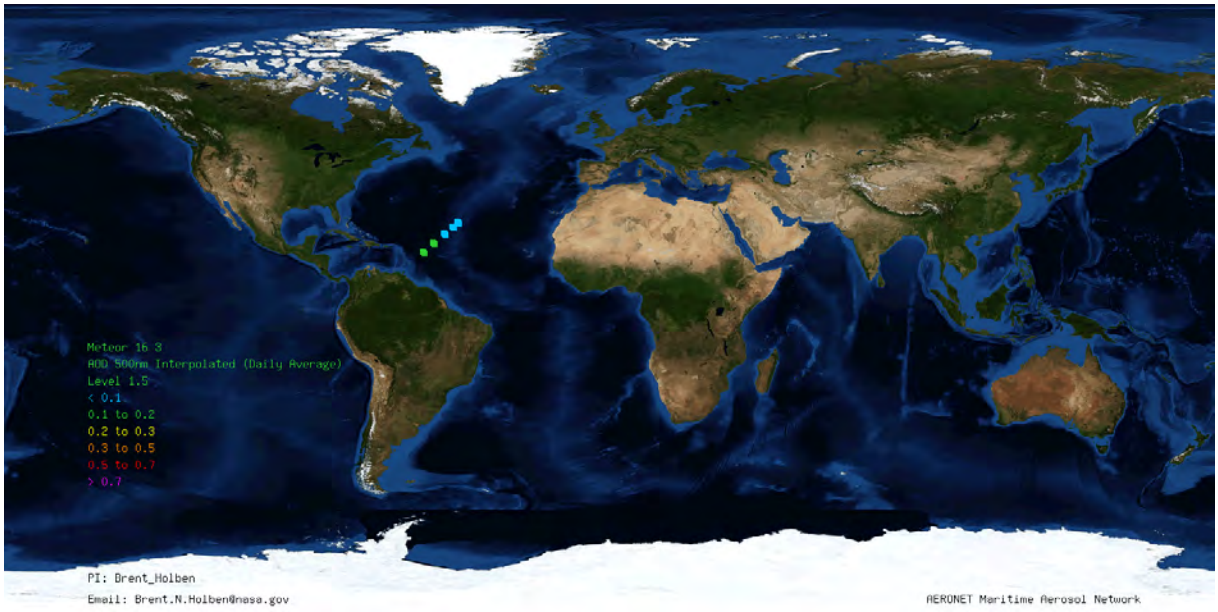

Fig. 5.5.5: *Aerosol optical depth at 500 nm, as daily means along the ship track of M127 (from the Level 2 dataset in http://aeronet.gsfc.nasa.gov/new_web/cruises_new/Meteor_16_3.html as of June 27th 2016).*

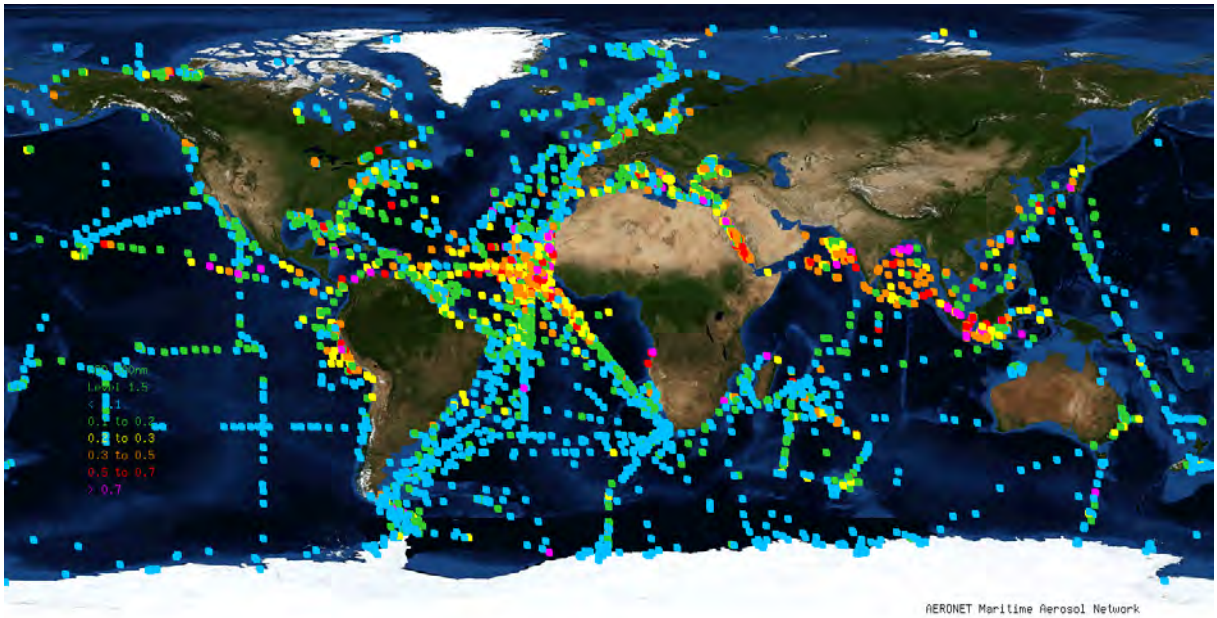

Fig. 5.5.6: *Level 2 aerosol optical depth at 500 nm (computed global average), as daily means along the ship tracks of all cruises (http://aeronet.gsfc.nasa.gov/new_web/maritime_aerosol_network.html). as of June 27th 2016)*

The new measurements show for the transit from Barbados to the TAG field at 26°N aerosol optical depth from 0.1 to 0.2, which is low, but in the working area the aerosol optical depth was even lower with < 0.1. This is accounted for by the fact that:

1. the working area (TAG field 26°N) is remote from land based aerosol sources
2. the region from 0-25°N latitude (within the transit to the TAG field) is influenced by sahara dust, hence, with a highly variable and seasonal dependence *(Smirnov et al., 2009)*

6 Weather data

(A. Raeke)

On the 25.05.2016 at about 09:00pm local time, the RV Meteor left the port of Bridgetown/Barbados for the cruise M127. At the beginning of the cruise the RV Meteor was transiting along the south flank of a high-pressure system centered above the North Atlantic. During the first days of the transit we encountered a steady trade wind from easterly direction with around 4 Bft. The significant wave height was 1.5 - 2m. The air- and water temperature was from 27 to 28°C. Below the trade wind inversion it resulted in isolated showers. During the transit the high-pressure influence increased slowly. A continuous easterly wind blew with around 4Bft until the 29.05. The high-pressure zone shifted a little to the south, so that from May 30th on the RV Meteor came into the central wind-weak field of the high-pressure zone. The wind blew weak from mostly northern directions and the significant wave height dropped to 1m.

A strong depression above the North Atlantic introduced an increasing northern swell (up to 3 m) starting in the evening of May 31st. In the night a weak cold front crossed the working area with isolated showers. On June 02nd and 03rd the swell decreased slowly related to a change from moderate to weak northeasterly trade winds. In the following days until June 05th the working area was located in the center of anticyclone. Smooth sea with a swell of 1 to 1.5m

guaranteed for good working conditions. From June 06th on, the high-pressure system became weaker and was replaced by the tail end of a strong cyclone approaching from the NW, west of the Azores, and moving in a northeasterly direction. The wind blew from west to northwest with around 4Bft and, during passing of the front on June 07th, temporarily with 5 to 6Bft.

Behind the front the high-pressure influence from the west increased again. On June 09th, the wind changed to an easterly direction. Until June 18th, the working area was mostly located to the south of the axis of trough of the Acores high-pressure system resulting in staedy easterly winds of between 3 to 4 Bft. The significant wave height reached 1 to 1.5m.

After June 18th, the high-pressure system near the Acores was moving in a westly direction. At the same time a new high-pressure system moved in from the United States**.** On June 22nd, a new high-pressure centre with up to 1031 hPa developed to the north of the working area. The wind force increased to 5 Bft. The significant wave height reached 1.5 to 2m. In order to be back in port against the swell and the wind, scientific station work ended in the evening of the June 22nd. During the transit the high-pressure system in the north of the vessel moved slowly north-eastwards to the Acores. On June 23rd, a cold front with moderate showers crossed the vessel track. Behind the cold front the wind blew from east to northeast with a force from 5-6 Bft, resulting in a significant wave hight of 2 to 2.5m that lasted until the June 26th. After that, the wind turned to a northeast direction and weakend to around 4 Bft. The significant wave height decreased to 1.5m. During the transit the air and water temperature decreased from 25/26°C at the start to 19/20°C when reaching the Acores. During the entire cruise we registered scattered showers below the Passat inversion. In the morning of June 28th 2016, RV Meteor reached Ponta Delgada.

7 Station list M127

Station	Gear Abbrev.	Date	Time	PositionLat	PositionLon	Depth [m]
ME127/557	XBT	29.05.16	15:45	22°57.30'N	048°45.16'W	4283
			15:52	22°57.75'N	048°44.63'W	4108
ME127/558	HYBIS (test)	29.05.16	15:47	22°57.43'N	048°45.01'W	4269
			18:16	22°58.42'N	048°43.38'W	-
ME127/559	AUV (test)	29.05.16	17:34	22°58.43'N	048°43.49'W	4348
			18:58	22°58.35'N	048°43.55'W	-
ME127/560	REL	29.05.16	19:07	22°58.35'N	048°43.65'W	4342
			21:21	22°58.23'N	048°43.74'W	-
ME127/561	ARGOS	29.05.16	21:28	22°58.30'N	048°43.81'W	4342
ME127/562	HYBIS (test)	30.05.16	13:34	24°44.20'N	046°32.81'W	3740
			14:05	24°44.20'N	046°32.81'W	3738
ME127/563	REL	30.05.16	14:15	24°44.20'N	046°32.81'W	3739
			15:12	24°44.20'N	046°32.81'W	-
ME127/564	XBT	31.05.16	01:57	26°01.60'N	044°53.93'W	4516
			02:05	26°02.12'N	044°53.28'W	4573
ME127/565	MB-PS	31.05.16	02:15	26°02.91'N	044°52.73'W	4488
			09:20	26°10.85'N	044°51.43'W	3719
ME127/566	AUV transp.	31.05.16	10:04	26°08.36'N	044°49.08'W	-
			13:19	26°07.75'N	044°49.09'W	-
ME127/567	OBEM	31.05.16	16:25	26°09.58'N	044°49.29'W	3588
			20:01	26°09.590'N	044°49.290'W	3586
ME127/568	AUV	31.05.16	20:33	26°07.87'N	044°48.26'W	-
		01.06.16	11:50	26°09.22'N	044°49.59'W	-
ME127/569	MB-PS	31.05.16	22:13	26°08.00'N	044°50.21'W	3773
		01.06.16	07:18	26°04.30'N	044°46.96'W	2881
ME127/570	OBEM	01.06.16	08:03	26°09.52'N	044°49.22'W	3593
			11:04	26°09.512'N	044°49.171'W	3578
ME127/571	OBEM	01.06.16	12:19	26°09.29'N	044°48.87'W	3537
			15:31	26°09.30'N	044°48.91'W	3562
ME127/572	AUV	01.06.16	18:03	26°07.83'N	044°48.62'W	3617
		02.06.16	10:34	26°10.47'N	044°49.65'W	3669
ME127/573	OBEM	01.06.16	18:49	26°09.33'N	044°48.99'W	3539
			21:45	26°09.305'N	044°48.875'W	3560
ME127/574	OBEM	01.06.16	22:11	26°09.09'N	044°48.56'W	3517
		02.06.16	01:16	26°09.076'N	044°48.562'W	3510
ME127/575	OBEM	02.06.16	01:34	26°08.80'N	044°48.19'W	3398
			04:25	26°08.808'N	044°48.185'W	3397
ME127/576	GC	02.06.16	04:57	26°10.422'N	044°48.318'W	343-4
			07:06	-	-	
ME127/577	MB-PS	02.06.16	08:00	26°04.10'N	044°47.08'W	2942
			09:23	26°11.15'N	044°42.24'W	3265
ME127/578	OBS	02.06.16	11:01	26°08.260'N	044°49.573'W	3680
ME127/579	OBS	02.06.16	11:11	26°08.217'N	044°49.507'W	3644
ME127/580	2D-MCS	02.06.16	11:56	26°07.71'N	044°48.56'W	3610
			18:18	26°08.25'N	044°50.10'W	3631
ME127/581	OBS	02.06.16	18:21	26°09.01'N	044°50.31'W	-
	(2 on deck)		20:50	26°09.15'N	044°50.52'W	-
ME127/582	AUV	02.06.16	21:25	26°07.91'N	044°48.80'W	-
		03.06.16	13:25	26°09.48'N	044°49.30'W	-
ME127/583	GC	02.06.16	22:14	26°09.659'N	044°48.818'W	3510
		03.06.16	00:27	-	-	-
ME127/584	GC	03.06.16	00:51	26°08.772'N	044°49.140'W	3605
			03:03	-	-	-

Station	Gear Abbrev.	Date	Time	PositionLat	PositionLon	Depth [m]
ME127/585	MB-PS	03.06.16	03:57	26°11.20'N	044°42.28'W	3263
			07:50	26°58.66'N	044°48.79'W	3290
ME127/586	HYBIS/OBS	03.06.16	09:20	26°09.79'N	044°49.56'W	-
			14:32	26°09.576'N	044°49.289'W	3593
ME127/587	HYBIS/OBS	03.06.16	16:13	26°09.56'N	044°49.23'W	-
			21:10	26°09.523'N	044°49.231'W	3548
ME127/588	HYBIS/OBS	03.06.16	21:48	26°09.54'N	044°49.21'W	3566
		04.06.16	01:22	26°09.514'N	044°49.210'W	3570
ME127/589	GC	04.06.16	01:59	26°08.779'N	044°49.134'W	3600
			04:36	-	-	-
ME127/590	GC	04.06.16	05:03	26°08.228'N	044°49.383'W	3628
			07:19	-	-	-
ME127/591	OBS	04.06.16	07:56	26°10.208'N	044°49.273'W	3458
ME127/592	OBS	04.06.16	08:17	26°09.958'N	044°49.029'W	3476
ME127/593	OBS	04.06.16	08:35	26°09.877'N	044°48.874'W	3441
ME127/594	OBS	04.06.16	08:57	26°09.315'N	044°48.667'W	3518
ME127/595	OBS	04.06.16	09:29	26°09.109’N	044°49.222’W	3591
ME127/596	HYBIS/OBS	04.06.16	11:07	26°09.51’N	044°49.27’W	3575
			14:33	26°09.492'N	044°49.248'W	3551
ME127/597	HYBIS/OBS	04.06.16	15:40	26°09.59’N	044°49.22’W	3594
			19:31	26°09.543'N	044°49.235'W	3597
ME127/598	OBS	04.06.16	19:55	26°09.593’N	044°49.212’W	3542
ME127/599	AUV (calibr)	04.06.16	21:41	26°07.95’N	044°48.49’W	3586
			23:21	26°08.10’N	044°48.97’W	3671
	AUV (mission)	04.06.16	23:54	26°08.09’N	044°48.69’W	3635
		05.06.16	13:42	26°09.43’N	044°48.99’W	3524
ME127/600	GC	05.06.16	00:33	26°09.184'N	044°49.042'W	3559
			02:48	-	-	-
ME127/601	GC	05.06.16	03:15	26°08.422'N	044°49.401'W	3664
			05:31	-	-	-
ME127/602	OBS	05.06.16	06:12	26°09.062'N	044°49.421'W	3571
ME127/603	OBS	05.06.16	06:34	26°09.158’N	044°49.577'W	3604
ME127/604	OBH	05.06.16	07:01	26°09.369’N	044°49.417’W	3608
ME127/605	OBS	05.06.16	07:43	26°09.895’N	044°49.709’W	3640
ME127/606	OBS	05.06.16	08:12	26°09.895’N	044°49.289’W	3520
ME127/607	OBH	05.06.16	08:39	26°10.189’N	044°48.946’W	3451
ME127/608	HYBIS/OBS	05.06.16	09:21	26°09.35’N	044°48.96’W	3568
			13:17	26°09.325'N	044°48.961'W	3514
ME127/609	HYBIS/OBS	05.06.16	14:40	26°09.32’N	044°48.92’W	3566
			19:14	26°09.368'N	044°48.966'W	3507
ME127/610	AUV	05.06.16	20:00	26°07.89’N	044°48.69’W	-
		06.06.16	11:12	26°09.46'N	044°49.34'W	3609
ME127/611	HYBIS/OBS	05.06.16	20:43	26°09.32’N	044°48.95’W	-
		06.06.16	00:23	26°09.304'N	044°48.943'W	3533
ME127/612	OBH	06.06.16	00:49	26°10.364’N	044°48.898’W	3437

Station	Gear Abbrev.	Date	Time	PositionLat	PositionLon	Depth [m]
ME127/613	OBH	06.06.16	01:02	26°10.438'N	044°48.815'W	3418
ME127/614	OBH	06.06.16	01:11	26°10.547'N	044°48.794'W	3425
ME127/615	GC	06.06.16	01:39	26°07.863'N	044°48.180'W	3555
			03:47	-	-	-
ME127/616	GC	06.06.16	05:00	26°09.391'N	044°48.464'W	3500
			07:08	-	-	-
ME127/617	GC	06.06.16	07:37	26°09.253'N	044°48.519'W	3462
			09:46	-	-	-
ME127/618	HYBIS/OBS	06.06.16	12:10	26°09.30'N	044°48.99'W	3543
			15:56	26°09.278'N	044°48.992'W	3560
ME127/619	HYBIS/OBS	06.06.16	16:38	26°09.37'N	044°49.02'W	-
			19:56	26°09.347'N	044°49.011'W	3507
ME127/620	AUV	06.06.16	20:35	26°08.00'N	044°48.52'W	-
		07.06.16	10:09	26°10.51'N	044°49.79'W	3647
ME127/621	MB-PS	06.06.16	22:36	26°04.67'N	044°55.75'W	3406
		07.06.16	09:11	26°13.89'N	044°53.27'W	3208
ME127/622	2D-MCS	07.06.16	11:54	26°08.56'N	044°49.72'W	-
		08.06.16	00:11	26°07.82'N	044°49.77'W	3698
	2D-MCS	08.06.16	01:07	26°07.97'N	044°49.65'W	3671
			13:58	26°11.29'N	044°51.27'W	3635
	2D-MCS	08.06.16	15:00	26°10.89'N	044°51.54'W	3724
			22:41	26°07.52'N	044°46.75'W	2763
ME127/623	AUV	08.06.16	23:06	26°07.83'N	044°48.66'W	3661
		09.06.16	14:30	26°07.90'N	044°48.41'W	3571
ME127/624	2D-MCS	08.06.16	23:59	26°07.52'N	044°47.15'W	2847
		09.06.16	12:59	26°11.77'N	044°50.82'W	3687
ME127/625	2D-MCS	09.06.16	15:05	26°07.97'N	044°49.15'W	3691
		10.06.16	01:54	26°11.68'N	044°50.86'W	3738
ME127/626	GC	10.06.16	02:42	26°10.401'N	044°48.747'W	3407
			04:46	-	-	-
ME127/627	GC	10.06.16	05:25	26°09.139'N	044°48.860'W	3519
			07:37	-	-	-
ME127/628	GC	10.06.16	08:12	26°09.639'N	044°49.270'W	3558
			10:24	-	-	-
ME127/629	OBH (rec)	10.06.16	09:55	26°09.64'N	044°49.27'W	-
					not released	
ME127/630	OBH (rec)	10.06.16	11:59	26°09.70'N	044°49.54'W	-
			13:46	26°11.13'N	044°49.02'W	
ME127/631	OBH (rec)	10.06.16	12:00	26°09.71'N	044°49.55'W	-
			13:56	26°11.07'N	044°48.91'W	
ME127/632	OBH (rec)	10.06.16	12:01	26°09.72'N	044°49.55'W	-
			13:37	26°11.15'N	044°48.91'W	
ME127/633	OBH (rec)	10.06.16	12:02	26°09.73'N	044°49.56'W	-
			14:09	26°11.02'N	044°49.08'W	
ME127/634	MB-PS	10.06.16	17:42	26°58.71'N	044°48.75'W	3216
			21:28	26°10.35'N	044°38.35'W	2761
ME127/635	AUV	10.06.16	22:43	26°07.88'N	044°48.70'W	3639
		11.06.16	15:02	26°08.56'N	044°48.36'W	3424
ME127/636	GC	11.06.16	00:07	26°09.088'N	044°49.540'W	3604
			02:17	-	-	-
ME127/637	GC	11.06.16	02:50	26°07.986'N	044°48.726'W	3639
			04:59	-	-	-
ME127/638	GC	11.06.16	05:30	26°08.015'N	044°50.158'W	3753
			07:45	-	-	-
ME127/639	OBH	11.06.16	08:35	26°10.570'N	044°48.285'W	3442

Station	Gear Abbrev.	Date	Time	PositionLat	PositionLon	Depth [m]
ME127/640	OBH	11.06.16	09:01	26°10.122'N	044°47.680'W	3229
ME127/641	OBH	11.06.16	09:33	26°09.678'N	044°47.088'W	3102
ME127/642	OBH	11.06.16	10:06	26°09.252'N	044°46.419'W	2824
ME127/643	MB-PS	11.06.16	16:08	26°13.87'N	044°53.35'W	3201
		12.06.16	14:18	26°16.29'N	044°33.87'W	3557
ME127/644	GC	12.06.16	15:54	26°09.006'N	044°48.695'W	3515
			18:06	-	-	-
ME127/645	GC	12.06.16	18:37	26°08.713'N	044°48.725'W	3562
			20:48	-	-	-
ME127/646	2D-MCS	12.06.16	22:57	26°12.99'N	044°48.26'W	3733
		13.06.16	16:05	26°06.86'N	044°52.01'W	4023
ME127/647	GC	13.06.16	18:35	26°09.146'N	044°48.858'W	3520
			20:51	-	-	-
ME127/648	AUV	13.06.16	22:11	26°08.05'N	044°48.58'W	3608
		15.06.16	16:02	26°18.89'N	045°01.11'W	-
ME127/649	GC	13.06.16	22:39	26°08.534'N	044°48.245'W	3423
		14.06.16	00:41	-	-	-
ME127/650	MB-PS	14.06.16	01:08	26°06.80'N	044°45.72'W	2321
			08:00	26°21.69'N	044°33.70'W	2912
ME127/651	HYBIS	14.06.16	10:14	26°09.08'N	044°48.66'W	3500
			13:46	26°09.091'N	044°48.580'W	3534
ME127/652	HYBIS	14.06.16	18:25	26°08.83'N	044°48.61'N	-
			21:36	26°08.805'N	044°48.483'N	3439
ME127/653	2D-MCS	14.06.16	21:49	26°08.47'N	044°49.74'W	3652
		15.06.16	17:37	26°12.27'N	044°45.07'W	3697
ME127/654	OBS (rec)	15.06.16	17:08	26°13.38'N	044°54.09'W	-
			18:24	26°09.84'N	044°49.48'W	
ME127/655	OBS (rec)	15.06.16	17:52	26°09.98'N	044°49.73'W	-
			18:55	26°09.48'N	044°49.03'W	
ME127/656	OBS (rec)	15.06.16	18:27	26°09.80'N	044°49.45'W	-
			19:41	26°10.49'N	044°49.55'W	
ME127/657	OBS (rec)	15.06.16	18:56	26°09.48'N	044°49.02'W	-
			20:00	26°10.14'N	044°49.09'W	
ME127/658	OBS (rec)	15.06.16	19:22	26°10.12'N	044°49.30'W	-
			20:28	26°10.02'N	044°48.93'W	
ME127/659	OBS (rec)	15.06.16	19:57	26°10.15'N	044°49.17'W	-
			20:48	26°10.15'N	044°49.41'W	
ME127/660	OBS (rec)	15.06.16	20:25	26°10.09'N	044°48.98'W	-
			21:26	26°09.27'N	044°49.23'W	
ME127/661	OBS (rec)	15.06.16	20:51	26°10.12'N	044°49.39'W	-
			21:58	26°09.22'N	044°49.37'W	
ME127/662	OBS (rec)	15.06.16	21:18	26°09.30'N	044°49.45'W	-
			22:25	26°09.27'N	044°49.55'W	
ME127/663	OBS (rec)	15.06.16	21:45	26°09.38'N	044°49.58'W	-
			23:04	26°09.60'N	044°49.24'W	
ME127/664	OBS (rec)	15.06.16	22:10	26°09.52'N	044°49.69'W	-
			23:29	26°10.06'N	044°49.74'W	
ME127/665	AUV	16.06.16	00:12	26°08.10'N	044°48.68'W	-
			13:55	26°07.90'N	044°48.30'W	
ME127/666	GC	16.06.16	00:58	26°08.593'N	044°46.920'W	3000
			02:52	-	-	-
ME127/667	GC	16.06.16	03:13	26°08.161'N	044°47.095'W	2992
			05:09	-	-	-
ME127/668	OBS (rec)	16.06.16	04:43	26°08.16'N	044°47.10'W	-
			05:48	26°09.63'N	044°49.34'W	

Station	Gear Abbrev.	Date	Time	PositionLat	PositionLon	Depth [m]
ME127/669	OBS (rec)	16.06.16	05:26	26°08.60'N	044°47.68'W	-
			06:54	26°09.75'N	044°49.45'W	
ME127/670	OBS (rec)	16.06.16	06:11	26°09.59'N	044°49.49'W	-
			07:58	26°09.61'N	044°49.33'W	
ME127/671	OBS (rec)	16.06.16	06:54	26°09.75'N	044°49.45'W	-
			08:48	26°09.75'N	044°49.04'W	
ME127/672	OBS (rec)	16.06.16	08:00	26°09.63'N	044°49.35'W	-
			09:14	26°09.40'N	044°49.01'W	
ME127/673	OBH (rec)	16.06.16	08:43	26°09.67'N	044°49.63'W	-
			10:00	26°10.71'N	044°48.35'W	
ME127/674	OBH (rec)	16.06.16	09:17	26°09.35'N	044°49.06'W	-
			10:26	26°10.21'N	044°47.75'W	
ME127/675	OBH (rec)	16.06.16	09:56	26°10.81'N	044°48.37'W	-
					not released	
ME127/676	OBH (rec)	16.06.16	10:14	26°10.42'N	044°48.04'W	-
			11:43	26°09.32'N	044°46.69'W	
ME127/677	HYBIS	16.06.16	14:32	26°10.30'N	044°48.82'W	-
			18:32	26°10.344'N	044°48.844'W	3418
ME127/678	OBH (rec)	16.06.16	19:01	26°09.68'N	044°49.36'W	-
ME127/679	OBH (rec)	16.06.16	19:42	26°09.96'N	044°47.28'W	-
ME127/680	MB-PS	16.06.16	21:57	26°10.54'N	044°49.97'W	3670
		17.06.16	02:29	26°08.47'N	044°47.99'W	3404
ME127/681	GC	17.06.16	02:58	26°10.444'N	044°49.076'W	3510
			05:05	-	-	-
ME127/682	GC	17.06.16	05:23	26°10.243'N	044°48.706'W	3445
			07:25	-	-	-
ME127/683	GC	17.06.16	07:55	26°08.341'N	044°49.933'W	3700
			10:08	-	-	-
ME127/684	HYBIS	17.06.16	10:42	26°08.75'N	044°49.30'W	3599
			15:32	26°08.711'N	044°49.190'W	3590
ME127/685	HYBIS	17.06.16	16:16	26°09.38'N	044°48.76'W	-
			19:51	26°09.373'N	044°48.825'W	3539
ME127/686	AUV	17.06.16	21:26	26°08.02'N	044°48.81'W	-
		18.06.16	13:09	26°09.57'N	044°47.56'W	
ME127/687	MB-PS	17.06.16	22:22	26°02.88'N	044°54.76'W	4157
		18.06.16	10:36	26°02.25'N	044°53.15'W	4603
ME127/688	HYBIS	18.06.16	13:41	26°08.32'N	044°50.05'W	-
			19:20	26°08.465'N	044°49.929'W	3632
ME127/689	AUV	18.06.16	20:10	26°08.00'N	044°48.81'W	3636
		19.06.16	09:40	26°10.04'N	044°46.99'W	3121
ME127/690	GC	18.06.16	20:46	26°10.774'N	044°49.041'W	3644
			22:57	-	-	-
ME127/691	GC	18.06.16	23:27	26°08.417'N	044°47.184'W	3067
		19.06.16	01:23	-	-	-
ME127/692	GC	19.06.16	01:47	26°08.559'N	044°48.397'W	3422
			03:48	-	-	-
ME127/693	GC	19.06.16	04:18	26°08.466'N	044°49.917'W	3654
			06:31	-	-	-
ME127/694	HYBIS	19.06.16	10:45	26°10.52'N	044°48.69'W	3434
			15:50	26°10.683'N	044°48.630'W	3436
ME127/695	OBEM	19.06.16	17:34	26°08.570'N	044°47.840'W	3348
			20:38	-	-	-
ME127/696	AUV	19.06.16	21:12	26°07.99'N	044°48.83'W	3631
		20.06.16	12:01	26°09.26'N	044°48.62'W	3512
ME127/697	2D-MCS	19.06.16	23:40	26°06.22'N	045°08.53'W	3141
		20.06.16	10:45	26°01.11'N	044°47.24'W	3173

Station	Gear Abbrev.	Date	Time	PositionLat	PositionLon	Depth [m]
ME127/698	2D-MCS	20.06.16	13:50	26°23.22'N	044°56.88'W	3009
		21.06.16	00:56	26°14.32'N	044°35.21'W	2967
ME127/699	AUV	21.06.16	03:16	26°07.95'N	044°49.03'W	-
			17:58	26°05.92'N	044°47.89'W	2693
ME127/700	GC	21.06.16	05:00	26°10.053'N	044°48.027'W	3345
			07:02	-	-	-
ME127/701	GC	21.06.16	07:24	26°09.367'N	044°47.611'W	3248
			09:28	-	-	-
ME127/702	GC	21.06.16	10:02	26°09.436'N	044°49.063'W	3560
			12:13	-	-	-
ME127/703	GC	21.06.16	12:41	26°08.984'N	044°48.576'W	3460
			14:49	-	-	-
ME127/704	OBH (rec)	21.06.16	16:00	-	-	-
			20:46	26°09.68'N	044°47.15'W	
ME127/705	OBH (rec)	21.06.16	16:01	-	-	-
			21:39	26°09.49'N	044°49.59'W	
ME127/706	AUV	21.06.16	22:02	26°07.93'N	044°48.89'W	-
		22.06.16	13:31	26°07.80'N	044°50.91'W	3973
ME127/707	MB-PS	21.06.16	23:39	26°18.59'N	044°58.98'W	2682
		22.06.16	11:01	25°59.41'N	044°39.74'W	2652
ME127/708	AUV-T	22.06.16	12:45	26°07.73'N	044°49.51'W	3703
			14:04	26°08.58'N	044°49.12'W	3573
ME127/709	AUV-T	22.06.16	12:46	26°07.73'N	044°49.51'W	3701
			14:19	26°08.21'N	044°49.25'W	3656
ME127/710	GC	22.06.16	15:38	26°05.485'N	044°38.763'W	2130
			16:59	-	-	-
ME127/711	GC	22.06.16	17:04	26°05.485'N	044°38.770'W	2130
			18:29	-	-	-
ME127/712	MB-PS	22.06.16	19:28	25°58.47'N	044°40.51'W	2753
			22:31	26°18.95'N	044°26.01'W	3434
ME127/713	ARGOS	25.06.16	09:07	31°56.75'N	036°16.86'W	3463
ME127/714	ARGOS	26.06.16	20:57	35°20.16'N	030°29.60'W	3127

Note: Locations for OBEM and HyBis are originally locations obtained using POSIDONIA USBL data; all OBS (also those deployed by HyBis) and OBH locations at the seafloor are further recalculated using results from seismic shooting.

Abbreviations:

ARGOS:	ships position for launch of floats
AUV:	ships position and time for launch and recovery
AUV-T:	ships position and time from release signal to transponder recovery on deck
GC:	time from launch to recovery of the instrument; location at bottom contact obtained by POSIDONIA; depth = cable out at contact
HYBIS/OBS:	ships position and time for launch; time of recovery; instrument deployment location is recalculated seafloor position
HYBIS:	ships position and time for launch; time of recovery; location at sampling point obtained by POSIDONIA
MB-PS:	ships position and time for begin / end of ships multibeam echosounding surveys
2D-MCS:	ships position and time for launch and recovery of seismic gear
OBS/H:	ships time for launch; bottom location is recalculated seafloor position / -
OBEM:	ships position and time for launch; time of recovery of cable; bottom location at end is recalculated seafloor position
OBS/H (rec):	ships position and time from release signal to instrument recovery on deck
REL:	ships position and time for launch and recovery; REL = function test of releasers in metal crate lowered to 1000m or 2000m
XBT:	ships position and time for launch / ships position and time for cutting the copper wire (reached max depth of 2000m)

8 Data and sample storage

All meta-data related to station work will be made publically available within 6 months of the cruise using the GEOMAR data management system.

Meta-data for AUV dives including bathymetry and sensor data will be stored at GEOMAR as well and will be made public at the end of 2016. Final data will be made available latest at the end of 2018. Responsible scientist for this data is: Dr. S. Petersen (email: spetersen@geomar.de).

Archive and working halves from gravity coring are stored at GEOMAR and the scientist responsible for getting access to the samples is: Dr. S. Petersen (email: spetersen@geomar.de). Subsample for geochemical analyses went to Dr. A. Lichtschlag (NOC) and to Prof. F. Barriga (FFCUL Lisbon). Chemical and geophysical data generated on-shore will be stored in the GEOMAR data management system after publication but latest at the end of 2018.

The ship-based bathymetric data is also stored at GEOMAR (responsible: Dr. N. Augustin; email: naugustin@geomar.de) and will be incorporated into PANGAEA in 2017. Transit data has been edited and gridded at 100m and is already available at PANGAEA under (https://doi.pangaea.de/10.1594/PANGAEA.864817).

All seismic data will be stored at GEOMAR (responsible: Dr. J. Bialas; email: jbialas@geomar.de) and will be incorporated into PANGAEA in 2018.

The M127 aerosol data for levels 1, 1.5 and 2, as processed by Dr. A. Smirnov at GSFC/NASA, are already made public. They are available at the following URL: http://aeronet.gsfc.nasa.gov/new_web/cruises_new/Meteor_16_3.html (Click on “data track” and a zip data file will be downloaded).

9 Acknowledgements

We gratefully acknowledge the expertise and help of captian Rainer Hammacher, his officers and the crew of the RV METEOR. The work was supported by a grant from the EU-FP7-Project “Blue Mining: Breakthrough Solutions for the Sustainable Deep Sea Mining Value Chain” under grant No. 604500. Additional support by GEOMAR, Helmholtz Centre for Ocean Research is greatfully acknowledged.

10 References

Ade-Hall, J.M., Palmer, H.C., and Hubbard, T.P. (1971), The magnetic and opaque petrological response of basalt to regional hydrothermal alteration, Geophys. J. R. Astron. Soc., 24, 137–174.

Balsam, W.L., Damuth, J.E. and Schneider, R.R. (1997) Comparison of shipboard vs. shore-based spectra data from Amazon Fan cores: implications for interpreting sediment composition. Proceedings of the ODP Sci. Results, v. 155, 193–215.

Blount, C.W., Dickson, F.W. (1969) The solubility of anhydrite (CaSO 4) in NaCl-H2O from 100 to 450°C and 1 to 1000 bars. Geochimica et Cosmochimica Acta 33, 227–245.

Brown, L. (2010) A new technique for depicting terrain relief [abstract]. NACIS Annual Meeting, 2010 Oct 13–17, St. Petersburg, Florida.

Caratori-Tontini, F., Davy, B., de Ronde, C.E.J., Embley, R.W., Leybourne, M., and Tivey, M.A. (2012) Crustal magnetization of Brothers Volcano, New Zealand, measured by autonomous underwater vehicles: Geophysical expression of a submarine hydrothermal system, Econ. Geol., 107, 1571–1581, doi:10.2113/econgeo.107.8.1571.

Cherkashov, G., Poroshina, I., Stepanova, T., Ivanov, V., Bel'tenev, V., Lazareva, L., Rozhdestvenskaya, I., Samovarov, M., Shilov, V., Glasby, G.P., Fouquet, Y., and Kuznetsov, V. (2010) Seafloor Massive Sulfides from the Northern Equatorial Mid-Atlantic Ridge: New Discoveries and Perspectives. Marine Georesources & Geotechnology 28, 222–239. doi:10.1080/1064119X.2010.483308

Cline, J.D. (1969) Spectrophotometric determination of hydrogen sulfide in natural waters. Limnol. Oceanogr., 14, 454–458.

de Ronde, C.E.J., et al. (2011) Submarine hydrothermal activity and gold-rich mineralization at Brothers volcano, Kermadec arc, New Zealand, Miner. Deposita, 46, 541–584, doi:10.1007/s00126-011-0345-8.

Hannington, M., Jamieson, J., Monecke, T., Petersen, S., and Beaulieu, S. (2011) The abundance of seafloor massive sulfide deposits. Geology 39, 1155–1158. doi:10.1130/G32468.1.

Heinson, G., White, A., Robinson, D., and Fathianpour, N. (2005) Marine self-potential gradient exploration of the continental margin, Geophysics, 50, 5, 109 – 118, doi : 10.1190/1.2057981.

Honsho, C., Dyment, J., Tamaki, K., Ravilly, M., Horen, H., and Gente, P. (2009) Magnetic structure of a slow spreading ridge segment: Insight from near-bottom magnetic measurements onboard a submersible, J. Geophys. Res., 114, B05101, doi:1 0.1029/ 2008 JB005915.

Honsho, C., Ura, T. and Kim, K. (2013) Deep-sea magnetic vector anomalies over the Hakurei hydrothermal field and the Bayonnaise knoll caldera, Izu-Ogasawara arc, Japan, J. Geophys. Res., 118, 5147–5164, doi:10.1002/jgrb.50382.

Humphris, S.E., Herzig, P.M., Miller, D.J., et al. (1995) The internal structure of an active sea-floor massive sulfide deposit. Nature 377, 713–716.

International Association of Geomagnetism and Aeronomy (IAGA) Working Group V-MOD (2010), International geomagnetic reference field: The eleventh generation, Geophys. J. Int., 183, 1216–1230, doi:10.1111/j.1365-246X.2010.04804.x.

Isezaki, N. (1986), A new shipboard three-component magnetometer, Geophysics, 51, 1992–1998.

Jamieson, J.W., Clague, D.A., and Hannington, M.D. (2014). Hydrothermal sulfide accumulation along the Endeavour Segment, Juan de Fuca Ridge. Earth and Planetary Science Letters 395, 136–148. doi:10.1016/j.epsl.2014.03.035.

Johnson, H.P., and Pariso, J.E. (1987) The effects of hydrothermal alteration on the magnetic properties of oceanic crust: Results from drill holes CY-2 and CY-2a, in Cyprus Crustal Study Project: Initial Report, Holes CY2 and 2a, edited by P. T. Robinson, I. L. Gibson and A. Panayiotou, Geol. Surv. Can. Pap. 85–29, pp. 283–293.

Knobelspiesse, K.D., Pietras, C., and Fargion, G.S. (2003) Sun-Pointing-Error Correction for Sea Deployment of the MICROTOPS II Handheld Sun Photometer, J. Atmos. Oceanic Technol., 20, 767-771.

Nakamura, K., T. Toki, N. Mochizuki, M. Asada, J. Ishibashi, Y. Nogi, S. Yoshikawa, J. Miyazaki, and K. Okino (2013) Discovery of a new hydrothermal vent based on an underwater, high-resolution geophysical survey, Deep Sea Res., Part I, 74, 1–10.

Peirce, C., et al. (2007) Morphology and genesis of slow-spreading ridges-seabed scattering and seismic imaging within the oceanic crust. Geophysical Journal International 168(1), 59-89.

Petersen, S., Herzig, P.M., Hannington, M.D. (2000) Third dimension of a presently forming VMS deposit: TAG hydrothermal mound, Mid-Atlantic Ridge, 26°N. Mineralium Deposita 35, 233–259.

Planert, L., et al. (2010) Crustal structure of a rifted oceanic core complex and its conjugate side at the MAR at 5°S: implications for melt extraction during detachment faulting and core complex formation. Geophysical Journal International 181, 113-126.

Porter, J. N., Miller, M., Pietras, C., and Mortell, C. (2001) Ship-Based Sun Photometer Measurements Using Microtops Sun Photometers, J. Atmos. Oceanic Technol., 18, 765-774.

Rona, P.A., Hannington, M.D., Raman, C.V., Thompson, G., Tivey, M.K., Humphris, S.E., Lalou, C., and Petersen, S. (1993) Active and relict sea-floor hydrothermal mineralization at the TAG hydrothermal field, Mid-Atlantic Ridge. Economic Geology 88, 1989–2017.

Seeberg-Elverfeldt, J., Schlüter, M., Feseker, T., and Kölling, M. (2005) Rhizon sampling of pore waters near the sediment/water interface of aquatic systems. Limnology and oceanography: Methods, 3(8), 361-37.

Shilov, V.V., Bel'tenev, V.E., Ivanov, V.N., Cherkashev, G.A., Rozhdestvenskaya, I.I., Gablina, I.F., Dobretsova, I.G., Narkevskii, E.V., Gustaitis, A.N., and Kuznetsov, V.Y. (2012) New hydrothermal ore fields in the Mid-Atlantic Ridge: Zenith-Victoria (20°08′N) and Petersburg (19°52′N). Doklady Earth Sciences 442, 63–69. doi:10.1134/S1028334X12010308.

Smirnov, A., et al. (2009) Maritime Aerosol Network as a component of Aerosol Robotic Network, J. Geophys. Res., 114, D06204, doi:10.1029/2008JD011257, 2009.

Szitkar, F., Dyment, J., Fouquet, Y., and Choi, Y. (2014) What causes low magnetization at basalt-hosted hydrothermal sites? Insights from inactive site Krasnov (MAR 168380N), Geochem. Geophys. Geosyst., 15, 1441–1451, doi:10.1002/2014GC005284.

Szitkar, F., Petersen, S., Caratori Tontini, F., and Cocchi, L. (2015a) High-resolution magnetics reveal the deep structure of a volcanic arc-related basalt-hosted hydrothermal site (Palinuro, Tyrrhenian Sea): Geochemistry, Geophysics, Geosystems, v.16, doi: 10.1002/ 2015GC005769.

Szitkar, F., and Dyment, J. (2015b) Near-seafloor magnetics reveal tectonic rotation and deep structure at TAG (Trans-Atlantic Geotraverse) hydrothermal site (Mid-Atlantic Ridge, 268N), Geology, 43, 87–90, doi:10.1130/G36086.1.

Tivey, M.A., Rona, P.A., and Schouten, H. (1993) Reduced crustal magnetization beneath the active sulfide mound, TAG hydrothermal field, Mid-Atlantic Ridge, at 268N, Earth Planet. Sci. Lett., 115, 101–115, doi:10.1016/0012-821X (93)90216-V.

Tivey, M.A., and Johnson, H.P. (2002) Crustal magnetization reveals subsurface structure of Juan de Fuca Ridge hydrothermal vent fields, Geology, 30, 979–982, doi:10.1130/0091-7613 (2002)030<0979:CMRSSO>2.0.CO;2.

Tivey, M.A., and Dyment, J. (2010) The magnetic signature of hydrothermal systems in slow-spreading environments, in Diversity of Hydrothermal Systems on Slow Spreading Ocean Ridges, AGU Geophys. Monogr., vol. 188, edited by P. A. Rona et al., pp. 43–66, AGU, Washington, D. C., doi:10.1029/2008GM000773.

Watkins, N.D., and Paster, T.P. (1971) The magnetic properties of igneous rocks from the ocean floor, Philos. Trans. R. Soc. London, 268, 507–550.

Zhu, J., Lin, J., Chen, Y.J., Tao, C., German, C.R., Yoerger, D.R., and Tivey, M.A. (2010) A reduced crustal magnetization zone near the first observed active hydrothermal vent field on the Southwest Indian Ridge, Geophys. Res. Lett., 37, L18303, doi:10.1029/2010GL043542.

Appendices

Appendix 1: Maps of ship-based multibeam data from transits

Appendix 2: AUV dive sheets

Appendix 3: Tables of sediment subsampling

Appendix 4: Core scans

Appendix 1

Maps of ship-based multibeam data from transits

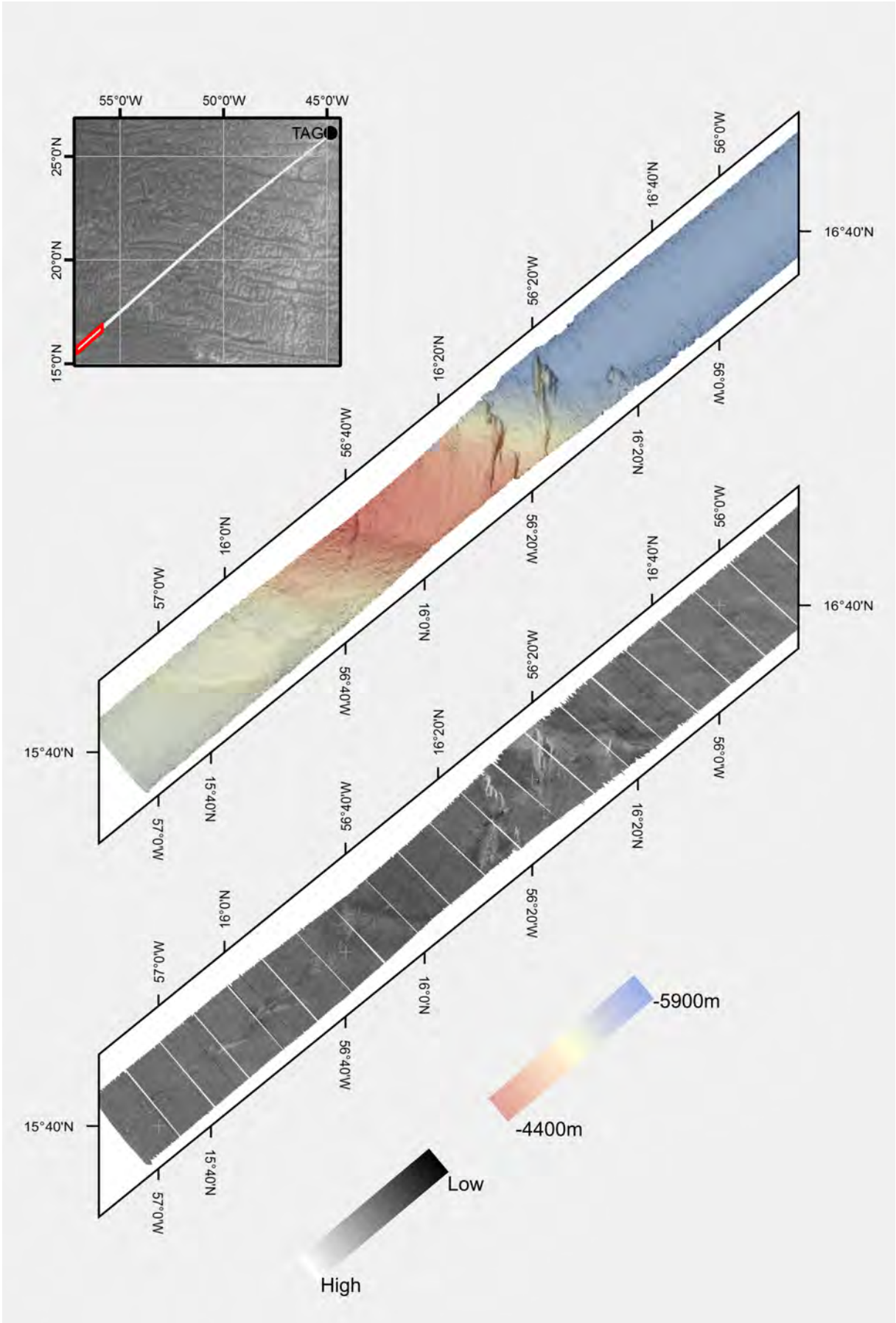

Appendix 1: Bathymetric and backscatter map of the transit to TAG. Map 1 of 10

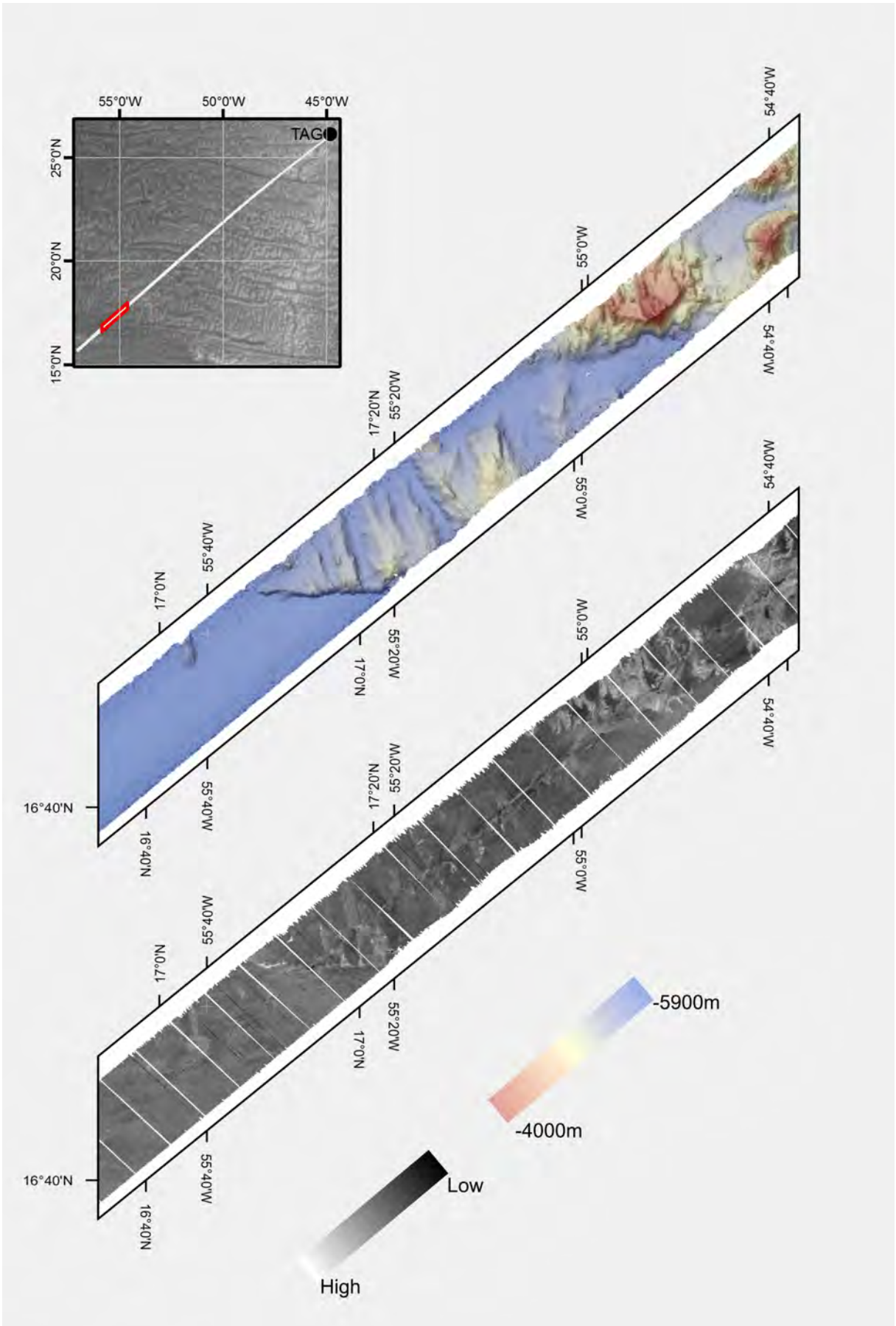

Appendix 1: Bathymetric and backscatter map of the transit to TAG. Map 2 of 10

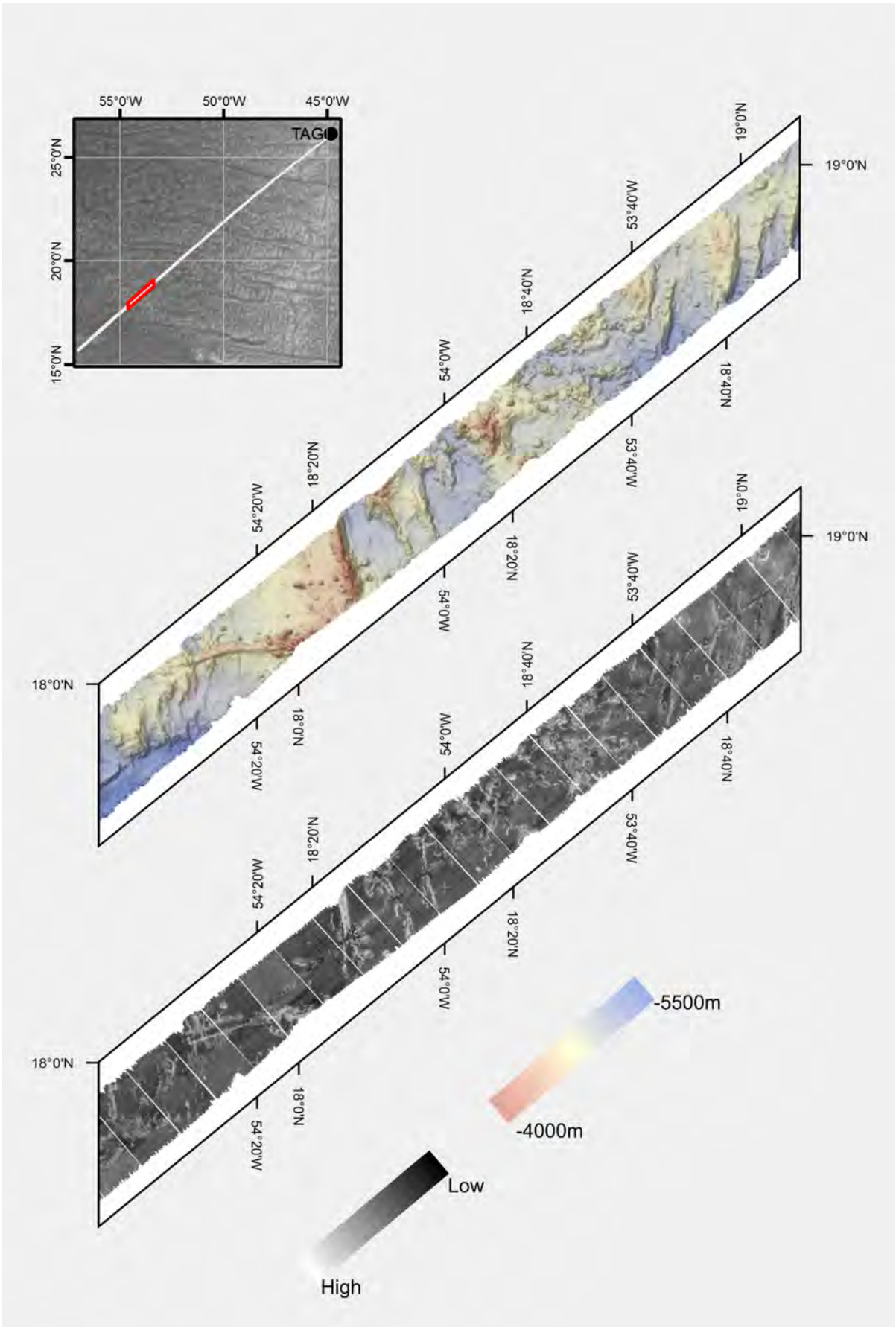

Appendix 1: Bathymetric and backscatter map of the transit to TAG. Map 3 of 10

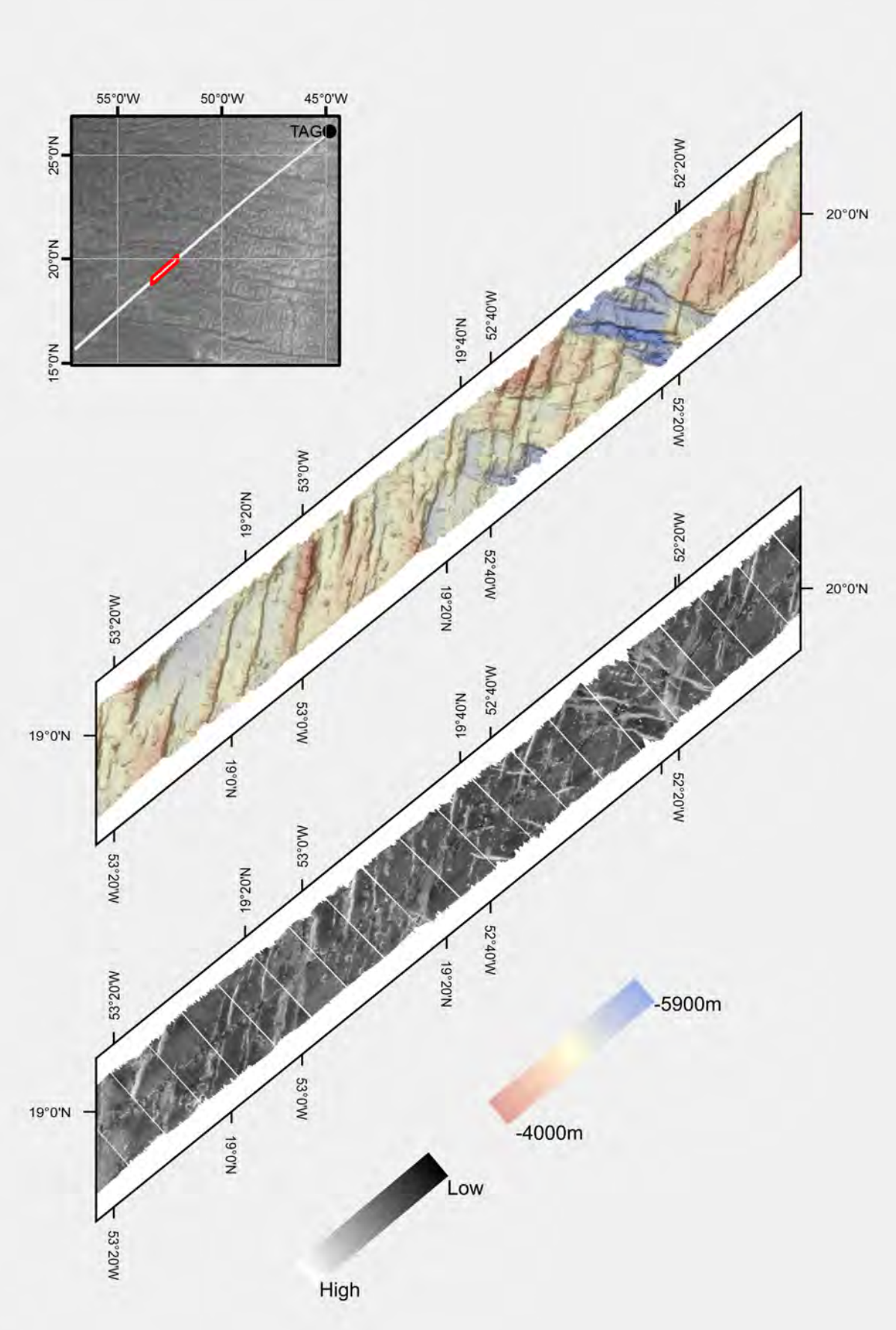

Appendix 1: Bathymetric and backscatter map of the transit to TAG. Map 4 of 10

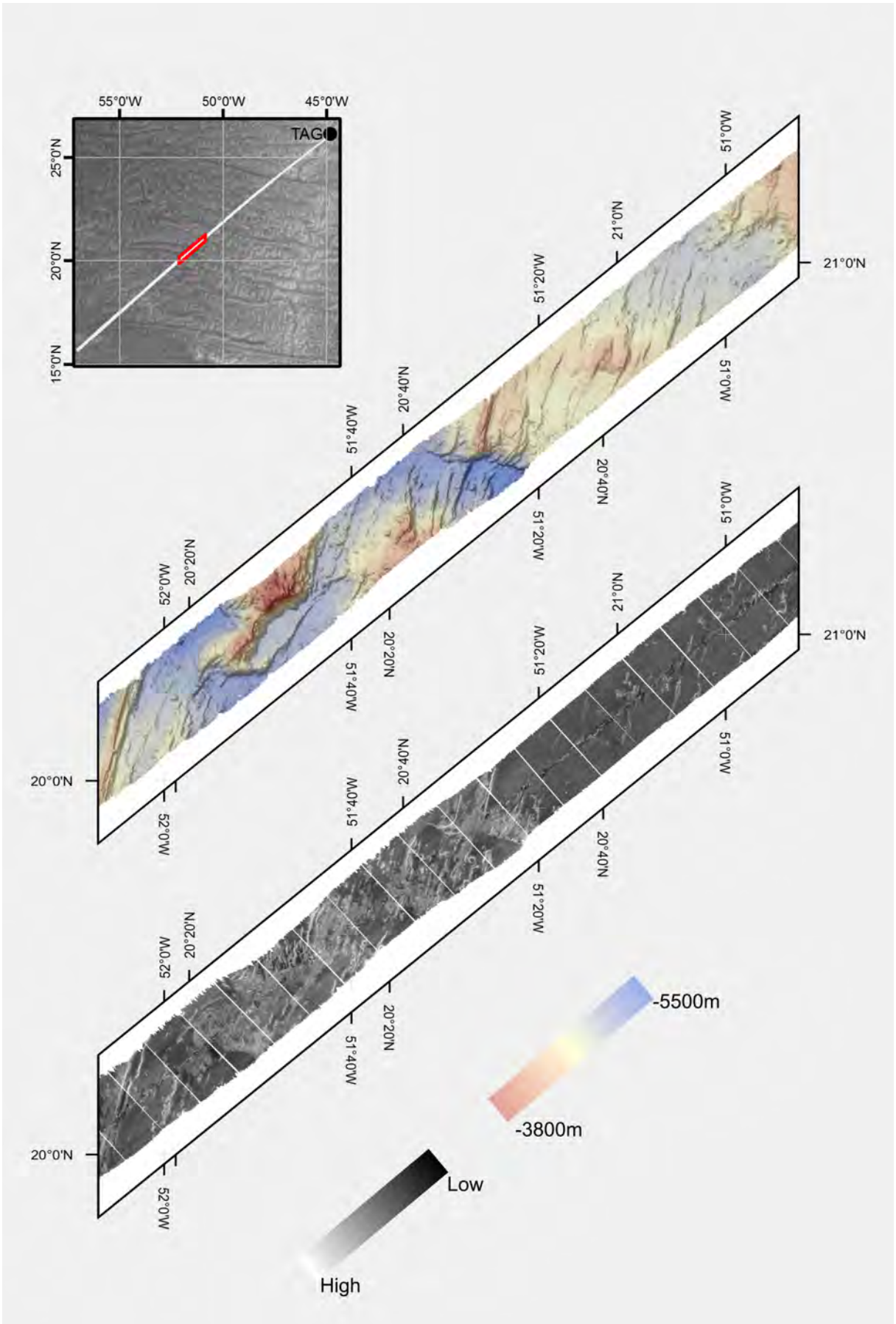

Appendix 1: Bathymetric and backscatter map of the transit to TAG. Map 5 of 10

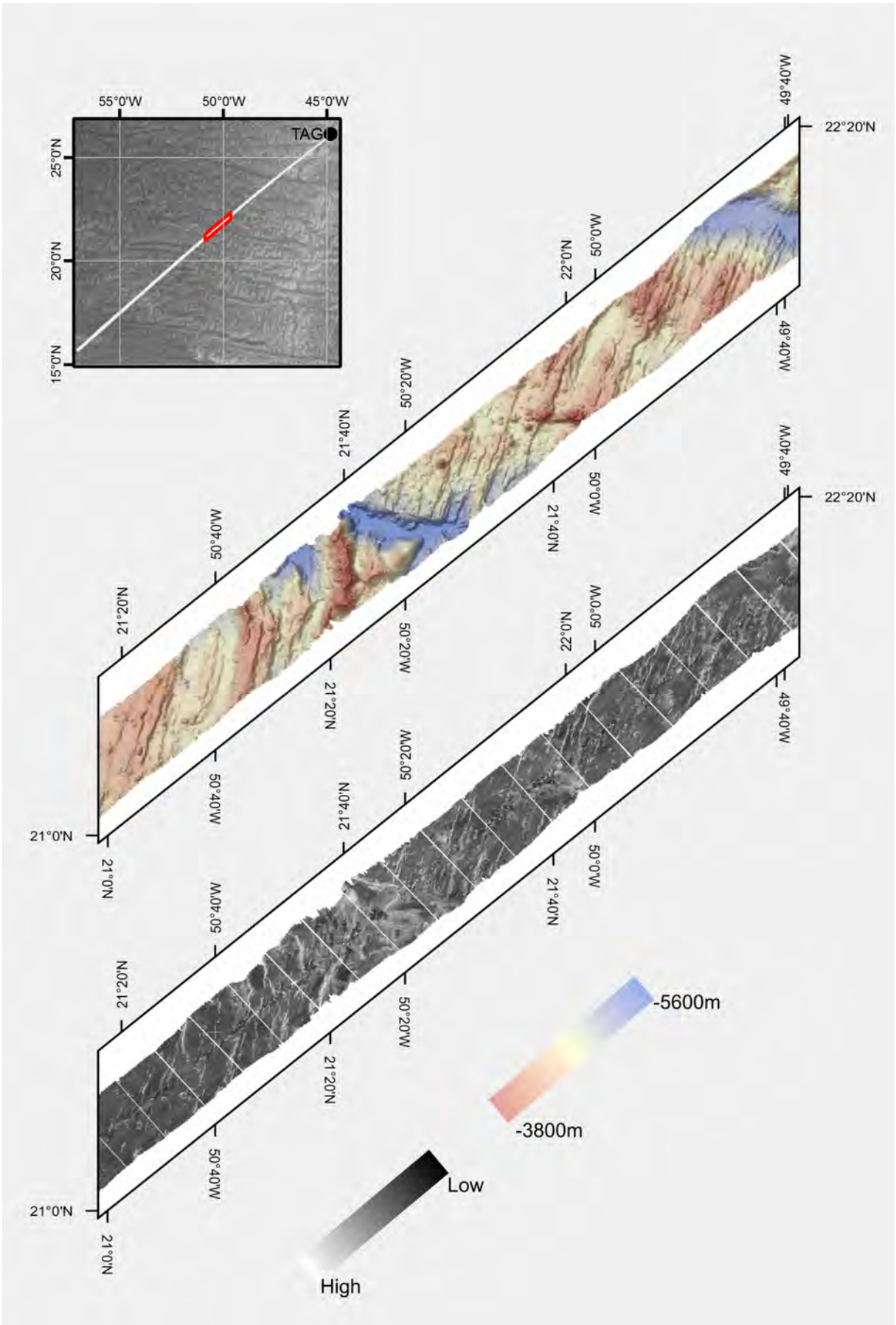

Appendix 1: Bathymetric and backscatter map of the transit to TAG. Map 6 of 10

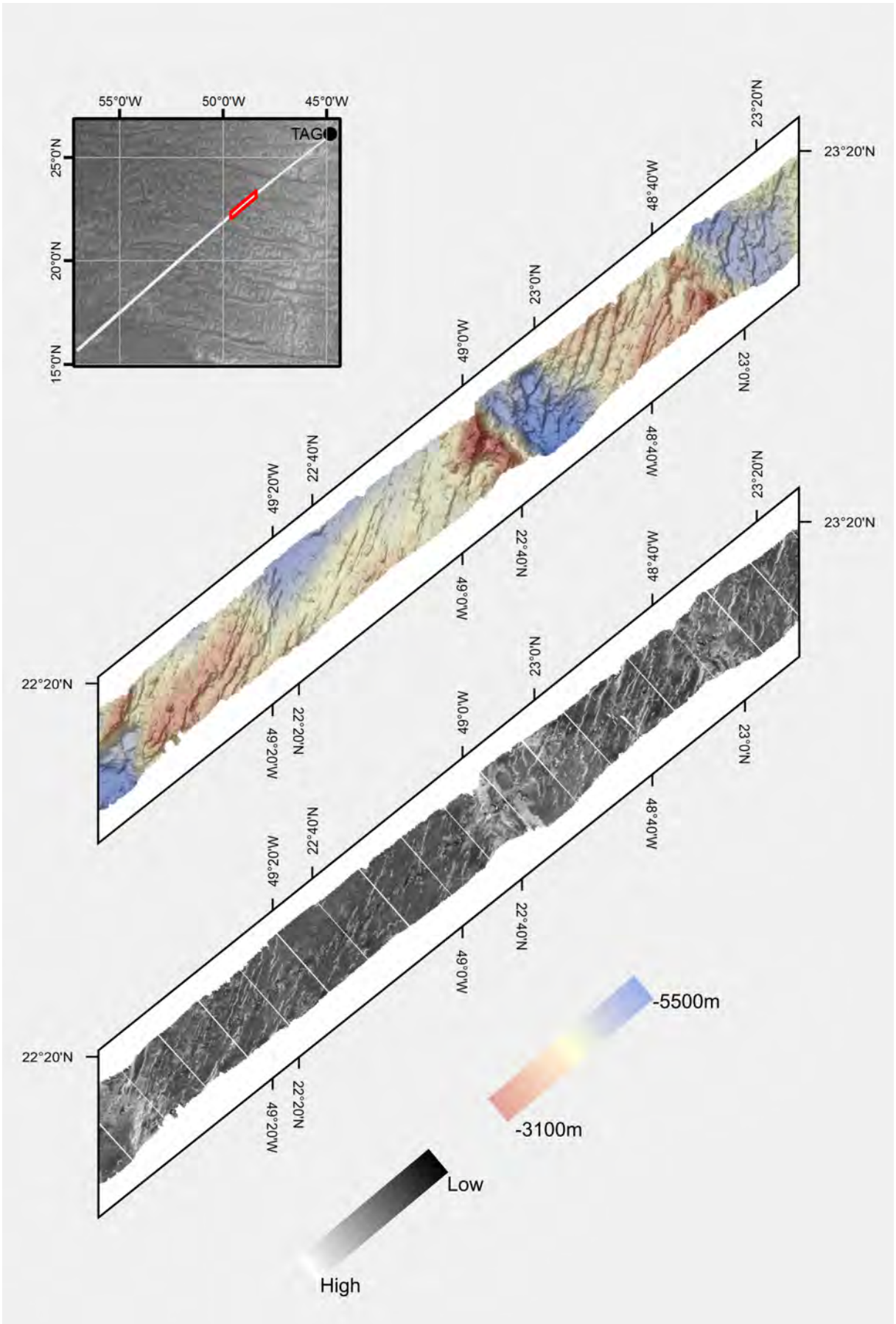

Appendix 1: Bathymetric and backscatter map of the transit to TAG. Map 7 of 10

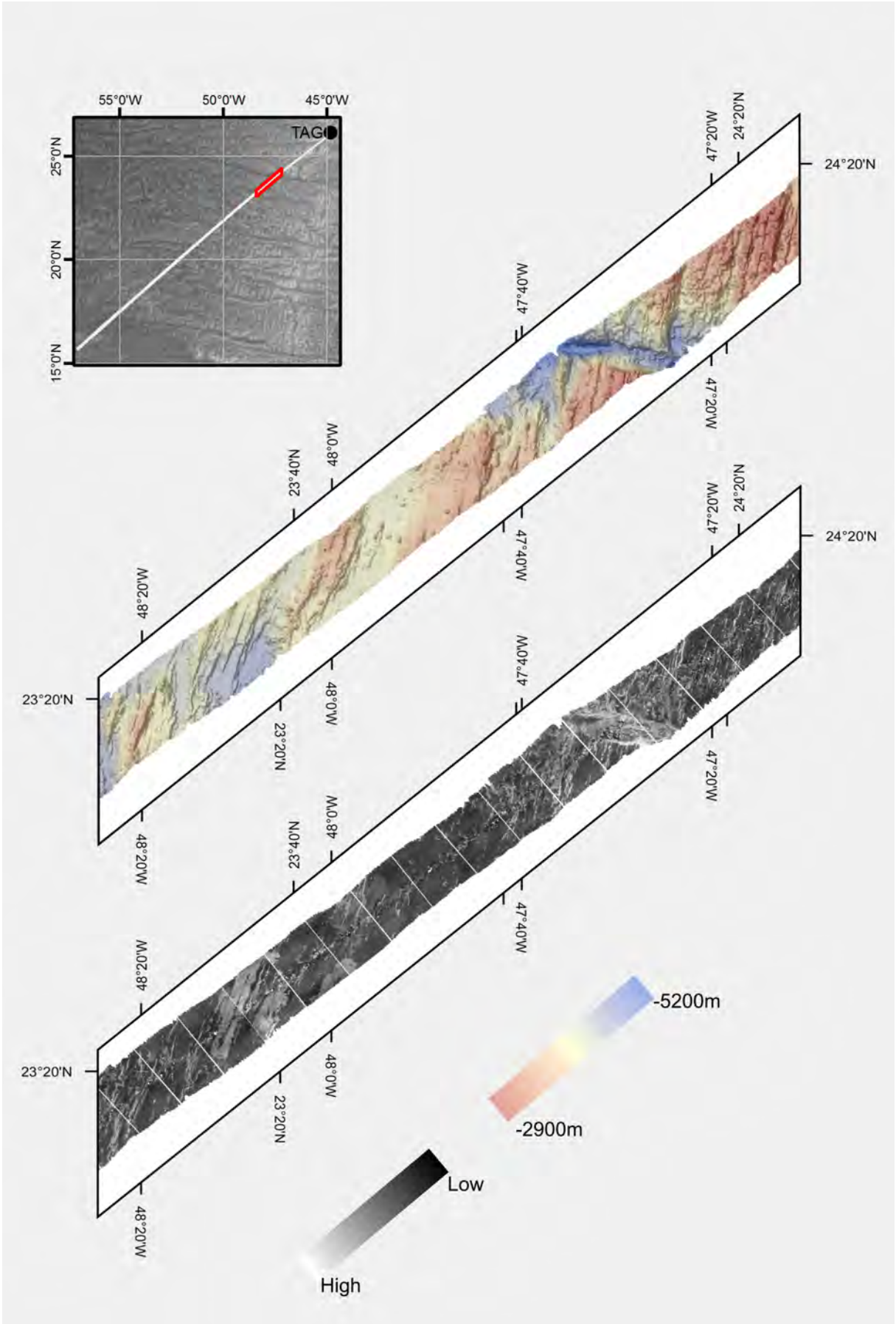

Appendix 1: Bathymetric and backscatter map of the transit to TAG. Map 8 of 10

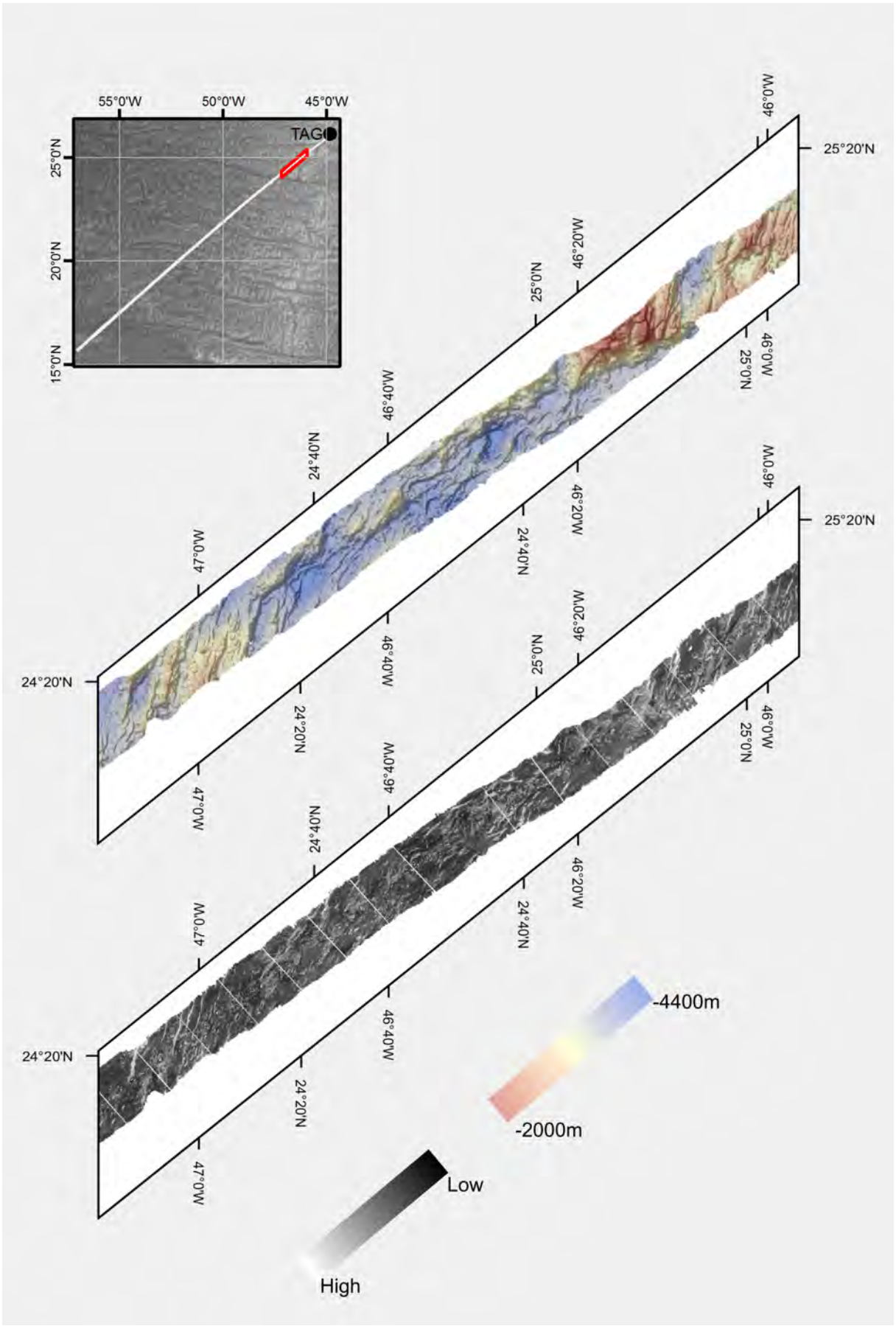

Appendix 1: Bathymetric and backscatter map of the transit to TAG. Map 9 of 10

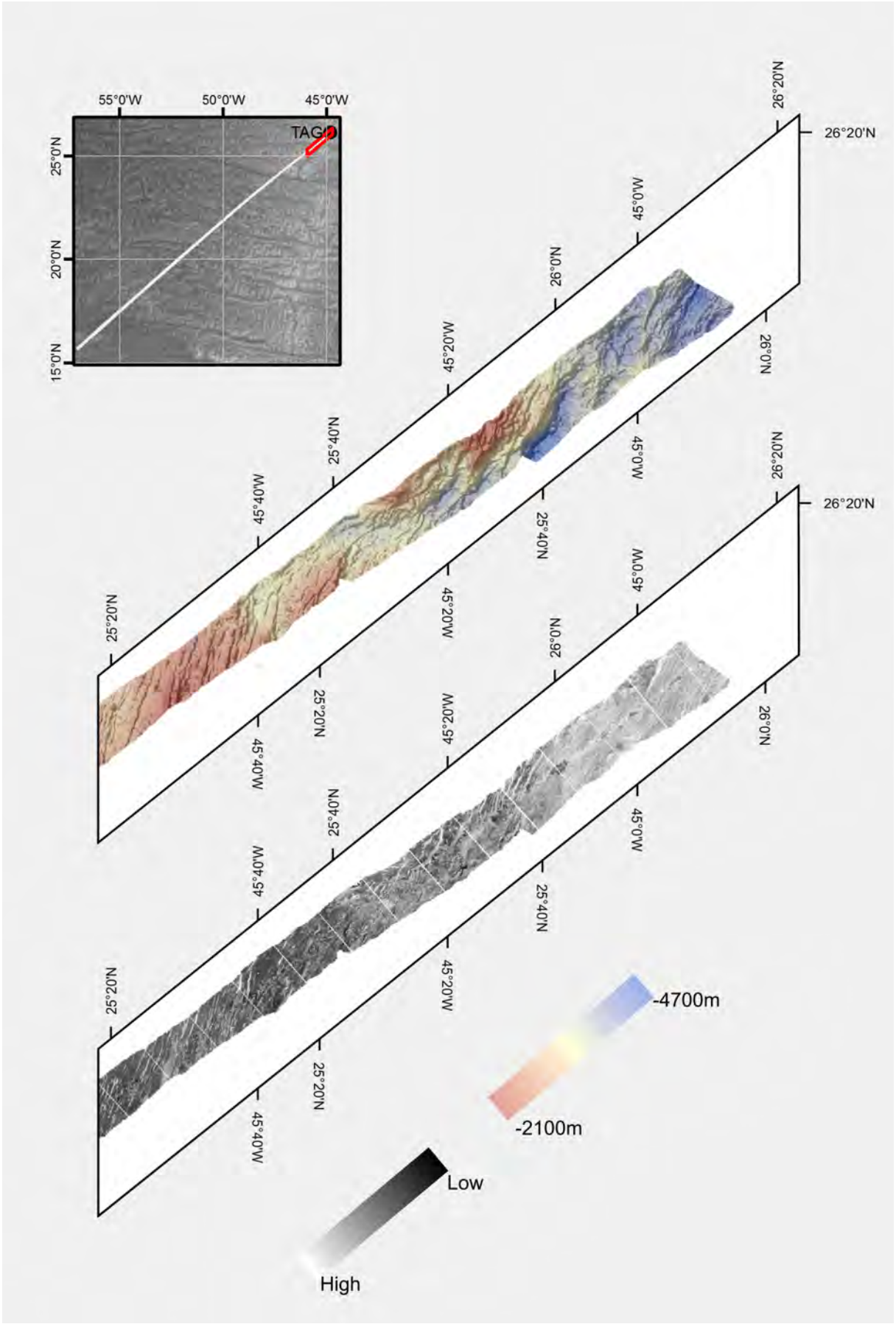

Appendix 1: Bathymetric and backscatter map of the transit to TAG. Map 10 of 10

Appendix 2

AUV dive sheets

Station	**M127/559**	GEOMAR	Day (UTC)	29.05.2016	
Dive	**Abyss0223**				

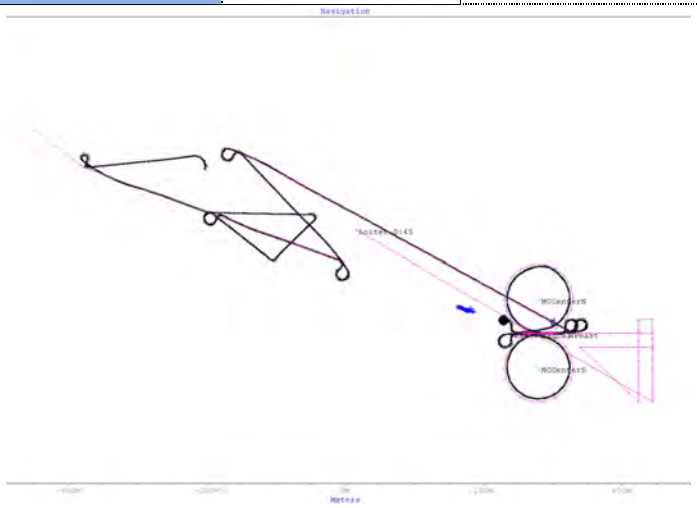

Mission goal:

Mission 223 was to check trim and buoyancy after the integration of the combined Magnetometer and Self Potential Sensor. Additionally a Magnetometer calibration should be done.

Times (UTC)	
Launch	17:15
Mission start	17:42
Survey start	18:05
Survey finished	18:17
Mission finished	18:29
Recovery	19:12
Distance travelled	2.93 km

Mission comments

- Mission took place while stopped ship during transit to work area
- Mission aborted due to leak in the tail section while Magnetometer calibration.

Depth / Altitude	- vehicle drove down to at a depth of 500 m during Magnetometer calibration (max. depth: 600 m)		
Line spacing	-		
Sensor	RESON Seabat 7125 200 kHz Multibeam		
Total raw files	Multibeam was tested (data not stored)	First file	-
Used raw files	-	Last file:	-
Survey area covered:	- Average coverage:	-	
Sensor	Magnetometer (APS-1540 S/N 0685) / Self Potential Sensor		
Total raw files	29 files (.B122) / 1.18 GB	First file	160529170500.B122
		Last file:	160529191500.B122
Comments	- Combined binary files include Magnetometer and Self Potential data		
Sensor	Eh / REDOX sensor (Koichi Nakamura)		
Total raw files	1 file (.txt) / 140 KB	File name	Abyss0223_REDOX.txt
Comments			
Sensor	SeaBird SBE49 FastCAT CTD (S/N: 4948793-0168)		
Total raw files	1 file (.txt) / 854 KB	File name	Abyss0223_CTD.txt
Comments	Sampling rate 4Hz		
Sensor	Wetlabs ECO FLNTU (Chlorophyll / Turbidity) (S/N: FLNTURTD-939)		
Total raw files	1 file (.txt) / 223 MB	File name	Abyss0223_ECO.txt
Comments			
Comments	- leak was caused by broken tail oil hose		

Station	**M127/568**		Day (UTC)	31.05.2016
Dive	**Abyss0224**			

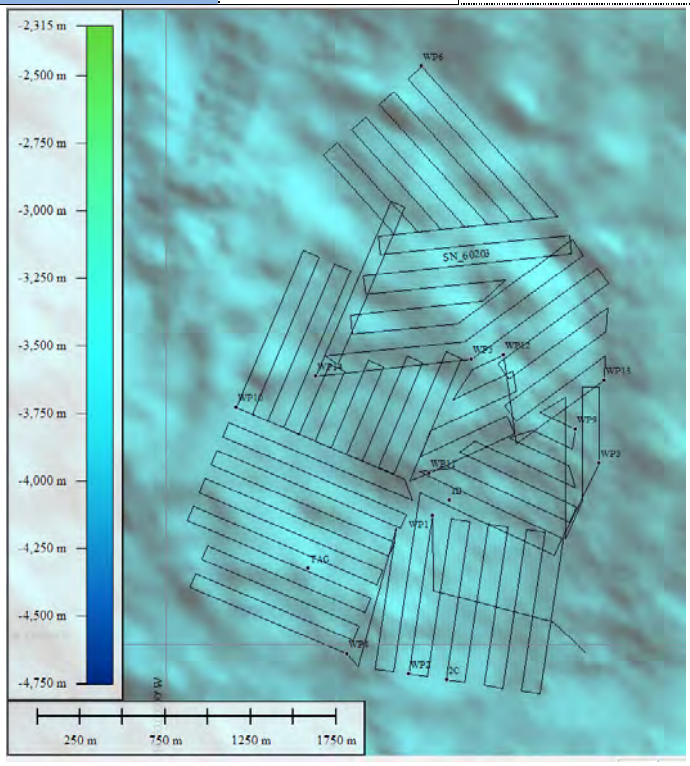

Mission goal:

Mission 224 was to map the southern part of the central box by using diverse fixed depths.

Times (UTC)	
Launch	20:35
Mission start	20:43
Survey start	21:48
Survey finished	09:55
Mission finished	11:16
Recovery	11:48
Distance travelled	80.91 km

Mission comments

- start position: 26°07.964'N 44°48.716'W
- transponders DT4B-LF and DT4C-LF were used for two legs, good fixes

Depth / Altitude	- survey pattern and legs planned with diverse fixed depths between 3470 and 3630 meters - vehicle flew in altitudes ranging from 20 and 110 m		
Line spacing	- line spacings were set considering slope; between 90-100 meters		
Sensor	RESON Seabat 7125 200 kHz Multibeam		
Total raw files	47 files (.s7k) / 12.4 GB	First file	20160531_214549.s7k
Used raw files	42 files (.s7k) / 11.42 GB	Last file:	20160601_094641.s7k
Survey area covered:	-	Average coverage:	-
Sensor	Magnetometer (APS-1540 S/N 0685) / Self Potential Sensor		
Total raw files	195 files (.B122) / 8.79 GB	First file	160531201500.B122
		Last file:	160601122500.B122
Comments	- Combined binary files include Magnetometer and Self Potential data		
Sensor	Eh / REDOX sensor (Koichi Nakamura)		
Total raw files	1 file (.txt) / 3.6 MB	File name	Abyss0224_REDOX.txt
Comments	Sampling rate 1Hz		
Sensor	SeaBird SBE49 FastCAT CTD (S/N: 4948793-0168)		
Total raw files	1 file (.txt) / 21.8 MB	File name	Abyss0224_CTD.txt
Comments	Sampling rate 4Hz		
Sensor	Wetlabs ECO FLNTU (Chlorophyll / Turbidity) (S/N: FLNTURTD-939)		
Total raw files	1 file (.txt) / 5.7 MB	File name	Abyss0224_ECO.txt
Comments	Sampling rate 1Hz		
Comments	- offset after descent phase: 108 m to 011° - strong interferences of another acoustic source (DVL) - Multibeam data were not used (Mission 226 re-mapped this area)		

Station	**M127/572**	Day (UTC)	01.06.2016
Dive	**Abyss0225**		

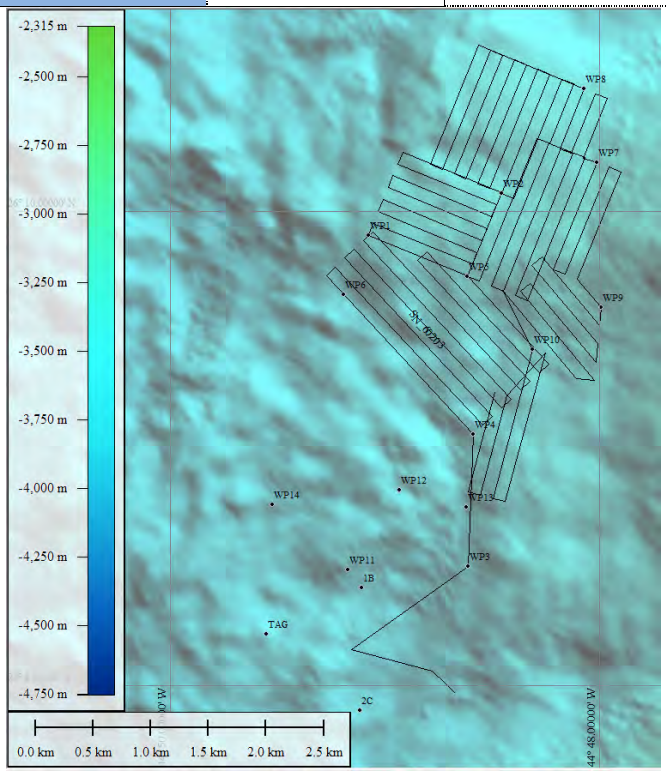

Mission goal:

Mission 225 was to map the northern part of the central box by using diverse fixed depths.

Times (UTC)	
Launch	18:05
Mission start	18:12
Survey start	19:24
Survey finished	05:22
Mission finished	06:39
Recovery	10:34
Distance travelled	68.99

Mission comments

- same mission start position than dive 224
- transponders DT4B-LF and DT4C-LF were used for two legs, good fixes

Depth / Altitude	- survey pattern and legs planned with diverse fixed depths between 3200 and 3600 meters - vehicle flew at altitudes ranging from 20 to 100 m		
Line spacing	- line spacings were set considering slope; between 90-100 meters		
Sensor	RESON Seabat 7125 200 kHz Multibeam		
Total raw files	185 files (.s7k) / 49.32 GB	First file	20160601_193454.s7k
Used raw files	147 files (.s7k) / 39.61 GB	Last file:	20160602_052035.s7k
Survey area covered:	-	Average coverage:	-
Sensor	Magnetometer (APS-1540 S/N 0685) / Self Potential Sensor		
Total raw files	199 files (.B122) / 8.97 GB	First file	160601180000.B122
		Last file:	160602103000.B122
Comments	- Combined binary files include Magnetometer and Self Potential data		
Sensor	Eh / REDOX sensor (Koichi Nakamura)		
Total raw files	1 file (.txt) / 3.1 MB	File name	Abyss0225_REDOX.txt
Comments	Sampling rate 1Hz		
Sensor	SeaBird SBE49 FastCAT CTD (S/N: 4948793-0168)		
Total raw files	1 file (.txt) / 18.6 MB	File name	Abyss0225_CTD.txt
Comments	Sampling rate 4Hz		
Sensor	Wetlabs ECO FLNTU (Chlorophyll / Turbidity) (S/N: FLNTURTD-939)		
Total raw files	1 file (.txt) / 4.8 MB	File name	Abyss0225_ECO.txt
Comments	Sampling rate 1Hz		
Comments	- offset after descent phase: 218 m to 342° - strong interferences of another acoustic source (DVL) - Multibeam data were not used (Mission 229 re-mapped this area)		

Station	**M127/582**		Day (UTC)	02.06.2016
Dive	**Abyss0226**			

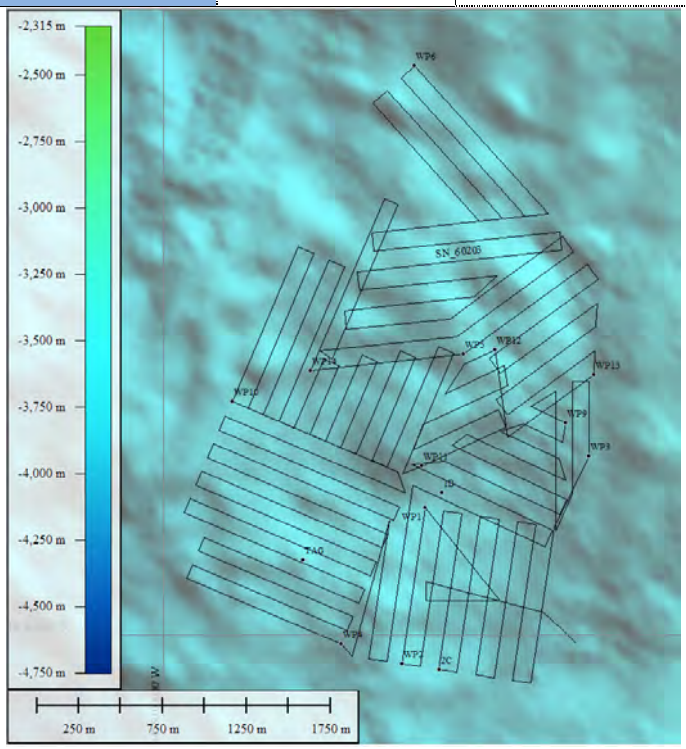

Mission goal:

Mission 226 was to repeat mission 224 in bottom following mode instead of fixes depths (Southern part of the central box).

Times (UTC)	
Launch	21:26
Mission start	21:31
Survey start	23:44
Survey finished	11:26
Mission finished	12:44
Recovery	13:25
Distance travelled	84.34 km

Mission comments

- same mission start position than dive 224
- transponders DT4B-LF and DT4C-LF were used for two legs, good fixes
- several test legs for RESON Multibeam setting before start survey pattern

Depth / Altitude	- bottom following at altitude of 80 metes - survey depths between 3410 and 3625 meters		
Line spacing	- line spacings were set considering slope; between 80-100 meters		
Sensor	RESON Seabat 7125 200 kHz Multibeam		
Total raw files	225 files (.s7k) / 58.79 GB	First file	20160602_234333.s7k
Used raw files	184 files (.s7k) / 49.57 GB	Last file:	20160603_112344.s7k
Survey area covered:	5.982 km^2 Average coverage:	0.51 km^2/hour @ 3.0 knots	
Sensor	Magnetometer (APS-1540 S/N 0685) / Self Potential Sensor		
Total raw files	189 files (.B122) / 8.52 GB	First file	160602210000.B122
		Last file:	160603124000.B122
Comments	- Combined binary files include Magnetometer and Self Potential data - Sensor data positions are not shifted to the corrected vehicle track		
Sensor	Eh / REDOX sensor (Koichi Nakamura)		
Total raw files	1 file (.txt) / 3.7 MB	File name	Abyss0226_REDOX.txt
Comments	- Sensor data positions are not shifted to the corrected vehicle track; Sampling rate 1Hz		
Sensor	SeaBird SBE49 FastCAT CTD (S/N: 4948793-0168)		
Total raw files	1 file (.txt) / 22.8 MB	File name	Abyss0226_CTD.txt
Comments	- Sensor data positions are not shifted to the corrected vehicle track; Sampling rate 4Hz		
Sensor	Wetlabs ECO FLNTU (Chlorophyll / Turbidity) (S/N: FLNTURTD-939)		
Total raw files	1 file (.txt) / 5.9 MB	File name	Abyss0226_ECO.txt
Comments	- Sensor data positions are not shifted to the corrected vehicle track; Sampling rate 1Hz		
Comments	- offset after descent phase: 165 m to 019° (LBL fix) - Sensor data positions (except RESON Multibeam) are not shifted to the corrected vehicle track - Corrected AUV track is stored in file Abyss0226_NEWNAVIGATION.xyz		

Station	**M127/599**		Day (UTC)	04.04.2016
Dive	**Abyss0227**			

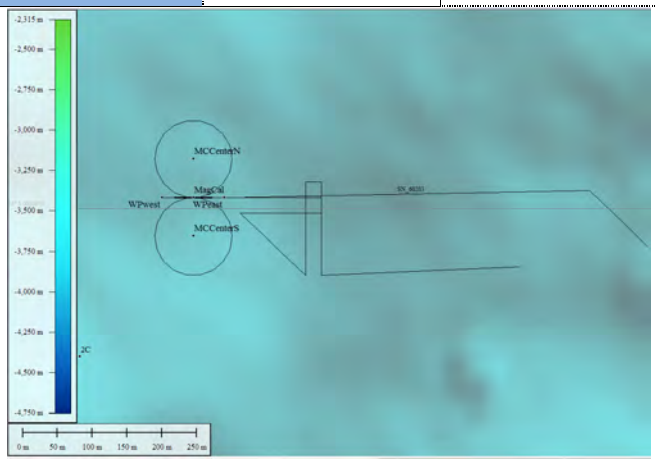

Mission goal:

Mission 227 was used to finish the magnetometer calibration.

Times (UTC)	
Launch	21:42
Mission start	21:46
Survey start	21:57
Survey finished	22:16
Mission finished	22:29
Recovery	-
Distance travelled	3.49 km

Mission comments

- same mission start position than dive 224

Depth / Altitude	The magnetometer calibration was done in 500 meters water depths (max. depth: 580 m)		
Line spacing	-		
Sensor	Magnetometer (APS-1540 S/N 0685) / Self Potential Sensor		
Total raw files	20 files (.B122) / 772.7 GB	First file	160604201000.B122
		Last file:	160604224103.B122
Comments	- Combined binary files include Magnetometer and Self Potential data		
Sensor	Eh / REDOX sensor (Koichi Nakamura)		
Total raw files	1 file (.txt) / 173 KB	File name	Abyss0227_REDOX.txt
Comments	Sampling rate 1Hz		
Sensor	SeaBird SBE49 FastCAT CTD (S/N: 4948793-0168)		
Total raw files	1 file (.txt) / 1.1 MB	File name	Abyss0227_CTD.txt
Comments	Sampling rate 4Hz		
Sensor	Wetlabs ECO FLNTU (Chlorophyll / Turbidity) (S/N: FLNTURTD-939)		
Total raw files	1 file (.txt) / 275 KB	File name	Abyss0227_ECO.txt
Comments	Sampling rate 1Hz		
Comments	-		

Station	**M127/599**	Day (UTC)	04.06.2016
Dive	**Abyss0228**		

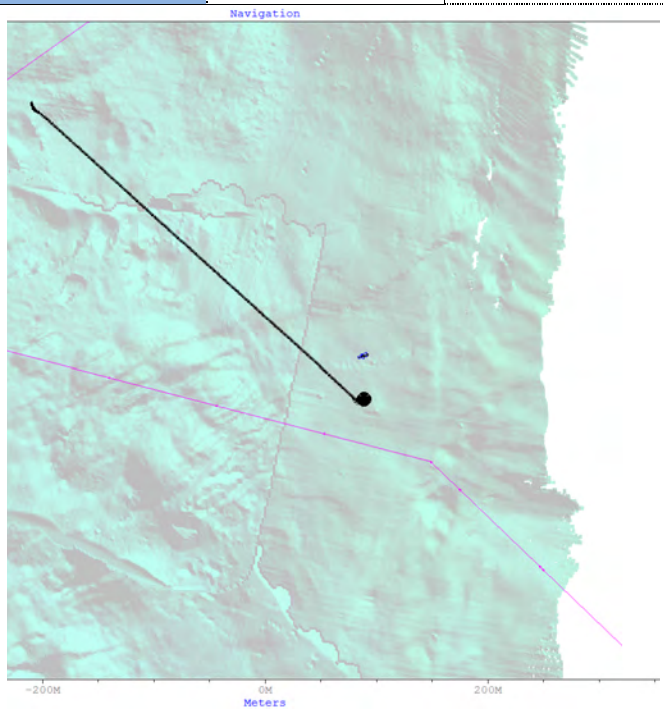

Mission goal:

Mission 228 was to repeat mission 225 in bottom following mode instead of flying at fixed depths.

Times (UTC)	
Launch	-
Mission start	22:50
Survey start	-
Survey finished	-
Mission finished	22:55
Recovery	23:19
Distance travelled	0.43 km

Mission comments

- Mission was started just after 227 without launch and recovery
- Mission was aborted on the first leg due to timeout.
- Dive was repeated in mission 229

Depth / Altitude	-		
Line spacing	-		
Sensor	Eh / REDOX sensor (Koichi Nakamura)		
Total raw files	1 file (.txt) / 20 KB	File name	Abyss0228_REDOX.txt
Comments	Sampling rate 1Hz		
Sensor	SeaBird SBE49 FastCAT CTD (S/N: 4948793-0168)		
Total raw files	1 file (.txt) / 120 KB	File name	Abyss0228_CTD.txt
Comments	Sampling rate 4Hz		
Sensor	Wetlabs ECO FLNTU (Chlorophyll / Turbidity) (S/N: FLNTURTD-939)		
Total raw files	1 file (.txt) / 31 KB	File name	Abyss0228_ECO.txt
Comments	Sampling rate 1Hz		
Comments	- Vehicle dropped ascent weight on 175 meters depth.		

Station	**M127/599**		Day (UTC)	04.06.2016
Dive	**Abyss0229**			

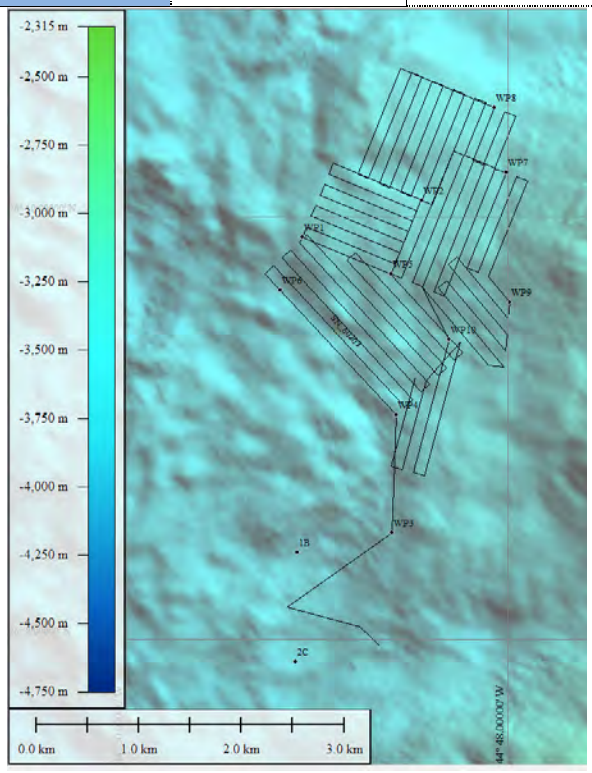

Mission goal:

Mission 229 was to repeat mission 225 in bottom following mode instead of flying at fixed depths.

Times (UTC)	
Launch	23:57
Mission start	23:59
Survey start	01:14
Survey finished	11:13
Mission finished	11:24
Recovery	13:42
Distance travelled	62.45 km

Mission comments

- same mission start position than dive 224
- transponders DT4B-LF and DT4C-LF were used for two legs
- good transponder position updates after descent phase

Depth / Altitude	- bottom following at altitude 80 metes - survey depths between 3260 and 3610 meters		
Line spacing	- line spacings: 100 meters		
Sensor	RESON Seabat 7125 200 kHz Multibeam		
Total raw files	189 files (.s7k) / 49.79 GB	First file	20160605_011227.s7k
Used raw files	158 files (.s7k) / 42.57 GB	Last file:	20160605_111145.s7k
Survey area covered:	5.802 km^2	Average coverage:	0.58 km^2/hour @ 3.0 knots
Sensor	Magnetometer (APS-1540 S/N 0685) / Self Potential Sensor		
Total raw files	158 files (.B122) / 7.11 GB	First file	160605000000.B122
		Last file:	160605130500.B122
Comments	- Combined binary files include Magnetometer and Self Potential data - Sensor data positions are not shifted to the corrected vehicle track		
Sensor	Eh / REDOX sensor (Koichi Nakamura)		
Total raw files	1 file (.txt) / 2.8 MB	File name	Abyss0229_REDOX.txt
Comments	- Sensor data positions are not shifted to the corrected vehicle track; Sampling rate 1Hz		
Sensor	SeaBird SBE49 FastCAT CTD (S/N: 4948793-0168)		
Total raw files	1 file (.txt) / 17.0 MB	File name	Abyss0229_CTD.txt
Comments	- Sensor data positions are not shifted to the corrected vehicle track; Sampling rate 4Hz		
Sensor	Wetlabs ECO FLNTU (Chlorophyll / Turbidity) (S/N: FLNTURTD-939)		
Total raw files	1 file (.txt) / 4.4 MB	File name	Abyss0229_ECO.txt
Comments	- Sensor data positions are not shifted to the corrected vehicle track; Sampling rate 1Hz		
Comments	- offset after descent phase: 124 m to 40° - Sensor data positions (except RESON Multibeam) are not shifted to the corrected vehicle track - Corrected AUV track is stored in file Abyss0229_NEWNAVIGATION.xyz - Multibeam raw files are larger because they contain record 7011 (compressed images)		

Station	**M127/610**	Day (UTC)	05.06.2016
Dive	**Abyss0230**		

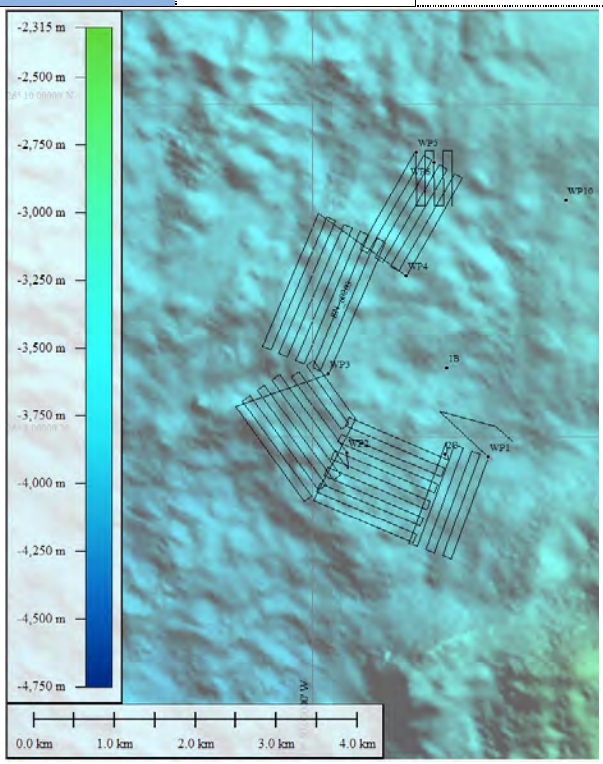

Mission goal:

Mission was to map the southwest region of the central box including the ATA position reffered to by IFREMER.

Times (UTC)	
Launch	20:00
Mission start	20:05
Survey start	21:11
Survey finished	09:25
Mission finished	10:47
Recovery	11:10
Distance travelled	80.19 km

Mission comments

- Same mission start position than dive 224
- Vehicle wasn't able to get LBL fix
- Vehicle only got ranges from Transponder DT4B-LF after descent phase

Depth / Altitude	- bottom following at altitude 80 metes - survey depths between 3450 and 3800 meters		
Line spacing	- line spacings: 100 meters		
Sensor	RESON Seabat 7125 200 kHz Multibeam		
Total raw files	56 files (.s7k) / 14.86 GB	First file	20160605_205827.s7k
Used raw files	48 files (.s7k) / 13.03 GB	Last file:	20160606_084220.s7k
Survey area covered:	7.508 km^2	Average coverage:	0.61 km^2/hour @ 3.0 knots
Sensor	Magnetometer (APS-1540 S/N 0685) / Self Potential Sensor		
Total raw files	177 files (.B122) / 7.98 GB	First file	160605200500.B122
		Last file:	160606104500.B122
Comments	- Combined binary files include Magnetometer and Self Potential data - Sensor data positions are not shifted to the corrected vehicle track		
Sensor	Eh / REDOX sensor (Koichi Nakamura)		
Total raw files	1 file (.txt) / 3.1 MB	File name	Abyss0230_REDOX.txt
Comments	- Sensor data positions are not shifted to the corrected vehicle track; Sampling rate 1Hz		
Sensor	SeaBird SBE49 FastCAT CTD (S/N: 4948793-0168)		
Total raw files	1 file (.txt) / 21.9 MB	File name	Abyss0230_CTD.txt
Comments	- Sensor data positions are not shifted to the corrected vehicle track; Sampling rate 4Hz		
Sensor	Wetlabs ECO FLNTU (Chlorophyll / Turbidity) (S/N: FLNTURTD-939)		
Total raw files	1 file (.txt) / 5.7 MB	File name	Abyss0230_ECO.txt
Comments	- Sensor data positions are not shifted to the corrected vehicle track; Sampling rate 1Hz		
Comments	- offset after descent phase: map 230 has to be shifted ca. 140 m to 291° (measured on New Mound 1) (no transponder fix) - Sensor data positions (except RESON Multibeam) are not shifted to the corrected vehicle track - Corrected AUV track is stored in file Abyss0230_NEWNAVIGATION.xyz		

Station	**M127/620**	GEOMAR	Day (UTC)	06.06.2016
Dive	**Abyss0231**			

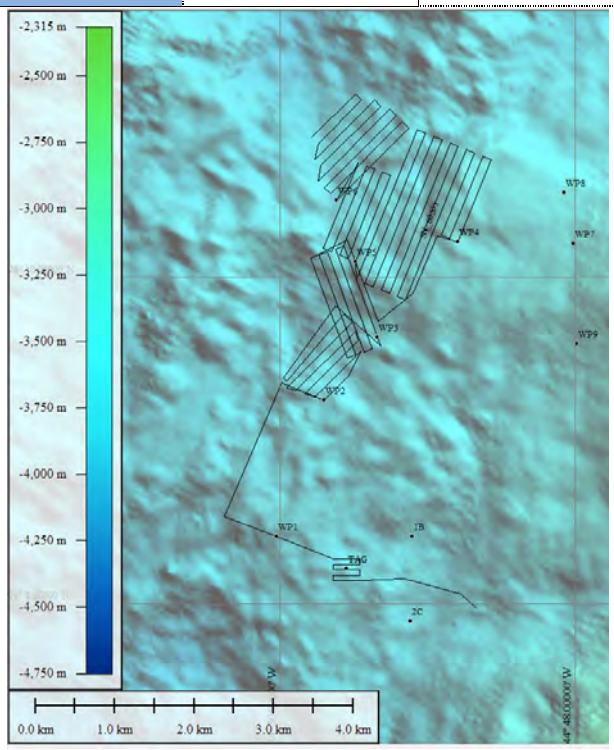

Mission goal:

Mission was to map the northwest area of the central box including "Shimmering mound" and repeated the mapping of the TAG mound by doing a survey pattern closer to the ground.

Times (UTC)	
Launch	20:38
Mission start	20:41
Survey start	21:45
Survey finished	07:40
Mission finished	09:07
Recovery	10:09
Distance travelled	67.69 km

Mission comments

- Same mission start position than dive 224
- Vehicle wasn't able to get LBL fix
- Vehicle only got ranges from Transponder DT4B-LF after descent phase

Depth / Altitude	- bottom following at altitude 80 metes (except survey pattern above TAG: fix depth 3590 m) - survey depths between 3320 and 3780 meters		
Line spacing	- line spacing (TAG area survey): 60 m - line spacing (northern survey pattern): 100 m		
Sensor	RESON Seabat 7125 200 kHz Multibeam		
Total raw files	45 files (.s7k) / 11.88 GB	First file	20160606_213520.s7k
Used raw files	39 files (.s7k) / 10.59 GB	Last file:	20160607_073134.s7k
Survey area covered:	6.679 km^2	Average coverage:	0.67 km^2/hour @ 3.0 knots
Sensor	Magnetometer (APS-1540 S/N 0685) / Self Potential Sensor		
Total raw files	208 files (.B122) / 8.57 GB	First file	160606181239.B122
		Last file:	160607113000.B122
Comments	- Combined binary files include Magnetometer and Self Potential data - Sensor data positions are not shifted to the corrected vehicle track		
Sensor	Eh / REDOX sensor (Koichi Nakamura)		
Total raw files	1 file (.txt) / 3.0 MB	File name	Abyss0231_REDOX.txt
Comments	- Sensor data positions are not shifted to the corrected vehicle track; Sampling rate 1Hz		
Sensor	SeaBird SBE49 FastCAT CTD (S/N: 4948793-0168)		
Total raw files	1 file (.txt) / 18.5 MB	File name	Abyss0231_CTD.txt
Comments	- Sensor data positions are not shifted to the corrected vehicle track; Sampling rate 4Hz		
Sensor	Wetlabs ECO FLNTU (Chlorophyll / Turbidity) (S/N: FLNTURTD-939)		
Total raw files	1 file (.txt) / 4.8 MB	File name	Abyss0231_ECO.txt
Comments	- Sensor data positions are not shifted to the corrected vehicle track; Sampling rate 1Hz		
Comments	- offset after descent phase: map 231 has to be shifted ca. 116 m to 293° (measures on TAG) -> no transponder fix - Sensor data positions (except RESON Multibeam) are not shifted to the corrected vehicle track - Corrected AUV track is stored in file Abyss0231_NEWNAVIGATION.xyz		

Station	**M127/623**	GEOMAR	Day (UTC)	08.06.2016	
Dive	**Abyss0232**				

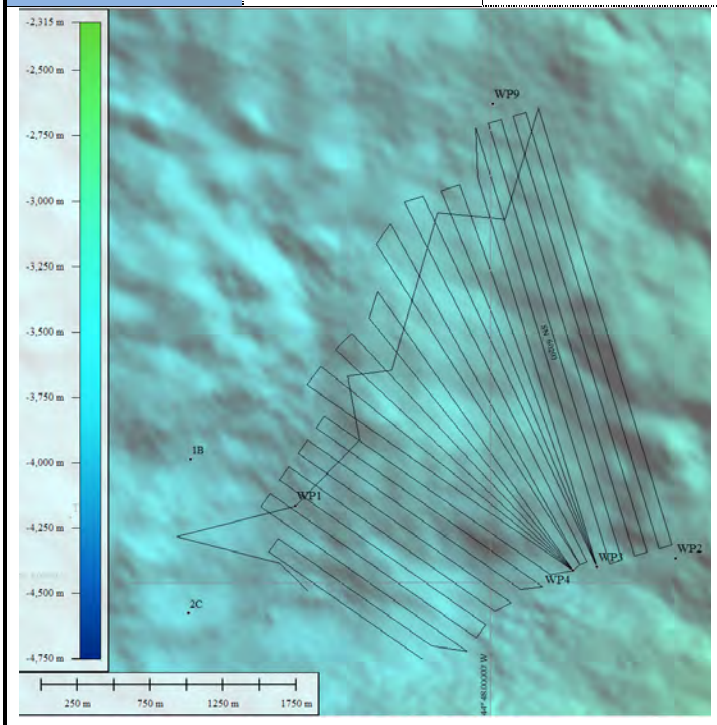

Mission goal:

Mission was to map the area southeast of the central box including the "MIR" zone.

Times (UTC)	
Launch	23:07
Mission start	23:12
Survey start	00:28
Survey finished	12:43
Mission finished	14:03
Recovery	14:31
Distance travelled	81.61 km

Mission comments

- same mission start position than dive 224
- transponders DT4B-LF and DT4C-LF were used for two legs
- good transponder position updates after descent phase

Depth / Altitude	- bottom following at altitude 80 metes - survey depths between 3100 and 3625 meters		
Line spacing	- line spacings were set considering slope; mainly between 80-100 meters - max. line spacing: 120 meters		
Sensor	RESON Seabat 7125 200 kHz Multibeam		
Total raw files	58 files (.s7k) / 14.78 GB	First file	20160609_002221.s7k
Used raw files	49 files (.s7k) / 13.31 GB	Last file:	20160609_123542.s7k
Survey area covered:	6.21 km^2	Average coverage:	0.51 km^2/hour @ 3.0 knots
Sensor	Magnetometer (APS-1540 S/N 0685) / Self Potential Sensor		
Total raw files	183 files (.B122) / 8.25 GB	First file	160608231000.B122
		Last file:	160609142000.B122
Comments	- Combined binary files include Magnetometer and Self Potential data - Sensor data positions are not shifted to the corrected vehicle track		
Sensor	Eh / REDOX sensor (Koichi Nakamura)		
Total raw files	1 file (.txt) / 3.6 MB	File name	Abyss0232_REDOX.txt
Comments	- Sensor data positions are not shifted to the corrected vehicle track; Sampling rate 1Hz		
Sensor	SeaBird SBE49 FastCAT CTD (S/N: 4948793-0168)		
Total raw files	1 file (.txt) / 22.1 MB	File name	Abyss0232_CTD.txt
Comments	- Sensor data positions are not shifted to the corrected vehicle track; Sampling rate 4Hz		
Sensor	Wetlabs ECO FLNTU (Chlorophyll / Turbidity) (S/N: FLNTURTD-939)		
Total raw files	1 file (.txt) / 5.8 MB	File name	Abyss0232_ECO.txt
Comments	- Sensor data positions are not shifted to the corrected vehicle track; Sampling rate 1Hz		
Comments	- offset after descent phase: 109 m to 342° - Sensor data positions (except RESON Multibeam) are not shifted to the corrected vehicle track - Corrected AUV track is stored in file Abyss0232_NEWNAVIGATION.xyz		

Station	**M127/635**	GEOMAR	Day (UTC)	10.06.2016
Dive	**Abyss0233**			

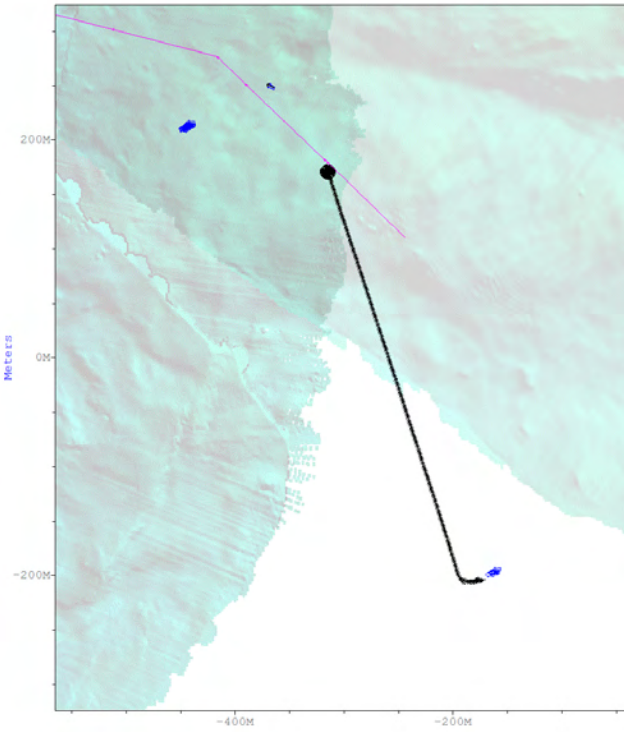

Mission goal:

Mission was to map the area of the "New Mounds" with higher resolution using the 400 kHz configuration.

Times (UTC)	
Launch	22:43
Mission start	22:46
Survey start	-
Survey finished	-
Mission finished	22:55
Recovery	23:09
Distance travelled	424 km

Mission comments

- Mission was aborted on the first leg due to timeout.
- Dive was repeated in mission 234

Depth / Altitude	-		
Line spacing	-		
Sensor	Eh / REDOX sensor (Koichi Nakamura)		
Total raw files	1 file (.txt) / 21.0 KB	File name	Abyss0233_REDOX.txt
Comments	Sampling rate 1Hz		
Sensor	SeaBird SBE49 FastCAT CTD (S/N: 4948793-0168)		
Total raw files	1 file (.txt) / 130.0 kB	File name	Abyss0233_CTD.txt
Comments	Sampling rate 4Hz		
Sensor	Wetlabs ECO FLNTU (Chlorophyll / Turbidity) (S/N: FLNTURTD-939)		
Total raw files	1 file (.txt) / 34.0 kB	File name	Abyss0233_ECO.txt
Comments	Sampling rate 1Hz		
Comments	- Vehicle dropped ascent weight on 174 meters depth.		

Station	**M127/635**		Day (UTC)	10.06.2016
Dive	**Abyss0234**			

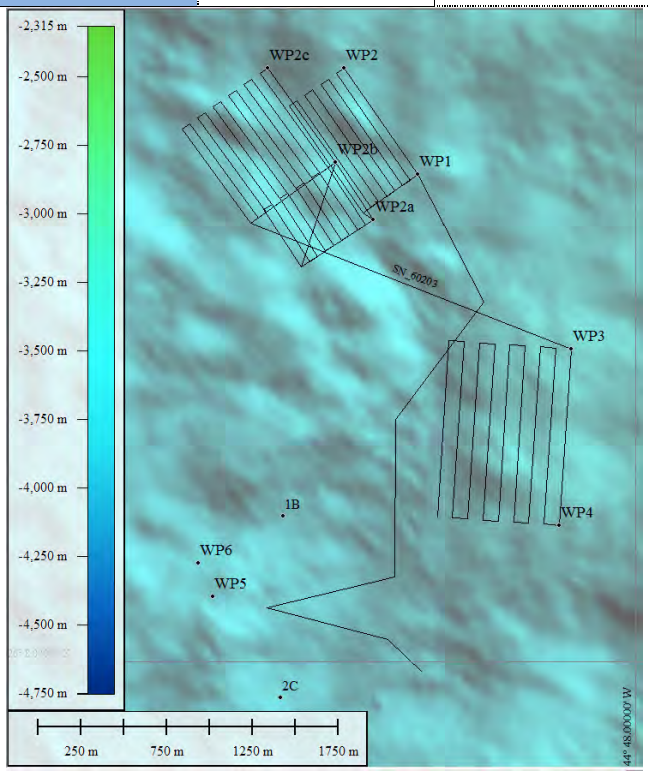

Mission goal:

Mission was to map the area of the "New Mounds" with higher resolution using the 400 kHz configuration.

Times (UTC)	
Launch	23:35
Mission start	23:37
Survey start	01:11
Survey finished	13:15
Mission finished	13:20
Recovery	15:02
Distance travelled	75.44 m

Mission comments

- same mission start position than dive 224
- transponders DT4B-LF and DT4C-LF were used for two legs; good fixes after descent
- Ground fault (50) as soon ascent weight was dropped (no surface objective)

Depth / Altitude	- fixed depths for the three survey patterns in the north (each split in three altitude levels) - survey depths between 3320 and 3590 meters		
Line spacing	- line spacing (northern survey pattern): 50 meters - line spacing (eastern survey pattern): 80 meters		
Sensor	RESON Seabat 7125 400 kHz Multibeam		
Total raw files	61 files (.s7k) / 16.19 GB	First file	20160611_010429.s7k
Used raw files	56 files (.s7k) / 15.09 GB	Last file:	20160611_130956.s7k
Survey area covered:	0.90 km^2 Average coverage:	0.07 km^2/hour @ 3.0 knots	
Sensor	Magnetometer (APS-1540 S/N 0685) / Self Potential Sensor		
Total raw files	182 files (.B122) / 8.2 GB	First file	160610233000.B122
		Last file:	160611143500.B122
Comments	- Combined binary files include Magnetometer and Self Potential data - Sensor data positions are not shifted to the corrected vehicle track		
Sensor	Eh / REDOX sensor (Koichi Nakamura)		
Total raw files	1 file (.txt) / 3.4 MB	File name	Abyss0234_REDOX.txt
Comments	- Sensor data positions are not shifted to the corrected vehicle track; Sampling rate 1Hz		
Sensor	SeaBird SBE49 FastCAT CTD (S/N: 4948793-0168)		
Total raw files	1 file (.txt) / 20.4 MB	File name	Abyss0234_CTD.txt
Comments	- Sensor data positions are not shifted to the corrected vehicle track; Sampling rate 4Hz		
Sensor	Wetlabs ECO FLNTU (Chlorophyll / Turbidity) (S/N: FLNTURTD-939)		
Total raw files	1 file (.txt) / 5.3 MB	File name	Abyss0234_ECO.txt
Comments	- Sensor data positions are not shifted to the corrected vehicle track; Sampling rate 1Hz		
Comments	- offset after descent phase: 80 m to 356° - Sensor data positions (except RESON Multibeam) are not shifted to the corrected vehicle track - Corrected AUV track is stored in file Abyss0234_NEWNAVIGATION.xyz		

Station	**M127/648**	Day (UTC)	13.06.2016
Dive	**Abyss0235**		

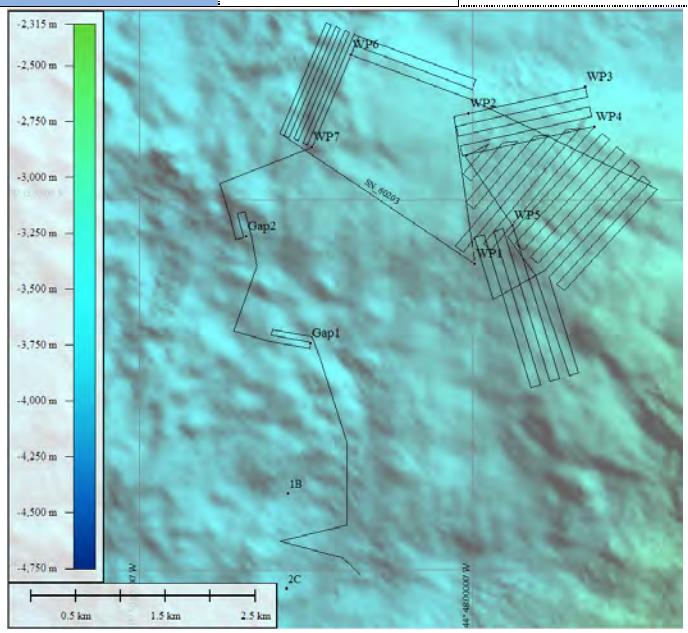

Mission goal:

Mission was to fill gaps in the central box (focused on the slope next to "shimmering") and to map the area northeast of the central box.

Times (UTC)	
Launch	22:12
Mission start	22:15
Survey start	23:32
Survey finished	11:51
Mission finished	13:11
Recovery	16:02 (15.06.16)
Distance travelled	81.29 m

Mission comments

- same mission start position than dive 224
- transponders DT4B-LF and DT4C-LF were used for two legs; good fixes after descent
- Ground fault (50) after mission finish
- vehicle couldn't be located for recovery since decreased acoustic performance

Depth / Altitude	- bottom following at altitude 80 metes - survey depths between 3050 and 3620 meters		
Line spacing	- line spacings were set considering slope; mainly between 50-100 meters		
Sensor	RESON Seabat 7125 200 kHz Multibeam		
Total raw files	80 files (.s7k) / 21.28 GB	First file	20160613_233249.s7k
Used raw files	48 files (.s7k) / 12.78 GB	Last file:	20160614_114917.s7k
Survey area covered:	6.37 km^2	Average coverage:	0.51 km^2/hour @ 3.0 knots
Sensor	Magnetometer (APS-1540 S/N 0685) / Self Potential Sensor		
Total raw files	153 files (.B122) / 6.88 GB	First file	160613231000.B122
		Last file:	160614115000.B122
Comments	- Combined binary files include Magnetometer and Self Potential data - Sensor data positions are not shifted to the corrected vehicle track		
Sensor	Eh / REDOX sensor (Koichi Nakamura)		
Total raw files	1 file (.txt) / 3.7 MB	File name	Abyss0235_REDOX.txt
Comments	- Sensor data positions are not shifted to the corrected vehicle track; Sampling rate 1Hz		
Sensor	SeaBird SBE49 FastCAT CTD (S/N: 4948793-0168)		
Total raw files	1 file (.txt) / 22.2 MB	File name	Abyss0235_CTD.txt
Comments	- Sensor data positions are not shifted to the corrected vehicle track; Sampling rate 4Hz		
Sensor	Wetlabs ECO FLNTU (Chlorophyll / Turbidity) (S/N: FLNTURTD-939)		
Total raw files	1 file (.txt) / 5.8 MB	File name	Abyss0235_ECO.txt
Comments	- Sensor data positions are not shifted to the corrected vehicle track; Sampling rate 1Hz		
Comments	- offset after descent phase: 48 m to 198° - Sensor data positions (except RESON Multibeam) are not shifted to the corrected vehicle track - Corrected AUV track is stored in file Abyss0235_NEWNAVIGATION.xyz		

Station	**M127/665**		Day (UTC)	16.06.2016
Dive	**Abyss0236**			

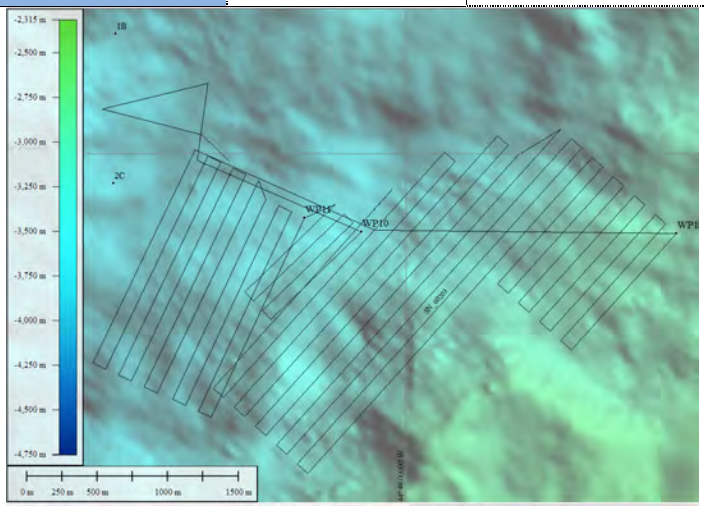

Mission goal:

Mission was to map the area east of mission 230 and south of mission 232.

Times (UTC)	
Launch	00:13
Mission start	00:19
Survey start	01:49
Survey finished	12:04
Mission finished	12:11
Recovery	13:54
Distance travelled	64.5 km

Mission comments

- same mission start position than dive 224
- transponders DT4B-LF and DT4C-LF were used for two legs; good fixes after descent
- Test after mission 235: no ground fault
- vehicle lost bottom lock very often

Depth / Altitude	- bottom following at altitude 80 metes (altitude changed between 50 – 135m) - survey depths between 2830 and 3700 meters		
Line spacing	- line spacings were set considering slope; mainly between 80-100 meters		
Sensor	RESON Seabat 7125 200 kHz Multibeam		
Total raw files	42 files (.s7k) / 11.8 GB	First file	20160616_013638.s7k
Used raw files	41 files (.s7k) / 11.8 GB	Last file:	20160616_115210.s7k
Survey area covered:	4.86 km^2	Average coverage:	0.47 km^2/hour @ 3.0 knots
Sensor	Magnetometer (APS-1540 S/N 0685) / Self Potential Sensor		
Total raw files	132 files (.B122) / 5.95 GB	First file	160616010000.B122
		Last file:	160616120000.B122
Comments	- Combined binary files include Magnetometer and Self Potential data - Sensor data positions are not shifted to the corrected vehicle track		
Sensor	Eh / REDOX sensor (Koichi Nakamura)		
Total raw files	1 file (.txt) / 2.9 MB	File name	Abyss0236_REDOX.txt
Comments	- Sensor data positions are not shifted to the corrected vehicle track; Sampling rate 1Hz		
Sensor	SeaBird SBE49 FastCAT CTD (S/N: 4948793-0168)		
Total raw files	1 file (.txt) / 17.7 MB	File name	Abyss0236_CTD.txt
Comments	- Sensor data positions are not shifted to the corrected vehicle track; Sampling rate 4Hz		
Sensor	Wetlabs ECO FLNTU (Chlorophyll / Turbidity) (S/N: FLNTURTD-939)		
Total raw files	1 file (.txt) / 4.6 MB	File name	Abyss0236_ECO.txt
Comments	- Sensor data positions are not shifted to the corrected vehicle track; Sampling rate 1Hz		
Comments	- offset after descent phase: 120° to 142° - Sensor data positions (except RESON Multibeam) are not shifted to the corrected vehicle track - Corrected AUV track is stored in file Abyss0236_NEWNAVIGATION.xyz - Multibeam data of the eastern survey pattern are shifted related to the western part during the mission		

Station	**M127/686**	Day (UTC)	17.06.2016
Dive	**Abyss0237**		

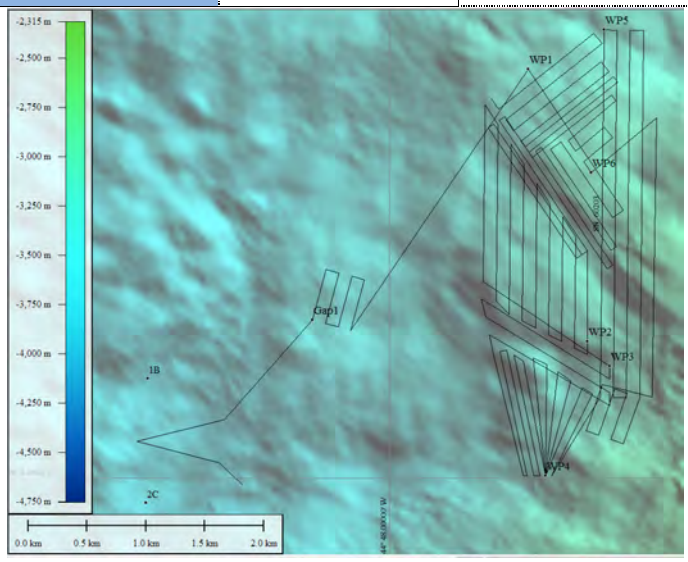

Mission goal:

The mission was to map the area southeast of dive 235 and east of 232 as well as filling a gap from previous dive.

Times (UTC)	
Launch	21:27
Mission start	21:29
Survey start	22:38
Survey finished	11:37
Mission finished	12:00
Recovery	13:10
Distance travelled	82.03 km

Mission comments

- same mission start position than dive 224
- transponders DT4B-LF and DT4C-LF were used for two legs; good fixes after descent
- vehicle lost bottom lock because of a wrong surface command
- lost legs were re-done in dive 238

Depth / Altitude	- bottom following at altitude 80 meters (altitude changed between 50 – 175 m / wrong surface command) - survey depths between 2840 and 3350 meters		
Line spacing	- line spacings were set considering slope; mainly between 50-100 meters		
Sensor	RESON Seabat 7125 200 kHz Multibeam		
Total raw files	49 files (.s7k) / 12.91 GB	First file	20160617_223818.s7k
Used raw files	49 files (.s7k) / 12.91 GB	Last file:	20160618_115925.s7k
Survey area covered:	5.24 km^2 Average coverage:	0,40 km^2/hour @ 3.0 knots	
Sensor	Magnetometer (APS-1540 S/N 0685) / Self Potential Sensor		
Total raw files	139 files (.B122) / 6.27 GB	First file	160617223000.B122
	Mind lack of data because of surface phase!!	Last file:	160618122500.B122
Comments	- Combined binary files include Magnetometer and Self Potential data - Sensor data positions are not shifted to the corrected vehicle track		
Sensor	Eh / REDOX sensor (Koichi Nakamura)		
Total raw files	1 file (.txt) / 3.6 MB	File name	Abyss0237_REDOX.txt
Comments	- Sensor data positions are not shifted to the corrected vehicle track; Sampling rate 1Hz		
Sensor	SeaBird SBE49 FastCAT CTD (S/N: 4948793-0168)		
Total raw files	1 file (.txt) / 21.7 MB	File name	Abyss0237_CTD.txt
Comments	- Sensor data positions are not shifted to the corrected vehicle track; Sampling rate 4Hz		
Sensor	Wetlabs ECO FLNTU (Chlorophyll / Turbidity) (S/N: FLNTURTD-939)		
Total raw files	1 file (.txt) / 5.7 MB	File name	Abyss0237_ECO.txt
Comments	- Sensor data positions are not shifted to the corrected vehicle track; Sampling rate 1Hz		
Comments	- offset after descent phase: 83 meters to 086° - Sensor data positions (except RESON Multibeam) are not shifted to the corrected vehicle track - Corrected AUV track is stored in file Abyss0237_NEWNAVIGATION.xyz		

Station	**M127/689**	Day (UTC)	18.06.2016
Dive	**Abyss0238**		

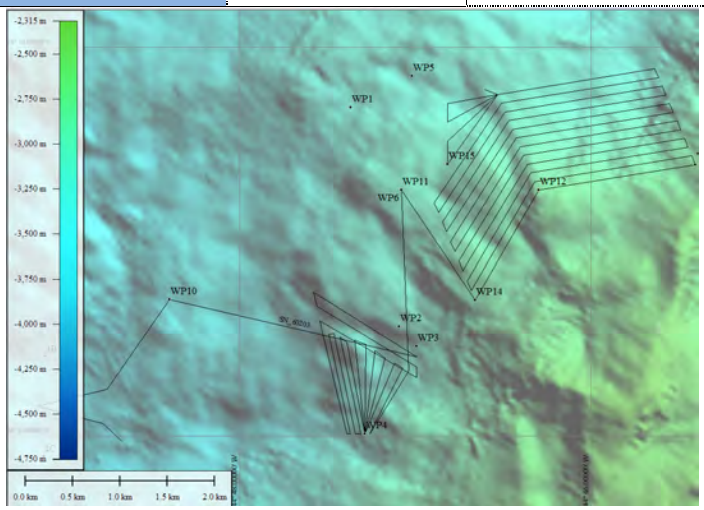

Mission goal:

Mission 238 was to re-map the southern part of dive 237 and to map the area east of 237.

Times (UTC)	
Launch	20:14
Mission start	20:14
Survey start	22:02
Survey finished	07:39
Mission finished	08:50
Recovery	09:43
Distance travelled	69.04

Mission comments

- same mission start position than dive 224
- transponders DT4B-LF and DT4C-LF were used for two legs; good fixes after descent

Depth / Altitude	- bottom following at altitude 80 meters (altitude changed between 45 – 135 m / wrong surface command) - survey depths between 2630 and 3625 meters		
Line spacing	- line spacings were set considering slope; mainly between 40-100 meters		
Sensor	RESON Seabat 7125 200 kHz Multibeam		
Total raw files	41 files (.s7k) / 10.88 GB	First file	20160618_215536.s7k
Used raw files	39 files (.s7k) / 10.34 GB	Last file:	20160619_073814.s7k
Survey area covered:	5.68 km^2	Average coverage:	0.56 km^2/hour @ 3.0 knots
Sensor	Magnetometer (APS-1540 S/N 0685) / Self Potential Sensor		
Total raw files	125 files (.B122) / 5.63 GB	First file	160618212000.B122
		Last file:	160619074000.B122
Comments	- Combined binary files include Magnetometer and Self Potential data - Sensor data positions are not shifted to the corrected vehicle track		
Sensor	Eh / REDOX sensor (Koichi Nakamura)		
Total raw files	1 file (.txt) / 3.1 MB	File name	Abyss0238_REDOX.txt
Comments	- Sensor data positions are not shifted to the corrected vehicle track; Sampling rate 1Hz		
Sensor	SeaBird SBE49 FastCAT CTD (S/N: 4948793-0168)		
Total raw files	1 file (.txt) / 18.7 MB	File name	Abyss0238_CTD.txt
Comments	- Sensor data positions are not shifted to the corrected vehicle track; Sampling rate 4Hz		
Sensor	Wetlabs ECO FLNTU (Chlorophyll / Turbidity) (S/N: FLNTURTD-939)		
Total raw files	1 file (.txt) / 4.9 MB	File name	Abyss0238_ECO.txt
Comments	- Sensor data positions are not shifted to the corrected vehicle track; Sampling rate 1Hz		
Comments	- offset after descent phase: 72 m to 033° - Sensor data positions (except RESON Multibeam) are not shifted to the corrected vehicle track - Corrected AUV track is stored in file Abyss0238_NEWNAVIGATION.xyz		

Station	**M127/696**		Day (UTC)	19.06.2016
Dive	**Abyss0239**			

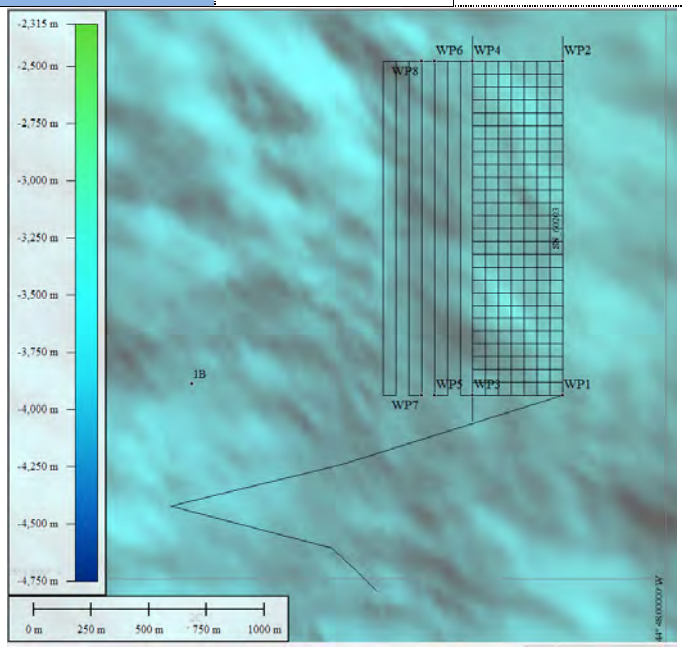

Mission goal:

Mission 239 was to re-map the around the MIR zone in higher resolution using the 400 kHz configuration.

Times (UTC)	
Launch	21:18
Mission start	21:21
Survey start	22:40
Survey finished	10:24
Mission finished	11:40
Recovery	11:58
Distance travelled	80.37

Mission comments

- same mission start position than dive 224
- transponders DT4B-LF and DT4C-LF were used for two legs; good fixes after descent

Depth / Altitude	- fixed depths for the three parts of the survey pattern (each split in three altitude levels) - Vehicle altitude between 12 and 120 meters - survey depths between 3370 and 3520 meters		
Line spacing	- line spacing: 50 meters		
Sensor	RESON Seabat 7125 200 kHz Multibeam		
Total raw files	60 files (.s7k) / 14.66 GB	First file	20160619_223948.s7k
Used raw files	58 files (.s7k) / 14.65 GB	Last file:	20160620_101015.s7k
Survey area covered:	1.11 km^2	Average coverage:	0.09 km^2/hour @ 3.0 knots (3 depth levels!!)
Sensor	Magnetometer (APS-1540 S/N 0685) / Self Potential Sensor		
Total raw files	149 files (.B122) / 6.73 GB	First file	160619223500.B122
		Last file:	160620110000.B122
Comments	- Combined binary files include Magnetometer and Self Potential data - Sensor data positions are not shifted to the corrected vehicle track		
Sensor	Eh / REDOX sensor (Koichi Nakamura)		
Total raw files	1 file (.txt) / 3.5 MB	File name	Abyss0239_REDOX.txt
Comments	- Sensor data positions are not shifted to the corrected vehicle track; Sampling rate 1Hz		
Sensor	SeaBird SBE49 FastCAT CTD (S/N: 4948793-0168)		
Total raw files	1 file (.txt) / 21.5 MB	File name	Abyss0239_CTD.txt
Comments	- Sensor data positions are not shifted to the corrected vehicle track; Sampling rate 4Hz		
Sensor	Wetlabs ECO FLNTU (Chlorophyll / Turbidity) (S/N: FLNTURTD-939)		
Total raw files	1 file (.txt) / 5.6 MB	File name	Abyss0239_ECO.txt
Comments	- Sensor data positions are not shifted to the corrected vehicle track; Sampling rate 1Hz		
Comments	- offset after descent phase: 71.0 m to 48° - Sensor data positions (except RESON Multibeam) are not shifted to the corrected vehicle track - Corrected AUV track is stored in file Abyss0239_NEWNAVIGATION.xyz		

Station	**M127/699**		Day (UTC)	21.06.2016
Dive	**Abyss0240**			

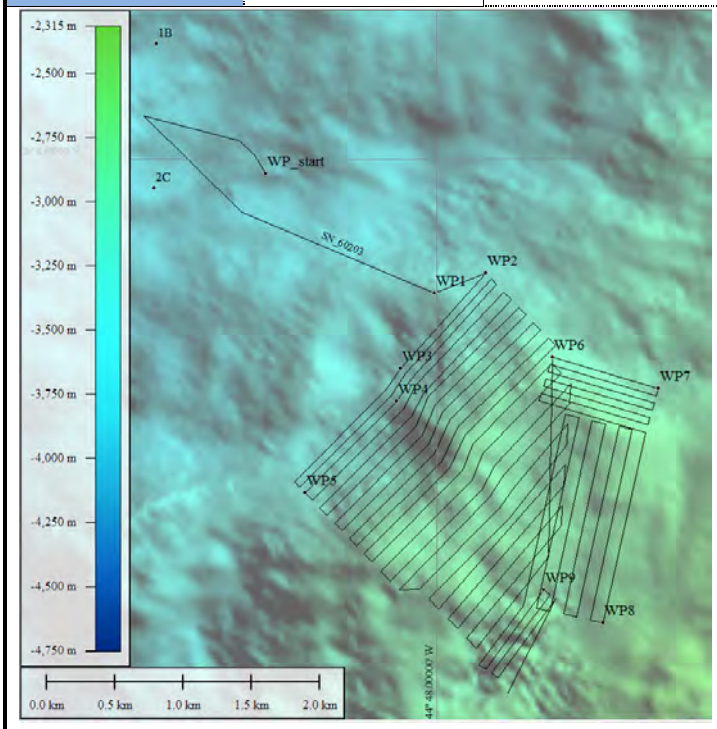

Mission goal:

Mission 240 was to map the area south of 236.

Times (UTC)	
Launch	04:23
Mission start	04:26
Survey start	06:04
Survey finished	16:26
Mission finished	16:45
Recovery	18:02
Distance travelled	66.53 km

Mission comments

- same mission start position than dive 224
- transponders DT4B-LF and DT4C-LF were used for two legs; good fixes after descent

Depth / Altitude	- bottom following at altitude 80 meters (altitude changed between 38 – 150 m / wrong surface command) - survey depths between 2620 and 3625 meters		
Line spacing	- line spacings were set considering slope; mainly between 40-100 meters		
Sensor	RESON Seabat 7125 200 kHz Multibeam		
Total raw files	41 files (.s7k) / 10.9 GB	First file	20160621_055924.s7k
Used raw files	41 files (.s7k) / 10.9 GB	Last file:	20160621_162401.s7k
Survey area covered:	4.29 km^2	Average coverage:	0.41 km^2/hour @ 3.0 knots
Sensor	Magnetometer (APS-1540 S/N 0685) / Self Potential Sensor		
Total raw files	218 files (.B122) / 9.13 GB	First file	160621040500.B122
		Last file:	160621234500.B122
Comments	- Combined binary files include Magnetometer and Self Potential data - Sensor data positions are not shifted to the corrected vehicle track		
Sensor	Eh / REDOX sensor (Koichi Nakamura)		
Total raw files	1 file (.txt) / 3.0 MB	File name	Abyss0240_REDOX.txt
Comments	- Sensor data positions are not shifted to the corrected vehicle track; Sampling rate 1Hz		
Sensor	SeaBird SBE49 FastCAT CTD (S/N: 4948793-0168)		
Total raw files	1 file (.txt) / 18.3 MB	File name	Abyss0240_CTD.txt
Comments	- Sensor data positions are not shifted to the corrected vehicle track; Sampling rate 4Hz		
Sensor	Wetlabs ECO FLNTU (Chlorophyll / Turbidity) (S/N: FLNTURTD-939)		
Total raw files	1 file (.txt) / 4.8 MB	File name	Abyss0240_ECO.txt
Comments	- Sensor data positions are not shifted to the corrected vehicle track; Sampling rate 1Hz		
Comments	- offset after descent phase: 135 m 139° - Sensor data positions (except RESON Multibeam) are not shifted to the corrected vehicle track - Corrected AUV track is stored in file Abyss0240_NEWNAVIGATION.xyz		

Station	**M127/706**	Day (UTC)	21.06.2016
Dive	**Abyss0241**		

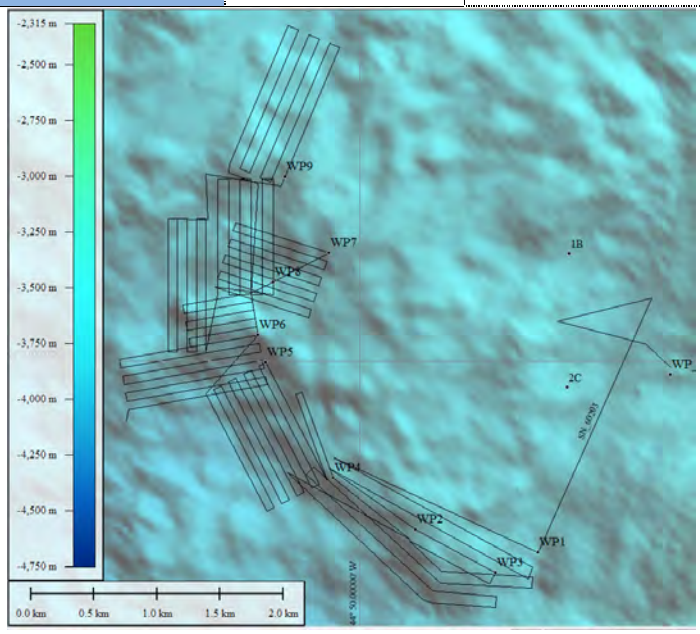

Mission goal:

Mission 241 was to map the neovolcanic section southwest of dive 230.

Times (UTC)	
Launch	22:02
Mission start	22:07
Survey start	23:40
Survey finished	11:40
Mission finished	11:52
Recovery	13:32
Distance travelled	74.71 km

Mission comments

- same mission start position than dive 224
- transponders DT4B-LF and DT4C-LF were used for two legs; good fixes after descent

Depth / Altitude	- bottom following at altitude 80 meters (altitude changed between 12 – 170 m / wrong surface command) - survey depths between 3535 and 3920 meters		
Line spacing	- line spacings were set considering slope; mainly between 40-100 meters		
Sensor	RESON Seabat 7125 200 kHz Multibeam		
Total raw files	47 files (.s7k) / 12.51 GB	First file	20160621_234054.s7k
Used raw files	47 files (.s7k) / 12.51 GB	Last file:	20160622_113657.s7k
Survey area covered:	4.63 km^2 Average coverage:	0.39 km^2/hour @ 3.0 knots	
Sensor	Magnetometer (APS-1540 S/N 0685) / Self Potential Sensor		
Total raw files	146 files (.B122) / 6.58 GB	First file	160621233500.B122
		Last file:	160622114000.B122
Comments	- Combined binary files include Magnetometer and Self Potential data - Sensor data positions are not shifted to the corrected vehicle track		
Sensor	Eh / REDOX sensor (Koichi Nakamura)		
Total raw files	1 file (.txt) / 3.4 MB	File name	Abyss0241_REDOX.txt
Comments	- Sensor data positions are not shifted to the corrected vehicle track; Sampling rate 1Hz		
Sensor	SeaBird SBE49 FastCAT CTD (S/N: 4948793-0168)		
Total raw files	1 file (.txt) / 20.5 MB	File name	Abyss0241_CTD.txt
Comments	- Sensor data positions are not shifted to the corrected vehicle track; Sampling rate 4Hz		
Sensor	Wetlabs ECO FLNTU (Chlorophyll / Turbidity) (S/N: FLNTURTD-939)		
Total raw files	1 file (.txt) / 5.3 MB	File name	Abyss0241_ECO.txt
Comments	- Sensor data positions are not shifted to the corrected vehicle track; Sampling rate 1Hz		
Comments	- offset after descent phase: 88 m to 047° - Sensor data positions (except RESON Multibeam) are not shifted to the corrected vehicle track - Corrected AUV track is stored in file Abyss0241_NEWNAVIGATION.xyz		

Appendix 3

Subsampling of gravity cores

Table Appendix 3.1: Summary of the distribution of pore water samples in sediments recovered by gravity coring. Shore-based analyses will be perfomed by A. Lichtschlag and A. Dutrieux (NOC).

Station	Recovery	No of pore water samples	Comment
M127/576GC	1.16 m	16	
M127/615GC	1.08 m	16	
M127/616GC	1.31 m	21	
M127/617GC	0.64 m	13	
M127/626GC	1.20 m	20	
M127/627GC	3.14 m	33	
M127/636GC	1.08 m	19	
M127/638GC	0.20 m	2	
M127/644GC	2.69 m	53	Very close sampling as we had sulfides in the core catcher
M127/645GC	1.31 m	17	
M127/647GC	3.00 m	35	
M127/649GC	1.78 m	18	
M127/666GC	0.37 m	/	Not sampled
M127/681GC	3.00 m	30	
M127/682GC	2.81 m	30	
M127/690GC	0.80 m	8	
M127/691GC	0.66 m	/	Not sampled
M127/692GC	0.79 m	15	
M127/693GC	0.71 m	12	
M127/702GC	0.92 m	17	
M127/703GC	3.00 m	22	
M127/711GC	3.00 m	14	
No of samples		**397**	

Table Appendix 3.2: Summary of on-board subsampling and measurements performed by FFCUL (Lisbon) on sediments from gravity corers and HyBis samples.

		on-board measurements						
Station	**No of subsamples**	**PIMA**	**XRD**	**XRF**	**pH**	**Eh**	**T**	**Spectro.**
M127/576GC	12	12	2	12	x	x	x	x
M127/615GC	15	15	2	15	x	x	x	x
M127/616GC	17	16	2	16	x	x	x	x
M127/617GC	8	8	3	8	x	x	x	x
M127/626GC	15	-	1	3	x	x	x	x
M127/627GC	49	16	1	16	x	x	x	x
M127/636GC	9	-	-	-	x	x	x	x
M127/638GC	3	-	-	-	x	x	x	x
M127/644GC	31	-	-	-	x	x	x	x
M127/645GC	6	-	-	-	x	x	x	x
M127/647GC	32	-	-	-	x	x	x	x
M127/649GC	11	-	-	-	x	x	x	x
M127/666GC	3	-	-	-	x	x	x	x
M127/681GC	15	-	-	-	x	x	x	x
M127/682GC	18	-	-	4	x	x	x	x
M127/690GC	4	-	-	-	x	x	x	x
M127/691GC	3	-	-	1	x	x	x	x
M127/692GC	11	-	-	1	x	x	x	x
M127/693GC	5	-	-	1	x	x	x	x
M127/702GC	7	-	-	-	x	x	x	x
M127/703GC	18	-	-	-	x	x	x	x
M127/711GC	17	-	-	-	x	x	x	x
HyBis samples	8	8	7	7	x	x	x	x
No of samples	**317**	**75**	**18**	**84**				

Note: Spectrophotometry was done every 5 cm downhole. The individual subsampling positions are indicated in the coring sheets in Appendix 4.

Table Appendix 3.3: Location of sediment subsamples by FFCUL in gravity cores from M127.

Station	Liner	depth
M127/576GC	B	010 cm
M127/576GC	B	020 cm
M127/576GC	A	030 cm
M127/576GC	A	040 cm
M127/576GC	A	050 cm
M127/576GC	A	060 cm
M127/576GC	A	070 cm
M127/576GC	A	080 cm
M127/576GC	A	090 cm
M127/576GC	A	100 cm
M127/576GC	A	113 cm
M127/576GC	cc	-
M127/615GC	B	002 cm
M127/615GC	B	009 cm
M127/615GC	A	015 cm
M127/615GC	A	018 cm
M127/615GC	A	020 cm
M127/615GC	A	025 cm
M127/615GC	A	035 cm
M127/615GC	A	045 cm
M127/615GC	A	055 cm
M127/615GC	A	065 cm
M127/615GC	A	075 cm
M127/615GC	A	085 cm
M127/615GC	A	095 cm
M127/615GC	A	102 cm
M127/615GC	cc	-
M127/616GC	B	005 cm
M127/616GC	B	015 cm
M127/616GC	B	025 cm
M127/616GC	B	035 cm
M127/616GC	B	045 cm
M127/616GC	A	050 cm
M127/616GC	A	060 cm
M127/616GC	A	070 cm
M127/616GC	A	080 cm
M127/616GC	A	090 cm
M127/616GC	A	100 cm
M127/616GC	A	106 cm
M127/616GC	A	110 cm
M127/616GC	A	115 cm
M127/616GC	A	122 cm
M127/616GC	A	127 cm
M127/616GC	cc	-
M127/617GC	A	005 cm
M127/617GC	A	015 cm
M127/617GC	A	025 cm

Station	Liner	depth
M127/617GC	A	035 cm
M127/617GC	A	045 cm
M127/617GC	A	055 cm
M127/617GC	A	062 cm
M127/617GC	cc	-
M127/626GC	B	005 cm
M127/626GC	B	010 cm
M127/626GC	B	015 cm
M127/626GC	A	025 cm
M127/626GC	A	035 cm
M127/626GC	A	045 cm
M127/626GC	A	055 cm
M127/626GC	A	065 cm
M127/626GC	A	075 cm
M127/626GC	A	085 cm
M127/626GC	A	095 cm
M127/626GC	A	100 cm
M127/626GC	A	104 cm
M127/626GC	A	110 cm
M127/626GC	cc	-
M127/627GC	D	005 cm
M127/627GC	D	015 cm
M127/627GC	C	030 cm
M127/627GC	C	040 cm
M127/627GC	C	043 cm
M127/627GC	C	047 cm
M127/627GC	C	050 cm
M127/627GC	C	053 cm
M127/627GC	C	057 cm
M127/627GC	C	065 cm
M127/627GC	C	072 cm
M127/627GC	C	075 cm
M127/627GC	C	080 cm
M127/627GC	C	085 cm
M127/627GC	C	090 cm
M127/627GC	C	098 cm
M127/627GC	C	106 cm
M127/627GC	C	111 cm
M127/627GC	C	118 cm
M127/627GC	B	122 cm
M127/627GC	B	130 cm
M127/627GC	B	136 cm
M127/627GC	B	146 cm
M127/627GC	B	151 cm
M127/627GC	B	156 cm
M127/627GC	B	163 cm
M127/627GC	B	170 cm
M127/627GC	B	175 cm

Station	Liner	depth
M127/627GC	B	184 cm
M127/627GC	B	197 cm
M127/627GC	B	207 cm
M127/627GC	B	212 cm
M127/627GC	B	216 cm
M127/627GC	B	219 cm
M127/627GC	A	222 cm
M127/627GC	A	226 cm
M127/627GC	A	235 cm
M127/627GC	A	241 cm
M127/627GC	A	250 cm
M127/627GC	A	256 cm
M127/627GC	A	263 cm
M127/627GC	A	271 cm
M127/627GC	A	280 cm
M127/627GC	A	284 cm
M127/627GC	A	285 cm
M127/627GC	A	290 cm
M127/627GC	A	300 cm
M127/627GC	A	307 cm
M127/627GC	cc	-
M127/636GC	B	010 cm
M127/636GC	B	020 cm
M127/636GC	A	030 cm
M127/636GC	A	046 cm
M127/636GC	A	060 cm
M127/636GC	A	075 cm
M127/636GC	A	090 cm
M127/636GC	A	105 cm
M127/636GC	cc	-
M127/638GC	A	005 cm
M127/638GC	A	015 cm
M127/638GC	cc	-
M127/644GC	C	005 cm
M127/644GC	C	020 cm
M127/644GC	C	030 cm
M127/644GC	C	040 cm
M127/644GC	C	050 cm
M127/644GC	C	052 cm
M127/644GC	C	060 cm
M127/644GC	C	070 cm
M127/644GC	B	080 cm
M127/644GC	B	095 cm
M127/644GC	B	110 cm
M127/644GC	B	118 cm
M127/644GC	B	122 cm
M127/644GC	B	126 cm
M127/644GC	B	135 cm

Station	Liner	depth
M127/644GC	B	144 cm
M127/644GC	B	150 cm
M127/644GC	B	155 cm
M127/644GC	B	162 cm
M127/644GC	B	170 cm
M127/644GC	A	185 cm
M127/644GC	A	195 cm
M127/644GC	A	205 cm
M127/644GC	A	215 cm
M127/644GC	A	225 cm
M127/644GC	A	235 cm
M127/644GC	A	245 cm
M127/644GC	A	253 cm
M127/644GC	A	260 cm
M127/644GC	A	269 cm
M127/644GC	cc	-
M127/645GC	B	015 cm
M127/645GC	B	030 cm
M127/645GC	A	060 cm
M127/645GC	A	100 cm
M127/645GC	A	125 cm
M127/645GC	cc	-
M127/647GC	C	005 cm
M127/647GC	C	015 cm
M127/647GC	C	030 cm
M127/647GC	C	034 cm
M127/647GC	C	037 cm
M127/647GC	C	042 cm
M127/647GC	C	054 cm
M127/647GC	C	064 cm
M127/647GC	C	072 cm
M127/647GC	C	080 cm
M127/647GC	C	090 cm
M127/647GC	C	096 cm
M127/647GC	B	105 cm
M127/647GC	B	118 cm
M127/647GC	B	122 cm
M127/647GC	B	140 cm
M127/647GC	B	150 cm
M127/647GC	B	160 cm
M127/647GC	B	178 cm
M127/647GC	B	184 cm
M127/647GC	B	187 cm
M127/647GC	B	193 cm
M127/647GC	B	199 cm
M127/647GC	A	213 cm
M127/647GC	A	227 cm
M127/647GC	A	235 cm
M127/647GC	A	245 cm

Station	Liner	depth
M127/647GC	A	257 cm
M127/647GC	A	273 cm
M127/647GC	A	274 cm
M127/647GC	A	280 cm
M127/647GC	cc	-
M127/649GC	B	015 cm
M127/649GC	B	025 cm
M127/649GC	B	045 cm
M127/649GC	B	070 cm
M127/649GC	A	092 cm
M127/649GC	A	100 cm
M127/649GC	A	120 cm
M127/649GC	A	135 cm
M127/649GC	A	150 cm
M127/649GC	A	167 cm
M127/649GC	cc	-
M127/666GC	A	010 cm
M127/666GC	A	030 cm
M127/666GC	cc	-
M127/681GC	C	010 cm
M127/681GC	C	030 cm
M127/681GC	C	055 cm
M127/681GC	C	080 cm
M127/681GC	B	103 cm
M127/681GC	B	125 cm
M127/681GC	B	136 cm
M127/681GC	B	151 cm
M127/681GC	B	153 cm
M127/681GC	B	170 cm
M127/681GC	B	190 cm
M127/681GC	A	220 cm
M127/681GC	A	250 cm
M127/681GC	A	280 cm
M127/681GC	cc	-
M127/682GC	C	010 cm
M127/682GC	C	020 cm
M127/682GC	C	045 cm
M127/682GC	C	078 cm
M127/682GC	B	090 cm
M127/682GC	B	116 cm
M127/682GC	B	132 cm
M127/682GC	B	138 cm
M127/682GC	B	155 cm
M127/682GC	B	160 cm
M127/682GC	B	165 cm
M127/682GC	B	180 cm
M127/682GC	A	198 cm

Station	Liner	depth
M127/682GC	A	209 cm
M127/682GC	A	220 cm
M127/682GC	A	235 cm
M127/682GC	A	260 cm
M127/682GC	cc	-
M127/690GC	A	025 cm
M127/690GC	A	045 cm
M127/690GC	A	070 cm
M127/690GC	cc	-
M127/691GC	A	020 cm
M127/691GC	A	040 cm
M127/691GC	cc	-
M127/692GC	A	010 cm
M127/692GC	A	016 cm
M127/692GC	A	022 cm
M127/692GC	A	032 cm
M127/692GC	A	037 cm
M127/692GC	A	043 cm
M127/692GC	A	050 cm
M127/692GC	A	060 cm
M127/692GC	A	064 cm
M127/692GC	A	070 cm
M127/692GC	cc	-
M127/693GC	A	015 cm
M127/693GC	A	035 cm
M127/693GC	A	045 cm
M127/693GC	A	060 cm
M127/693GC	cc	-
M127/702GC	A	020 cm
M127/702GC	A	030 cm
M127/702GC	A	045 cm
M127/702GC	A	053 cm
M127/702GC	A	063 cm
M127/702GC	A	075 cm
M127/702GC	cc	-
M127/703GC	C	014 cm
M127/703GC	C	049 cm
M127/703GC	C	070 cm
M127/703GC	C	097 cm
M127/703GC	B	110 cm
M127/703GC	B	118 cm
M127/703GC	B	125 cm
M127/703GC	B	135 cm
M127/703GC	B	148 cm
M127/703GC	B	157 cm

Station	Liner	depth
M127/703GC	B	165 cm
M127/703GC	B	180 cm
M127/703GC	B	196 cm
M127/703GC	A	221 cm
M127/703GC	A	234 cm
M127/703GC	A	250 cm
M127/703GC	A	279 cm
M127/703GC	cc	-
M127/711GC	C	035 cm
M127/711GC	C	060 cm

Station	Liner	depth
M127/711GC	C	085 cm
M127/711GC	B	107 cm
M127/711GC	B	120 cm
M127/711GC	B	148 cm
M127/711GC	B	160 cm
M127/711GC	B	175 cm
M127/711GC	B	197 cm
M127/711GC	A	235 cm
M127/711GC	A	268 cm
M127/711GC	A	278 cm
M127/711GC	A	296 cm

Appendix 4

Gravity Core Scans

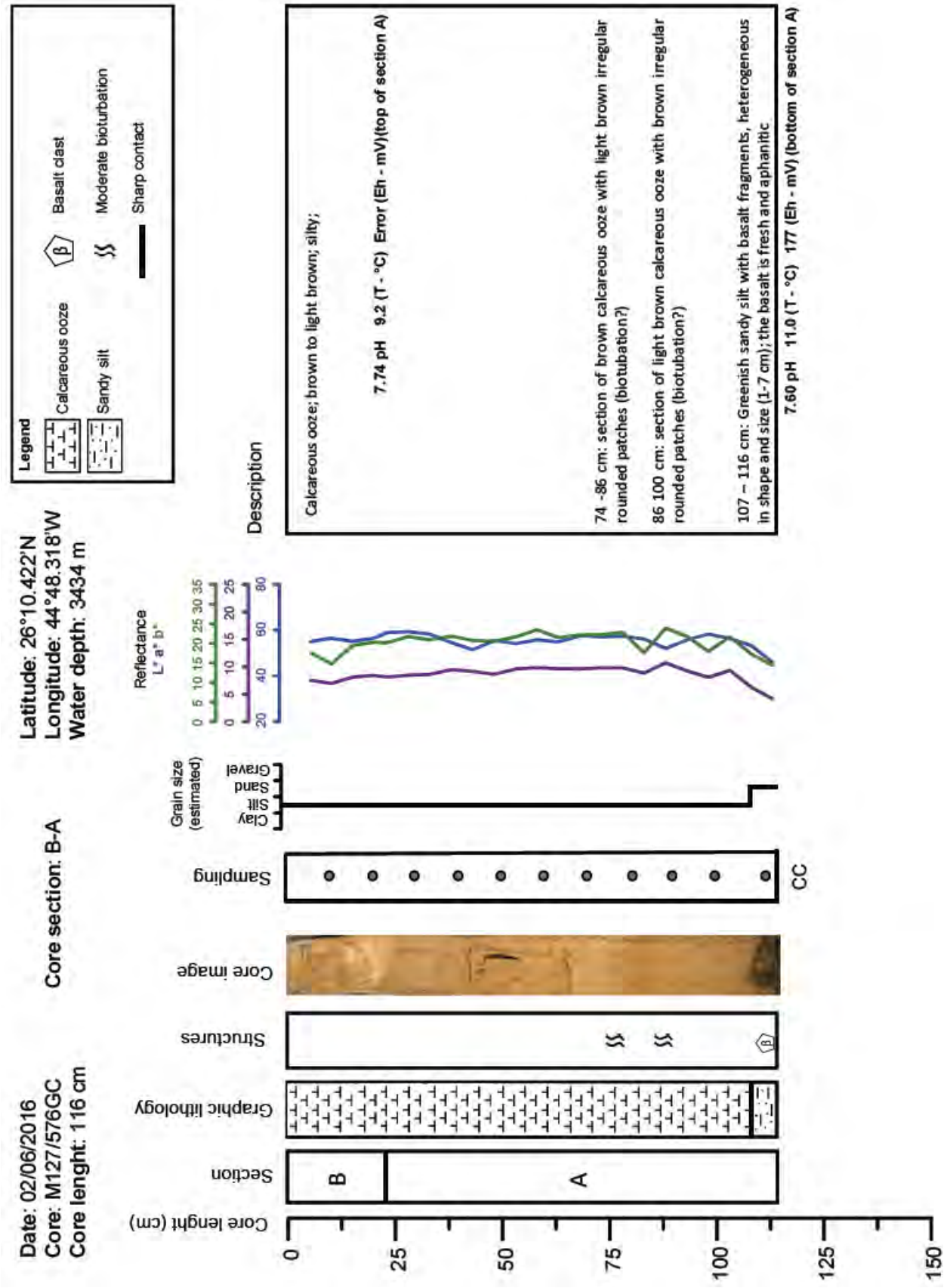
Legend
Calcareous ooze
Basalt clast
Sandy silt
Moderate bioturbation
Sharp contact
Description
Calcareous ooze; brown to light brown; silty;
7.74 pH 9.2 (T - °C) Error (Eh - mV)(top of section A)
74 -86 cm: section of brown calcareous ooze with light brown irregular rounded patches (biotubation?)
86 100 cm: section of light brown calcareous ooze with brown irregular rounded patches (biotubation?)
107 – 116 cm: Greenish sandy silt with basalt fragments, heterogeneous in shape and size (1-7 cm); the basalt is fresh and aphanitic
7.60 pH 11.0 (T - °C) 177 (Eh - mV) (bottom of section A)
Date: 02/06/2016
Core: M127/576GC
Core lenght: 116 cm
Core section: B-A
Latitude: 26°10.422'N
Longitude: 44°48.318'W
Water depth: 3434 m
Reflectance L* a* b*
Grain size (estimated)
Clay
Silt
Sand
Gravel
Sampling
Core image
Structures
Graphic lithology
Section
Core lenght (cm)
B
A
CC
0
25
50
75
100
125
150

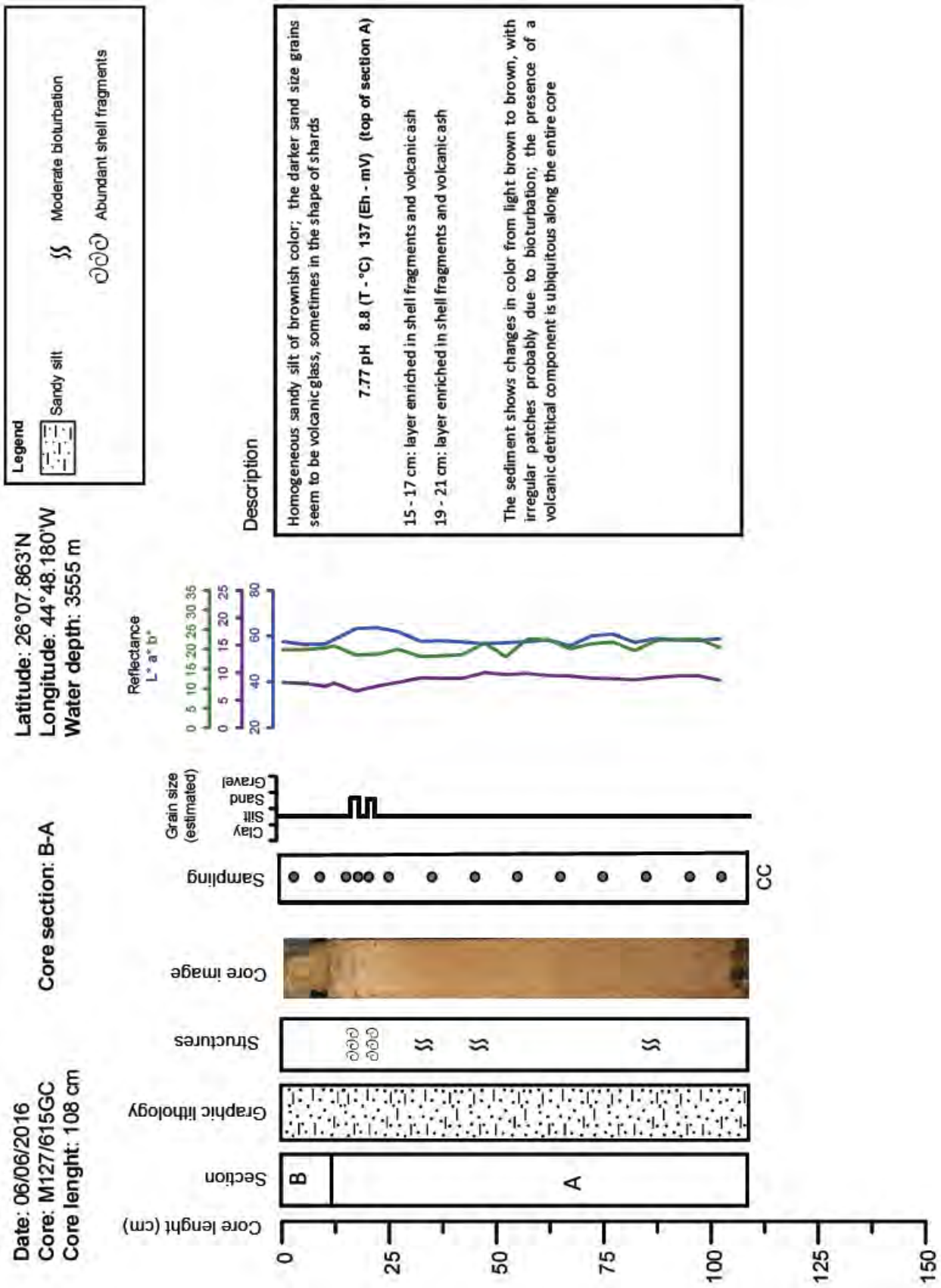
Legend
Sandy silt
Moderate bioturbation
Abundant shell fragments
Description
Homogeneous sandy silt of brownish color; the darker sand size grains seem to be volcanic glass, sometimes in the shape of shards
7.77 pH 8.8 (T - °C) 137 (Eh - mV) (top of section A)
15 - 17 cm: layer enriched in shell fragments and volcanic ash
19 - 21 cm: layer enriched in shell fragments and volcanic ash
The sediment shows changes in color from light brown to brown, with irregular patches probably due to bioturbation; the presence of a volcanic detritical component is ubiquitous along the entire core
Latitude: 26°07.863'N
Longitude: 44°48.180'W
Water depth: 3555 m
Core section: B-A
Date: 06/06/2016
Core: M127/615GC
Core lenght: 108 cm
Reflectance L* a* b*
Grain size (estimated)
Clay
Silt
Sand
Gravel
Sampling
CC
Core image
Structures
Graphic lithology
Section
B
A
Core lenght (cm)
0
25
50
75
100
125
150

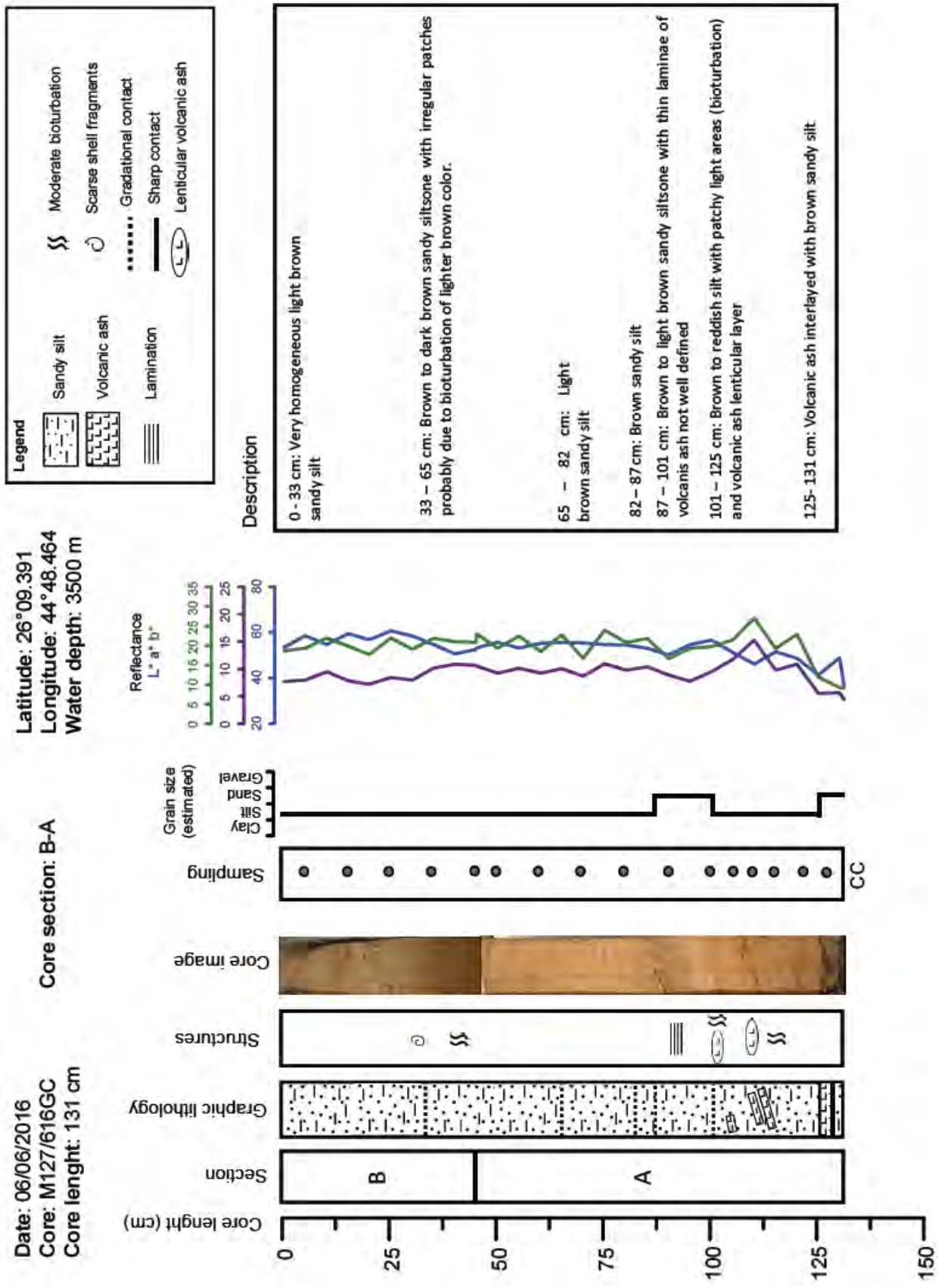
Legend
Sandy silt
Volcanic ash
Lamination
Moderate bioturbation
Scarse shell fragments
Gradational contact
Sharp contact
Lenticular volcanic ash
Description
0 - 33 cm: Very homogeneous light brown sandy silt
33 – 65 cm: Brown to dark brown sandy siltsone with irregular patches probably due to bioturbation of lighter brown color.
65 – 82 cm: Light brown sandy silt
82 – 87 cm: Brown sandy silt
87 – 101 cm: Brown to light brown sandy siltsone with thin laminae of volcanis ash not well defined
101 – 125 cm: Brown to reddish silt with patchy light areas (bioturbation) and volcanic ash lenticular layer
125- 131 cm: Volcanic ash interlayed with brown sandy silt
Latitude: 26°09.391
Longitude: 44°48.464
Water depth: 3500 m
Core section: B-A
Date: 06/06/2016
Core: M127/616GC
Core lenght: 131 cm
Reflectance L* a* b*
Grain size (estimated)
Clay
Silt
Sand
Gravel
Sampling
Core image
Structures
Graphic lithology
Section
Core lenght (cm)
B
A
CC
0
25
50
75
100
125
150

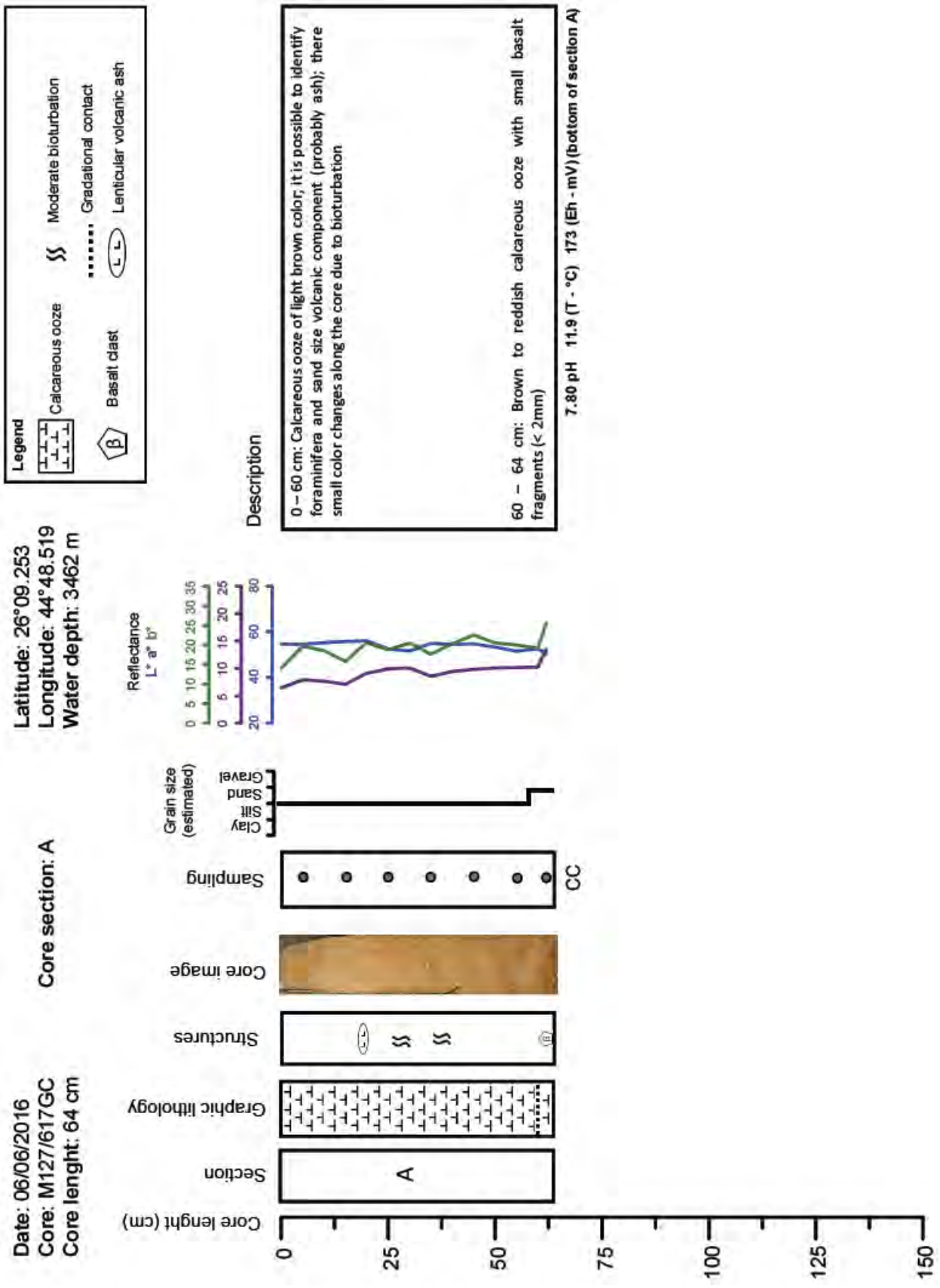
Date: 06/06/2016
Core: M127/617GC
Core lenght: 64 cm
Core section: A
Latitude: 26°09.253
Longitude: 44°48.519
Water depth: 3462 m
Legend
Calcareous ooze
Moderate bioturbation
Gradational contact
Basalt clast
Lenticular volcanic ash
Description
0 – 60 cm: Calcareous ooze of light brown color; it is possible to identify foraminifera and sand size volcanic component (probably ash); there small color changes along the core due to bioturbation
60 – 64 cm: Brown to reddish calcareous ooze with small basalt fragments (< 2mm)
7.80 pH 11.9 (T - °C) 173 (Eh - mV) (bottom of section A)
Reflectance L* a* b*
Grain size (estimated)
Clay
Silt
Sand
Gravel
Sampling
Core image
Structures
Graphic lithology
Section
Core lenght (cm)
A
CC
0
25
50
75
100
125
150

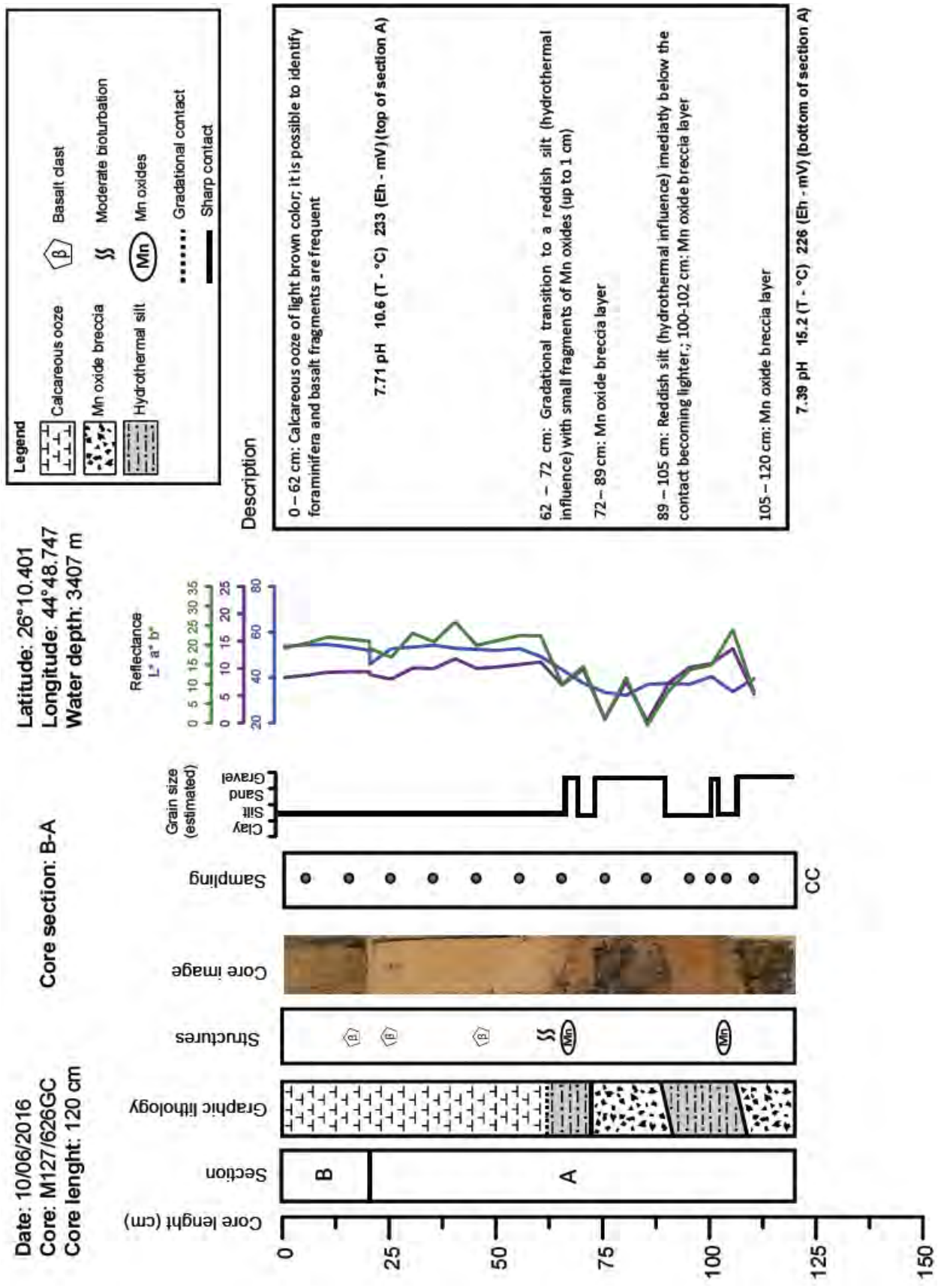
Legend
Calcareous ooze
Basalt clast
Mn oxide breccia
Moderate bioturbation
Hydrothermal silt
Mn oxides
Gradational contact
Sharp contact
Description
0 – 62 cm: Calcareous ooze of light brown color; it is possible to identify foraminifera and basalt fragments are frequent
7.71 pH 10.6 (T - °C) 233 (Eh - mV) (top of section A)
62 – 72 cm: Gradational transition to a reddish silt (hydrothermal influence) with small fragments of Mn oxides (up to 1 cm)
72 – 89 cm: Mn oxide breccia layer
89 – 105 cm: Reddish silt (hydrothermal influence) imediatly below the contact becoming lighter.; 100-102 cm: Mn oxide breccia layer
105 – 120 cm: Mn oxide breccia layer
7.39 pH 15.2 (T - °C) 226 (Eh - mV) (bottom of section A)
Latitude: 26°10.401
Longitude: 44°48.747
Water depth: 3407 m
Core section: B-A
Date: 10/06/2016
Core: M127/626GC
Core lenght: 120 cm
Reflectance L* a* b*
Grain size (estimated)
Clay
Silt
Sand
Gravel
Sampling
Core image
Structures
Graphic lithology
Section
Core length (cm)
B
A
CC
0
25
50
75
100
125
150

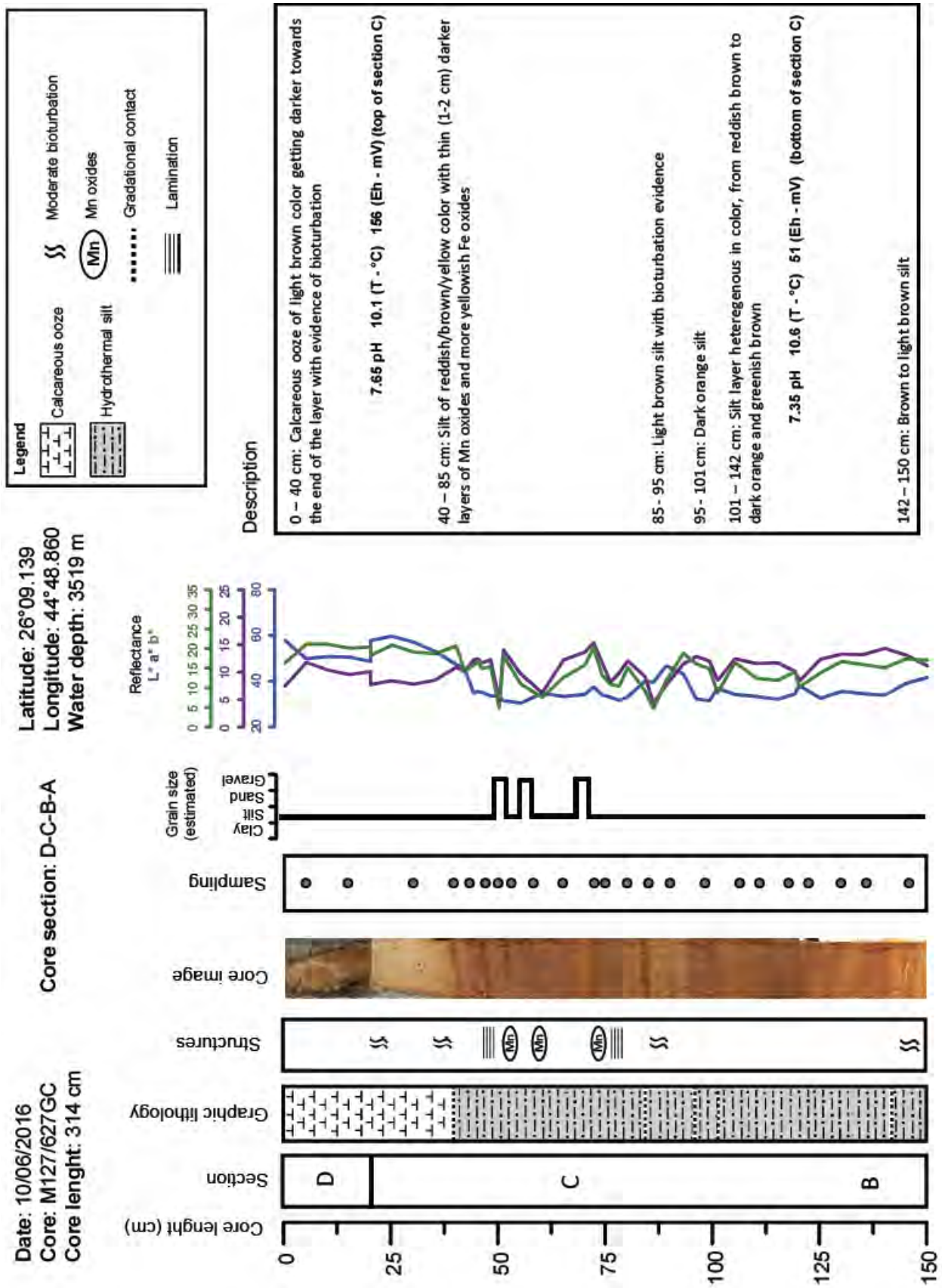
Legend
Calcareous ooze
Moderate bioturbation
Hydrothermal silt
Mn oxides
Gradational contact
Lamination
Description
0 – 40 cm: Calcareous ooze of light brown color getting darker towards the end of the layer with evidence of bioturbation
7.65 pH 10.1 (T - °C) 156 (Eh - mV) (top of section C)
40 – 85 cm: Silt of reddish/brown/yellow color with thin (1-2 cm) darker layers of Mn oxides and more yellowish Fe oxides
85 - 95 cm: Light brown silt with bioturbation evidence
95 - 101 cm: Dark orange silt
101 – 142 cm: Silt layer heteregenous in color, from reddish brown to dark orange and greenish brown
7.35 pH 10.6 (T - °C) 51 (Eh - mV) (bottom of section C)
142 – 150 cm: Brown to light brown silt
Latitude: 26°09.139
Longitude: 44°48.860
Water depth: 3519 m
Core section: D-C-B-A
Date: 10/06/2016
Core: M127/627GC
Core lenght: 314 cm
Reflectance
L* a* b*
Grain size (estimated)
Clay
Silt
Sand
Gravel
Sampling
Core image
Structures
Graphic lithology
Section
Core lenght (cm)
D
C
B
0
25
50
75
100
125
150

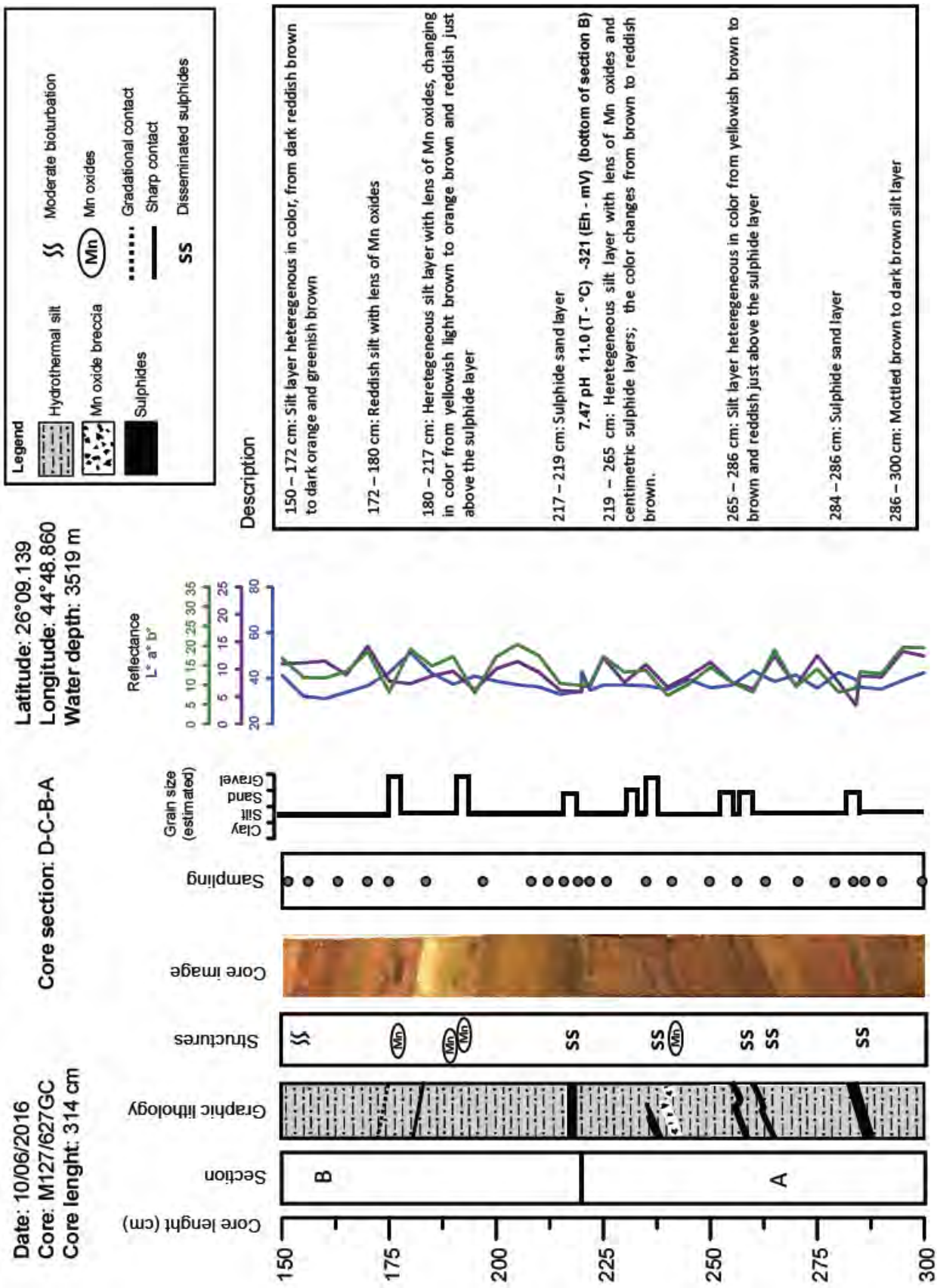
Legend
Hydrothermal silt
Moderate bioturbation
Mn oxide breccia
Mn oxides
Sulphides
Gradational contact
Sharp contact
SS Disseminated sulphides
Description
150 – 172 cm: Silt layer heteregenous in color, from dark reddish brown to dark orange and greenish brown
172 – 180 cm: Reddish silt with lens of Mn oxides
180 – 217 cm: Heretegeneous silt layer with lens of Mn oxides, changing in color from yellowish light brown to orange brown and reddish just above the sulphide layer
217 – 219 cm: Sulphide sand layer
7.47 pH 11.0 (T - °C) -321 (Eh - mV) (bottom of section B)
219 – 265 cm: Heretegeneous silt layer with lens of Mn oxides and centimetric sulphide layers; the color changes from brown to reddish brown.
265 – 286 cm: Silt layer heteregeneous in color from yellowish brown to brown and reddish just above the sulphide layer
284 – 286 cm: Sulphide sand layer
286 – 300 cm: Mottled brown to dark brown silt layer
Latitude: 26°09.139
Longitude: 44°48.860
Water depth: 3519 m
Core section: D-C-B-A
Date: 10/06/2016
Core: M127/627GC
Core lenght: 314 cm
Reflectance L* a* b*
Grain size (estimated)
Clay
Silt
Sand
Gravel
Sampling
Core image
Structures
Graphic lithology
Section
Core lenght (cm)
B
A
SS
Mn
150
175
200
225
250
275
300

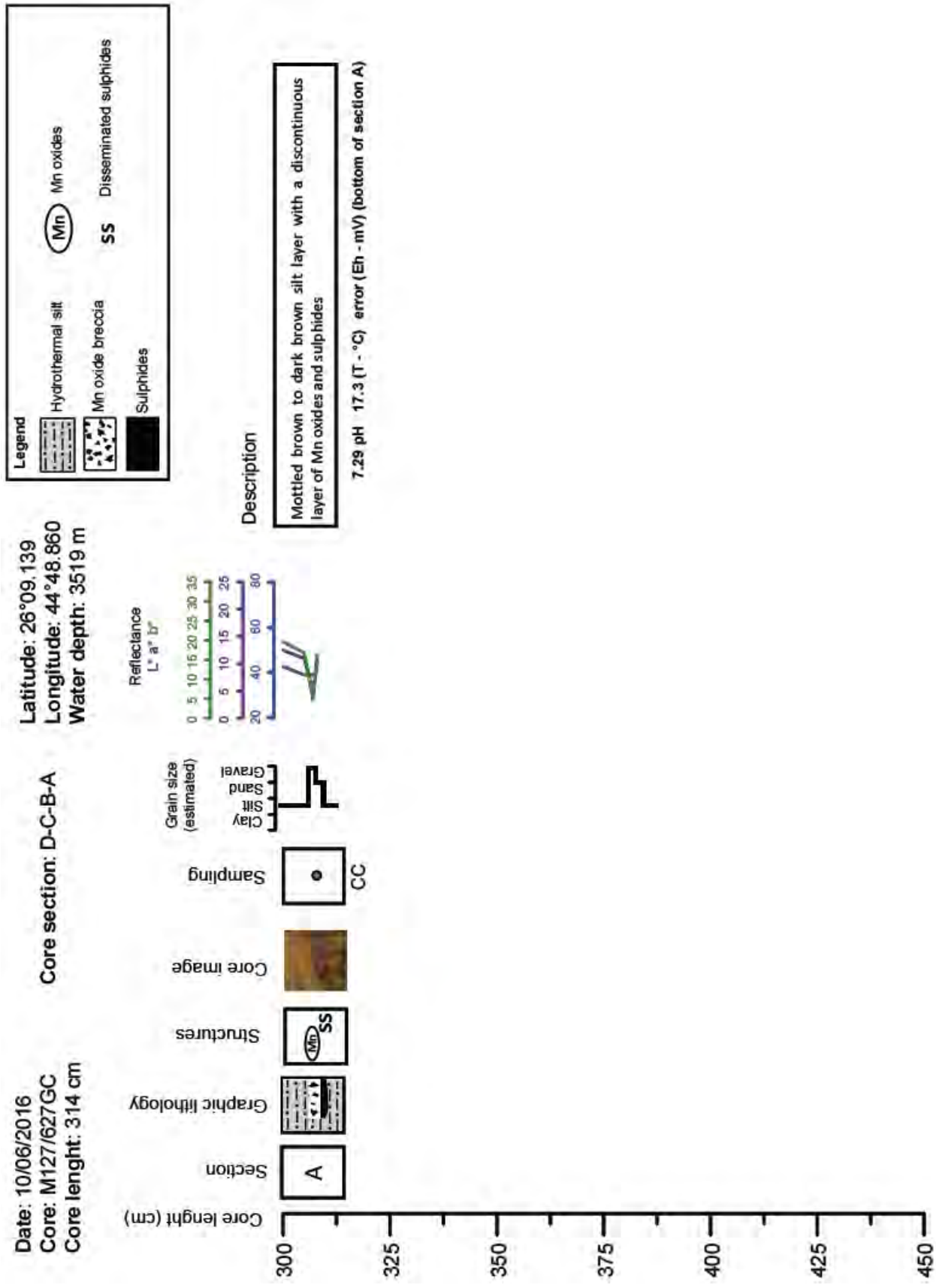
Date: 10/06/2016
Core: M127/627GC
Core lenght: 314 cm
Core section: D-C-B-A
Latitude: 26°09.139
Longitude: 44°48.860
Water depth: 3519 m
Legend
Hydrothermal silt
Mn oxides
Mn oxide breccia
SS Disseminated sulphides
Sulphides
Description
Mottled brown to dark brown silt layer with a discontinuous layer of Mn oxides and sulphides
7.29 pH 17.3 (T - °C) error (Eh - mV) (bottom of section A)
Reflectance L* a* b*
Grain size (estimated)
Clay
Silt
Sand
Gravel
Sampling
CC
Core image
Structures
Graphic lithology
Section
Core length (cm)
300
325
350
375
400
425
450

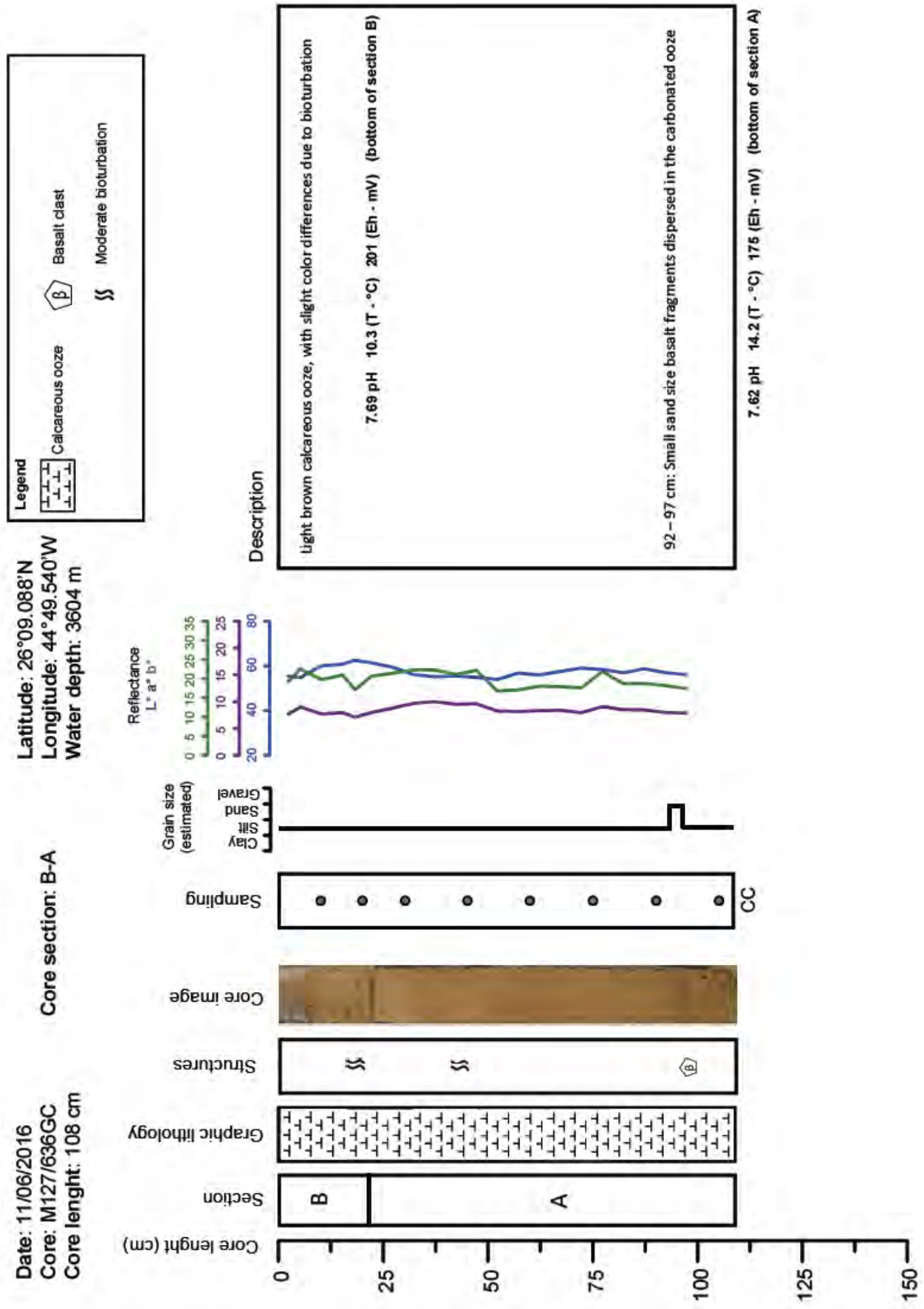
Date: 11/06/2016
Core: M127/636GC
Core lenght: 108 cm
Core section: B-A
Latitude: 26°09.088'N
Longitude: 44°49.540'W
Water depth: 3604 m
Legend
Calcareous ooze
Basalt clast
Moderate bioturbation
Description
light brown calcareous ooze, with slight color differences due to bioturbation
7.69 pH 10.3 (T - °C) 201 (Eh - mV) (bottom of section B)
92 – 97 cm: Small sand size basalt fragments dispersed in the carbonated ooze
7.62 pH 14.2 (T - °C) 175 (Eh - mV) (bottom of section A)
Reflectance
L* a* b*
Grain size (estimated)
Clay
Silt
Sand
Gravel
Sampling
CC
Core image
Structures
Graphic lithology
Section
B
A
Core lenght (cm)
0
25
50
75
100
125
150

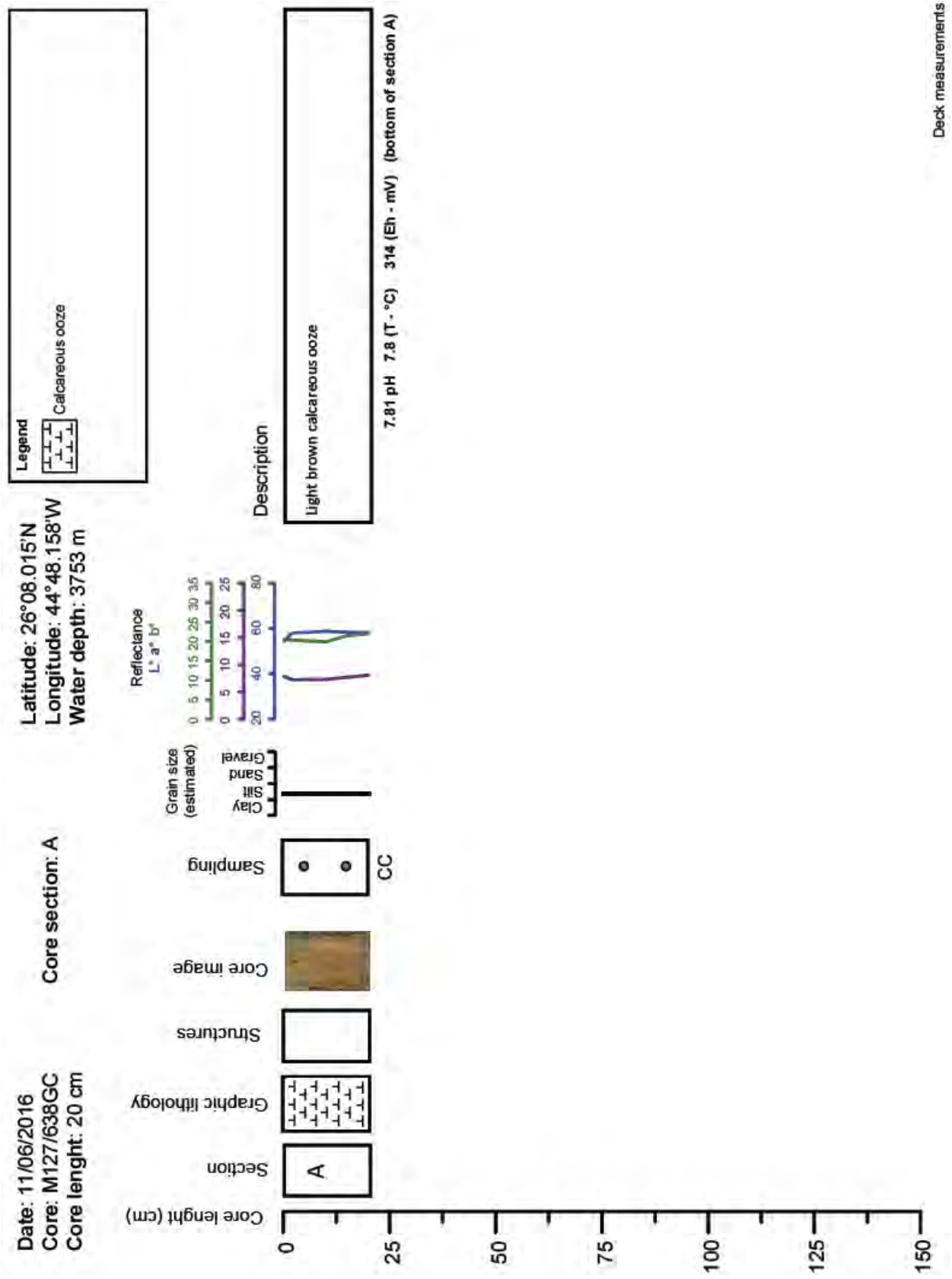
Date: 11/06/2016
Core: M127/638GC
Core lenght: 20 cm
Core section: A
Latitude: 26°08.015'N
Longitude: 44°48.158'W
Water depth: 3753 m
Legend
Calcareous ooze
Core lenght (cm)
Section
Graphic lithology
Structures
Core image
Sampling
Grain size (estimated)
Clay
Silt
Sand
Gravel
Reflectance
L* a* b*
Description
Light brown calcareous ooze
CC
7.81 pH 7.8 (T - °C) 314 (Eh - mV) (bottom of section A)
Deck measurements

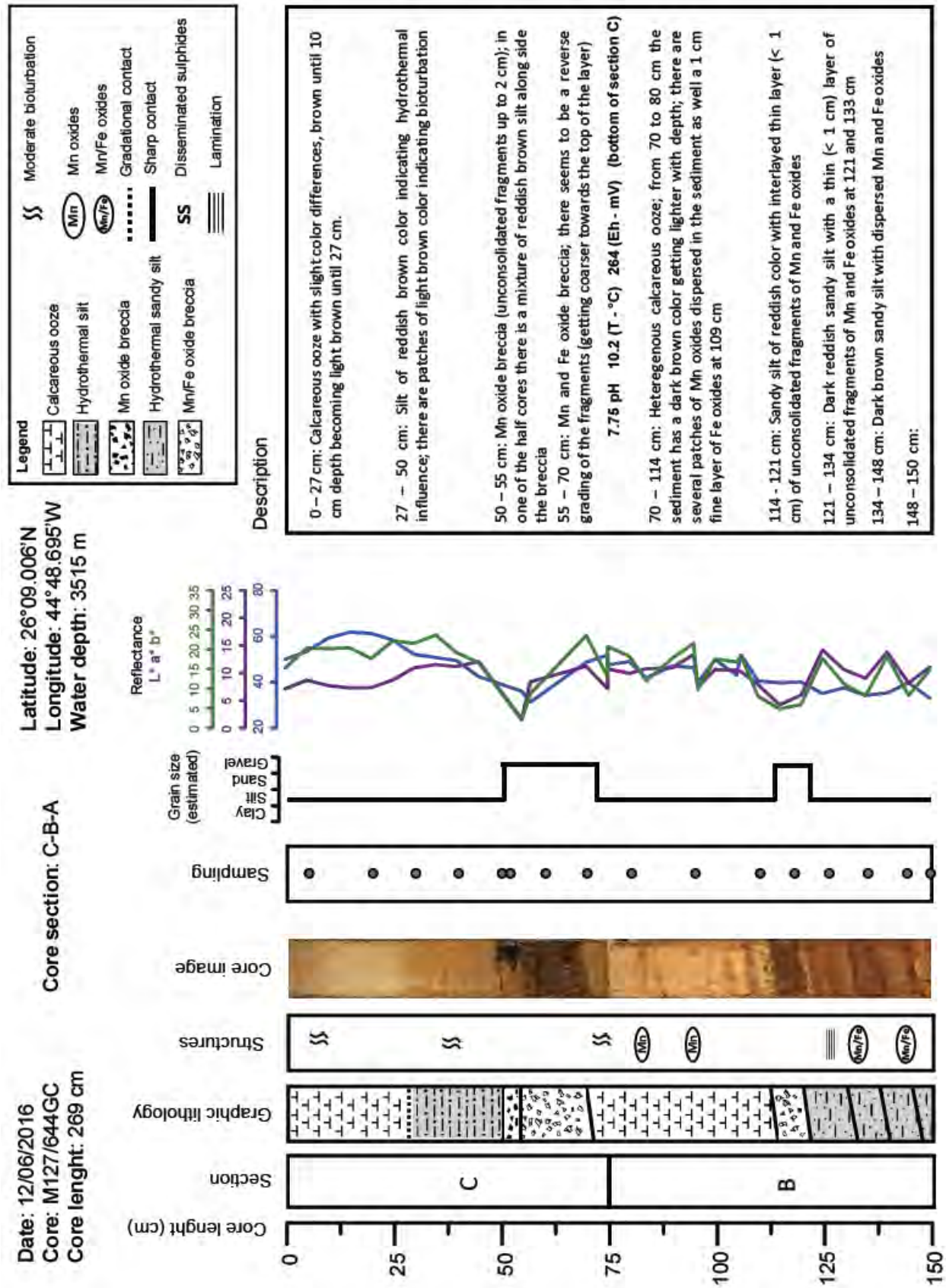
Date: 12/06/2016
Core: M127/644GC
Core lenght: 269 cm
Core section: C-B-A
Latitude: 26°09.006'N
Longitude: 44°48.695'W
Water depth: 3515 m
Core lenght (cm)
Section
Graphic lithology
Structures
Core image
Sampling
Grain size (estimated)
Clay
Silt
Sand
Gravel
Reflectance
L* a* b*
Legend
Calcareous ooze
Hydrothermal silt
Mn oxide breccia
Hydrothermal sandy silt
Mn/Fe oxide breccia
Moderate bioturbation
Mn oxides
Mn/Fe oxides
Gradational contact
Sharp contact
Disseminated sulphides
Lamination
Description
0 – 27 cm: Calcareous ooze with slight color differences, brown until 10 cm depth becoming light brown until 27 cm.
27 – 50 cm: Silt of reddish brown color indicating hydrothermal influence; there are patches of light brown color indicating bioturbation
50 – 55 cm: Mn oxide breccia (unconsolidated fragments up to 2 cm); in one of the half cores there is a mixture of reddish brown silt along side the breccia
55 – 70 cm: Mn and Fe oxide breccia; there seems to be a reverse grading of the fragments (getting coarser towards the top of the layer)
7.75 pH 10.2 (T - °C) 264 (Eh - mV) (bottom of section C)
70 – 114 cm: Heteregenous calcareous ooze; from 70 to 80 cm the sediment has a dark brown color getting lighter with depth; there are several patches of Mn oxides dispersed in the sediment as well a 1 cm fine layer of Fe oxides at 109 cm
114 - 121 cm: Sandy silt of reddish color with interlayed thin layer (< 1 cm) of unconsolidated fragments of Mn and Fe oxides
121 – 134 cm: Dark reddish sandy silt with a thin (< 1 cm) layer of unconsolidated fragments of Mn and Fe oxides at 121 and 133 cm
134 – 148 cm: Dark brown sandy silt with dispersed Mn and Fe oxides
148 – 150 cm:

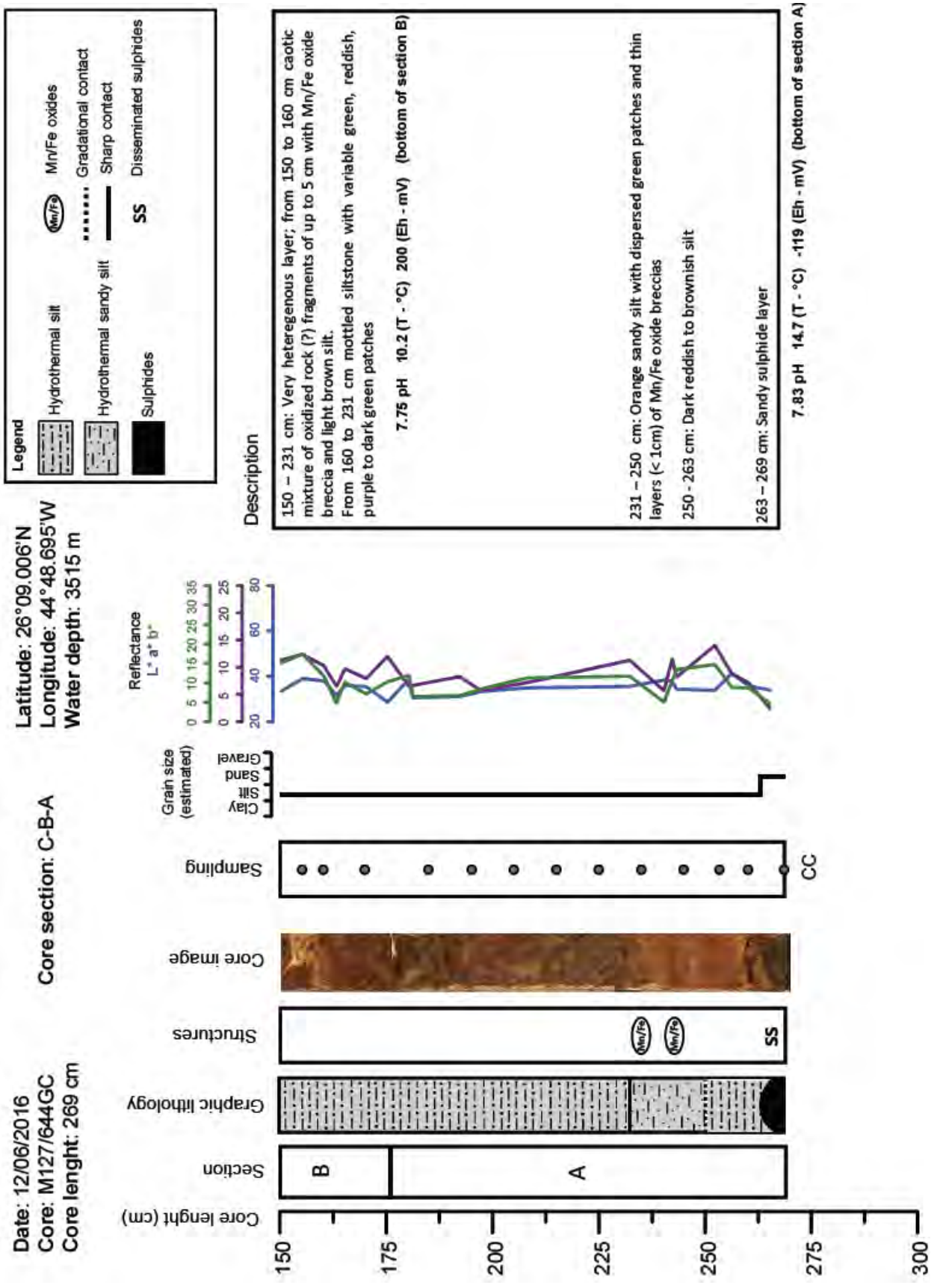
Date: 12/06/2016
Core: M127/644GC
Core lenght: 269 cm
Core section: C-B-A
Latitude: 26°09.006'N
Longitude: 44°48.695'W
Water depth: 3515 m
Legend
Hydrothermal silt
Mn/Fe oxides
Hydrothermal sandy silt
Gradational contact
Sharp contact
Sulphides
SS Disseminated sulphides
Description
150 – 231 cm: Very heteregenous layer; from 150 to 160 cm caotic mixture of oxidized rock (?) fragments of up to 5 cm with Mn/Fe oxide breccia and light brown silt.
From 160 to 231 cm mottled siltstone with variable green, reddish, purple to dark green patches
7.75 pH 10.2 (T - °C) 200 (Eh - mV) (bottom of section B)
231 – 250 cm: Orange sandy silt with dispersed green patches and thin layers (< 1cm) of Mn/Fe oxide breccias
250 - 263 cm: Dark reddish to brownish silt
263 – 269 cm: Sandy sulphide layer
7.83 pH 14.7 (T - °C) -119 (Eh - mV) (bottom of section A)
Reflectance L* a* b*
Grain size (estimated)
Clay
Silt
Sand
Gravel
Sampling
Core image
Structures
Graphic lithology
Section
Core lenght (cm)
B
A
SS
CC
150
175
200
225
250
275
300

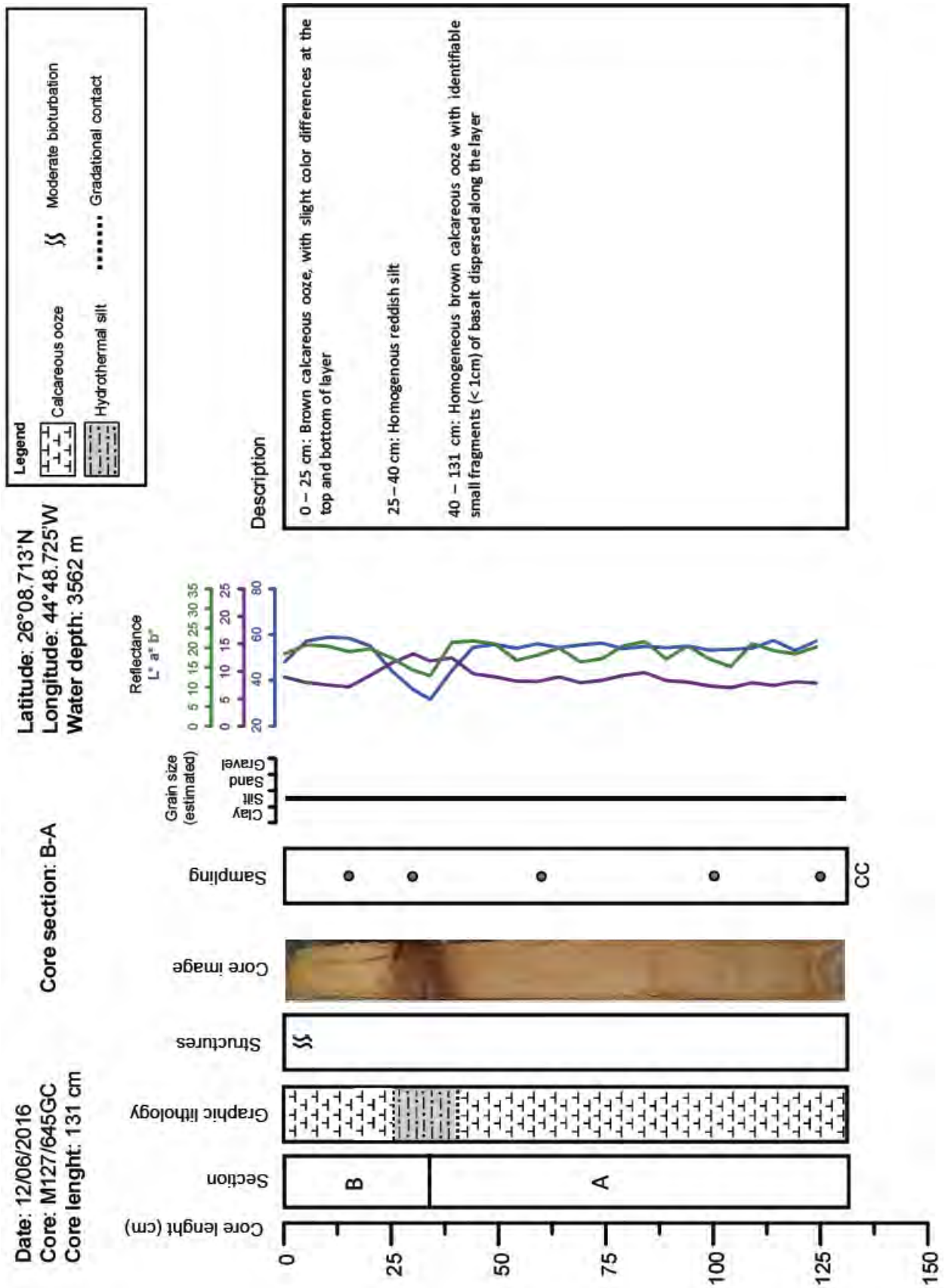
Date: 12/06/2016
Core: M127/645GC
Core lenght: 131 cm
Core section: B-A
Latitude: 26°08.713'N
Longitude: 44°48.725'W
Water depth: 3562 m
Legend
Calcareous ooze
Moderate bioturbation
Hydrothermal silt
Gradational contact
Description
0 – 25 cm: Brown calcareous ooze, with slight color differences at the top and bottom of layer
25 – 40 cm: Homogenous reddish silt
40 – 131 cm: Homogeneous brown calcareous ooze with identifiable small fragments (< 1cm) of basalt dispersed along the layer
Reflectance L* a* b*
Grain size (estimated)
Clay
Silt
Sand
Gravel
Sampling
Core image
Structures
Graphic lithology
Section
Core lenght (cm)
B
A
CC
0
25
50
75
100
125
150

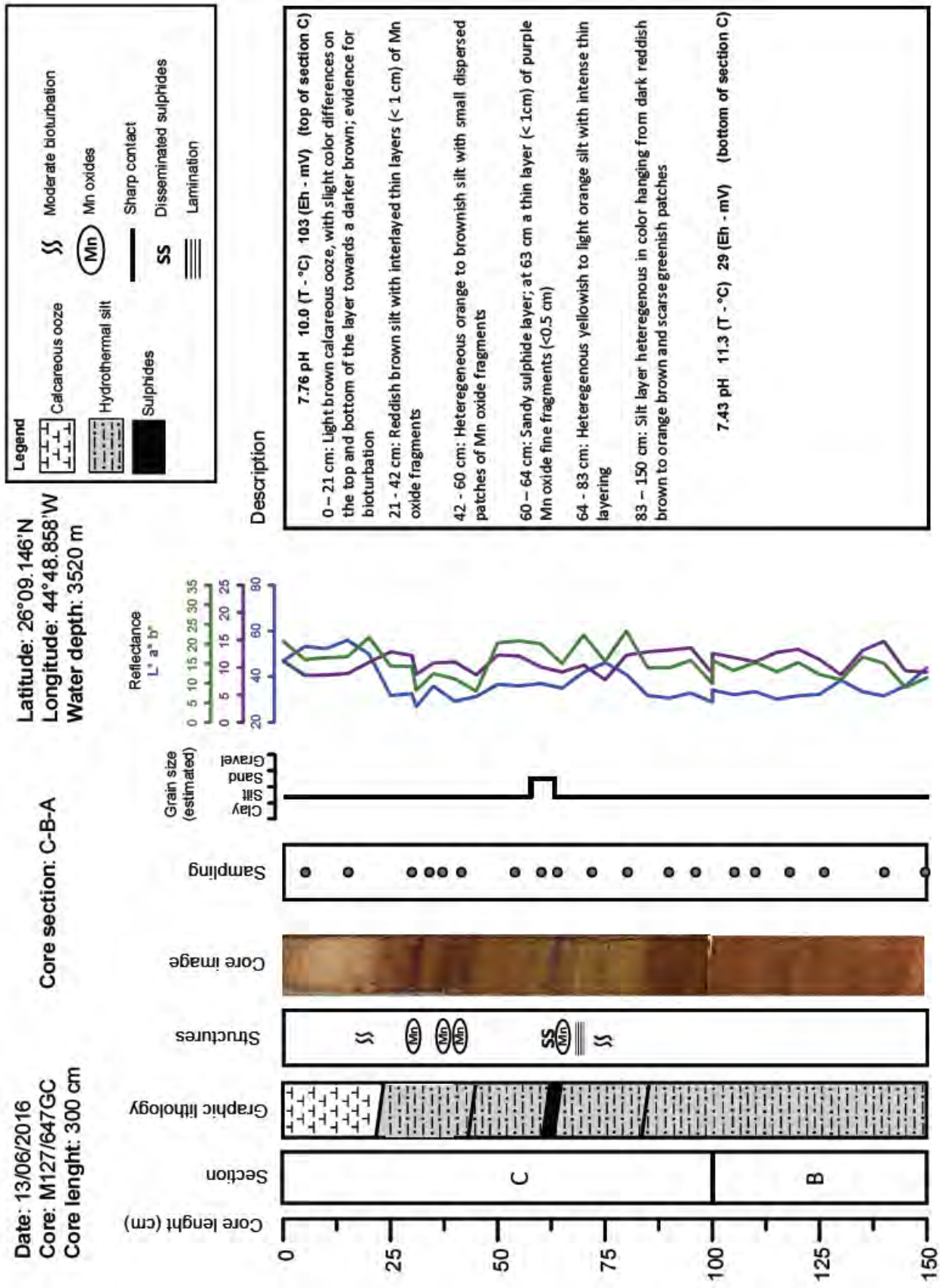
Legend
Calcareous ooze
Hydrothermal silt
Sulphides
Moderate bioturbation
Mn oxides
Sharp contact
Disseminated sulphides
Lamination
Description
7.76 pH 10.0 (T - °C) 103 (Eh - mV) (top of section C)
0 – 21 cm: Light brown calcareous ooze, with slight color differences on the top and bottom of the layer towards a darker brown; evidence for bioturbation
21 - 42 cm: Reddish brown silt with interlayed thin layers (< 1 cm) of Mn oxide fragments
42 - 60 cm: Heteregeneous orange to brownish silt with small dispersed patches of Mn oxide fragments
60 – 64 cm: Sandy sulphide layer; at 63 cm a thin layer (< 1cm) of purple Mn oxide fine fragments (<0.5 cm)
64 - 83 cm: Heteregenous yellowish to light orange silt with intense thin layering
83 – 150 cm: Silt layer heteregenous in color hanging from dark reddish brown to orange brown and scarse greenish patches
7.43 pH 11.3 (T - °C) 29 (Eh - mV) (bottom of section C)
Latitude: 26°09.146'N
Longitude: 44°48.858'W
Water depth: 3520 m
Core section: C-B-A
Date: 13/06/2016
Core: M127/647GC
Core lenght: 300 cm
Reflectance L* a* b*
Grain size (estimated)
Clay
Silt
Sand
Gravel
Sampling
Core image
Structures
Graphic lithology
Section
Core lenght (cm)
C
B
0
25
50
75
100
125
150

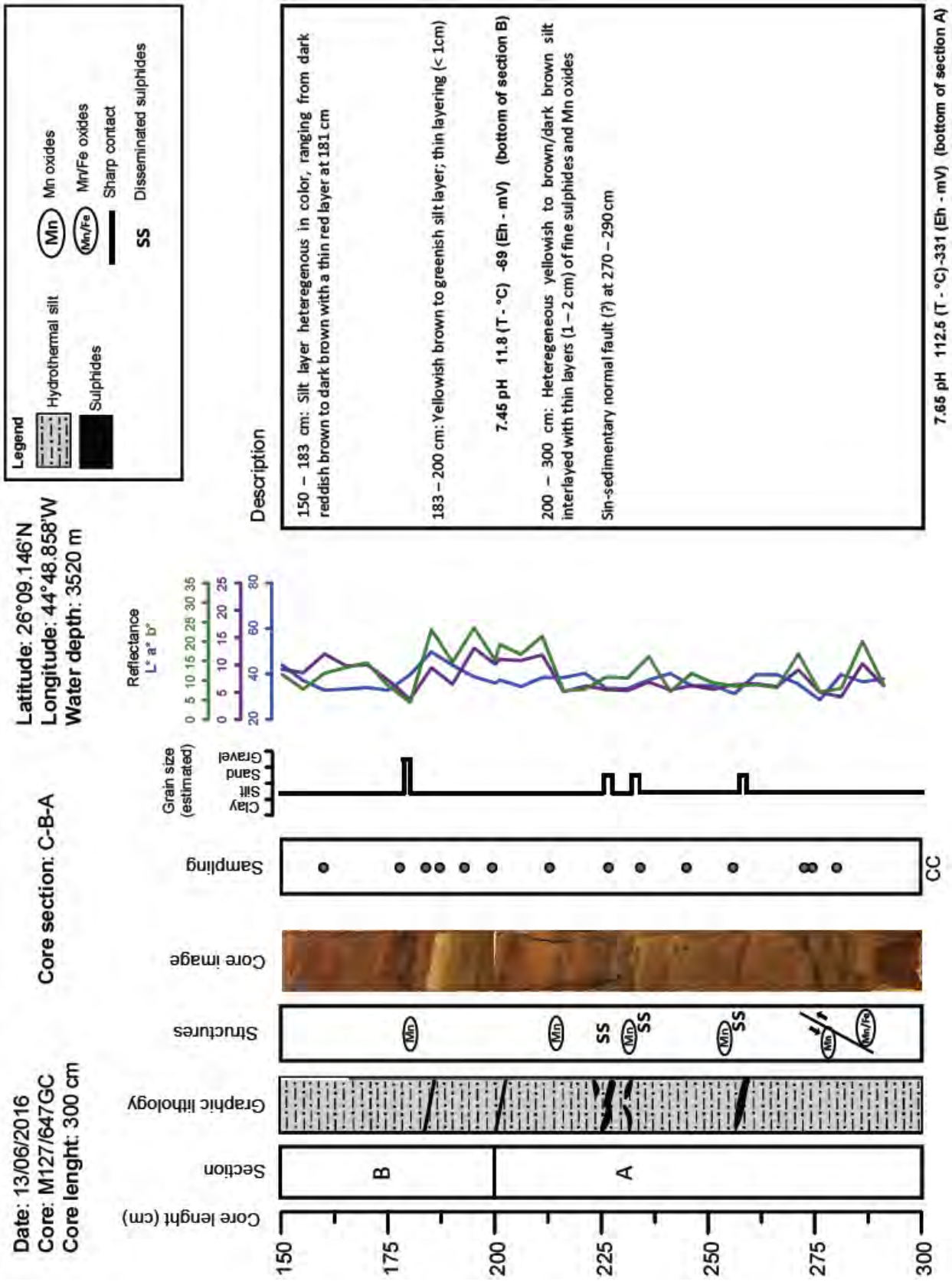
Legend
Hydrothermal silt
Sulphides
Mn oxides
Mn/Fe oxides
Sharp contact
SS Disseminated sulphides
Description
150 – 183 cm: Silt layer heteregenous in color, ranging from dark reddish brown to dark brown with a thin red layer at 181 cm
183 – 200 cm: Yellowish brown to greenish silt layer; thin layering (< 1cm)
7.45 pH 11.8 (T - °C) -69 (Eh - mV) (bottom of section B)
200 – 300 cm: Heteregeneous yellowish to brown/dark brown silt interlayed with thin layers (1 – 2 cm) of fine sulphides and Mn oxides
Sin-sedimentary normal fault (?) at 270 – 290 cm
7.65 pH 112.5 (T - °C) -331 (Eh - mV) (bottom of section A)
Latitude: 26°09.146'N
Longitude: 44°48.858'W
Water depth: 3520 m
Core section: C-B-A
Date: 13/06/2016
Core: M127/647GC
Core lenght: 300 cm
Reflectance L* a* b*
Grain size (estimated)
Clay
Silt
Sand
Gravel
Sampling
Core image
Structures
Graphic lithology
Section
Core lenght (cm)
CC
B
A
SS
Mn
Mn/Fe

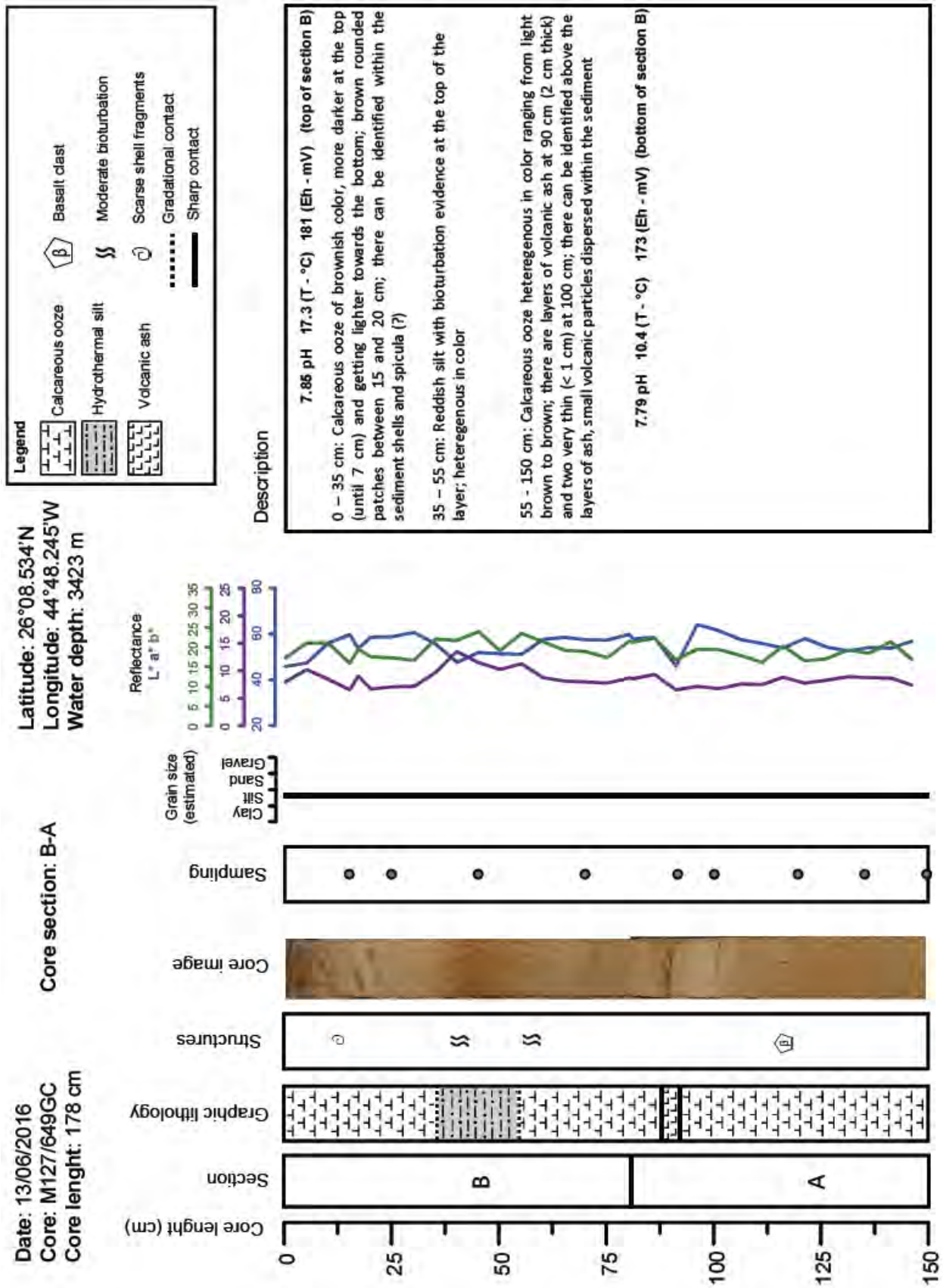
Date: 13/06/2016
Core: M127/649GC
Core lenght: 178 cm
Core section: B-A
Latitude: 26°08.534'N
Longitude: 44°48.245'W
Water depth: 3423 m
Legend
Calcareous ooze
Basalt clast
Hydrothermal silt
Moderate bioturbation
Volcanic ash
Scarse shell fragments
Gradational contact
Sharp contact
Description
7.85 pH 17.3 (T - °C) 181 (Eh - mV) (top of section B)
0 – 35 cm: Calcareous ooze of brownish color, more darker at the top (until 7 cm) and getting lighter towards the bottom; brown rounded patches between 15 and 20 cm; there can be identified within the sediment shells and spicula (?)
35 – 55 cm: Reddish silt with bioturbation evidence at the top of the layer; heteregenous in color
55 - 150 cm: Calcareous ooze heteregenous in color ranging from light brown to brown; there are layers of volcanic ash at 90 cm (2 cm thick) and two very thin (< 1 cm) at 100 cm; there can be identified above the layers of ash, small volcanic particles dispersed within the sediment
7.79 pH 10.4 (T - °C) 173 (Eh - mV) (bottom of section B)
Reflectance L* a* b*
Grain size (estimated)
Clay
Silt
Sand
Gravel
Sampling
Core image
Structures
Graphic lithology
Section
Core lenght (cm)
B
A
0
25
50
75
100
125
150

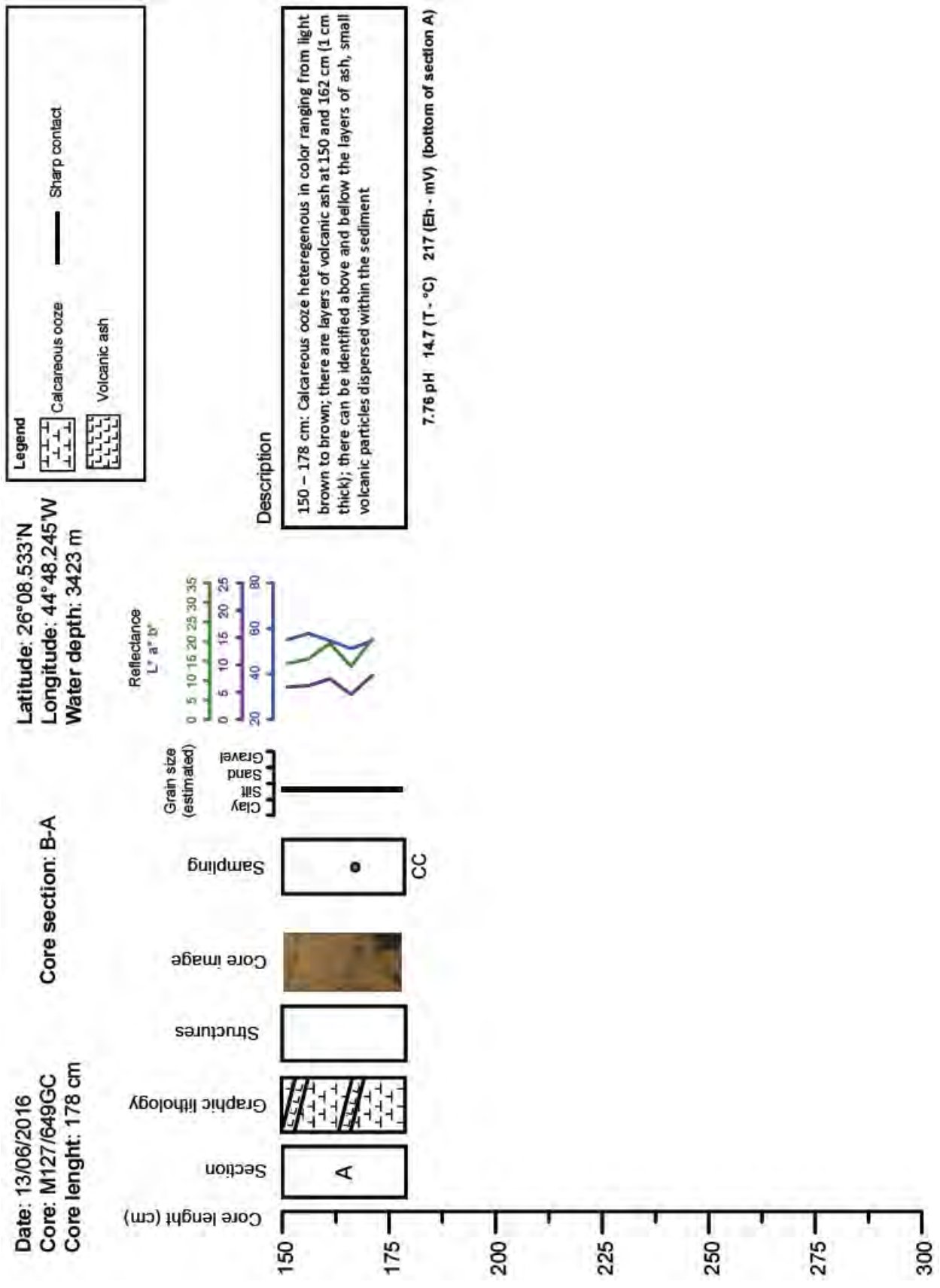
Date: 13/06/2016
Core: M127/649GC
Core lenght: 178 cm
Core section: B-A
Latitude: 26°08.533'N
Longitude: 44°48.245'W
Water depth: 3423 m
Legend
Calcareous ooze
Sharp contact
Volcanic ash
Description
150 – 178 cm: Calcareous ooze heteregenous in color ranging from light brown to brown; there are layers of volcanic ash at 150 and 162 cm (1 cm thick); there can be identified above and bellow the layers of ash, small volcanic particles dispersed within the sediment
7.76 pH 14.7 (T - °C) 217 (Eh - mV) (bottom of section A)
Core lenght (cm)
Section
Graphic lithology
Structures
Core image
Sampling
Grain size (estimated)
Clay
Silt
Sand
Gravel
Reflectance
L* a* b*
A
CC
150
175
200
225
250
275
300

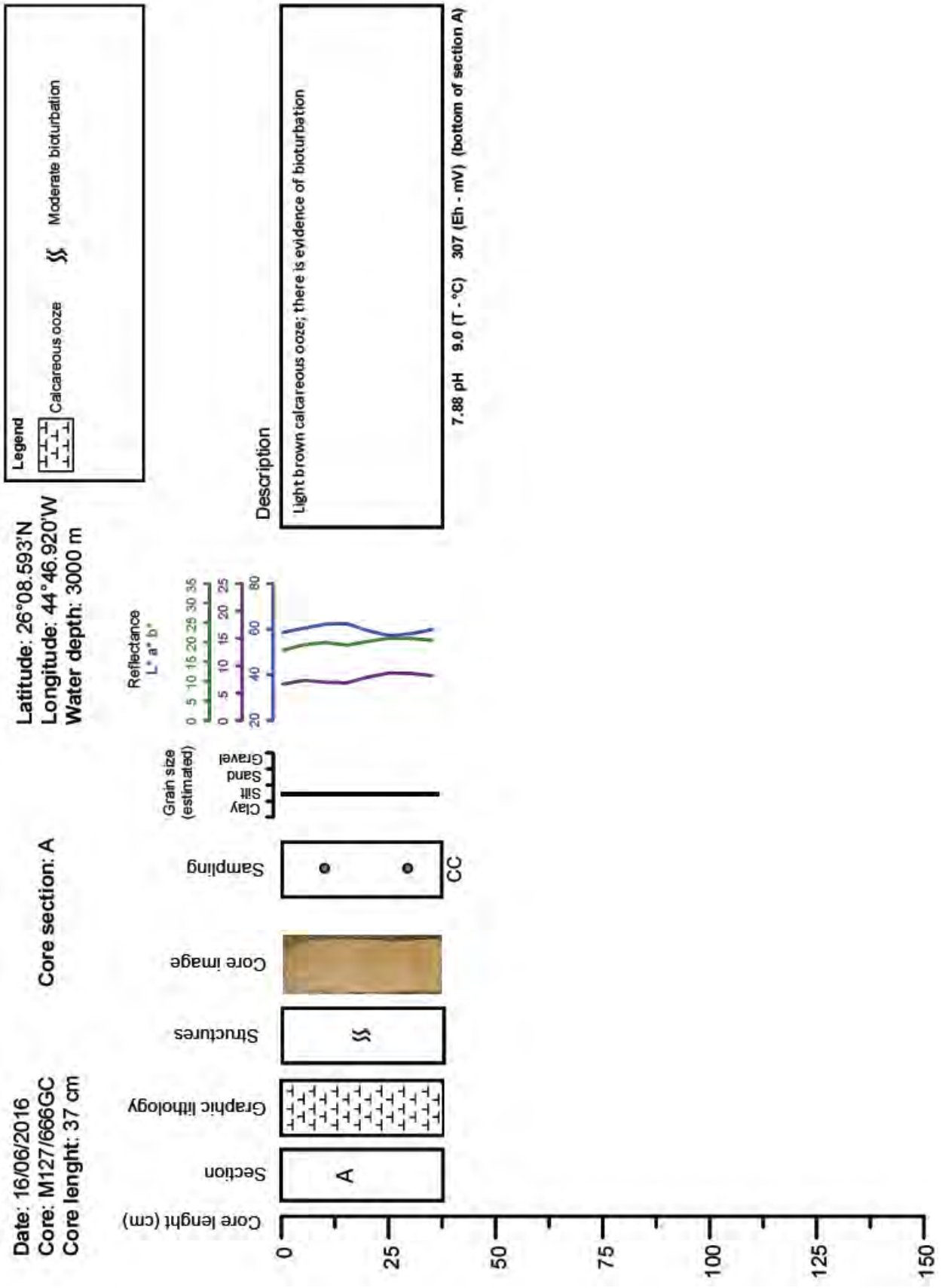
Date: 16/06/2016
Core: M127/666GC
Core lenght: 37 cm
Core section: A
Latitude: 26°08.593'N
Longitude: 44°46.920'W
Water depth: 3000 m
Legend
Calcareous ooze
Moderate bioturbation
Description
Light brown calcareous ooze; there is evidence of bioturbation
7.88 pH 9.0 (T - °C) 307 (Eh - mV) (bottom of section A)
Core lenght (cm)
Section
Graphic lithology
Structures
Core image
Sampling
Grain size (estimated)
Clay
Silt
Sand
Gravel
Reflectance
L* a* b*
A
CC
0
25
50
75
100
125
150

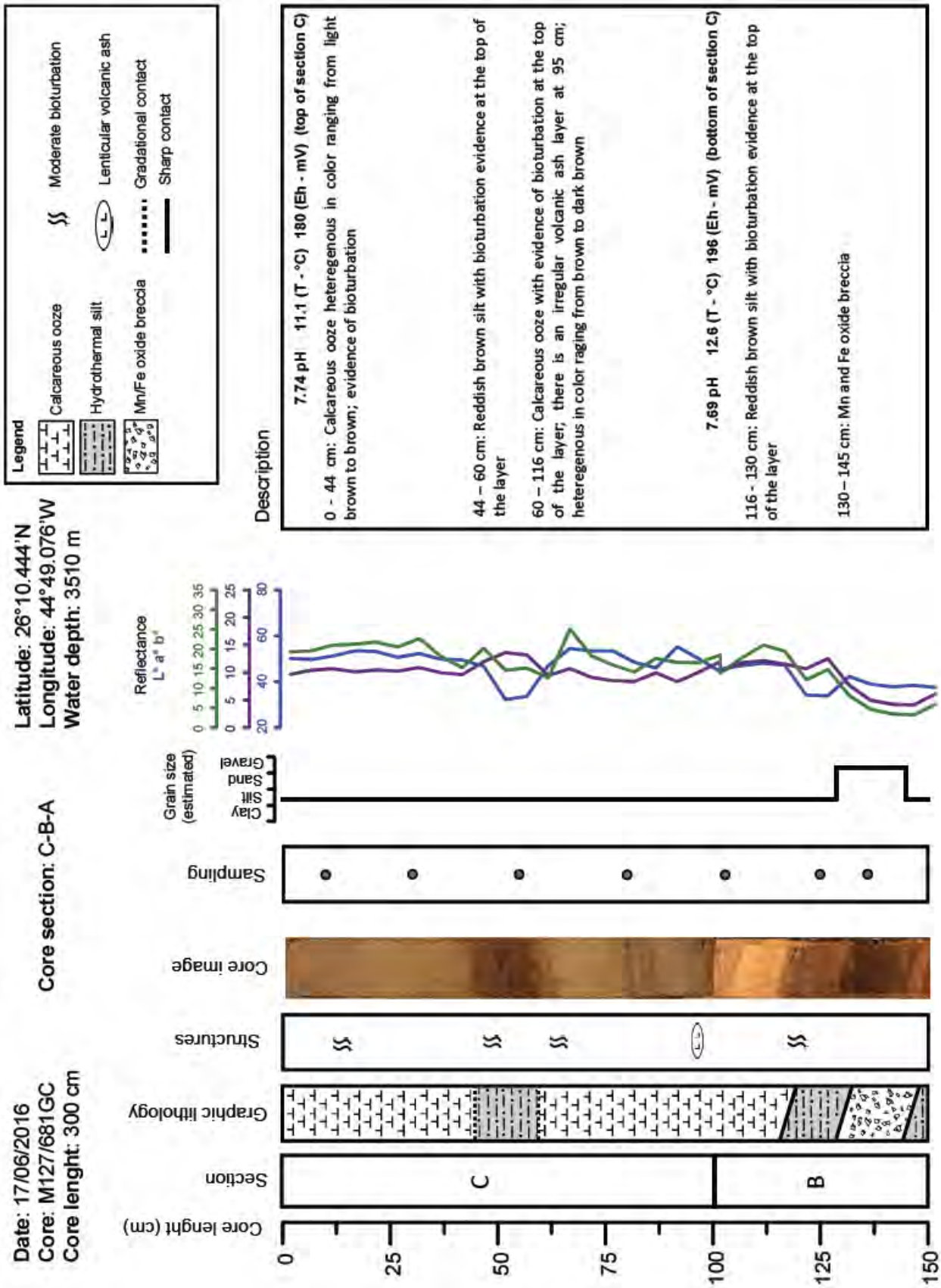
Date: 17/06/2016
Core: M127/681GC
Core lenght: 300 cm
Core section: C-B-A
Latitude: 26°10.444'N
Longitude: 44°49.076'W
Water depth: 3510 m
Legend
Calcareous ooze
Moderate bioturbation
Hydrothermal silt
Lenticular volcanic ash
Mn/Fe oxide breccia
Gradational contact
Sharp contact
Description
7.74 pH 11.1 (T - °C) 180 (Eh - mV) (top of section C)
0 - 44 cm: Calcareous ooze heteregenous in color ranging from light brown to brown; evidence of bioturbation
44 – 60 cm: Reddish brown silt with bioturbation evidence at the top of the layer
60 – 116 cm: Calcareous ooze with evidence of bioturbation at the top of the layer; there is an irregular volcanic ash layer at 95 cm; heteregenous in color raging from brown to dark brown
7.69 pH 12.6 (T - °C) 196 (Eh - mV) (bottom of section C)
116 - 130 cm: Reddish brown silt with bioturbation evidence at the top of the layer
130 – 145 cm: Mn and Fe oxide breccia
Reflectance
L* a* b*
Grain size (estimated)
Clay
Silt
Sand
Gravel
Sampling
Core image
Structures
Graphic lithology
Section
Core lenght (cm)
C
B
0
25
50
75
100
125
150

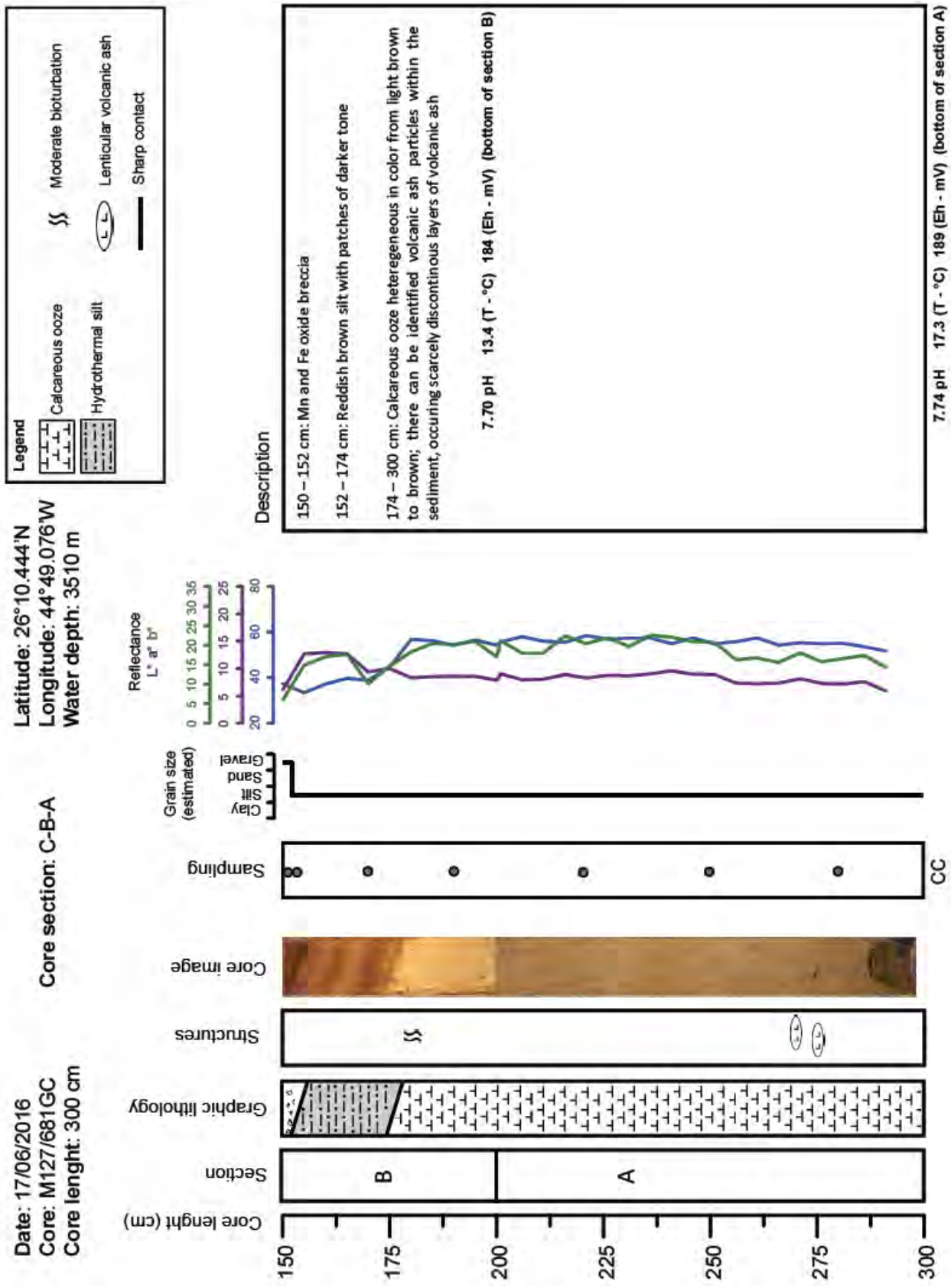
Date: 17/06/2016
Core: M127/681GC
Core lenght: 300 cm
Core section: C-B-A
Latitude: 26°10.444'N
Longitude: 44°49.076'W
Water depth: 3510 m
Legend
Calcareous ooze
Hydrothermal silt
Moderate bioturbation
Lenticular volcanic ash
Sharp contact
Description
150 – 152 cm: Mn and Fe oxide breccia
152 – 174 cm: Reddish brown silt with patches of darker tone
174 – 300 cm: Calcareous ooze heteregeneous in color from light brown to brown; there can be identified volcanic ash particles within the sediment, occuring scarcely discontinous layers of volcanic ash
7.70 pH 13.4 (T - °C) 184 (Eh - mV) (bottom of section B)
7.74 pH 17.3 (T - °C) 189 (Eh - mV) (bottom of section A)
Reflectance L* a* b*
Grain size (estimated)
Clay
Silt
Sand
Gravel
Sampling
Core image
Structures
Graphic lithology
Section
Core lenght (cm)
B
A
CC
150
175
200
225
250
275
300

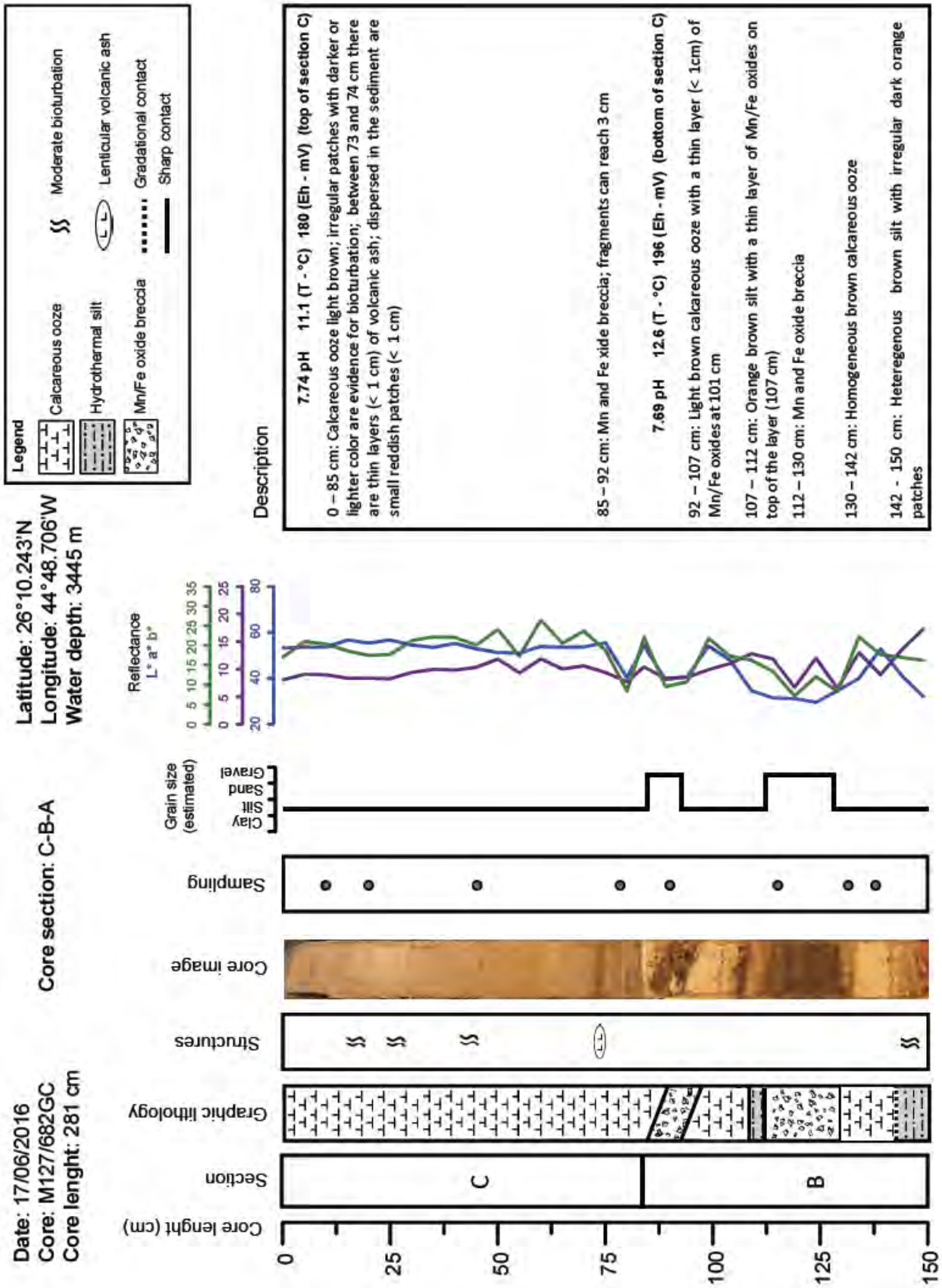
Date: 17/06/2016
Core: M127/682GC
Core lenght: 281 cm
Core section: C-B-A
Latitude: 26°10.243'N
Longitude: 44°48.706'W
Water depth: 3445 m
Legend
Calcareous ooze
Hydrothermal silt
Mn/Fe oxide breccia
Moderate bioturbation
Lenticular volcanic ash
Gradational contact
Sharp contact
Description
7.74 pH 11.1 (T - °C) 180 (Eh - mV) (top of section C)
0 – 85 cm: Calcareous ooze light brown; irregular patches with darker or lighter color are evidence for bioturbation; between 73 and 74 cm there are thin layers (< 1 cm) of volcanic ash; dispersed in the sediment are small reddish patches (< 1 cm)
85 – 92 cm: Mn and Fe xide breccia; fragments can reach 3 cm
7.69 pH 12.6 (T - °C) 196 (Eh - mV) (bottom of section C)
92 – 107 cm: Light brown calcareous ooze with a thin layer (< 1cm) of Mn/Fe oxides at 101 cm
107 – 112 cm: Orange brown silt with a thin layer of Mn/Fe oxides on top of the layer (107 cm)
112 – 130 cm: Mn and Fe oxide breccia
130 – 142 cm: Homogeneous brown calcareous ooze
142 - 150 cm: Heteregenous brown silt with irregular dark orange patches
Reflectance L* a* b*
Grain size (estimated)
Clay
Silt
Sand
Gravel
Sampling
Core image
Structures
Graphic lithology
Section
Core lenght (cm)
C
B
0
25
50
75
100
125
150

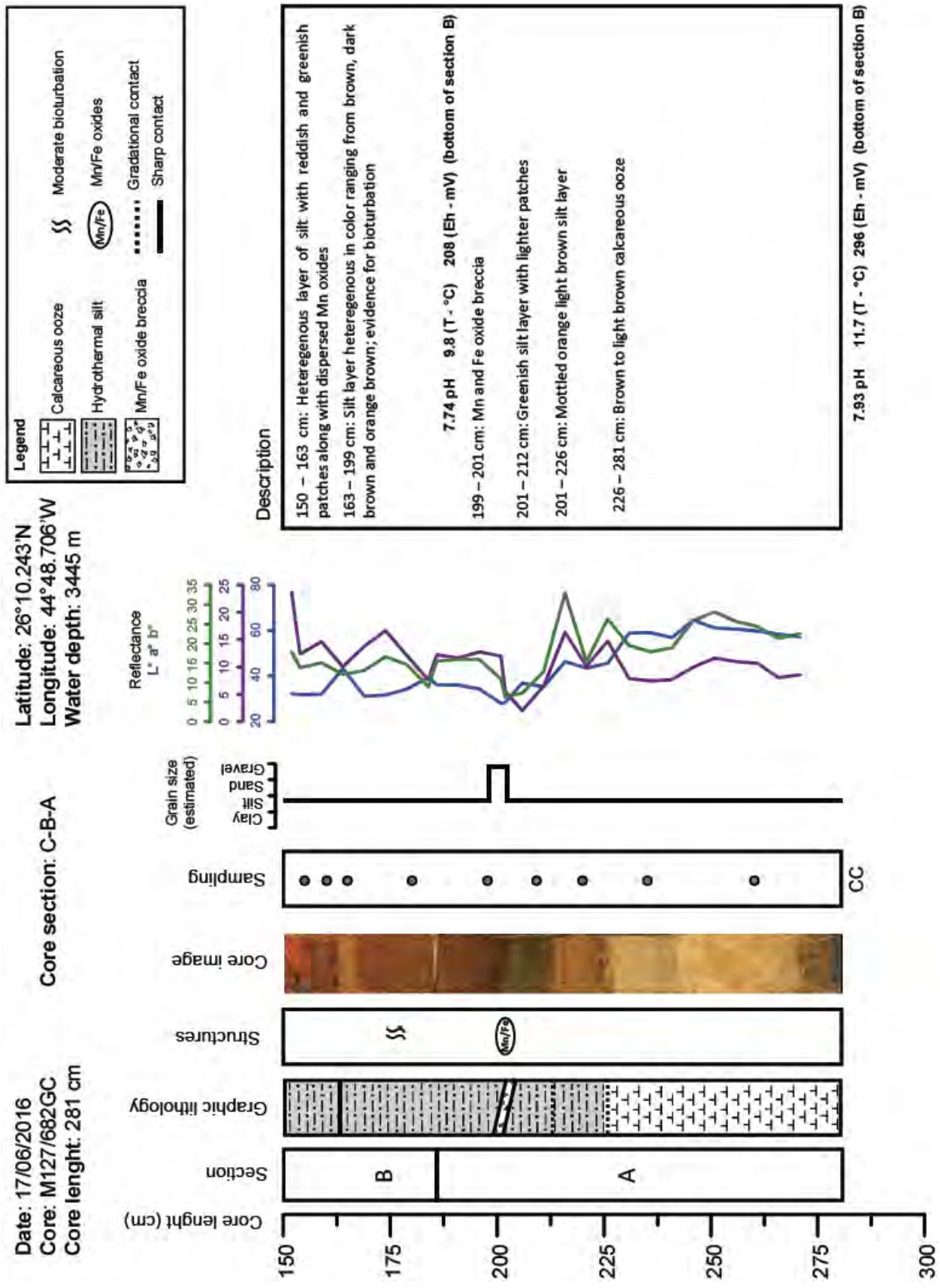
Date: 17/06/2016
Core: M127/682GC
Core lenght: 281 cm
Core section: C-B-A
Latitude: 26°10.243'N
Longitude: 44°48.706'W
Water depth: 3445 m
Legend
Calcareous ooze
Moderate bioturbation
Hydrothermal silt
Mn/Fe oxides
Mn/Fe oxide breccia
Gradational contact
Sharp contact
Description
150 – 163 cm: Heteregenous layer of silt with reddish and greenish patches along with dispersed Mn oxides
163 – 199 cm: Silt layer heteregenous in color ranging from brown, dark brown and orange brown; evidence for bioturbation
7.74 pH 9.8 (T - °C) 208 (Eh - mV) (bottom of section B)
199 – 201 cm: Mn and Fe oxide breccia
201 – 212 cm: Greenish silt layer with lighter patches
201 – 226 cm: Mottled orange light brown silt layer
226 – 281 cm: Brown to light brown calcareous ooze
7.93 pH 11.7 (T - °C) 296 (Eh - mV) (bottom of section B)
Reflectance L* a* b*
Grain size (estimated)
Clay
Silt
Sand
Gravel
Sampling
CC
Core image
Structures
Graphic lithology
Section
A
B
Core lenght (cm)
150
175
200
225
250
275
300

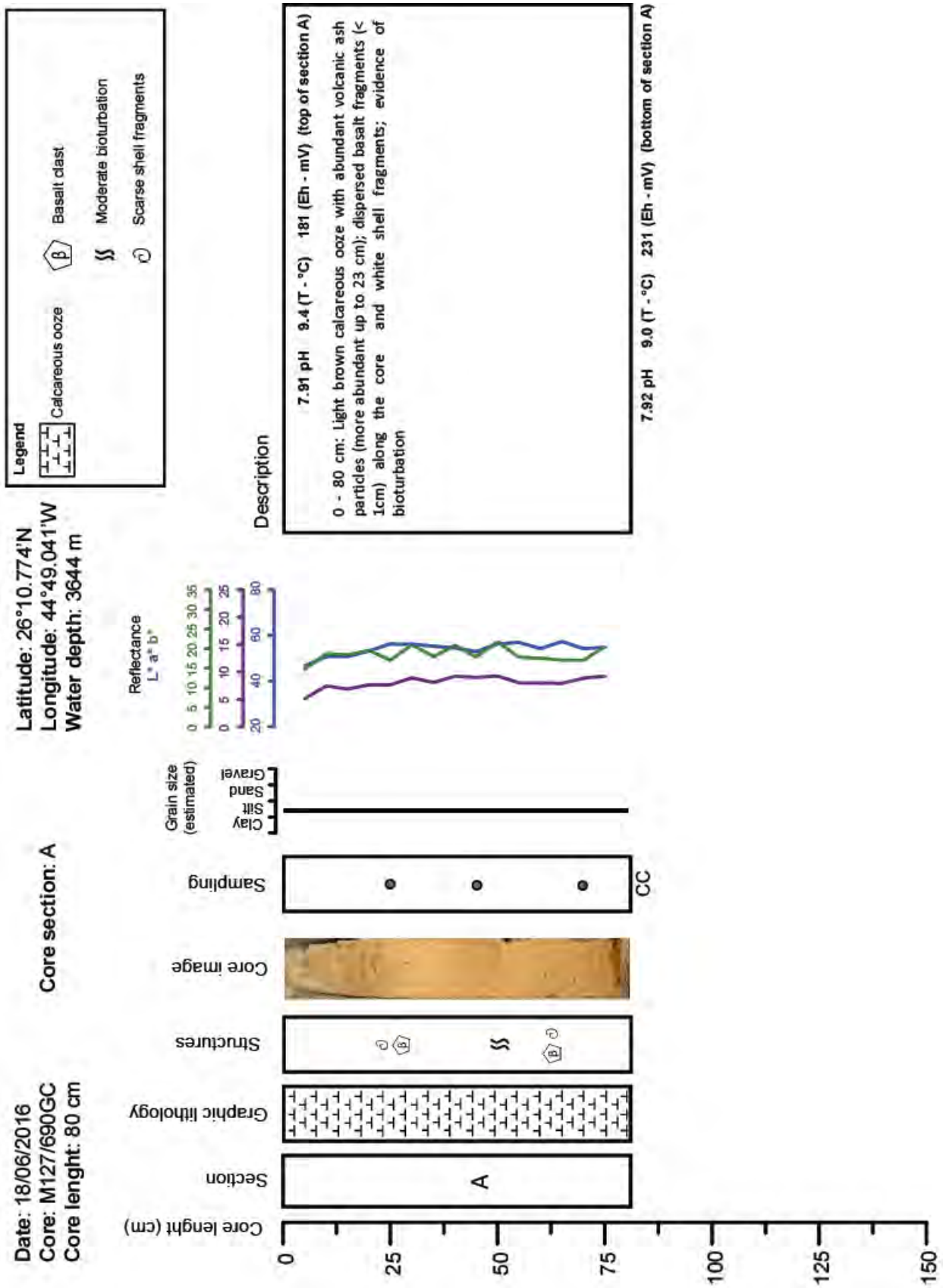
Date: 18/06/2016
Core: M127/690GC
Core lenght: 80 cm
Core section: A
Latitude: 26°10.774'N
Longitude: 44°49.041'W
Water depth: 3644 m
Legend
Calcareous ooze
Basalt clast
Moderate bioturbation
Scarse shell fragments
Description
7.91 pH 9.4 (T - °C) 181 (Eh - mV) (top of section A)
0 - 80 cm: Light brown calcareous ooze with abundant volcanic ash particles (more abundant up to 23 cm); dispersed basalt fragments (< 1cm) along the core and white shell fragments; evidence of bioturbation
7.92 pH 9.0 (T - °C) 231 (Eh - mV) (bottom of section A)
Reflectance L* a* b*
Grain size (estimated)
Clay
Silt
Sand
Gravel
Sampling
CC
Core image
Structures
Graphic lithology
Section
A
Core lenght (cm)
0
25
50
75
100
125
150

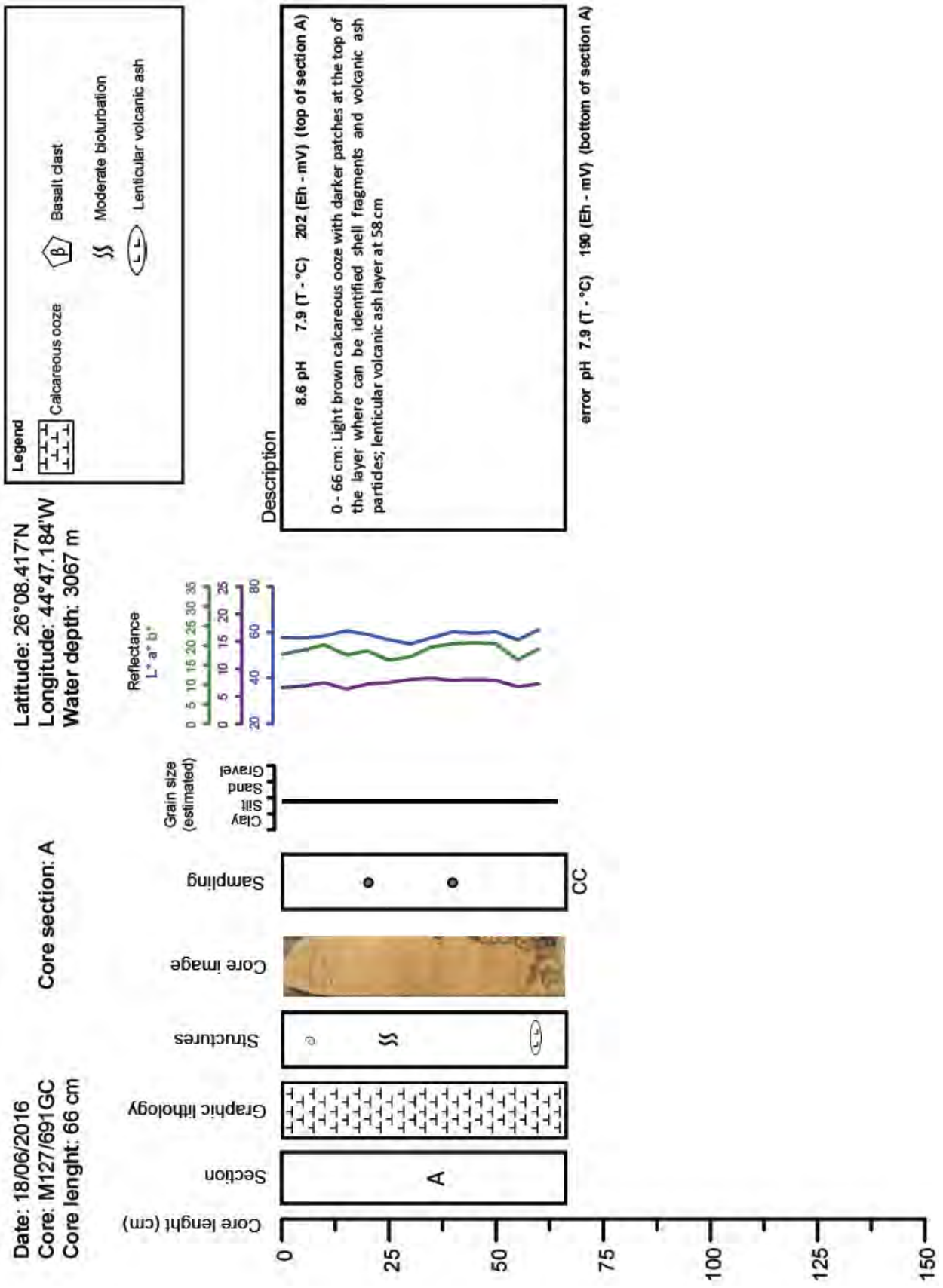
Date: 18/06/2016
Core: M127/691GC
Core lenght: 66 cm
Core section: A
Latitude: 26°08.417'N
Longitude: 44°47.184'W
Water depth: 3067 m
Legend
Calcareous ooze
Basalt clast
Moderate bioturbation
Lenticular volcanic ash
Description
8.6 pH 7.9 (T - °C) 202 (Eh - mV) (top of section A)
0 - 66 cm: Light brown calcareous ooze with darker patches at the top of the layer where can be identified shell fragments and volcanic ash particles; lenticular volcanic ash layer at 58 cm
error pH 7.9 (T - °C) 190 (Eh - mV) (bottom of section A)
Reflectance L* a* b*
Grain size (estimated)
Clay
Silt
Sand
Gravel
Sampling
Core image
Structures
Graphic lithology
Section
Core lenght (cm)
A
CC
0
25
50
75
100
125
150

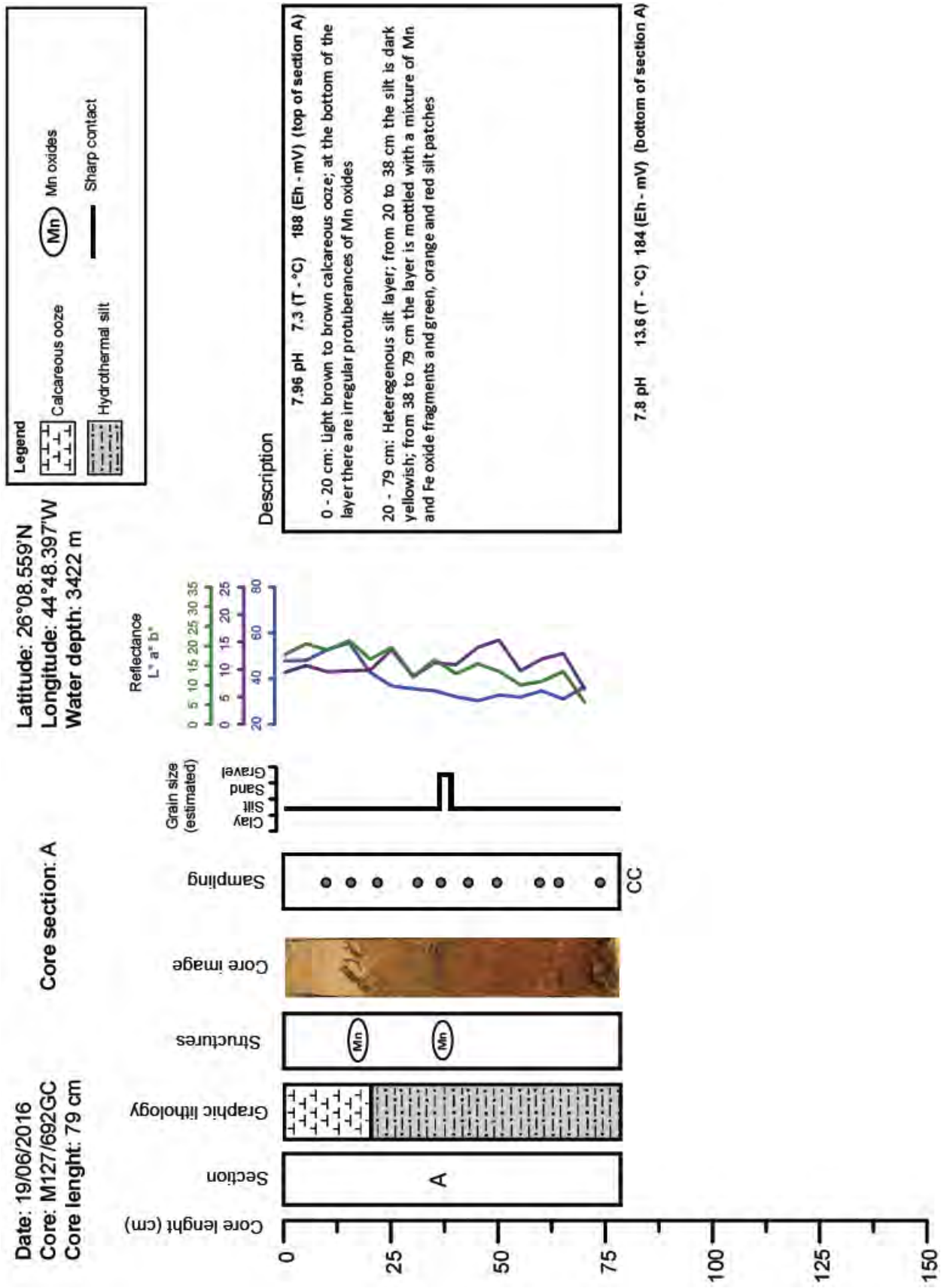
Date: 19/06/2016
Core: M127/692GC
Core lenght: 79 cm
Core section: A
Latitude: 26°08.559'N
Longitude: 44°48.397'W
Water depth: 3422 m
Legend
Calcareous ooze
Hydrothermal silt
Mn oxides
Sharp contact
Description
7.96 pH 7.3 (T - °C) 188 (Eh - mV) (top of section A)
0 - 20 cm: Light brown to brown calcareous ooze; at the bottom of the layer there are irregular protuberances of Mn oxides
20 - 79 cm: Heteregenous silt layer; from 20 to 38 cm the silt is dark yellowish; from 38 to 79 cm the layer is mottled with a mixture of Mn and Fe oxide fragments and green, orange and red silt patches
7.8 pH 13.6 (T - °C) 184 (Eh - mV) (bottom of section A)
Reflectance L* a* b*
Grain size (estimated)
Clay
Silt
Sand
Gravel
Sampling
CC
Core image
Structures
Mn
Graphic lithology
Section
A
Core lenght (cm)
0
25
50
75
100
125
150

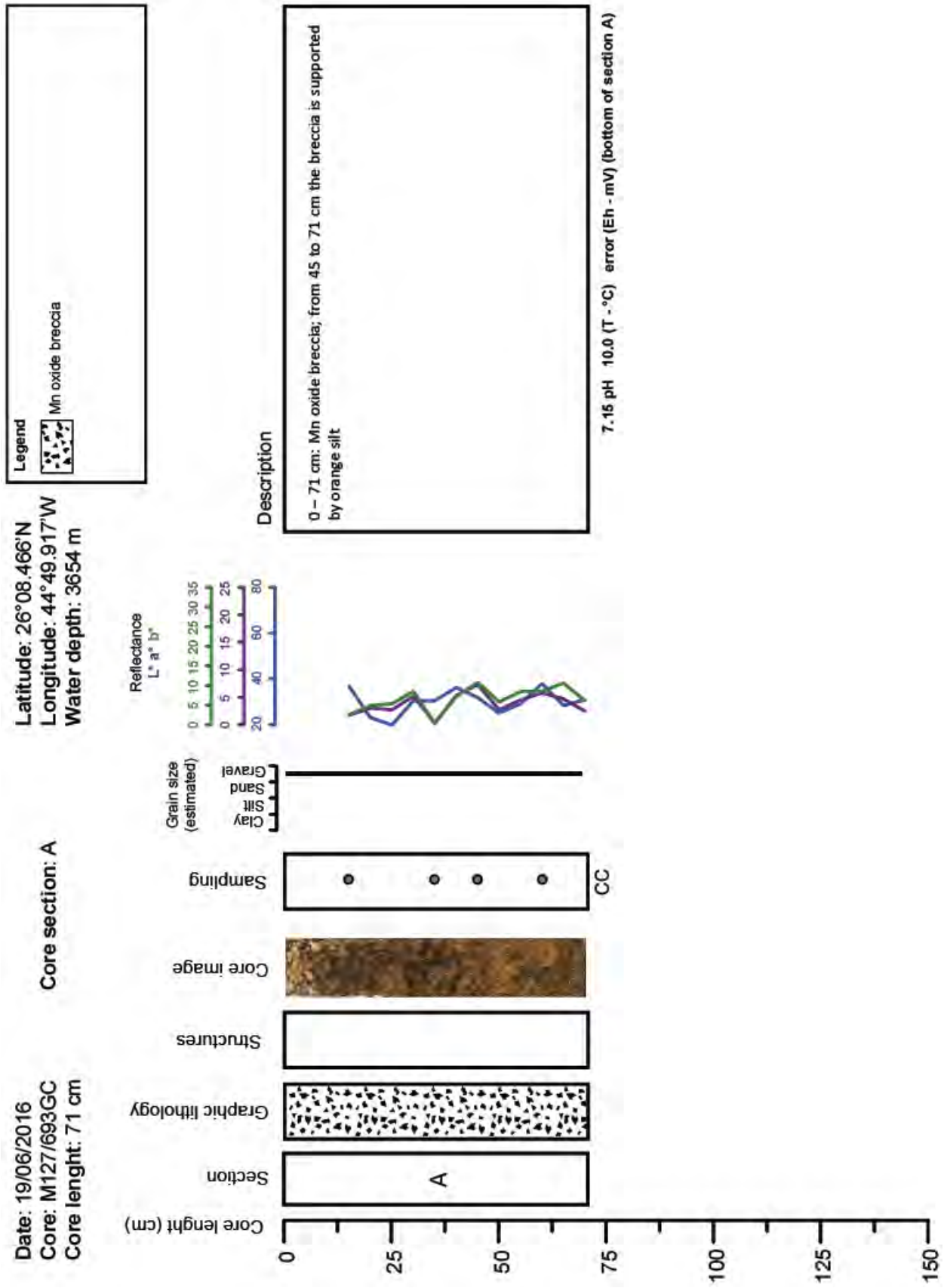
Date: 19/06/2016
Core: M127/693GC
Core lenght: 71 cm
Core section: A
Latitude: 26°08.466'N
Longitude: 44°49.917'W
Water depth: 3654 m
Legend
Mn oxide breccia
Description
0 – 71 cm: Mn oxide breccia; from 45 to 71 cm the breccia is supported by orange silt
7.15 pH 10.0 (T - °C) error (Eh - mV) (bottom of section A)
Reflectance L* a* b*
Grain size (estimated)
Clay
Silt
Sand
Gravel
Sampling
Core image
Structures
Graphic lithology
Section
Core lenght (cm)
A
CC
0
25
50
75
100
125
150

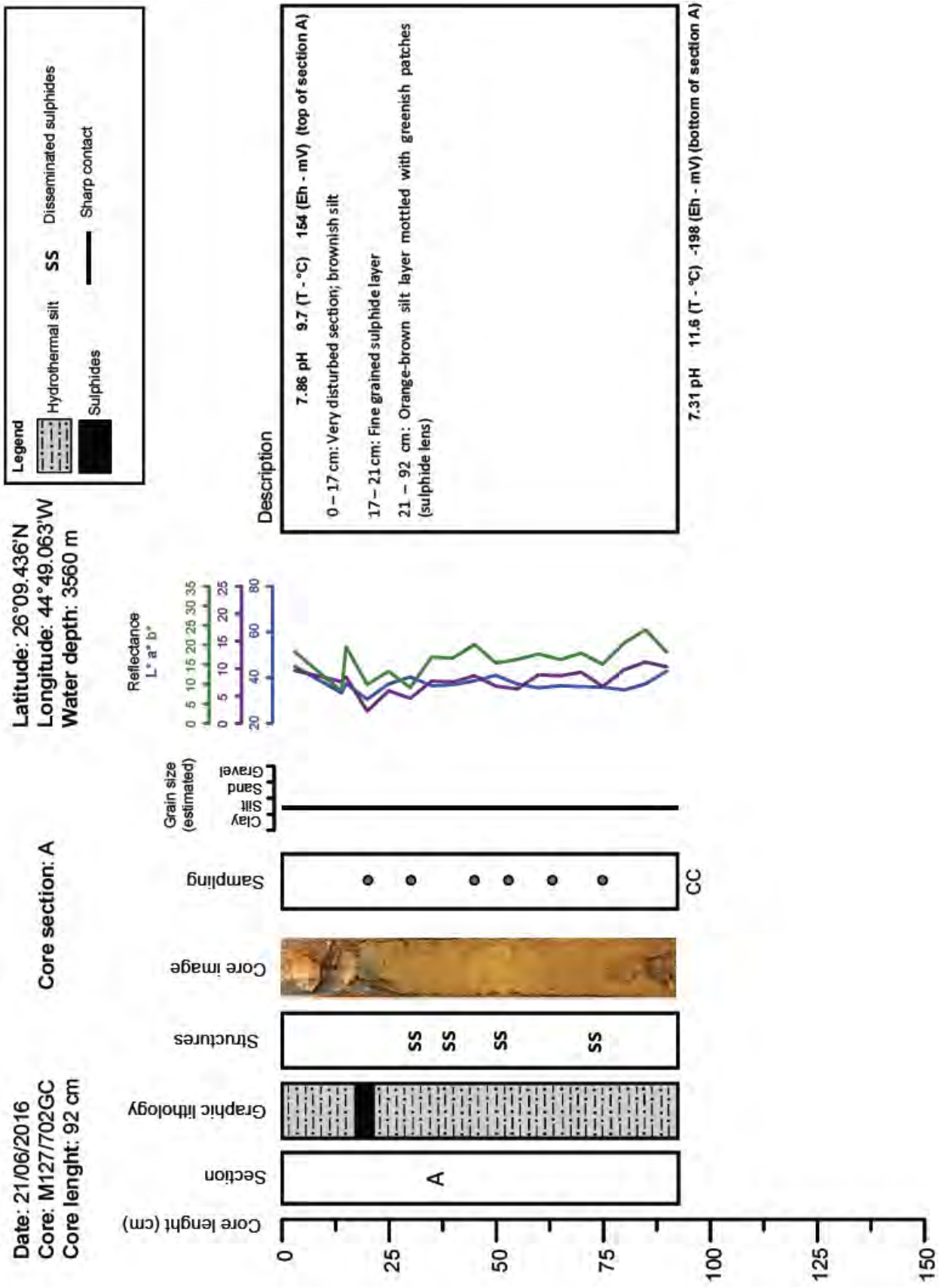
Legend
Hydrothermal silt
SS Disseminated sulphides
Sulphides
Sharp contact
Description
7.86 pH 9.7 (T - °C) 154 (Eh - mV) (top of section A)
0 – 17 cm: Very disturbed section; brownish silt
17 – 21 cm: Fine grained sulphide layer
21 – 92 cm: Orange-brown silt layer mottled with greenish patches (sulphide lens)
7.31 pH 11.6 (T - °C) -198 (Eh - mV) (bottom of section A)
Latitude: 26°09.436'N
Longitude: 44°49.063'W
Water depth: 3560 m
Date: 21/06/2016
Core: M127/702GC
Core lenght: 92 cm
Core section: A
Reflectance L* a* b*
Grain size (estimated)
Clay
Silt
Sand
Gravel
Sampling
Core image
Structures
Graphic lithology
Section
Core lenght (cm)
A
SS
CC
0
25
50
75
100
125
150

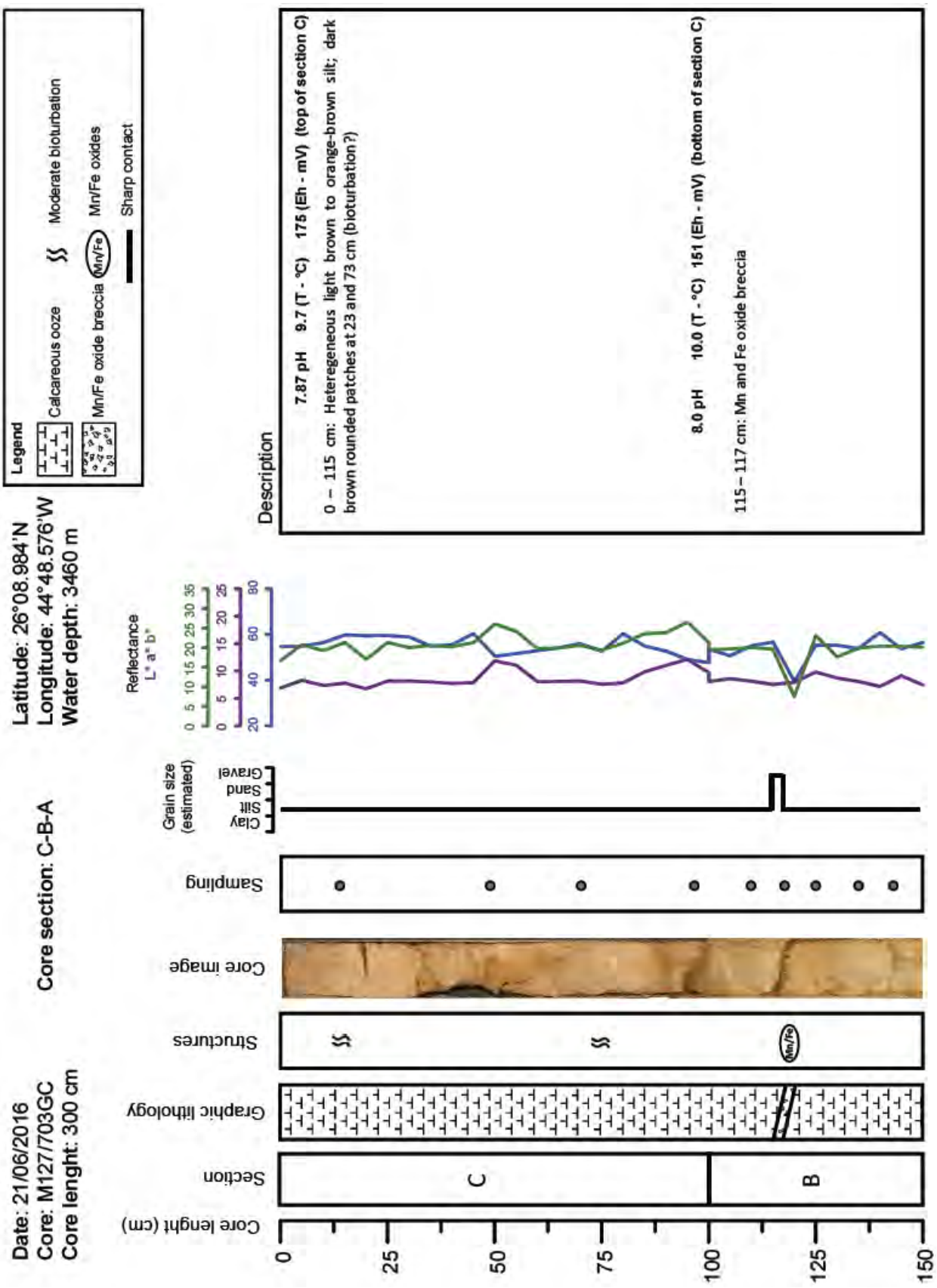
Legend
Calcareous ooze
Moderate bioturbation
Mn/Fe oxide breccia
Mn/Fe oxides
Sharp contact
Description
7.87 pH 9.7 (T - °C) 175 (Eh - mV) (top of section C)
0 – 115 cm: Heteregeneous light brown to orange-brown silt; dark brown rounded patches at 23 and 73 cm (bioturbation?)
8.0 pH 10.0 (T - °C) 151 (Eh - mV) (bottom of section C)
115 – 117 cm: Mn and Fe oxide breccia
Latitude: 26°08.984'N
Longitude: 44°48.576'W
Water depth: 3460 m
Core section: C-B-A
Date: 21/06/2016
Core: M127/703GC
Core lenght: 300 cm
Reflectance L* a* b*
Grain size (estimated)
Clay
Silt
Sand
Gravel
Sampling
Core image
Structures
Graphic lithology
Section
Core lenght (cm)
C
B
Mn/Fe
0
25
50
75
100
125
150

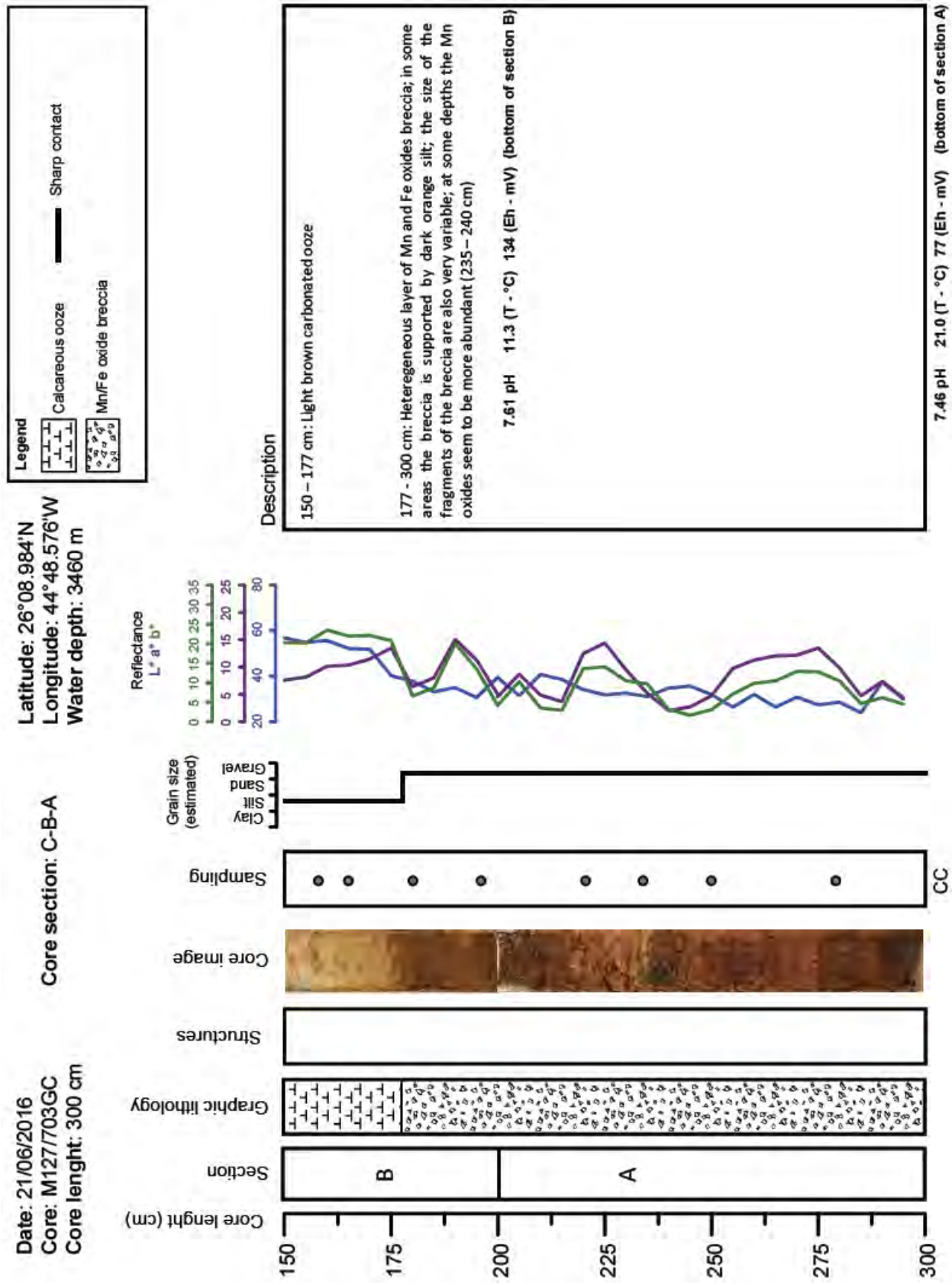
Legend
Calcareous ooze
Sharp contact
Mn/Fe oxide breccia
Latitude: 26°08.984'N
Longitude: 44°48.576'W
Water depth: 3460 m
Core section: C-B-A
Date: 21/06/2016
Core: M127/703GC
Core lenght: 300 cm
Description
150 – 177 cm: Light brown carbonated ooze
177 - 300 cm: Heteregeneous layer of Mn and Fe oxides breccia; in some areas the breccia is supported by dark orange silt; the size of the fragments of the breccia are also very variable; at some depths the Mn oxides seem to be more abundant (235 – 240 cm)
7.61 pH 11.3 (T - °C) 134 (Eh - mV) (bottom of section B)
7.46 pH 21.0 (T - °C) 77 (Eh - mV) (bottom of section A)
Reflectance
L* a* b*
Grain size (estimated)
Clay
Silt
Sand
Gravel
Sampling
Core image
Structures
Graphic lithology
Section
Core lenght (cm)
B
A
CC
150
175
200
225
250
275
300

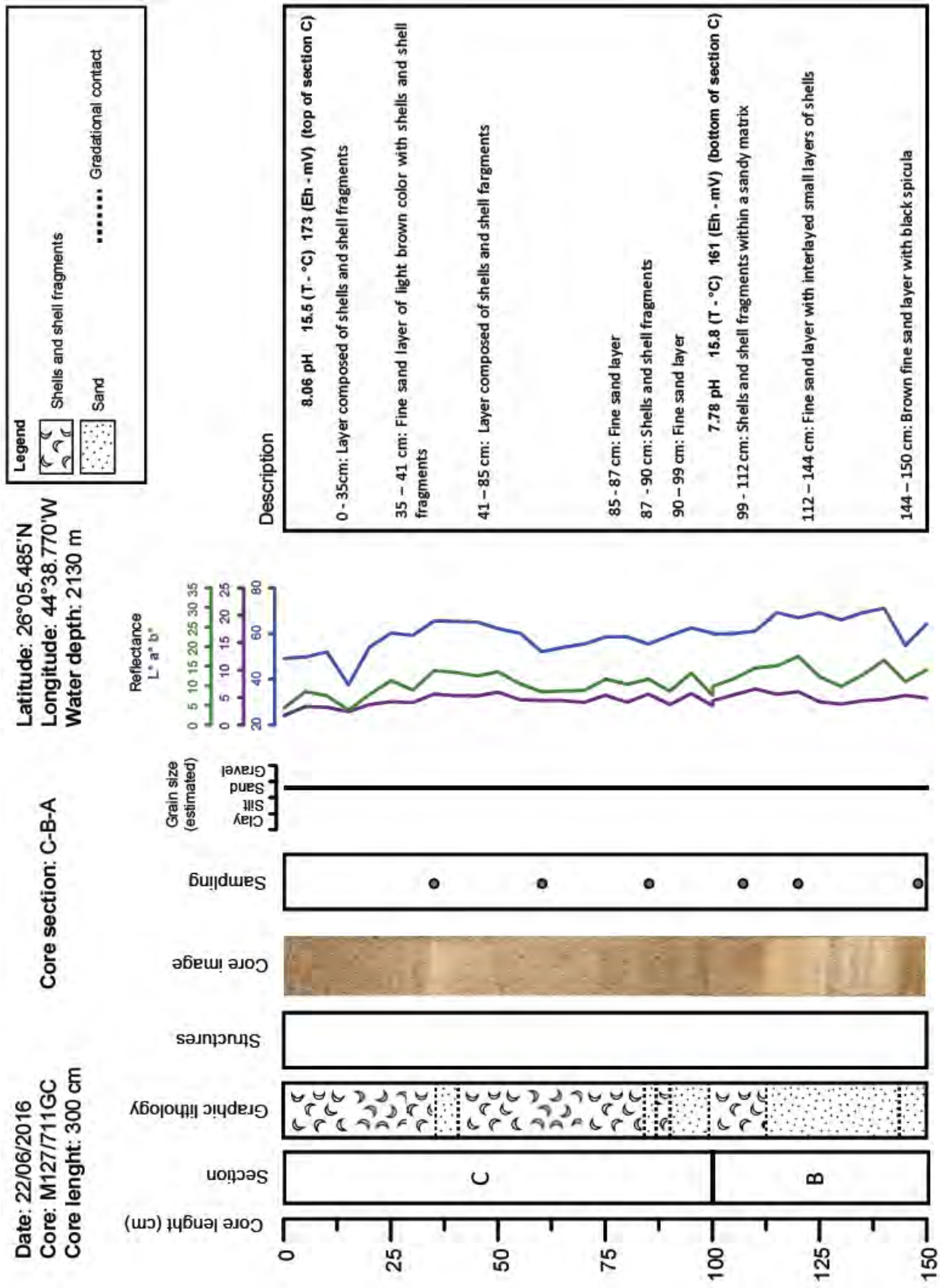
Legend
Shells and shell fragments
Sand
Gradational contact
Description
8.06 pH 15.5 (T - °C) 173 (Eh - mV) (top of section C)
0 - 35cm: Layer composed of shells and shell fragments
35 – 41 cm: Fine sand layer of light brown color with shells and shell fragments
41 – 85 cm: Layer composed of shells and shell fargments
85 - 87 cm: Fine sand layer
87 - 90 cm: Shells and shell fragments
90 – 99 cm: Fine sand layer
7.78 pH 15.8 (T - °C) 161 (Eh - mV) (bottom of section C)
99 - 112 cm: Shells and shell fragments within a sandy matrix
112 – 144 cm: Fine sand layer with interlayed small layers of shells
144 – 150 cm: Brown fine sand layer with black spicula
Latitude: 26°05.485'N
Longitude: 44°38.770'W
Water depth: 2130 m
Core section: C-B-A
Date: 22/06/2016
Core: M127/711GC
Core lenght: 300 cm
Reflectance L* a* b*
Grain size (estimated)
Clay
Silt
Sand
Gravel
Sampling
Core image
Structures
Graphic lithology
Section
Core lenght (cm)
C
B
0
25
50
75
100
125
150

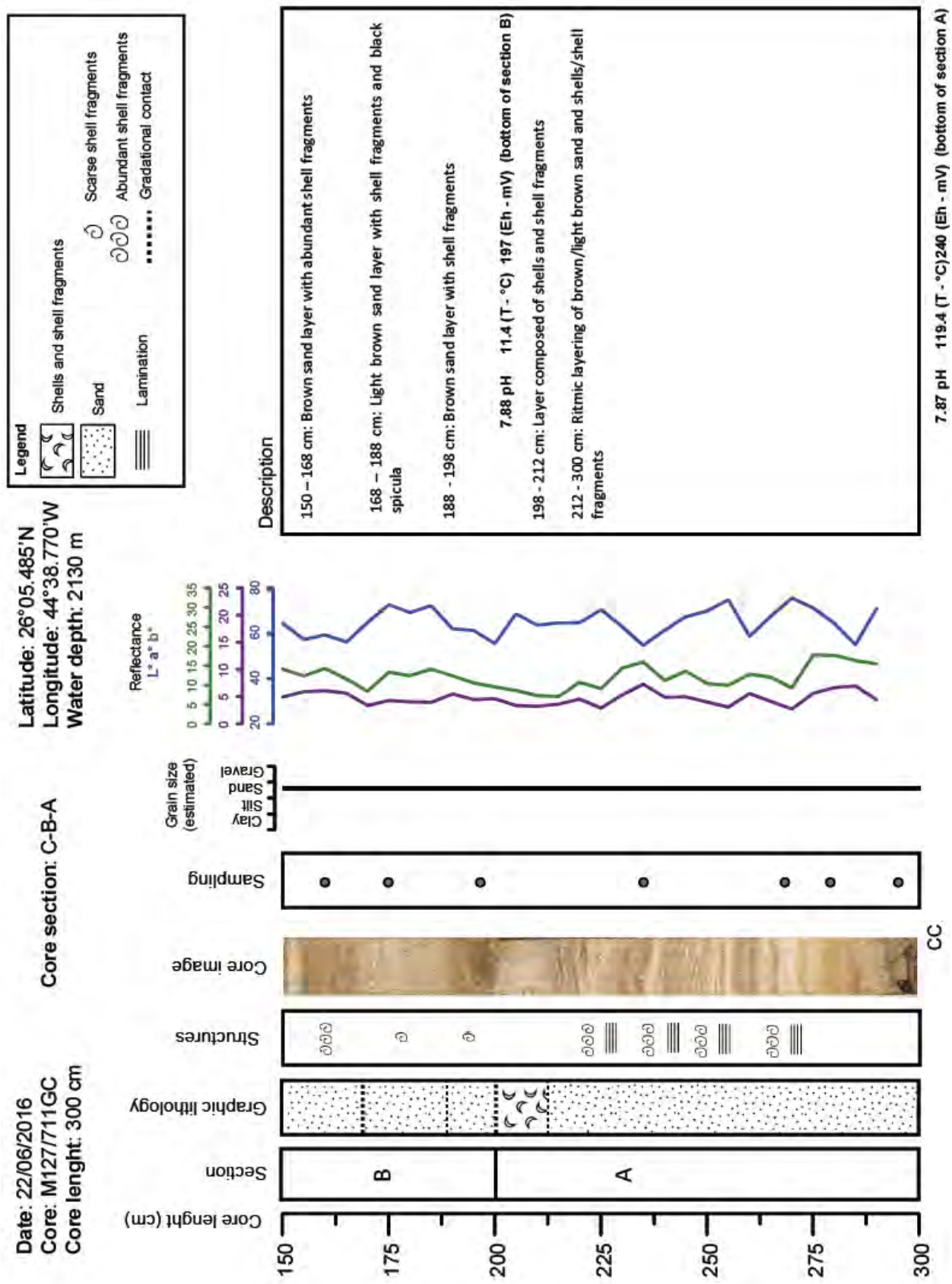
Date: 22/06/2016
Core: M127/711GC
Core lenght: 300 cm
Core section: C-B-A
Latitude: 26°05.485'N
Longitude: 44°38.770'W
Water depth: 2130 m
Legend
Shells and shell fragments
Sand
Lamination
Scarse shell fragments
Abundant shell fragments
Gradational contact
Description
150 – 168 cm: Brown sand layer with abundant shell fragments
168 – 188 cm: Light brown sand layer with shell fragments and black spicula
188 - 198 cm: Brown sand layer with shell fragments
7.88 pH 11.4 (T - °C) 197 (Eh - mV) (bottom of section B)
198 - 212 cm: Layer composed of shells and shell fragments
212 - 300 cm: Ritmic layering of brown/light brown sand and shells/shell fragments
7.87 pH 119.4 (T - °C)240 (Eh - mV) (bottom of section A)
Reflectance L* a* b*
Grain size (estimated)
Clay
Silt
Sand
Gravel
Sampling
Core image
Structures
Graphic lithology
Section
Core lenght (cm)
B
A
CC
150
175
200
225
250
275
300

GEOMAR
Helmholtz-Zentrum für Ozeanforschung Kiel

GEOMAR Reports

No.	Title
1	FS POSEIDON Fahrtbericht / Cruise Report POS421, 08. – 18.11.2011, Kiel - Las Palmas, Ed.: T.J. Müller, 26 pp, DOI: 10.3289/GEOMAR_REP_NS_1_2012
2	Nitrous Oxide Time Series Measurements off Peru – A Collaboration between SFB 754 and IMARPE –, Annual Report 2011, Eds.: Baustian, T., M. Graco, H.W. Bange, G. Flores, J. Ledesma, M. Sarmiento, V. Leon, C. Robles, O. Moron, 20 pp, DOI: 10.3289/GEOMAR_REP_NS_2_2012
3	FS POSEIDON Fahrtbericht / Cruise Report POS427 – Fluid emissions from mud volcanoes, cold seeps and fluid circulation at the Don-_Kuban deep sea fan (Kerch peninsula, Crimea, Black Sea) – 23.02. – 19.03.2012, Burgas, Bulgaria - Heraklion, Greece, Ed.: J. Bialas, 32 pp, DOI: 10.3289/GEOMAR_REP_NS_3_2012
4	RV CELTIC EXPLORER EUROFLEETS Cruise Report, CE12010 – ECO2@NorthSea, 20.07. – 06.08.2012, Bremerhaven – Hamburg, Eds.: P. Linke et al., 65 pp, DOI: 10.3289/GEOMAR_REP_NS_4_2012
5	RV PELAGIA Fahrtbericht / Cruise Report 64PE350/64PE351 – JEDDAH-TRANSECT -, 08.03. – 05.04.2012, Jeddah – Jeddah, 06.04 - 22.04.2012, Jeddah – Duba, Eds.: M. Schmidt, R. Al-Farawati, A. Al-Aidaroos, B. Kürten and the shipboard scientific party, 154 pp, DOI: 10.3289/GEOMAR_REP_NS_5_2013
6	RV SONNE Fahrtbericht / Cruise Report SO225 - MANIHIKI II Leg 2 The Manihiki Plateau - Origin, Structure and Effects of Oceanic Plateaus and Pleistocene Dynamic of the West Pacific Warm Water Pool, 19.11.2012 - 06.01.2013 Suva / Fiji – Auckland / New Zealand, Eds.: R. Werner, D. Nürnberg, and F. Hauff and the shipboard scientific party, 176 pp, DOI: 10.3289/GEOMAR_REP_NS_6_2013
7	RV SONNE Fahrtbericht / Cruise Report SO226 – CHRIMP CHatham RIse Methane Pockmarks, 07.01. - 06.02.2013 / Auckland – Lyttleton & 07.02. – 01.03.2013 / Lyttleton – Wellington, Eds.: Jörg Bialas / Ingo Klaucke / Jasmin Mögeltönder, 126 pp, DOI: 10.3289/GEOMAR_REP_NS_7_2013
8	The SUGAR Toolbox - A library of numerical algorithms and data for modelling of gas hydrate systems and marine environments, Eds.: Elke Kossel, Nikolaus Bigalke, Elena Piñero, Matthias Haeckel, 168 pp, DOI: 10.3289/GEOMAR_REP_NS_8_2013
9	RV ALKOR Fahrtbericht / Cruise Report AL412, 22.03.-08.04.2013, Kiel – Kiel. Eds: Peter Linke and the shipboard scientific party, 38 pp, DOI: 10.3289/GEOMAR_REP_NS_9_2013
10	Literaturrecherche, Aus- und Bewertung der Datenbasis zur Meerforelle (Salmo trutta trutta L.) Grundlage für ein Projekt zur Optimierung des Meerforellenmanagements in Schleswig-Holstein. Eds.: Christoph Petereit, Thorsten Reusch, Jan Dierking, Albrecht Hahn, 158 pp, DOI: 10.3289/GEOMAR_REP_NS_10_2013
11	RV SONNE Fahrtbericht / Cruise Report SO227 TAIFLUX, 02.04. – 02.05.2013, Kaohsiung – Kaohsiung (Taiwan), Christian Berndt, 105 pp, DOI: 10.3289/GEOMAR_REP_NS_11_2013
12	RV SONNE Fahrtbericht / Cruise Report SO218 SHIVA (Stratospheric Ozone: Halogens in a Varying Atmosphere), 15.-29.11.2011, Singapore - Manila, Philippines, Part 1: SO218- SHIVA Summary Report (in German), Part 2: SO218- SHIVA English reports of participating groups, Eds.: Birgit Quack & Kirstin Krüger, 119 pp, DOI: 10.3289/GEOMAR_REP_NS_12_2013
13	KIEL276 Time Series Data from Moored Current Meters. Madeira Abyssal Plain, 33°N, 22°W, 5285 m water depth, March 1980 – April 2011. Background Information and Data Compilation. Eds.: Thomas J. Müller and Joanna J. Waniek, 239 pp, DOI: 10.3289/GEOMAR_REP_NS_13_2013

GEOMAR
Helmholtz-Zentrum für Ozeanforschung Kiel

GEOMAR Reports

No.	Title
14	RV POSEIDON Fahrtbericht / Cruise Report POS457: ICELAND HAZARDS Volcanic Risks from Iceland and Climate Change:The Late Quaternary to Anthropogene Development Reykjavík / Iceland – Galway / Ireland, 7.-22. August 2013. Eds.: Reinhard Werner, Dirk Nürnberg and the shipboard scientific party, 88 pp, DOI: 10.3289/GEOMAR_REP_NS_14_2014
15	RV MARIA S. MERIAN Fahrtbericht / Cruise Report MSM-34 / 1 & 2, SUGAR Site, Varna – Varna, 06.12.13 – 16.01.14. Eds: Jörg Bialas, Ingo Klaucke, Matthias Haeckel, 111 pp, DOI: 10.3289/GEOMAR_REP_NS_15_2014
16	RV POSEIDON Fahrtbericht / Cruise Report POS 442, "AUVinTYS" High-resolution geological investigations of hydrothermal sites in the Tyrrhenian Sea using the AUV "Abyss", 31.10. – 09.11.12, Messina – Messina, Ed.: Sven Petersen, 32 pp, DOI: 10.3289/GEOMAR_REP_NS_16_2014
17	RV SONNE, Fahrtbericht / Cruise Report, SO 234/1, "SPACES": Science or the Assessment of Complex Earth System Processes, 22.06. – 06.07.2014, Walvis Bay / Namibia - Durban / South Africa, Eds.: Reinhard Werner and Hans-Joachim Wagner and the shipbord scientific party, 44 pp, DOI: 10.3289/GEOMAR_REP_NS_17_2014
18	RV POSEIDON Fahrtbericht / Cruise Report POS 453 & 458, "COMM3D", Crustal Structure and Ocean Mixing observed with 3D Seismic Measurements, 20.05. – 12.06.2013 (POS453), Galway, Ireland – Vigo, Portugal, 24.09. – 17.10.2013 (POS458), Vigo, Portugal – Vigo, Portugal, Eds.: Cord Papenberg and Dirk Klaeschen, 66 pp, DOI: 10.3289/GEOMAR_REP_NS_18_2014
19	RV POSEIDON, Fahrtbericht / Cruise Report, POS469, "PANAREA", 02. – 22.05.2014, (Bari, Italy – Malaga, Spain) & Panarea shallow-water diving campaign, 10. – 19.05.2014, Ed.: Peter Linke, 55 pp, DOI: 10.3289/GEOMAR_REP_NS_19_2014
20	RV SONNE Fahrtbericht / Cruise Report SO234-2, 08.-20.07.2014, Durban, -South Africa - Port Louis, Mauritius, Eds.: Kirstin Krüger, Birgit Quack and Christa Marandino, 95 pp, DOI: 10.3289/GEOMAR_REP_NS_20_2014
21	RV SONNE Fahrtbericht / Cruise Report SO235, 23.07.-07.08.2014, Port Louis, Mauritius to Malé, Maldives, Eds.: Kirstin Krüger, Birgit Quack and Christa Marandino, 76 pp, DOI: 10.3289/GEOMAR_REP_NS_21_2014
22	RV SONNE Fahrtbericht / Cruise Report SO233 WALVIS II, 14.05-21.06.2014, Cape Town, South Africa - Walvis Bay, Namibia, Eds.: Kaj Hoernle, Reinhard Werner, and Carsten Lüter, 153 pp, DOI: 10.3289/GEOMAR_REP_NS_22_2014
23	RV SONNE Fahrtbericht / Cruise Report SO237 Vema-TRANSIT Bathymetry of the Vema-Fracture Zone and Puerto Rico TRench and Abyssal AtlaNtic BiodiverSITy Study, Las Palmas (Spain) - Santo Domingo (Dom. Rep.) 14.12.14 - 26.01.15, Ed.: Colin W. Devey, 130 pp, DOI: 10.3289/GEOMAR_REP_NS_23_2015
24	RV POSEIDON Fahrtbericht / Cruise Report POS430, POS440, POS460 & POS467 Seismic Hazards to the Southwest of Portugal; POS430 - La-Seyne-sur-Mer - Portimao (7.4. - 14.4.2012), POS440 - Lisbon - Faro (12.10. - 19.10.2012), POS460 - Funchal - Portimao (5.10. - 14.10.2013), POS467 - Funchal - Portimao (21.3. - 27.3.2014), Ed.: Ingo Grevemeyer, 43 pp, DOI: 10.3289/GEOMAR_REP_NS_24_2015
25	RV SONNE Fahrtbericht / Cruise Report SO239, EcoResponse Assessing the Ecology, Connectivity and Resilience of Polymetallic Nodule Field Systems, Balboa (Panama) – Manzanillo (Mexico), 11.03. -30.04.2015, Eds.: Pedro Martínez Arbizu and Matthias Haeckel, 204 pp, DOI: 10.3289/GEOMAR_REP_NS_25_2015

GEOMAR
Helmholtz-Zentrum für Ozeanforschung Kiel

GEOMAR Reports

No.	Title
26	RV SONNE Fahrtbericht / Cruise Report SO242-1, JPI OCEANS Ecological Aspects of Deep-Sea Mining, DISCOL Revisited, Guayaquil - Guayaquil (Equador), 29.07.-25.08.2015, Ed.: Jens Greinert, 290 pp, DOI: 10.3289/GEOMAR_REP_NS_26_2015
27	RV SONNE Fahrtbericht / Cruise Report SO242-2, JPI OCEANS Ecological Aspects of Deep-Sea Mining DISCOL Revisited, Guayaquil - Guayaquil (Equador), 28.08.-01.10.2015, Ed.: Antje Boetius, 552 pp, DOI: 10.3289/GEOMAR_REP_NS_27_2015
28	RV POSEIDON Fahrtbericht / Cruise Report POS493, AUV DEDAVE Test Cruise, Las Palmas - Las Palmas (Spain), 26.01.-01.02.2016, Ed.: Klas Lackschewitz, 17 pp, DOI: 10.3289/GEOMAR_REP_NS_28_2016
29	Integrated German Indian Ocean Study (IGIOS) - From the seafloor to the atmosphere - A possible German contribution to the International Indian Ocean Expedition 2 (IIOE-2) programme – A Science Prospectus, Eds.: Bange, H.W. , E.P. Achterberg, W. Bach, C. Beier, C. Berndt, A. Biastoch, G. Bohrmann, R. Czeschel, M. Dengler, B. Gaye, K. Haase, H. Herrmann, J. Lelieveld, M. Mohtadi, T. Rixen, R. Schneider, U. Schwarz-Schampera, J. Segschneider, M. Visbeck, M. Voß, and J. Williams, 77pp, DOI: 10.3289/GEOMAR_REP_NS_29_2016
30	RV SONNE Fahrtbericht / Cruise Report SO249, BERING – Origin and Evolution of the Bering Sea: An Integrated Geochronological, Volcanological, Petrological and Geochemical Approach, Leg 1: Dutch Harbor (U.S.A.) - Petropavlovsk-Kamchatsky (Russia), 05.06.2016-15.07.2016, Leg 2: Petropavlovsk-Kamchatsky (Russia) - Tomakomai (Japan), 16.07.2016-14.08.2016, Eds.: Reinhard Werner, et al., DOI: 10.3289/GEOMAR_REP_NS_30_2016
31	RV POSEIDON Fahrtbericht/ Cruise Report POS494-2, HIERROSEIS Leg 2: Assessment of the Ongoing Magmatic-Hydrothermal Discharge of the El Hierro Submarine Volcano, Canary Islands by the Submersible JAGO, Valverde – Las Palmas (Spain), 07.02.-15.02.2016, Eds.: Hannington, M.D. and Shipboard Scientific Party, DOI: 10.3289/GEOMAR_REP_NS_31_2016
32	RV METEOR Fahrtbericht/ Cruise Report M127, Extended Version, Metal fluxes and Resource Potential at the Slow-spreading TAG Midocean Ridge Segment (26°N, MAR) – Blue Mining@Sea, Bridgetown (Barbados) – Ponta Delgada (Portugal) 25.05.-28.06.2016, Eds.: Petersen, S. and Shipboard Scientific Party, DOI: 10.3289/GEOMAR_REP_NS_32_2016

For GEOMAR Reports, please visit:
https://oceanrep.geomar.de/view/series/GEOMAR_Report.html

Reports of the former IFM-GEOMAR series can be found under:
https://oceanrep.geomar.de/view/series/IFM-GEOMAR_Report.html

GEOMAR
Helmholtz-Zentrum für Ozeanforschung Kiel

Das GEOMAR Helmholtz-Zentrum für Ozeanforschung Kiel ist Mitglied der Helmholtz-Gemeinschaft Deutscher Forschungszentren e.V.

The GEOMAR Helmholtz Centre for Ocean Research Kiel is a member of the Helmholtz Association of German Research Centres

Helmholtz-Zentrum für Ozeanforschung Kiel / Helmholtz Centre for Ocean Research Kiel
GEOMAR
Dienstgebäude Westufer / West Shore Building
Düsternbrooker Weg 20
D-24105 Kiel
Germany

Helmholtz-Zentrum für Ozeanforschung Kiel / Helmholtz Centre for Ocean Research Kiel
GEOMAR
Dienstgebäude Ostufer / East Shore Building
Wischhofstr. 1-3
D-24148 Kiel
Germany

Tel.: +49 431 600-0
Fax: +49 431 600-2805
www.geomar.de